(1)

EURO MBE -91

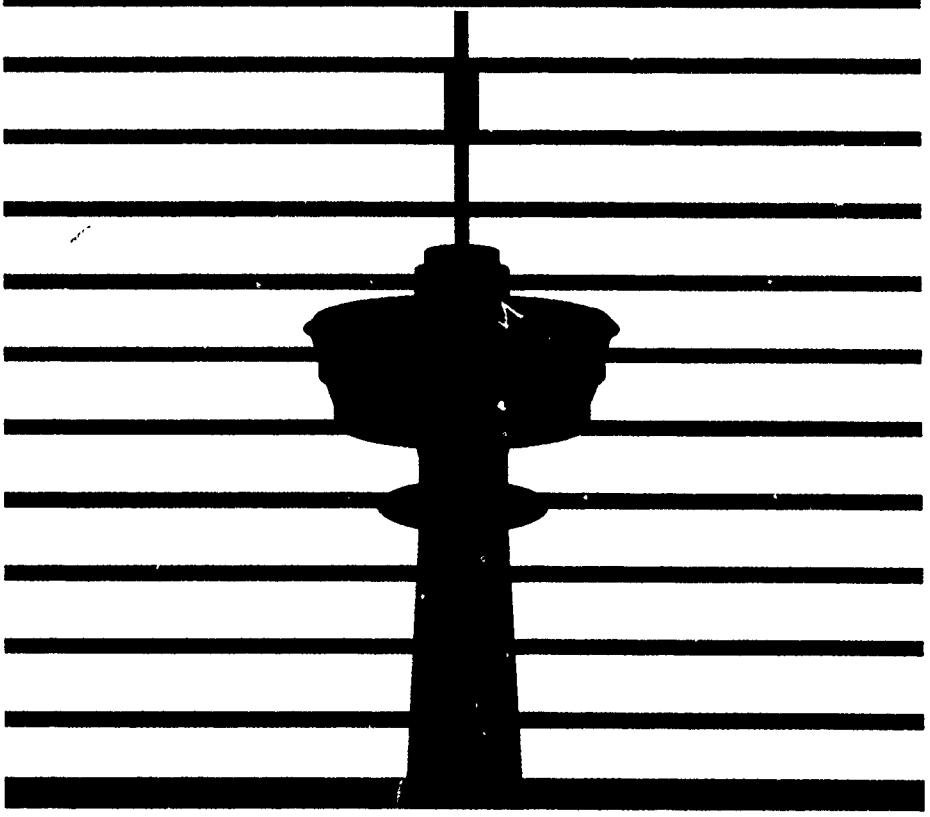

Sixth European Conference on Molecular Beam Epitaxy and Related Growth Methods

April 21-24, 1991
Tampere Hall, Tampere, Finland

R&D No:- 6403-EE-02
DAJA45-90-M-0312.

Tampere University of Technology

General Information

Registration and Conference Desk
The registration desk will be open from 16:00 to 21:00 on Sunday, April 21, from 8:00 to 18:00 on Monday, and from 8:00 to 15:00 on Tuesday and Wednesday. It is situated in Tampere Hall.

Exhibition
There is an exhibition of equipment, materials, books, etc. in the Exhibition Hall which is open from Monday, 9:00, to Wednesday, 12:00. The poster viewing sessions and the coffee breaks will also be held in the Exhibition Hall.

Social Functions

Sunday April 21:	18.00-21.00 Welcome Party in Tampere Hall
Monday April 22:	19.30-21.00 Reception by the Major of the City of Tampere
Tuesday April 23:	15.30-18.30 Visit to Spa Eden, Nokia City
	20.00 Conference Dinner in Restaurant "Kaijakka".

Attendees' companions are welcome to all these social functions. Companions' registration fee is FIM 500, which can be paid at the Registration Desk. There will also be an additional companions' programme on Monday and Tuesday. This programme including sightseeing, lunches, and visits to art galleries and a shopping mall will cost FIM 350.

Programme Committee
Prof. F. Alexandre, CNET, Bagneux
Prof. T. Andersson, Chalmers University of Technology, Gothenburg
Prof. I. Eisele, Universität der Bundeswehr München, Neubiberg
Dr. T. Foxon, Philips Research Laboratories, Redhill
Dr. F. Genova, CSELT, Torino
Dr. L. Goldstein, Laboratoires de Marcoussis, Marcoussis
Dr. H. Meier, IBM Zürich
Prof. M. Pessa (Chairman), TUT, Tampere
Prof. K. Singer, UMIST, Manchester
Prof. G. Weimann, Technical Universität München, Garching.

International Advisory Committee
Dr. R. Bicknell-Tassius, Universität Würzburg
Dr. F. Briones, CNM-CSIC, Madrid
Prof. R. Enderlein, Humboldt-Universität Berlin
Prof. D. Ferry, Arizona State University, Tempe
Prof. A. Gossard, University of California, Santa Barbara
Dr. M. Herman, Inst. Phys. of Academy of Poland, Warsaw
Dr. J.P. Hirtz, Thomson CSF/LCR, Paris
Dr. H. van Houten, Philips Research Laboratories, Eindhoven

Prof. B.A. Joyce, Imperial College, London
Dr. M. Laznicka, Institute of Physics, Prague
Prof. J. Massies, CNRS, Valbonne
Dr. M. Mizerov, A.F. Ioffe Institute, Leningrad
Dr. K. Ohno, Hokkaido University, Sapporo
Prof. K. Ploog, Max-Planck Institut, Stuttgart
Dr. H. Riechert, Siemens, München
Prof. Y. Shiraki, University of Tokyo, Tokyo
Dr. H. Sitter, Johannes Kepler Universität, Linz
Prof. S. Stenin, Academy of Science of USSR, Novosibirsk
Dr. W.T. Tsang, AT&T Bell Laboratories, Murray Hill
Prof. C. Whitehouse, RSRE, Malvern
Prof. R. H. Williams, University of Wales, Cardiff

Organizing Committee

Prof. M. Pessa (Chairman), TUT, phone +358 31 162 548, fax +358 31 162 600
Dr. H. Asonen, TUT, phone +358 31 162 554
Prof. J. Sinkkonen, Helsinki University of Technology, Espoo
Dr. I. Suni, Technical Research Centre, Espoo.
Ms R. Siekkinen (Secretary), TUT, phone +358 31 162 441, fax +358 31 162 164
Ms L. Kivipelto-Mattila (Social Programme), TUT, phone +358 31 162 452
Ms T. Taipale (Exhibition and Press Information), TVP Ltd

Sponsoring Societies and Organizations

EURO MBE-91 is sponsored by the Ministry of Education, the Ministry of Trade and Industry, the Finnish Physical Society, the Finnish Vacuum Society, and European Research Office of The US Army.

Acknowledgements

EURO MBE-91 has also been supported, in part, by DCA Instruments, Finnair, Isa Riber, and VG Semicon, to whom the organizers are most grateful.

The following companies attend the exhibition:

	Stand #
Aixtron GmbH	1
DCA Instruments Oy	10
DeMaCo Cryogenics	
EPI	19
Fisons Instruments Nordic AB	15
Intevac Inc. - MBE Equipment Division	9
Isa Riber	5
Johnson Matthey Electronics	2
Metaux Speciaux	12
Nippon Mining (U.K.) Ltd.	17
Nordiska Balzers AB	4
Outokumpu Semitronic	6
Oxford Applied Research	7
Oy Philips Ab, Analytical	8
Promecome	16
Springer	
Staib Instrumente GmbH	11
Superior Vacuum Technology	3
Union Carbide Corporation Advanced Ceramics	13
Vacuum Barrier Corp.	14
VSW Scientific Instruments	18

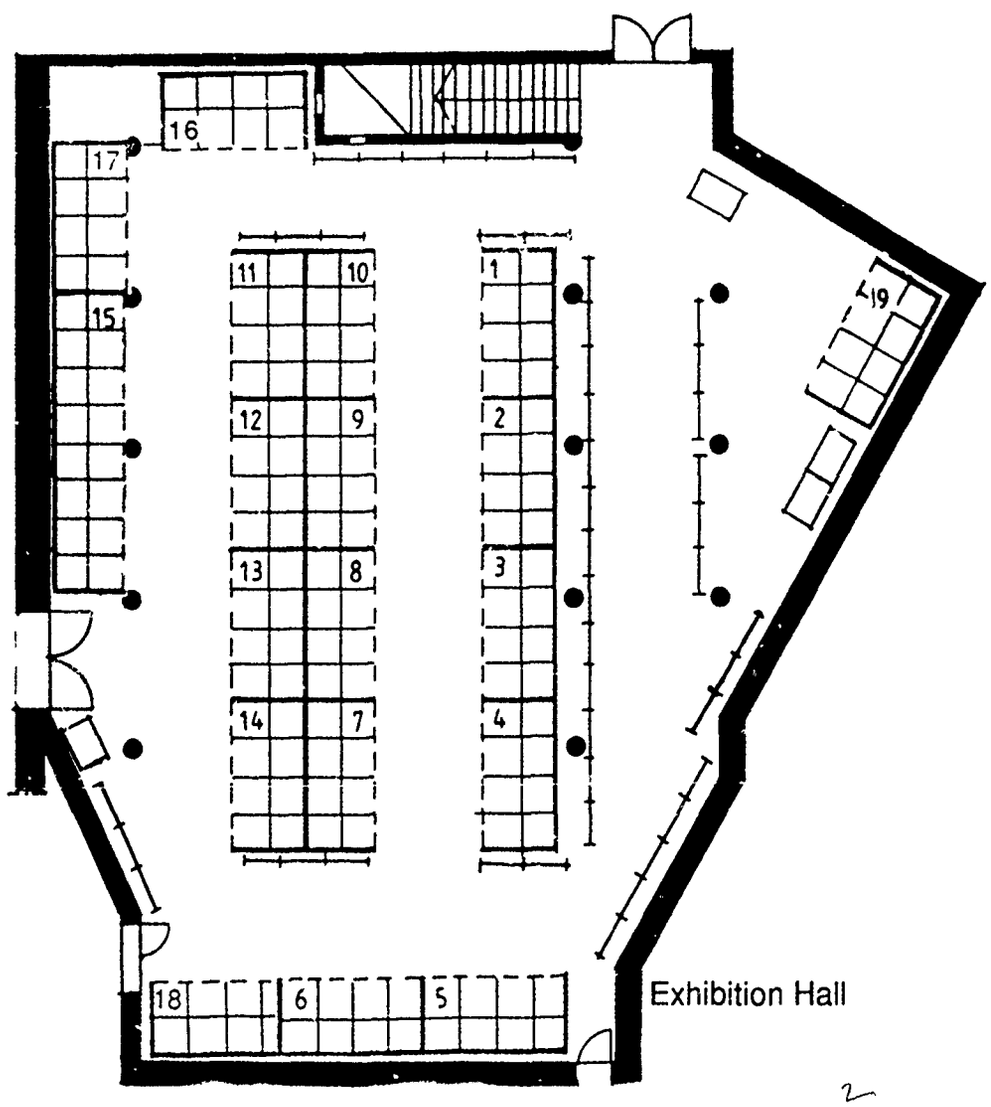

Programme
Sunday, 21 April

18.00-21.00 Registration and Get-together in Tampere Hall

Monday, 22 April

8.00-18.00 Registration

9.00-9.10 Opening Remarks

Session A
Si MBE

Chairman: I. Eisele

Topics covered during this symposium include: (1)

Ao1 Local growth of silicon MBE layers;

9.10-9.25 W. Kiunke, E. Hammerl, and I. Eisele, Fakultät für Elektrotechnik, Institut für Physik, Neubiberg, Germany

(2)

Ao2 Doping during growth; and δ doping by low energy implantation of As and Sb in Si MBE

9.25-9.40 H. Charki[1], E. Gergam[1], G. Prudon[2], and A. Vapaille[1*], [1]Institut d'Electronique Fondamentale, Université de Paris Sud, Orsay, [2]Laboratoire de Physique de la Matière, INSA, Villeurbanne, France

(3)

Ao3 Electrical characterisation for silicon; B delta-doped layers

9.40-9.55 N.L. Mattey[1], P.J. Phillips[1], R.A.A. Kubiak[1] S.N. Newstead[1], E.H.C. Parker[1], T.E. Whall[1], A. Wood[2], and A O'Neill[2], [1]Physics Department, University of Warwick, Coventry, and [2]Department of Electrical and Electronic Engineering, University of Newcastle, Newcastle, UK

(to pg 5)

Poster Summaries

Ap1 Electrical and optical properties of the Si-SiGe interface

9.55-10.00 J.C. Brighten[1] R.A.A. Kubiak[1], T.E. Whall[1], E.H.C. Parker*[1], S. Gardelis[2], J. Rimmer[2], and B. Hamilton[2], [1]Department of Physics, University of Warwick, Warwick, and [2]Department of Pure and Applied Physics, University of Manchester Institute of Science and Technology, Manchester, UK

Ap2 Molecular beam epitaxy with synchronization of nucleation

10 00-10.05 V.A. Markov[1], O.P. Pchelyakov[1], L.V. Sokolov[1], S.I. Stenin[1], and S. Stoyanov[2], [1]Institute of Semiconductor Physics, Siberian Branch of the USSR Academy of Sciences, Novosibirsk, USSR, and [2]Institute of Physical Chemistry, Bulgarian Academy of Sciences, Sophia, Bulgaria

Ap3 Influence of the surface structure on the Sb doping efficiency at low-temperature Si-MBE

10.05-10.10 A.I. Nikiforov, B.Z. Kanter, and S.I. Stenin, Institute of Semiconductor Physics, Siberian Branch of the USSR Academy of Sciences, Novosibirsk, USSR

Ap4 Negative differential resistance in silicon epitaxial structure

10.10-10.15 V.V. Suprunchik*, A.V. Dvurechenskii, D.L. Damchuk, and Yu.P. Stepantsev, Institute of Semiconductor Physics, Siberian Branch of the USSR Academy of Sciences, Novosibirsk, USSR

Ap5 Si solid phase epitaxy on Si-Sb and Si-B surface phases

10.15-10.20 A.V. Zotov and V.G. Lifshits, Institute of Automation and Control Processes, USSR Academy of Sciences, Vladivostok, USSR

Session B
Growth and Characterization of II-VI's

Chairman: H. Zogg

Bo1 10.20-10.35 **Growth of (111) CdTe studied by RHEED and X-ray photoelectron diffraction**

S. Tatarenko*[1], J. Cibert[1], R. Duszak[1], K. Saminadayar[2], and C. Deshayes[1]. [1]Laboratoire de Spectrométrie Physique, Université Joseph Fourier, CNRS, Grenoble, France, and [2]Centre d'Etudes Nucléaires, Grenoble, France

Bo2 10.35-10.50 **MBE growth and optical properties of $CdTe/Cd_{0.5}Hg_{0.5}Te$ heterostructures**

L. Ulmer*[1], E. Monterrat[1], N. Magnea[1], H. Mariette[2], P. Gentile[1], and J.L. Pautrat[1], Groupe Physique des Semiconducteurs, CEN - Grenoble, and [2]Laboratoire de Spectrométrie Physique Université J. Fourier, Grenoble, France

Bo3 10.50-11 05 **N-type doping of MBE zinc selenide using an electrochemical iodine cell**

J. Simpson, J.M. Wallace, H. Stewart, S.J.A. Adams, K.A. Prior *, and B.C. Cavenett, Department of Physics, Heriot-Watt University, Riccarton, UK

Poster Summaries

Bp1 11.05-11.10 **Growth and doping of $Cd_xHg_{(1-x)}Te(111)$ in molecular beam epitaxy**

T. Colin* and A. Million, LETI / Laboratoire Infrarouge, Grenoble, France

Bp2 11.10-11.15 **MBE growth of zinc selenide under intense UV laser irradiation**

J. Simpson, S.J.A. Adams, J.M. Wallace, K.A. Prior*, and B.C. Cavenett, Department of Physics, Heriot-Watt University, Riccarton, UK

Bp3 11.15-11.20 **Asymmetric azimuth angle dependence of X-ray rocking curves in N-ion implanted ZnSe**

K. Imai*, M. Hovinen, E. Kuusisto, J. Lilja, and M. Pessa, Department of Physics, Tampere University of Technology, Tampere, Finland

11.20-11 45 Coffee Break (Exhibition Hall)

Session C
Instrumentation
Chairman: H. Asonen

Co1 11.45-12.00 **Design and perfomance of multi-wafer MBE system used in HEMT production;**
H. Gotoh[1], Y, Higuchi[1], V.J. Mifsud[2], and D. Williams*[2], Mitsubishi Kasei Corporation, Ushiku-shi, Japan, and [2]VG Semicon Ltd, East Grinstead, England

Co2 12.00-12.15 **Indium free mounting technique retrofit to a 2 inch In bonded wafer substrate holder;**
D. Martin*, F. Morier-Genrud, and F.K. Reinhart, Institut de Micro et optoelectronique, Ecole Polytechnique Fédérale de Lausanne, Lausanne, Switzerland

Co3 12.15-12.30 **Structure, properties, and purity of pyrolytic boron nitride crucibles for molecular beam epitaxy**
A.W. Moore, Union Carbide Coatings Service Corporation, Parma, USA

(to pg 7)

Poster Summaries

Cp1 12.30-12.35 **MBE system for research**
M. Láznicka*[1], M. Cukr[1], J. Krautwurm[1], P. Svoboda[1], P. Doubrava[1], Z. Sourek[1], I. Gregora[1], V. Vorlicek[1], J. Oswald[1], and G. Nachtwei[2], [1]Institute of Physics, Czechoslovak Academy of Sciences, Prague, Czechoslovakia, and [2]Department of Physics, Institute of Solid State Physics, Humboldt University, Berlin, Germany

Cp2 12.35-12.40 **On the accuracy of MBE cell-temperature calibration investigated by frequency domain analysis of RHEED intensity oscillations**
J. Kraus*, J. Weyers, W. Prost, and F.J.Tegude, Universität-GH-Duisburg, Halbleitertechnik/Halbleitertechnologie, Duisburg, Germany

Cp3 12.40-12.45 **Optical simulation of effusion molecular beam for MBE**
B. Adamczyk*, L. Michalak, and E. Marcinkowska, Institute of Physics, Maria Curie-Sklodowska University, Lublin, Poland

Cp4 12.45-12.50 **Mathematical modeling of heating and Knudsen flow in effusion cell for MBE technology**
A.V. Bune and T.M. Makhviladze, Modeling Laboratory of Microelectronics Processes , Institute of Physics and Technology, Academy of Science of the USSR, Moscow , USSR

12.50-14.00 Lunch

Session D
Surfaces and Interfaces
Chairman: F. Alexandre

Do1 14.00-14.15 **A comparative study of InP oxide desorption under fluxes of As_4 and P_2**
R. Averbeck[1], H. Riechert*[1], H. Schlötterer[1], and G. Weimann[2], [1]Siemens Research Laboratories, München, and [2]Walter-Schottky-Institut, TU München, Garching, Germany

Do2 14.15-14.30 **Realization of atomically abrupt InAs/GaAs heterointerfaces by flashoff of the In floating layer**
O. Brandt*[1], K. Ploog[1], L. Tapper[1], M. Hohenstein[2], and F. Phillipp[2], [1]Max-Planck-Institut für Festkörperforschung, Stuttgart, and [2]Max-Planck-Institut für Metallforschung, Stuttgart, Germany

Do3 14.30-14.45 **The impact of the MBE growth conditions on the $Al_{0.48}In_{0.52}As$/$Ga_{0.47}In_{0.53}As$ interface**
H. Künzel*, H.G. Bach, A. Hase, and C. Schramm, Heinrich-Hertz-Institut für Nachrichtentechnik Berlin GmbH, Berlin, Germany

Do4 14.45-15.00 **Si delta dipole doping to tune AlAs/GaAs heterostructure band offsets**
L. Sorba[1,2], G. Bratina[1], G. Ceccone[1,3], A. Antonini[1], and A. Franciosi[1,3], [1]Laboratorio TASC dell´ INFM, Trieste, [2]Instituto di Acustica O.M. Corbiono del C.N.R., Roma, Italy, and [3]Department of Chemical Engineering and Materials Science, University of Minnesota, Minneapolis, USA

Do5 15.00-15.15 **Surface structures of epitaxial $CoSi_2$ thin films grown on Si(111) studied *in-situ* by scanning tunneling microscopy**
R. Stalder*, N. Onda, H. Sirringhaus, and H. von Känel, Laboratorium für Festkörperphysik, ETH, Zürich, Switzerland

Poster Summaries

Dp1 15.15-15.20 **Capping and decapping of MBE-grown GaAs(001) investigated with ASP, XPS and RHEED**
R.W. Bernstein[1], B.O. Fimland*[2], A. Borg[2], A.P. Grande[2], and J.K. Grepstad[2], [1]Norwegian Telecom Research Institute. Kjeller, and [2]Division of Physical Electronics, University of Trondheim - NTH, Trondheim, Norway

Dp2 15.20-15.25 **Strain measurement of molecular beam epitaxially grown $In_xGa_{1-x}As$ on InP(100) by double crystal X-ray diffraction: The effect of InAs interfacial layers**
S.A. Clark*[1], J.E. Macdonald[1], D.I. Westwood[1], R.H. Williams[1], and S.J. Barnett[2], [1]University of Wales College of Cardiff, Cardiff, and [2]Royal Signals Research Establishment, Great Malvern, UK

Dp3 15.25-15.30 **Scattering properties of GaAs/AlGaAs single quantum well grown by MBE**
X. Wang[1] and H. Zheng[2], [1]National Laboratory for Superlattices and Related Microstructures, and [2]Institute of Semiconductors, Academia Sinica, Beijing, China

Dp4 15.30-15.35 **RHEED studies of the CdTe growth surface and the orientation independence of the CdTe-HgTe valence band offset**
C.R. Becker*[1], Y.S. Wu[2], A. Waag[1], R.N. Bicknell-Tassius[1], and G. Landwehr[1], [1]Physikalisches Institut der Universität Würzburg, Würzburg, Germany, and [2]Institute of Physics, Chinese Academy of Sciences, Beijing, China

15.35-18.30 Poster viewing session
Exhibition of equipment, materials and books (Exhibition Hall)

19.30-21.00 Reception by the City of Tampere, City Hall

Tuesday, 23 April

8.00- Registration
8.30

Session E
Strained Layers and Quantum Wells

Chairman: F. Genova

Eo1 8.30-8.45 **Photoluminescence characterization of strained $Ga_xIn_{1-x}As/Ga_xIn_{1-x}As_yP_{1-y}$ quantum wells grown by gas-source molecular beam epitaxy**

R.J. Simes*[1], A. Perales[1], F. Mollot[2], M. Boulou[1], C. Starck[1], D. Bonnevie[1], M. Lambert[3], and L. Goldstein[1], Alcatel-Alsthom Recherche, Marcoussis, [2]L2M-CNRS, Bagneux, and [3]Alcatel-CIT, La Ville du Bois, France

(cont'd) → (7)

Eo2 8.45-9.00 **The temperature dependence of the critical layer thickness in $In_{0.36}Ga_{0.64}As$/GaAs single quantum wells grown by molecular beam epitaxy**

M.J. Ekenstedt, S.M. Wang, and T.G. Andersson, Department of Physics, Chalmers University of Technology, Göteborg, Sweden

Eo3 9.00-9.15 **Observation of type-I to type-II transition in strained $In_{0.22}Al_yGa_{0.78-y}As$/GaAs quantum wells grown by MBE**

S.M. Wang, T.G. Andersson, M.J. Ekenstedt, and V.D. Kulakovskii, Department of Physics, Chalmers University of Technology, Göteborg, Sweden

Eo4 9.15-9.30 **Strained layer devices for optical computing applications**

R. Grey*[1], P.A. Claxton[1], J. Woodhead[1], A.S. Pabla[1], M.H. Moloney[2], Department of Electronic and Electrical Engineering, The University of Sheffield, Sheffield, UK, and [2]Department of Pure and Applied Physics, Optronics Ireland Research Centre, The University of Dublin Trinity College, Dublin, Ireland

Eo5 9.30-9.45 **MBE growth of doped CdTe thin films and CdTe-CdMnTe quantum wells and their characterization**

A. Waag*[1], S. Schmeusser[1], R.N. Bicknell-Tassius[1], Y.S. Wu[2], T. Kuhn[1], B. Schmied[1], D. Yakovlev[3], W. Ossau[1], and G. Landwehr[1], Physikalisches Institut der Universität Würzburg, Würzburg, Germany, [2]Insitute of Physics, Chinese Academy of Sciences, Beijing, China, [3]Ioffe Physico-Technical Institute, Leningrad, USSR

(8) →

Eo6 9.45-10.00 **Large piezoelectric fields in (111) CdTe-CdZnTe quantum wells** (to pg 13)

J. Cibert*[1], R. André[1], C. Deshayes[1], Le Si Dang[1], S. Tatarenko[1], G. Feuillet[2], P.H. Jouneau[2], R. Mallard[2], and K. Saminadayar[2], [1]Laboratoire de Spectrométrie Physique, Université Joseph Fourier, Grenoble, and Département de Recherche Fondamentale, Centre d'Etudes Nucléaires, Grenoble, France

Poster Summaries

Ep1 10.00-10.05 **Enhanced excitonic transitions and electro-optical bistability in strained $In_xGa_{1-x}As/Al_{0.15}Ga_{0.85}As$ multiple quantum wells**

K. Fujiwara*[1], K. Kawashima[1], K. Kobayashi[1], and N. Sano[2], [1]ATR Optical and Radio Communications Research Laboratories, Kyoto, and [2]Department of Physics, School of Science, Kwansei Gakuin University, Nishinomiya, Japan

Ep2 10.05-10.10 **MBE growth and relaxation of strained $In_xGa_{1-x}As$ layers ($0.53 < x \leq 1.0$) on InP**

M. Gendry*, V. Drouot, J.L. Duvault, D. Gallet, C. Santinelli, and G. Hollinger, Laboratoire d'électronique, Ecole Centrale de Lyon, Ecully, France

Ep3 10.10-10.15 **MBE grown MQW in the InGaAlAs/InGaAs system: Non-radiative lifetime monitoring**

M. Quillec*, K.Satzke, and B. Sermage, Centre National d'Etudes des Télécommunications, Bagneux, France

Ep4 10.15-10.20 **The application of flux variations for the MBE growth of laterally graded GaAs/AlGaAs quantum well structures**

V.M. Airaksinen*[1], R. Salo[1], U. Gyllenberg[2], and H. Lipsanen[3], [1]Electron Physics Laboratory, Helsinki University of Technology, Espoo, [2]Semiconductor Laboratory, Technical Research Centre of Finland, Espoo, and [3]Optoelectronics Laboratory, Helsinki University of Technology, Espoo, Finland

Ep5 10.20-10.25 **MBE growth and characterization of strained GaSb layers on GaAs(100) for GaSb/InAs/GaSb QW structures**

S.V. Ivanov*, A.A. Budza, A.A. Dzamashvili, P.S. Kop'ev, B.Ya. Meltser, V.M. Ustinov, and S.V. Shaposhnikov, A.F.Ioffe Physico-Technical Institute, The Academy of Sciences of USSR, Leningrad, USSR

Ep6 10.25-10.30 **On the growth of InGaAs/InP QW structures by CBE**

A. Antolini[1], D. Campi[1], G. Gastaldi[1], F. Genova[1], M. Iori[1], C. Lamberti[2], G. Morello[1], and C. Rigo*[1], [1]Centro Studi E Laboratori Telecommunicazioni, Torino, and [2]Dottorato di Ricerca Universita' di Torino, Torino, Italy

Ep7 10.30-10.35 **Molecular beam epitaxy of $PbSe/Pb_{1-x}Mn_xSe$ multiquantum wells**

N. Frank, E. Koppensteiner, and G. Bauer, Institut für Halbleiterphysik, Johannes Kepler Universität Linz, Linz, Austria

10.35-11.05 Coffee Break, (Exhibition Hall)

Session F
Heteroepitaxy of Dissimilar Materials

Chairman: J. Massies

Fo1 11.05-11.20 **Defect self-annihilation in surfactant-mediated hetero epitaxial growth**

M. Horn-von Hoegen[1], F.K. LeGoues[2], M. Copel[2], and R.M. Tromp[2], [1]Institut für Festkörperphysik, Universität Hannover, Hannover, Germany, and [2]IBM Research Division, Thomas J. Watson Research Center, Yorktown Heights, USA

Fo2 11.20-11.35 **Low temperature process of GaAs/AlAs heterostructures on Si by atomic layer molecular beam epitaxy**

Y. González*, L. González, and F. Briones, Centro Nacional de Microelectrónica, Madrid, Spain

Fo3 11.35-11.50 **First stages of the molecular beam epitaxy growth of ZnTe on GaAs(001) studied by grazing incidence X-ray diffraction**

V.H. Etgens*[1], R. Pinchaux[2], M. Sauvage-Simkin[3], J. Massies[4], N. Jedrecy[3], A. Waldhauer[5], S. Tatarenko[6], and P.H. Jouneau[7], [1]LURE, Orsay, [2]Université P. et M.Curie, Paris, [3]Laboratoire de Minéralogie-Cristallographie, Paris, [4]Laboratoire Physique du Solide et Energie Solaire, CNRS, Sophia Antipolis, [5]DSM/DPhG/SPAS, Gif sur Yvete, [6]Laboratoire de Spectrométrie Physique, Université Joseph Fourier-CNRS, Grenoble, [7]CEN-Grenoble, Grenoble, France

Fo4 11.50-12.05 **Growth of InP on GaAs by gas-source MBE**

K. Rakennus*, T. Hakkarainen, K. Tappura, and M. Pessa, Department of Physics, Tampere University of Technology, Tampere, Finland

Poster Summaries

Fp1 12.05-12.10 **Molecular beam epitaxy of III-VI layered compounds InSe and GaSe**

J.-Y. Emery*[1], L. Brahim-Otsmane[1], and A. Chevy[2], [1]Laboratoire de Physique des Solides, Université Pierre et Marie Curie, Paris, and [2]Laboratoire de Physique des Milieux Condensés, Université Pierre et Marie Curie, Paris, France

Fp2 12.10-12.15 **MBE-growth of InSb bulk-layers on GaAs substrates and observation of resonant tunneling in InSb/AlInSb double-barrier structures**

J.R. Söderström*, M.M. Cumming, J.Y. Yao, and T.G. Andersson, Department of Physics, Chalmers University of Technology, Göteborg, Sweden

Fp3 12.15-12.20 **MBE growth of $In_xGa_{1-x}As$ (x=0.53) on Silicon**

A. Georgakilas[1], M. Lagadas[1], J. Stoemenos[2], and A. Christou[3], [1]Institute of Electronic Structure and Laser, Foundation for Research and Technology-Hellas, Heraklion, [2]Physics Department, University of Thessaloniki, Thessaloniki, Greece, and [3]Department of Electrical Engineering, University of Maryland, College Park, USA

Fp4 12.20-12.25 **MBE growth of GaAs on Si with a Si buffer layer**

A. Georgakilas[1], J. Stoemenos[2], P. Panayotatos[3], and A. Christou[4], [1]Institute of Electronic Structure and Laser, Foundation for Research and Technology-Hellas, Heraklion, [2]Physics Department, University of Thessaloniki, Thessaloniki, Greece, [3]Department of Electrical and Computer Engineering, Rutgers University, Piscataway, [4]Department of Electrical Engineering, University of Maryland, College Park, USA

Fp5 12.25-12.30 **MBE process compatible plasma enhanced growth of silicon-based dielectric films**

I. Eisele[1], H. Lorenz[1], J. Ramm[2], E. Bech[2], A. Züger[2], [1]Fakultät für Elektrotechnik, Institut für Physik, Neubiberg, Germany, and [2]FL-Balzers AG, Liechtenstein

Fp6 12.30-12.35 **Initial stage of epitaxially grown ZnSe on GaAs: Experiment and theory**

D. Schikora*, J. Grieshe, A. Josiek, and R. Enderlein, Department of Physics, Humboldt-University Berlin, Germany

Fp7 12.35-12.40 **Structural properties of MBE grown BaF_2/CaF_2 bilayers on both Si(111) and Si(100)**

F. Nguyen-Van-Dau*, V. Mathet, J. Siejka[1], P. Galtier, and D.G. Crété, Thomson CSF, Orsay, [1]GPSENS, University of Paris, Paris, France

Fp8 12.40-12.45 **RHEED intensity oscillations during CaF_2 and SrF_2 MBE growth on Si(111) and GaAs(111)B**

S.V. Novikov, N.S. Sokolov*, and N.L. Yakovlev, A.F. Ioffe Physico-Technical Institute, Leningrad, USSR

Fp9 12.45-12.50 **Layer by layer molecular beam epitaxy of BiSrCaCuO: Study of the bismuth incorporation**

M. Laguës[1], L. Ranno[1], M. Viret[1], X.Z. Xu[1], J.P. Contour*[2], and P.Bernstein[2], [1]Laboratoire de Physique Quantique, CNRS, Paris, and [2]Laboratoire de Physique du Solice, ESPCI, Paris, France

Fp10 12.50-12.55 **Epitaxial growth of lattice matched $Sc_{0.2}Yb_{0.8}As$/(001)GaAs and GaAs/$Sc_{0.2}Yb_{0.8}As$/(001) and (111)GaAs heterostructures**

V. Durel, J. Caulet, Y. Ballini, M. Minier, B. Guenais, G. Dupas, and A. Guivarc'h*, LAB/OCM/MPA, CNET, Lannion, France

12.55-14.10 Lunch

14.10-15.30 Poster viewing session
Exhibition of equipment, materials and books (Exhibition Hall)

15.30-18.30 Visit to Spa EDEN, Nokia City
(Bus transportation, 20 min)

20.00 Banquet, Restaurant "Kaijakka" near the quay by Lake Pyhäjärvi

Wednesday, 24 April

8.00- Exhibition
8.30

Session G
Growth of III-V's by GSMBE, MOMBE, and CBE

Chairman: L. Goldstein

Go1 8.30-8.45 **Growth of GaInAs and GaInAsP by CBE**

A. Rudra*[1], J.F. Carlin[1], M. Gailhanou[1], J.L. Staehli[2], P. Ruterana[1], and M. Ilegems[1], [1]Institute for Micro- and Opto-electronics and [2]Insitute for Applied Physics, Ecole Polytechnique Fédérale de Lausanne, Lausanne, Switzerland

Go2 8.45-9.00 **Growth of InP/InGaAs multiple quantum well structures with exceptional lateral uniformity by chemical beam epitaxy**

P.J. Skevington*, S.J. Amin, G.J. Davies, British Telecom Research Laboratories, Ipswich, UK

Go3 9.00-9.15 **Carbon incorporation in MOMBE grown $Ga_xIn_{1-x}P$ layers**

Ph. Maurel*, J.C. Garcia, Ph. Bove, C. Grattepain, and J.P. Hirtz, Thomson CSF, Orsay, France

Poster Summaries

Gp1 9.15-9.20 **APAH - A coordinatively saturated aluminium precursor for MOMBE**

M. Kamp*[1], F. König[1], G. Mörsch[1], H. Lüth[1], L. Pohl[2], and M. Hostalek[2], [1]Institut für Schicht- und Ionen-technik, Forschungszentrum Jülich, Jülich, and [2]E. Merck, Darmstadt, Germany

Gp2 9.20-9.25 **Observation of electro-optical effects in InGaAsP/InP quantum wells and superlattice grown by GSMBE**

F. Mollot*, M. Boulou, and C. Starck, Alcatel Alsthom Recherche, Marcoussis, *L2M, CNRS, Bagneux, France

Session H
Devices

Chairman: H. Schlötterer

Ho1 9.30-9.45 **Growth of PBH laser by GSMBE**
D. Bonnevie, J-L. Lievin, C. Starck, F. Poingt, D. Sigogne, and L. Goldstein*, Alcatel Alsthom Recherche, Marcoussis, France

Ho2 9.45-10.00 **Strained GRIN-MQW lasers for λ = .5 µm grown by gas-source MBE**
H. Asonen*, J. Keskinen, J. Näppi, M. Korteoja, K. Tappura, K. Rakennus, T. Hakkarainen, and M. Pessa, Department of Physics, Tampere University of Technology, Tampere, Finland

Ho3 10.00-10.15 **High power AlGaAs-SQW-SCH-lasers and laser arrays prepared by molecular beam epitaxy**
V.P. Chalyi, S.Y. Karpov, Yu.V. Kovalchuck, V.E. Myachin*, A.Yu. Ostrovski , A.P. Shkurko, N.A. Strugov, and A.L. Ter-Martirosyan, A.F.Ioffe Physico-Technical Institute, Leningrad, USSR

Ho4 10.15-10.30 **Improved MBE growth of heavily doped GaAs(Be)/GaAlAs HBTs with high device performances and high thermal stability**
N. Jourdan, F. Alexandre*, C. Dubon-chevallier, J. Dangla, Y. Gao, and A.C. Papadopoulo, Centre National d'études des Télé-communications, Bagneux, France

Ho5 10.30-10.45 **Influence of MBE growth temperature on the device performance of AlGaAs/GaAs HBT's and their characterization by photoluminescence**
C. Wölk, H. Leier, and F.J. Berlec, Daimler Benz AG, Ulm, Germany

Poster Summaries

Hp1 10.45-10.50 **InP solar cells grown by gas-source molecular beam epitaxy**
J.P. Zibin*, K. Rakennus, K. Tappura, G. Zhang, J. Lammasniemi, and H. Asonen, Department of Physics, Tampere University of Technology, Tampere, Finland

Hp2 10.50-10.55 **AlInAs/GaInAs metal-semiconductor-metal photodiode with graded AlGaInAs transition regions**
A. Temmar, J.P. Praseuth*, and A. Scavennec, Centre National d'Etudes des Télécommunications, Bagneux, France

Hp3 10.55-11.00 **Properties of pseudomorphic $In_xGa_{1-x}As/Al_{0.3}Ga_{0.7}As/GaAs$ high electron mobility transistors ($0 < x < 0.5$)**
T. Schweizer*, K. Köhler, P. Ganser, A. Hülsmann, and P. Tasker, Fraunhofer Insitut für Angewandte Festkörperphysik, Freiburg, Germany

11.00-11.30 Coffee break (Exhibition Hall)

Session I
MBE Growth and Characterization of III-V's

Chairman: C. Stanley

Io1 11.30-11.45 **STM imaging of MBE-grown (Al)GaAs (110) cross sections**
U. Albrektsen[1], H.W. Salemink*[2], and H.P. Meier[2], [1]Telecommunications Research Laboratory, Hørsholm, Denmark, and [2]IBM Research Division, Zürich Research Laboratory, Rüschlikon, Switzerland

Io2 11.45-12.00 ***In situ* monitoring of III-V MBE growth processes using laser light scattering;**
G.W. Smith*, C.R. Whitehouse, J.L. Glasper, and D.J. Robbins, Royal Signals and Radar Establishment, Malvern, UK

Io3 12.00-12.15 ***In situ* control of epitaxial growth using reflectance difference;**
L. Samuelson*, J. Jönsson, and G. Paulsson, Department of Solid State Physics, University of Lund, Lund, Sweden

Io4 12.15-12.30 **Selective area n-type doping in MBE growth of GaAs using tin ions**
J.H. Thompson*[1], E.H. Linfield[1], D.A. Ritchie[1], G.A.C. Jones[1], J.E.F. Frost[1], A.C. Churchill[1], Q.W. Smith[2], D. Lee[2], M. Houlton[2], and C.R. Whitehouse[2], [1]Cavendish Laboratory, Cambridge, and [2]RSRE, Malvern, UK

Poster Summaries

Ip1 12.30-12.35 **283000 cm²/Vs mobility in GaAs grown by MBE using As_4**
R. Sivertsen and A. Paulsen, Norwegian Telecom Research Institute, Kjeller, Norway

Ip2 12.35-12.40 **Low-oxygen arsenic for AlGaAs MBE**
R.G.L. Barnes*[1] and A. Chew[2], [1]Johnson Matthey PLC, Royston, and [2]Institute of Surface Science and Technology, Loughborough University of Technology, Loughborough, UK

Ip3 12.40-12.45 **Surface stoichiometry variation in "atomic layer" molecular beam epitaxy of ~~GaAs~~ gallium arsinide;**
C. Deparis and J. Massies*, Laboratoire Physique du Solide et Energie Solaire, CNRS, Sophia Antipolis, France

Ip4 12.45-12.50 **MBE-overgrowth of patterned substrates by an $Al_{0.4}Ga_{0.6}As$-GaAs superlattice: Contours and defects analyzed by TEM**
K. Johannessen*[1], Y.X. Guo[2], B. Skurdal[2], and R. Høier[3], [1]ELAB-RUNIT, Trondheim, [2]Department of Physics, University of Trondheim NTH, Trondheim, and [3]SINTEF Applied Physics, Trondheim, Norway

Ip5 12.50-12.55 **Influence of growth temperature on MBE grown $Al_{0.48}In_{0.52}As$**
H. Künzel*, J. Böttcher, A. Hase, and C. Schramm, Heinrich-Hertz-Institut für Nachrichtentechnik Berlin GmbH, Berlin, Germany

(cont'd) → (9) → (10) → (11) → (12) → and (13) → Nonlinear optic in situ diagnostic of crystalline film.

Ip6 12.55-13.00 **Dependence of $Al_xGa_{1-x}As$ crystalline quality on surface reconstruction during growths in molecular beam epitaxy**
M.I. Etinberg, N.N. Faleev, G.A. Fokin, G. de la Kruz, V.E. Myachin, Y.V. Pogorelski*, I.Y. Rusanovich, and I.A. Sokolov, A.F. Ioffe Physico-technical Institute, Leningrad, USSR

Ip7 13.00-13.05 **Non-linear optic "in situ" diagnostic of a crystalline film in molecular beam epitaxy facilities**
V.F. Krasnov*, N.A. Kultchitsky, S.L. Musher, L.A. Osadchev, V.I. Prots, A.M. Rubenchik, V.E. Ryabchenko, and M.F. Stupak, Institute of Automation and Electrometry of Siberian Branch of USSR Academy of Science, Novosibirsk, USSR

13.05-14.00 Lunch

14.00-16.00 Discussion on
(a) Problems encountered in MBE and related growth methods, and
(b) Do we need EURO MBE CLUB?

16.00 Closing Remarks

Post-Deadline Papers

P1 **Resonant tunneling structures based on the GaAs/AlAs system**
A. Förster[1], H. Lüth, H. Brugger[2], and U. Meiners[2], [1]Institute für Schicht und Ionentechnik, Forschungszentrum Jülich, [2]Daimler Benz Forschungsinstitut, Germany

P2 **Doping of CdTe(100) on BaF_2/CaF_2 covered Si(100) for solar cell fabrication**
A.N. Tiwari, H. Zogg*, and S. Blunier, AFIF at Swiss Federal Institute of Technology, ETH-Hönggerberg, Zürich, Switzerland

P3 **Low temperature growth and IR-device fabrication with $Pb_{1-x}Sn_xSe/BaF_2$-CaF_2 on Si(111) substrates**
H. Zogg, S. Blunier, T. Hoshino, C. Maissen, and J. Masek,
AFIF at Swiss Federal Institute of Technology, ETH-Hönggerberg, Zürich, Switzerland

P4 **Observation of reflected-high-energy-electron diffraction oscillations during atomic layer epitaxy growth of CdTe**
W. Faschinger, P. Juza, and H. Sitter, Institut für Experimental physik, University of Linz, Austria

P5 **Deep level analysis of undoped $Ga_xIn_{1-x}P$/GaAs heterostructures grown by MOMBE and MOVPE**
E.C. Paloura[1], A. Ginoudi[2], G. Konstandinidis[2], and G. Kiriakidis[2], [1]Aristotle University of Thessaloniki, Thessaloniki, [2]FORTH-IESL, Heraklion, Greece

P6 **RHEED studies and the growth of high mobility indium phosphide by solid source MBE**
C.R. Stanley*, V.M. Airaksinen, R.H. Hutchins, and M. McElhinney, MBE Research Group, Department of Electronics and Electrical Engineering, University of Glasgow, Glasgow, U.K.

LOCAL GROWTH OF SILICON MBE LAYERS

W. Kiunke, E. Hammerl, and I. Eisele, Institut für Physik, Fakultät für Elektrotechnik, W-8014 Neubiberg, Germany
Tel.: 089/6004-3519
Fax: 089/6004-3560

The accurate control of growth parameters by MBE allows doping layers with nm thickness and thus multilayer systems become feasible. In such a 3 dimensional device the lateral as well as vertical transport can be studied if selective contacts to the layers are available. This can be achieved either by etching down to the individual layers, or by local growth of the layers. Because the control of etching processes for nm dimensions is very difficult, local epitaxy is a propriate alternative. For this reason we have investigated two ways of shadow masking: (1) a patterned BN plate is mechanically positioned in front of the silicon wafer, or (2) the substrate is pre-patterned by photolithographic processing in such a way that local epitaxy down to micrometer scale can be achieved.

Using different mechanical masks, vertical electronic devices with laterally structured delta-doping layers have been grown. The patterns have been designed in order to overlap only in the active regions. The contacts to the local deltas can then be formed by classical means. Several local n^+-Delta - p-n^+-Delta systems have been grown. The buffer, the intermediate, and the top layer are p doped and conventionally deposited over the whole substrat. Only the two n^+ Deltalayers with a thickness of 2-3 nm were grown as crossing stripes with a size of 1×7 mm. Ohmic contacts were prepared with alloyed aluminium at each end of local delta stripes. The active region has a size of approximately 1×1 mm. Secondary Ion Mass Spectrometry measurements have been carried out in order to verify the desired structure. Electrical transport measurements in the vertical MBE devices performed at 4.2 K will be reported.

A novel method for the mesa growth of silicon with lateral dimensions on a micrometer scale has also been investigated. Before the MBE pro-

cess, conventional photolithography has been applied to an oxide-nitride sandwich, deposited onto a silicon substrate, in order to obtain shadow masks with micrometer lateral dimensions. First the nitride layer on top is patterned, which defines the windows for the local MBE growth. After that the SiO_2 layer, which serves as a spacer between the substrate and the nitride layer, is selectively etched down to the substrate within these windows. The nitride cantilever, resulting from underetching, acts as a shadow mask for the molecular beam during the subsequent MBE process.

Scanning Electron Micrographs show the geometrical shape of the grown structures, whereas Electron Channeling Pattern and Transmission Electron Micrographs reveal high crystalline quality. To demonstrate the possible application of the growth mode for electronic device fabrication, unipolar and bipolar devices such as triangular barrier and p-i-n diodes have been prepared. The electrical device characteristics between 300 K and 4.2 K show that the device quality compares to that of mesa etched structures.

Doping during Growth and δ Doping

by Low Energy Implantation of As and Sb in Si MBE

H Charki (1), E. Gergam (1), G. Prudon (2), A. Vapaille (1)*
(1) Institut d'Electronique Fondamentale - URA 22 - Université de Paris Sud
Bat. 220 - 91405 Orsay Cedex (France) - Tel (33) 1 69417843 - Fax (33) 1 60192593
(2) Laboratoire de Physique de la Matière INSA - 69621 Villeurbanne Cedex (France)

Introduction - It has been shown (1) that the atomic size of a dopant relative to the matrix elements is the key parameter which determines wether or not a dopant exhibits surface accumulation behaviour during MBE growth. In Silicon MBE, N doping impurities commonly used (As and Sb) have an atomic radius much higher than silicon and are therefore strongly segregated. This drawback can be avoided if doping is made by low energy (100 - 1keV) implantation of As or Sb atoms which are deposited no longer on but under the surface of the epitaxial layer. This is the I2MBE method (Ion Implantation Molecular Beam Epitaxy) (2)(3)(4) whose potential advantages are : 1) incorporation probability near unity - 2) possibility of high doping level without degradation of the crystallographic quality of the layer - 3) steep doping profiles - 4) easy and continuous control of the doping level by measurement of the ion current - 5) good uniformity of the doping level over the whole wafer owing to XY sweeping of the ion beam.

In this paper we present results obtained on I2MBE layers doped with As or Sb either during growth (DDG layers) or during an interruption of the growth (δ doped layers)

Incorporation probability and electrical activity of the doping atoms - The table compares for As or Sb doped layers (DDG and δ) : 1) dopants concentration expected from implanted ions current measurement assuming a sticking coefficient equal to unity - 2) dopants concentration determined by SIMS - 3) carriers concentration deduced from Hall van der Pauw measurement. p_{inc} is the ratio of SIMS to expected dopants concentrations and represents then the incorporation probability. p_{elec} is the ratio of carrier to SIMS dopants concentrations and represents then the electrical activity.

Sample	Energy eV		$N_{exp.}$ cm^{-3}	N_{SIMS} cm^{-3}	p_{inc}	n_{Hall} cm^{-3}	p_{elec}
As29	1k		$4{,}2.10^{18}$	$4{,}4.10^{18}$	1	4.10^{18}	0,9
As34	1k		$3{,}2.10^{18}$	3.10^{18}	0,9	$3{,}2.10^{18}$	1
As36	1k		$2{,}1.10^{18}$	2.10^{18}	1	$2{,}2.10^{18}$	1
As44	500		2.10^{18}	$2{,}1.10^{18}$	1	$1{,}9.10^{18}$	1
As45	500		$1{,}9.10^{18}$	$1{,}8.10^{18}$	1	$1{,}9.10^{18}$	1
As27	500		$1{,}2.10^{19}$	$1{,}3.10^{19}$	1		
Sb4	1k		$8{,}5.10^{18}$	6.10^{18}	0,7	$6{,}4.10^{18}$	1
		duration	cm^{-2}	cm^{-2}		cm^{-2}	
δAs1	1k	2mn	$1{,}7.10^{13}$	$1{,}6.10^{13}$	0,9	$1{,}6.10^{13}$	1
δAs3	1k	10	$5{,}8.10^{13}$	$2{,}3.10^{13}$	0,4	$2{,}2.10^{13}$	1
δAs4	1k	10	$5{,}8.10^{13}$	3.10^{13}	0,5	3.10^{13}	1
δSb1	1k	2	$1{,}1.10^{13}$	$4{,}6.10^{12}$	0,4	$4{,}7.10^{12}$	1

For As DDG layers, it can be seen that p_{inc} and p_{elec} are in every cases nearly equal to unity. These results lead us to the following conclusions : at the growth

temperature (750°C) and even at low implantation energy (500eV) - 1) there is no exodiffusion nor segregation of the implanted atoms - 2) the As conversion from interstitial to substitutional sites has a kinetics faster than that of the layer growth - 3) doping level can be easily controlled by controling growth rate and ion current.

For Sb DDG, p_{inc} is slightly smaller than unity. Two facts can explain the difference observed between Sb and As : 1) atomic radius of Sb is larger than As therefore silicon lattice has a stronger tendency to reject the former - 2) for the same implantation energy, Sb projected range is smaller than As one, being nearer from the surface Sb atoms are more easily expelled. However Sb p_{elec} is equal to unity as for As : all Sb incorporated is in substitutional site.

For δ doping, p_{inc} is in every case found smaller than unity, moreover its value decreases for the same element with the dose (i.e. the growth interruption time) and between the two elements with the atomic radius. Interpretation of these behaviors could be that in the case of δ doping, the implanted dopants are not continuously buried by the silicon flux, then if the implantation time is long (high dose) they have time enough to exodiffuse. Here again this effect must be stronger for Sb than for As. In all cases studied p_{elec} is equal to unity. This is a superiority of I2MBE method for processing δ doped layers, indeed it has been shown that a large fraction of the dopants are electrically inactives in channels processed by SPE (5) (6).

Profiles Characterisation - I2MBE is potentially able to realize hyperabrupt doping profiles, the steepness being limited only by the dispersion on the penetration depth of the implanted doping ions which is in the range of 1 nm for the low energies used (10^2 eV). It is thus important to characterize this parameter on δ doped layers where profiles are expected steepest.

Figure 1 gives, for 1 keV As and Sb δ doped layers, SIMS profiles obtained with 5,5 keV O_2^+ primary ions. The FWHM (nm), the up and down slopes (nm/decade) of the profiles are specified on the figure. The values obtained are in good agrement with those reported by Zeindl (6), van Gorkum (5), Denhoff (4) for δ doped layers processed by SPE or I2MBE. Nevertheless these values are pessimistics, SIMS profiles being smeared by three effects : ion mixing. beam incorporation and surface roughness induced sputtering. As shown by N. L Mattey et al (8) these effects are function of the SIMS primary ions energy.

The asymetry of the profile has two origins : asymetry of the actual profile, which is non

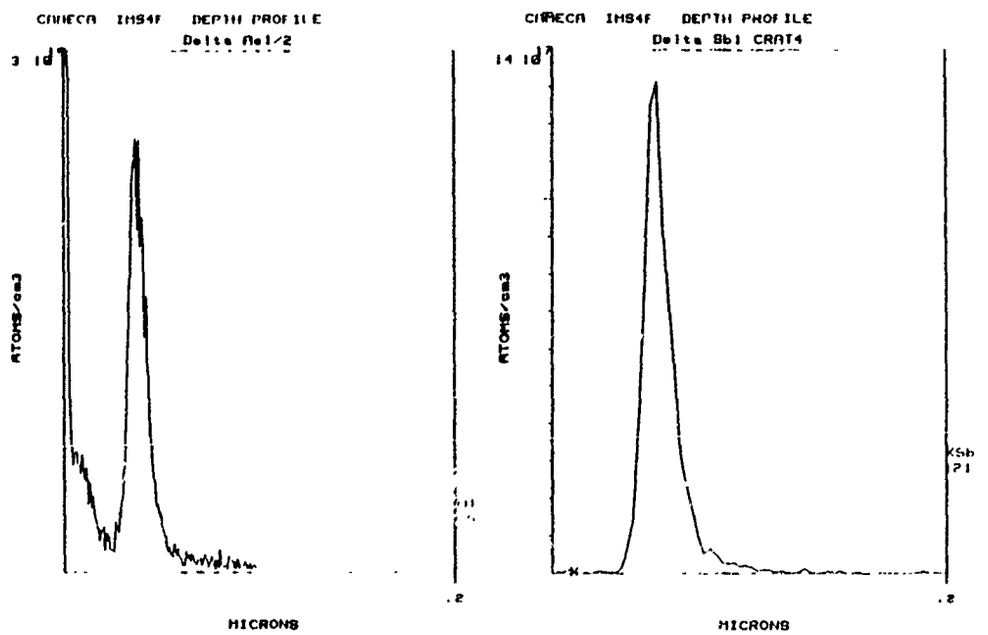

Fig 1 δ As : FWHM 9 nm - Upslope 4, Downslope 12 nm/decade
δ Sb : FWHM 12 nm - Upslope 9, Downslope 18 nm/decade

gaussian, and beam incorporation effect which gives an exponentially decreasing profile behind the delta.

δ As doped layers show As surface concentration peak on SIMS profiles. These peaks are also observed on non implanted layers processed with the ion source on, but the beam shutter closed. They are probably due to surface accumulation of neutral As after film deposition. However Hall measurements have shown that this "surface" As is electrically inactive. Note that no surface peaks are observed on δ Sb samples.

Doping profile can also be characterized by C(V) measurement, figure 2a gives the result obtained for a δ As doped layer : FWHM is 2nm. In fact C(V) profile is more representative of the free carrier profile - or of the spreading of the 2 DEG wave function (8) - than of the actual doping profile. Figure 2b compares doping and free carriers profiles, the former caculated by TRIM (9) the latter deduced from the first by resolution of Poisson equation. We see that free carrier profile is more spread but that FWHM are of the same order of magnitude for both. The experimental value of 2 nm is then probably representative of the actual thickness of the "doping plane".

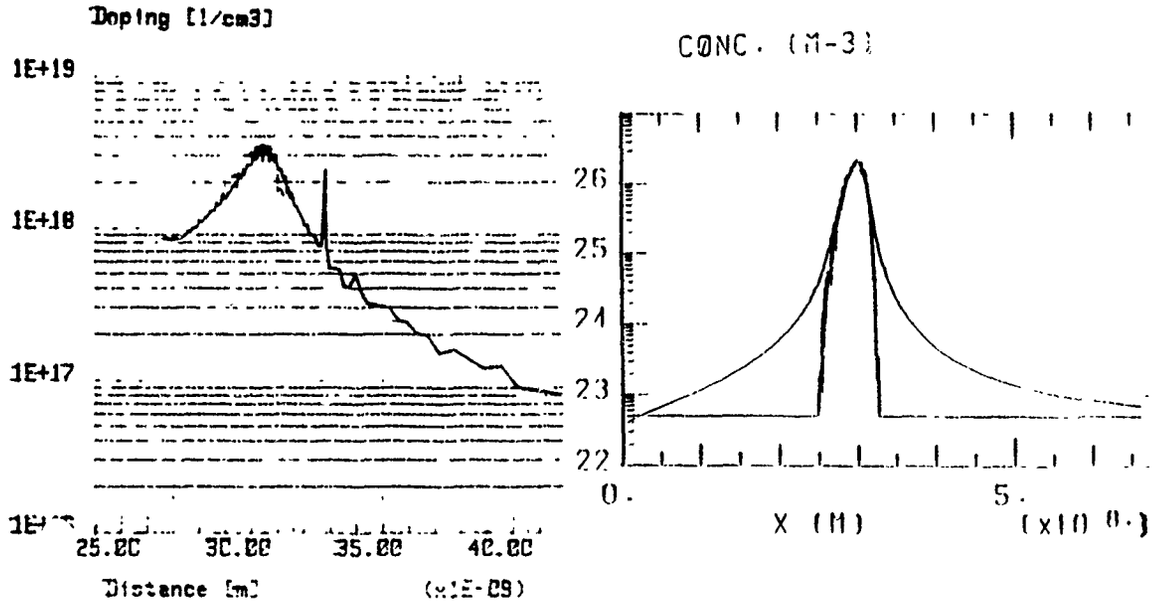

Fig 2 : δ As - (a) C(V) profile - (b) simulated doping profile and free carrier profile

Conclusion - I2MBE method improves incorporation of doping atoms in Silicon. Incorporation probability is better for DDG than for δ doping. Seen by SIMS δ As profiles are thinner than δ Sb profiles but residual doping is higher with As and a surface concentration peak is observed with As. FWHM of C(V) profile seems more representative of the actual thickness of the "doping plane" than FWHM of SIMS profile.

(1) G Pindora, RAA Kubiak, SM Newstead, DP Woodruff - Surf Sci 234 p17 (1990)
(2) Y Ota - J Electrochem Soc 126 (10) p1761 (1979)
(3) MA Hasan, J Knall, J Barnett, SA Rockett, JE Sundgren, JE Green - JVST B 5 (5) p1332 (1987)
(4) MW Denhoff, TE Jackman, JP Mac Caffrey - APL 54 (14) p 1332 (1989)
(5) AA Van Gorkum, K Nakagawa, Y Shiraki JAP 66 (6) p2485 (1989)
(6) HP Zeindl, T Wegenhaupt, J Eisele - Thin Solid Film 184 p21 (1990)
(7) NL Mattey, MG Dowsett, EHC Parker, TE Whall - APL 57 (16) p1648 (1990)
(8) EF Shubert, RF Kopf, JM Kuo, HS Luftmann, PA Grabinski - APL 57 (15) p497 (1990)
(9) JP Biersack, LG Haggmark - Nucl Inst and Methods 184 p 257 (1980)

Ao3

ELECTRICAL CHARACTERISATION OF SILICON: B DELTA-DOPED LAYERS

N.L. Mattey, P.J. Phillips, R.A.A. Kubiak
S.N. Newstead, E.H.C. Parker and T.E. Whall*.
Physics Department, University of Warwick,
Coventry, CV4 7AL, UK.

A. Wood and A O'Neill, Department of Electrical
and Electronic Engineering, University of
Newcastle, NE1 7RU, UK.

Delta-doped layers are attracting considerable interest for their possible application in FET devices and also provide a vehicle for studies of fundamental low dimensional phenomena.

Following our early work(1), delta-doped spikes of width 0.4nm as deduced by X-ray diffraction(2) and of sheet concentrations in the range $1x10^{12}$ to $4x10^{14}$ cm^{-2} have been grown in silicon by coevaporation of elemental boron at a growth temperature of 480°C. The dopant is fully activated up to the maximum sheet concentration, but the 4K mobilities are smaller than bulk values and "metallic" behaviour sets in at higher equivalent 3D concentrations than in the bulk. The widths of the CV profiles appear to be determined by the spatial extent of the wave function rather than the classical Debye length. Resistivity and Hall measurements down to 0.3K are used to demonstrate the 2D nature of the carrier gas.

References

(1) N.L. Mattey, M. Hopkinson, R.F. Houghton, D.S. McPhail, T.E. Whall and E.H.C. Parker, Thin Solid Films, 184, 177, (1990).

(2) A.R. Powell, N.L. Mattey, R.A.A. Kubiak, T.E. Whall and D.K. Bowen, Semicon. Sci. Technol, (1991).

Ap1

ELECTRICAL AND OPTICAL PROPERTIES OF THE Si-SiGe INTERFACE

J.C.Brighten, R.A.A.Kubiak, T.E.Whall and E.H.C.Parker*
Department of Physics
University of Warwick, Coventry, CV4 7AL, UK.

S.Gardelis, J.Rimmer and B.Hamilton
Dept of Pure and Applied Physics
University of Manchester Institute of Science and Technology,
PO Box 88, Manchester, M60 1QD, UK.

We have carried out fundamental measurements on the properties of the Si-SiGe interface; the systems measured are all fully strained single p-type epitaxial layers (Ge close to 5%) grown onto Si buffer layers using Molecular Beam Epitaxy. Although heterojunctions of this basic form are central to heterojunction bipolar technology, detailed information on the carrier distributions, local point defect and interface state densities, and on the role of the interface as a recombination plane are difficult to obtain.

We have used a novel approach to making C-V profiles of carrier densities and fixed charge assessment of this interface. We have further used the structure to make detailed DLTS measurements of deeply bound holes at or close to the interface.

We have further studied the photoluminescence behaviour of these structures, and have observed that large changes in the PL behaviour correlate with changes seen in the electrical data.

We therefore present in this paper, new data on the electronic properties of the interface and evidence that the interface plays an important role in carrier recombination and luminescence.

Ap2

MOLECULAR BEAM EPITAXY WITH SYNCHRONIZATION OF NUCLEATION

V. A. Markov, O. P. Pchelyakov, L. V. Sokolov, S. I. Stenin, S. Stoyanov*

Institute of Semiconductor Physics, Siberian Branch of the USSR Academy of Sciences Novosibirsk, 630090, USSR
Phone: 83832-354286 Fax:(83832)-357502

*Institute of Physical Chemistry, Bulgarian Academy of Sciences, Bulgaria

This paper deals with a new MBE technique based on the possibility to maintain undamping RHEED oscillations by periodic conditions giving rise for two dimensional nucleation which can be achieved by different means suitable for each particular case, for example by short duration increase of surface supersaturation or supercooling. This technique being named by the authors MBE with nucleation synchronization (MBE-NS) allows the growth of epistructures of any thickness with in situ control of their properties by RHEED or automatic ellipsometry. The new MBE technique can be applied both to elementally semiconductors and compounds like A_3B_5, A_2B_6 , etc.

The first test of MBE-NS was performed during Ge homoepitaxy. Two implementations of MBE-NS vere realized in experiments. A RHEED specular beam oscillation that was registered during Ge growth without any synchronization is shown in Fig. 1a and Fig. 2a. At the first method the nucleation synchronization was realized by periodical variation of the flux intensity (Fig. 1b). At the second method it was a periodical variation of the substrate temperature as a synchronizing influence (Fig. 2b). All these experiments were realized in a one-chamber home-made system supplied by RHEED and automatic ellipsometry [1].

1. A. V. Arkhipenko, Y. A. Blumkina, M. A. Lamin, O. P. Pchelyakov, L. V. Sokolov, S. I. Stenin, N. I. Kozlov, A. A. Kroshkov, Poverhnost, 1985, N1, P93.

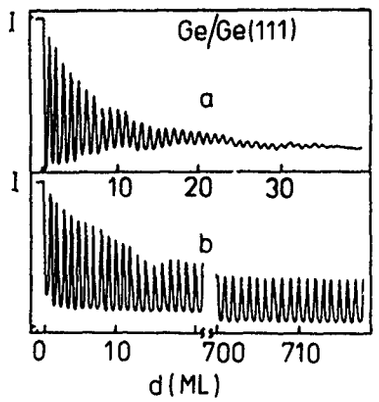

Fig. 1. A RHEED oscillation without any synchronization (a) and during MBE-NS (the first method) (b).

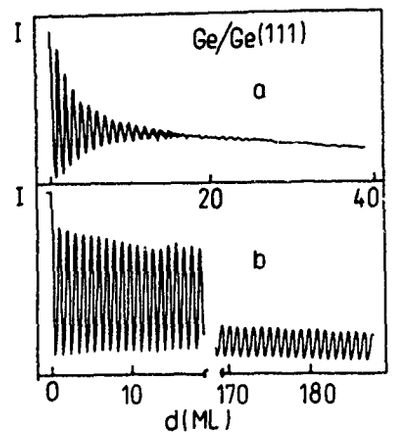

Fig. 2. A RHEED oscillation without any synchronization (a) and during MBE-NS (the second method) (b).

INFLUENCE OF THE SURFACE STRUCTURE ON THE Sb DOPING EFFICIENCY AT LOW-TEMPERATURE Si-MBE

A.I.Nikiforov, B.Z.Kanter and S.I.Stenin

Institute of Semiconductor Physics,
Academy of Science of the USSR, Siberian Branch,
pr. Lavrentjeva 13, 630090, Novosibirsk 90, USSR

An arbitrary doping profile with abrupt transitions has been produced by molecular-beam epitaxy (MBE) at low temperatures (600-800^{o}C) when thermal diffusion of the dopant atoms can be avoided. However, surface segregation may still be present at such temperatures, disturbing dopant profile, especially for the delta-doping layers. In [1,2] a decrease of the substrate temperature (T_s) up to 200-400^{o}C has been attempted, but there were no data about dopant distribution in the epitaxial layers. In the present work the Sb incorporation by measuring carrier profiles in Sb periodic doping structures and an influence of the surface structure on the dopant incorporation was investigated.

All samples have been grown in a non-commercial MBE system. Si and Sb beams were evaporated from an electron-beam evaporator and effusion cell respectively. The epitaxial layers were deposited onto (111) and (100) 60 millimeter diameter substrates. Silicon wafers were precleaned by chemical treatment and a protective oxide layer with a thickness of 1-1.5 nm was desorbed by a Si beam at 800^{o}C. Then an undoped Si buffer layer was grown at 700^{o}C. To obtain a dopant profile the spreading resistance method was used and samples were beveled by chemical etching.

The Sb doping during the homoepitaxial growth on Si(111) and Si(100) surfaces has been studied at temperatures of 300-600^{o}C for the growth rate V_g=0.3 nm s^{-1}. In Fig.1 the incorporation coefficient (K) and maximum concentration versus T_s are presented. High-temperature and low-temperature growth regimes

are observed, with a transition temperature for the (111) orientation is 500°C. Over the first range the exponential dependence of the Sb incorporation coefficient with the activation energy of 1.2 ± 0.2 eV takes place. The transition to the low-temperature regime is accompanied by the change of surface structure from Si(111)-7x7 to Si(111)-1x1 (7x7→1x1) and the transition temperature is determined only by V_g and doesn't depend on the Sb beam. In this regime the Sb incorporation coefficient tends to unity. The low-temperature doping regime is distinguished by the sharp decrease of Sb surface segregation.

The doping process for Si(100) is rather different from the one described for the Si(111). In this case the exponential increase of K within the investigated temperature range with activation energy of 1.43 ± 0.2 eV is observed. The transition to the low-temperature regime is assumed to take place at about T_S=250°C and be close to the lower limit for epitaxy for this growth rate.

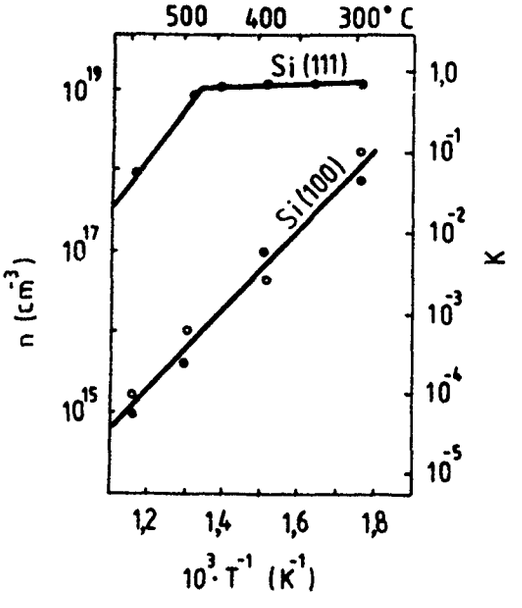

Fig.1.Sb maximum concentration and incorporation coefficient versus T_S.

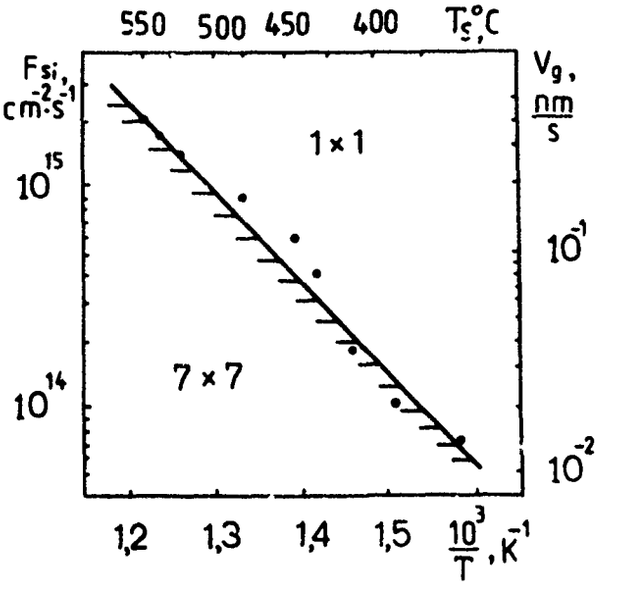

Fig.2. The dependence of transition temperature versus T_S.

As the transition to the low-temperature doping regime is accompanied by the structure change 7x7→1x1, the Si(111) surface structures during epitaxial growth are investigated at T_s=350-550°C and V_g=0.01-0.4 nm s^{-1} by reflection high energy electron diffraction. It is found that at silicon beams (F_{Si}) more some critical ones the phase transition 7x7→1x1 occur. There is region of T_s and F_{Si} where crushing of the Si(111)-7x7 superstructure by means of the silicon beam is occurred. Moreover, this transition has reversible character. Fig.2 shows the dependence of transition temperature versus F_{Si}. A transition activation energy have a value of 0.85 ± 0.2 eV. The shaded field represents the transition region. Over this region can be observed under definite condition the Si(111)-5x5 superstructure.

The impurity incorporation change and structure transition can be explained by the high density of Si adatoms on the growing surface during crushing of the Si(111)-7x7 superstructure [3]. From reflection electron microscopy data, the Si adatoms concentration reaches 0.2-0.3 of a monolayer at the transition 7x7→1x1. The low-temperature Si-MBE regime can be used to create complicated epitaxial structures with large concentration gradients.

1. K.Nakagawa, M.Miyao, and Y.Shiraki - Thin Solid Films, 1989, v.183, No. 1/2, p.315-322.
2. H.Jorke, H.Kibbel, F.Schaffler, A.Casel, H.-J. Herzog, and E.Kasper - Appl.Phys.Lett., 1989, v.54. No.9, p.819-821.
3. A.V.Latyshev, A.L.Assev, A.V.Krasilnikov, and S.I.Stenin - Surf.Sci., 1990, v.227,No.1, p.24-34.

Negative differential resistance in silicon epitaxial structure

*Suprunchik V.V., Dvurechenskii A.V., Demchuk D.L., Stepantsov Yu.P.
Institute of Semiconductor Physics, Academy of Sciences of the USSR, Novosibirsk
630090 Novosibirsk, Pr. Ac.Lawrenteva 13, USSR

The structures with blocked impurity band (BIB) is interesting for infrared photodetectors /1/. Theoretical calculation of the current-voltage (I-V) characteristics gives $I \sim \sqrt{V}$ law for this structure /2/.

We had observed negative differential resistance (NDR) in BIB structure with Si-molecular-beam-epitaxy (MBE) grown layer.

Epitaxial layer of 4.5 μm thick and acceptor content $\approx 6 \cdot 10^{14}$ cm^{-3} was grown at Si (111) substrate with boron content $\approx 1 \cdot 10^{17}$ cm^{-3}. Structural quality of the epitaxial layer was monitored with (7x7) reflection high energy electron diffraction (RHEED) patterns characteristic of Si (111) clean surface. By planar technology ohmic contacts were prepared in BIB-structure. Similar technology of contact preparation was used for samples without epitaxial layer. At (6÷60) K I-V characteristics were studied. We have found NDR at U = +0.5 V (on epitaxial layer) and saturation current area at U $\leq$ -0.2 V for epitaxial structure (Fig.1). Temperature dependence of carrier transport was investigated. I-V characteristics of sample without layer had near ohmic law at any investigated temperatures. Conductance has well known activation law with ε_1 and ε_3 energies for impurity activation and hopping conduction (Fig. 2). As was measured $\varepsilon_1 = 38$, $\varepsilon_3 = 6$ meV and $\varepsilon_1 = 31$, $\varepsilon_3 = 2$ meV for sample without and with epitaxial layer respectively. Also hopping conductance saturation was observed in epitaxial structure at (12÷20) K area (Fig.2). NDR and current saturation (see Fig.1) were appeared only at this temperature area. Epitaxial structure had near ohmic law at another temperatures.

The nature of the strong non-ohmic characteristic observed is discussed.

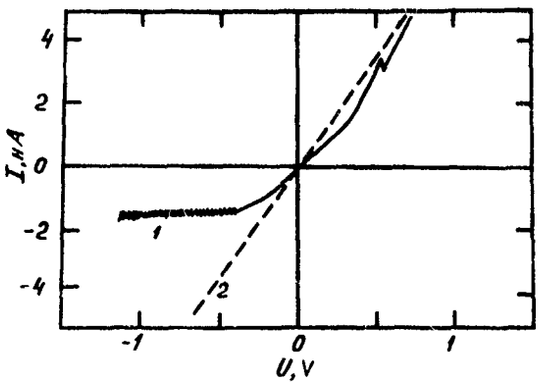

Fig.1. I-V characteristic for samples with (1) and without epitaxial layer (2). T = 15.0 K.

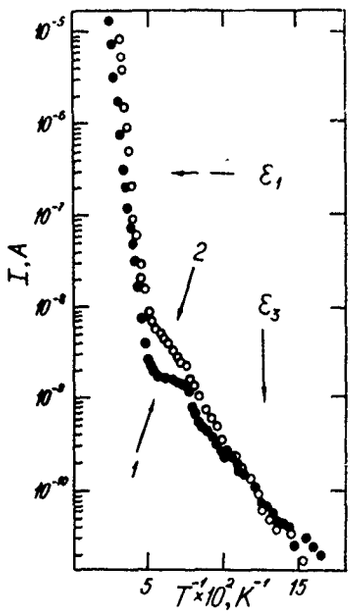

Fig.2. Ln I versus T^{-1} for samples with (1) and without epitaxial layer (2). U = -0.5 V.

/1/ Petroff M.D. and Stapelbroek, United States Patent No. 4 568 960 (1986)

/2/ Martin B.G. Sol.St.Electron. 33, 427 (1990)

Si SOLID PHASE EPITAXY ON Si-Sb AND Si-B SURFACE PHASES

A.V.ZOTOV and V.G.LIFSHITS
Institute of Automation and Control Processes,
USSR Academy of Sciences, Vladivostok 690032, USSR

1.INTRODUCTION

The delta-doped structures in which the dopant atoms are confined to a single atomic plane in semiconductor are of considerable scientific interest and finds application in a number of novel devices.

In the present paper, the main stages of the delta-doped structure fabrication in silicon have been considered, including formation of surface phases of antimony and boron atoms on the silicon surfaces and subsequent solid phase epitaxial (SPE) growth of silicon on the surface phases (SP's).

2.EXPERIMENTAL

The formation of surface phases and experiments on epitaxial growth were carried out in modified DEL-300 Riber ultrahigh-vacuum system. The vacuum chamber contains Si sublimation source and a Knudsen cell for deposition of antimony. LEED and AES facilities enable the monitoring of the crystalline structure and composition of the sample surface. The samples used were rectangular Si bars ($15\times5\times0.4$ mm^3) with (111) and (100) orientations.

3.FORMATION OF SURFACE PHASES

3.1.Si-Sb surface phases

The Si-Sb SP's were formed by deposition of antimony onto the Si(111) and Si(100) substrates held at 900K. During deposition, Sb coverage reaches the saturation value corresponding to the stable Si-Sb SP. LEED observations revealed that the stable Si-Sb SP formed on Si(111) substrate has $(\sqrt{3}\times\sqrt{3})$-R30° structure and the stable Si(100)-Sb SP is disordered . The saturated stable Sb coverage for both substrate orientations was found to be about 1 monolayer [1].

3.2.Si-B surface phases

The Si-B SP's were formed by annealing of highly B-doped Si samples at 1520 to 1620K [2]. The accumulation of boron at the sample surface occurs since the evaporation rate of B atoms from a silicon surface is considerably lower than that of Si atoms.Combined LEED-AES data revealed that the sample surface undergoes structural transformations during the surface accumulation of boron. The ($\sqrt{3}\times\sqrt{3}$) reconstruction was detected for the B-enriched Si(111) surface and disordered Si-B phase is formed on the Si(100) surface.

4.Si EPITAXY ON SURFACE PHASES

In order to avoid surface segregation of impurities and smearing of the concentration profile, the Si epitaxial films were grown by means of solid phase epitaxy [3]. Amorphous Si was deposited at a rate of 0.2nm/s. The pressure during deposition was below $5\cdot10^{-8}$Pa. The amorphous Si films were crystallized *in situ* at temperatures of epitaxial crystallization (conventionally, at about 900K).

4.1.Quality of epitaxial Si films

The structure of the grown Si films were characterized by LEED intensity measurements.The Si films grown on the disordered Si(100)-Sb SP exhibit good crystalline quality comparable to that of Si(100) substrate over the entire thickness range studied (20-80nm). The SPE Si films grown on the ordered Si(111)$\sqrt{3}\times\sqrt{3}$-Sb SP show considerable disorder. Such an anisotropy is consistent with the results for SPE growth of Si films on "pure" Si(100) and Si(111) substrates [3].

The similar results were obtained for epitaxial films grown on the Si-B SP's, i.e. Si films grown on Si(100)-B SP demonstrate good structural quality and Si films grown on the Si(111)$\sqrt{3}\times\sqrt{3}$-B SP show residual disorder similar to that in Si films grown on "pure" Si(111)7×7 surface.

4.2.Preservation of buried surface phases

Suppression of smearing of SP during subsequent epitaxial growth of Si is a key problem of the formation of buried SP. The possible smearing of sharp concentration

profile can occur both at the stage of amorphous Si film deposition and during the crystallization of amorphous film induced by annealing.

The AES observations of sample surface during initial stages of Si deposition onto the Si(100)-Sb SP revealed that at temperatures below 350K the decrease of Sb Auger peak (454eV) amplitude fits the equation $I=I_o exp(-d/\lambda \cdot cos\phi)$, where λ=0.83nm is the escape depth of 454eV Auger electrons and d is Si film thickness. This suggests the absence of Sb segregation.

The results obtained in Ref.[2] have shown that boron redistribution during SPE crystallization is determined solely by bulk diffusion in the already crystallized Si film. Thus, the diffusion smearing at the crystallization stage can be avoided, since annealing at about 870K for several minutes is sufficient for complete crystallization of Si film, while the diffusion length ($2\sqrt{Dt}$) of B and Sb in Si corresponding to such an annealing procedure is less than one interatomic distance.

4.CONCLUSIONS

The SPE growth of Si films on Si-Sb and Si-B surface phases has been studied by LEED and AES techniques. The SP's studied do not effect the SPE growth of Si films, and the structural quality of the grown Si films coincides with that of Si films grown on "pure" Si surfaces, i.e. Si films grown on (100) substrates exhibit good crystalline quality and Si films grown on (111) substrates are faulted. It has been shown that smearing of buried SP's in the growth direction can be avoided by the use of deposition of amorphous Si films at temperatures close to room temperature and "gentle" annealing at about 900K.

[1] A.V.Zotov, A.A.Saranin, V.G.Lifshits and E.A.Khramtsova, Surf.Sci. 230 (1990) L147.

[2] V.V.Korobtsov, V.G.Lifshits and A.V.Zotov, Surf.Sci.195 (1988) 466.

[3] A.V.Zotov and V.V.Korobtsov, J.Cryst.Growth 98 (1989) 519

AIXTRON

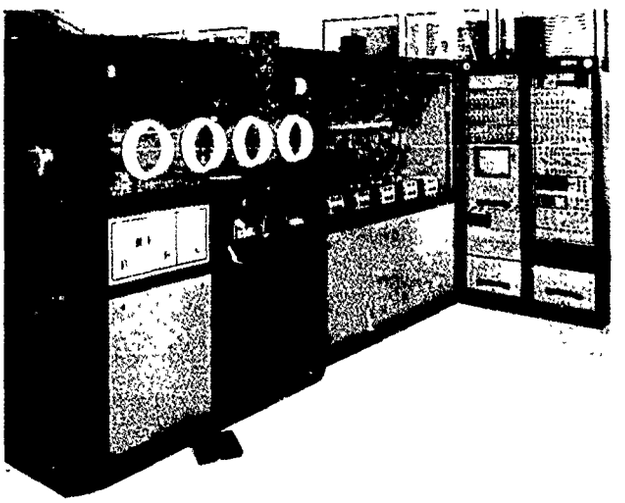

AIX 2000/2400

Multiwafer Planetary Reactor

AIXTRON's concepts
for advanced III-V production systems include

- Equipment
- Processes
- Technologies
- Training
- Support

AIXTRON: Committed to AIXcellence

AIXTRON GmbH
Kackertstr 15-17
D-5100 Aachen, FRG

Phone: + 49 (241) 89 09-0
Fax: + 49 (241) 89 09-40
Telex 8 329 908 aix d

US Sales and Service
AIXTRON Inc.
9150 S W Pioneer Court, Suite D1

Wilsonville, OR 97070 USA
Phone: (503) 682-45 64
Fax (503) 682-56 73

The R&D efforts for the AIX 2000 MOVPE reactor and processes are partly supported by the Commission of the European Communities under ESPRIT 5003 'PLANET'

Growth of (111) CdTe studied by RHEED and X-Ray Photoelectron Diffraction.

S. TATARENKO*(a), J. CIBERT (a), R. DUSZAK (a), K. SAMINADAYAR (b), C. DESHAYES (a).

(a) Laboratoire de Spectrométrie Physique, Université Joseph Fourier, CNRS, Grenoble, France.
(b) Centre d'Etudes Nucléaires, Grenoble.
Mailing adress: CENG, DRF/SPH/PSC, BP 85X, 38041 GRENOBLE, FRANCE.

We present an extensive study of (111)B CdTe growth, including investigations of the different stabilized surfaces. The CdTe surfaces are studied by RHEED and XPS while MBE growth is monitored by RHEED intensity oscillations.

First we present in figure 1 a phase diagram of the surface reconstructions as observed by RHEED. These surfaces are obtained by varying the Te fluxes up to 10^{-6} Torr and/or the substrate temperature. Several structures, namely (1x1), (2x2), (2√3x2√3)R 30° and C(8x4) are found.

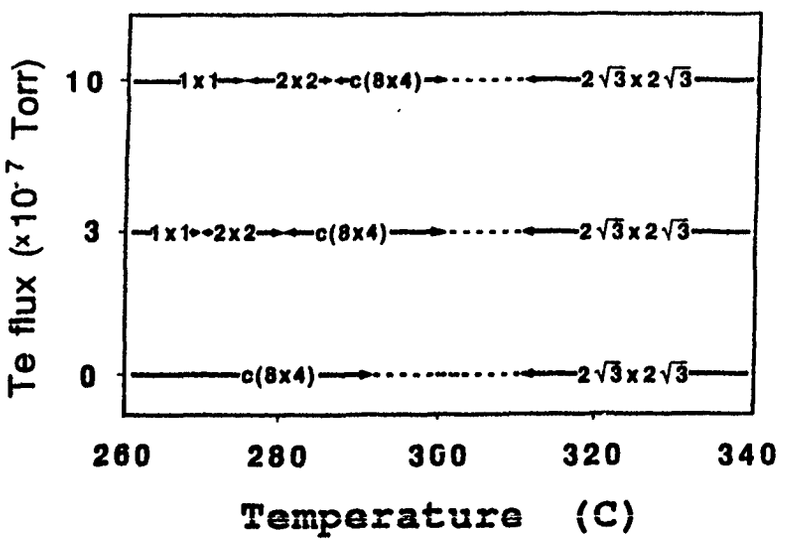

Figure 1

The (1x1) and (2x2) surfaces are observed in the lower temperature range. All transitions between adjacent structures are observed to be reversible, however it takes several minutes

for the transformation from the C(8x4) to the (2√3x2√3)R 30° to be completed as indicated by the dashed line.

We propose model for (111)B CdTe using a bilayer surface representation derived from the "hexagonal ring model" recently suggested for the (111)B GaAs surface. This model gives electrically neutral surfaces for each observed reconstruction. It is shown in figure 2.

Such a model is conforted for the (2√3x2√3)R30° surface by X-Ray Photoelectron Diffraction results. In these studies, in agreement with the model, a Cd surface state different from that of Cd bulk is observed. The surface geometry suggested by the model is pointed out. Moreover the directions of the Cd-Te surface bonds are found to be tilted by about 5° above the equivalent bulk axis (outwards relaxation).

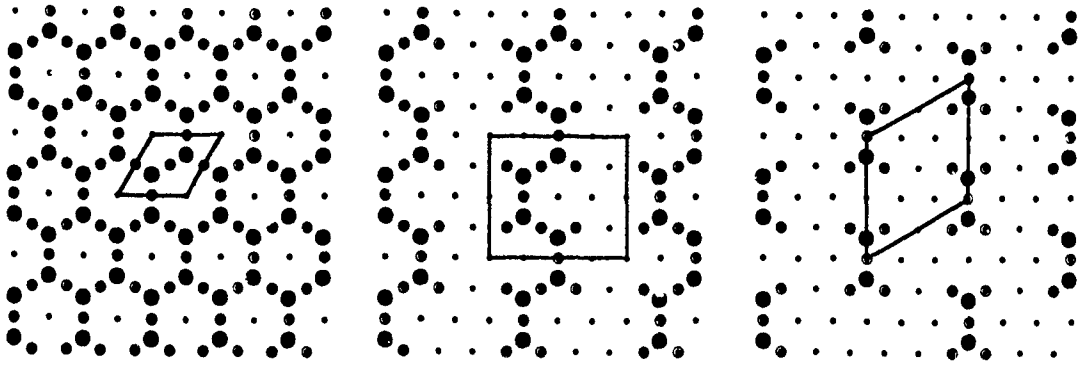

Figure 2

The variety of reconstructions which can be induced under different tellurium pressures and sample temperatures suggests that the MBE growth of (111) CdTe may be very sensitive to the initial conditions. In order to get a better insight into the growth mechanisms, a set of RHEED Intensity Oscillations was monitored when starting from the previous reconstructed surfaces. Some of the results are shown in figure 3.

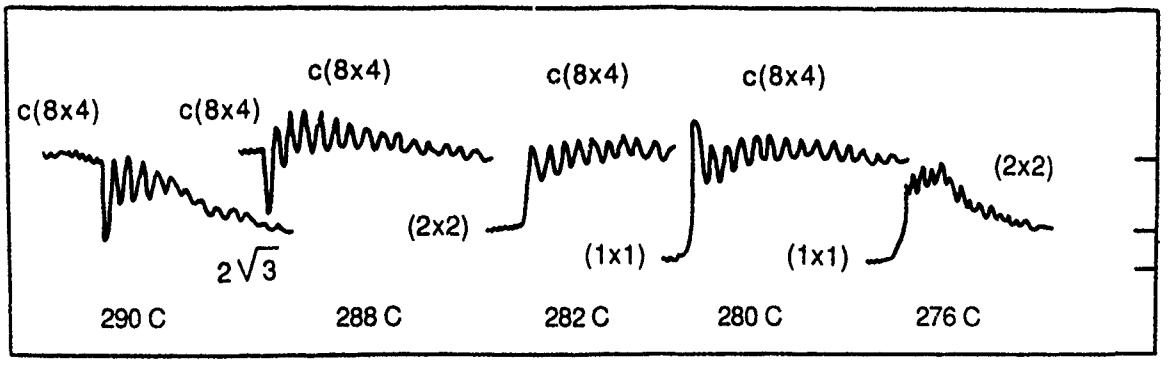

Figure 3

As seen in the figure there exists a strong correlation between the RHEED oscillations feature and the surface reconstruction observed before and during growth. A change in the mean level of the RHEED intensity is recorded when the surface reconstruction is modified. The most intense signal is obtained for the C(8x4) surface while the 2√3, (2x2), (1x1) surfaces give lower and lower levels (as indicated on the right side of the figure). Note that the levels recorded under static or growth conditions are the same.

Moreover an inversion in the initial phase of RHEED oscillations is seen in the figure when growth starts on the C(8x4) surface as compared the other ones. This can be interpreted in terms of reconstruction change when the CdTe cell is obtained : the intense and abrupt decrease of the signal observed for the C(8x4) could be associated to the formation of the (2x2) surface by completion of the CdTe chains proposed in the model. In the same way, when growth starts on the (2x2) surface the increase of the signal corresponds to the formation of the C(8x4) growing layer.

MBE GROWTH AND OPTICAL PROPERTIES OF $CdTe/Cd_{0,5}Hg_{0,5}Te$ HETEROSTRUCTURES

L. Ulmer * , E. Monterrat, N. Magnea ,
H. Mariette ^, P. Gentile, J.L. Pautrat

DRF / Service de Physique / Groupe Physique des Semiconducteurs
CEN- Grenoble, 85X, 38041 Grenoble Cedex
Tel : 76883499. Fax number : 885153
^Laboratoire de Spectrométrie Physique,
Université J. Fourier, Grenoble

The development of high quality CdTe / $Cd_XHg_{1-X}Te$ heterostructures for infrared detection or emission systems requires a tight control of layers thicknesses and interface smoothness. Today molecular beam epitaxy monitored by Reflexion High Energy Electron diffraction (RHEED) oscillations measurements appears as a powerful tool for growing such systems.

We have grown by MBE $Cd_XHg_{1-X}Te$ (CMT) based quantum wells and superlattices ($X \approx 0.5$) on (100) $Cd_{.96}Zn_{.04}Te$ substrates, at 180°C, using a constant level Hg cell, a CdTe cell and a Te cell. To maintain a Hg pressure over the sample, the Hg cell is always open, even during growth interruptions, and the surface exhibits the C(2X2) structure caracteristic of a cation rich surface. During the growth we observe intense RHEED oscillations, which show that the growth of Hg compounds takes place by a 2D layer by layer mode.

Moreover we can observe also RHEED oscillations, corresponding to HgTe (Te cell open) and to "CdTe"-meaning CdTe grown under Hg flux- (CdTe cell open). The three kinds of RHEED oscillations are shown in Figure 1. For each component one oscillation corresponds to the growth of one monolayer so the growth rates r are deduced and we verify that $r_{CMT} = r_{HgTe} + r_{"CdTe"}$. In principle the composition X in Cd can also be deduced : $X = r_{"CdTe"}/r_{CMT}$. But the characterization of thick layers by electron microprobe and infrared transmission shows that this formula is not correct because "CdTe" contains in fact an important amount of Hg, about 30%, depending on the growth parameters. Thus, even at temperatures as low as 180°C, the sticking coefficient of Cd, S_{Cd}, is far from unity -around 0.7- so "CdTe" is in fact

$Cd_{0.7}Hg_{0.3}Te$ and $X = S_{Cd} \cdot r_{"CdTe"}/r_{CMT}$. After this correction we verify that the RHEED oscillations measurements are in agreement with the chemical analysis.

This low value of S_{Cd} shows that the growth of CMT is highly dependent on surface kinetics phenomena. This is confirmed by the fact that for the same growth conditions, we find $S_{Cd} = 0.75$ for (100) misoriented substrats and $S_{Cd} = 0.94$ for (111) substrates. To obtain "CdTe" richer in Cd, the low value of S_{Cd} can be compensated by an additional flux of Cd, emitted by a Cd cell. Under these conditions, we reduce the incorporation of Hg in "CdTe" which falls from 30% to 5%.

The study of the structural quality of the layers is performed on 50 periods 80Å/90Å $Cd_{0.75}Hg_{0.25}Te/Cd_{0.48}Hg_{0.52}Te$ superlattices. The High Resolution Transmission Electronic Microscopy images reveal smooth interfaces and constant thicknesses for all periods. The regularity of the period is confirmed by the satellite peaks observed on X-ray diffraction rocking curves. This tight control of the layers thicknesses and composition is due to the very stable flux of the constant level Hg cell.

In order to study electronic properties of CMT heterostructures we have determined the calibration curve of the band gap Eg versus the concentration X in $Cd_XHg_{1-X}Te$ 4µm-thick layers in the domain of concentration of our wells and barriers (X between 0.4 and 0.8) shown in Figure 2. For each layer Eg and X are determined respectively by infrared transmission and electron microprobe.

The basic structure, designed for low temperature photoluminescence (PL), of our samples is a 4 µm thick buffer layer of CMT followed by $Cd_{Xb}Hg_{1-Xb}Te$ / CMT quantum wells, Xb= 0.7, or 0.95 with the additional Cd flux during the growth of the barriers. The buffer layer allows the determination of X_{Cd} (IR transmission, electronic microprobe and PL). The quantum wells have thicknesses between a few monolayers and 500Å. They provide strong luminescence with important quantum effects (Figure 3): the maximum of luminescence is shifted from 2.5 µm to 1 µm by decreasing the thickness of the wells, in good agreement with the calculations of the confinement energies.

These results show that CMT based heterostructures with high IR emission efficiency can be obtained by MBE. Moreover with variations of refractive index greater than 10% between barriers and wells,and barriers heights of about 0.8 eV for the electrons and 0.2 eV for the holes, these systems are very promising for the elaboration of infrared lasers.

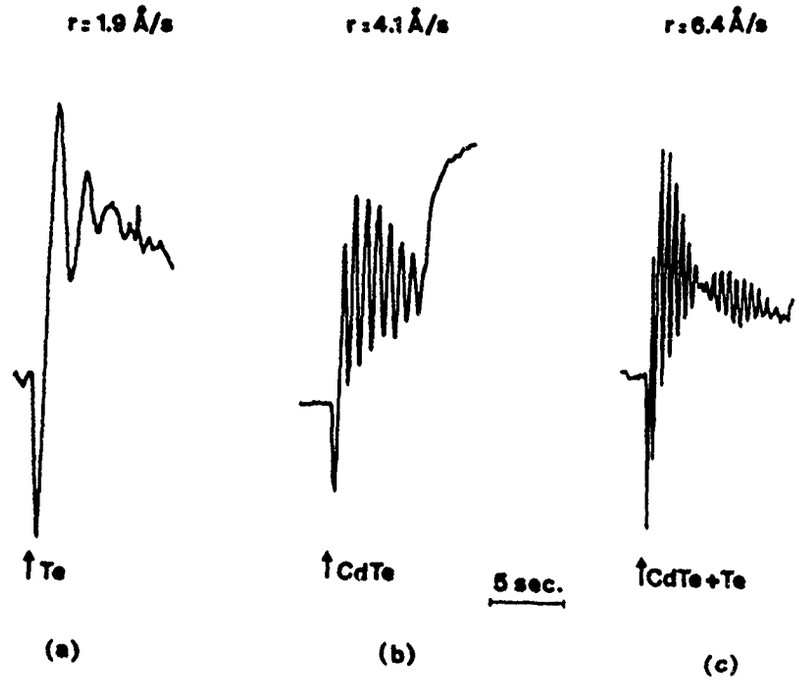

Figure 1 : RHEED oscillations at TS= 180°C for (a) HgTe (b) "CdTe" under Hg flux and (c) $Cd_{.45}Hg_{.55}Te$ growth. The Hg cell shutter is kept open during the growth and the interruptions.

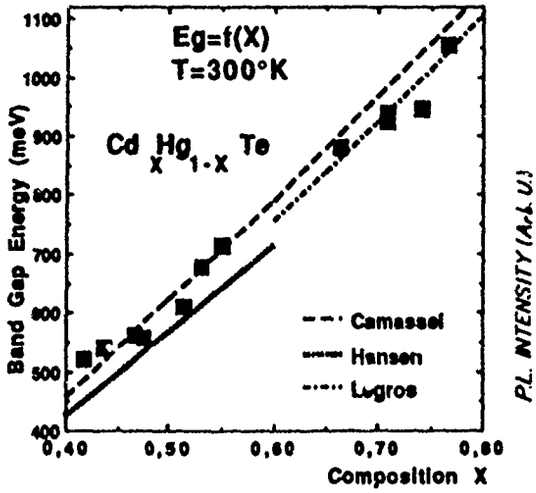

Figure 2 : Band Gap Energy (by IR transmission) versus composition X_{Cd} (by electronic microprobe) at 300°K. The curves correspond to data published by other authors.

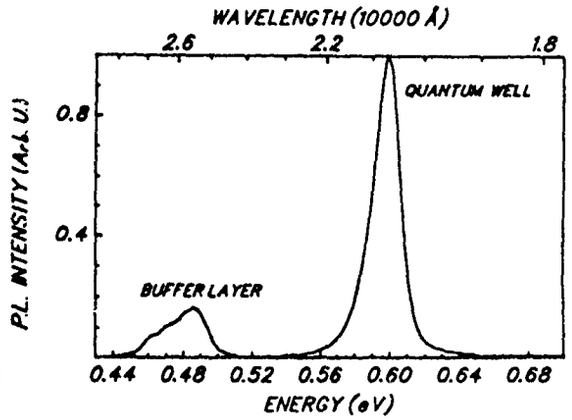

Figure 3 : Photoluminescence spectrum of a 4µm-thick buffer layer $Cd_{0.45}Hg_{0.55}Te$ followed by a 150 Å quantum well of same composition (X_{Cd}= 0.70 in the barriers).

N-TYPE DOPING OF MBE ZINC SELENIDE USING AN ELECTROCHEMICAL IODINE CELL

J. Simpson, J.M. Wallace, H. Stewart, S.J.A. Adams, K.A. Prior* and B.C. Cavenett
Department of Physics, Heriot-Watt University,
Riccarton, Edinburgh EH14 4AS, UK.
Phone: +44(0)31 451 3035
Fax: +44(0)31 451 3088/3136

1 Introduction

Recent results have shown that it is possible to grow n-type ZnSe by MBE and MOCVD with dopants from the group III or group VII elements. Gallium was originally used in MBE (1), but typically this material has low mobilities and carrier concentrations which saturate at $8x10^{17}$ cm^{-3}. A comparison of the effectiveness of group III and group VII dopants, including iodine, has been carried out in MOCVD (2,3) where it was noted that higher dopant activation was obtained for the group VII elements with carrier concentrations greater than $1x10^{19}$ cm^{-3}. More recently, the use of Cl as a dopant was demonstrated in MBE grown material by Ohkawa et al. (4) using $ZnCl_2$ but, as yet, there have been no reported attempts of doping MBE ZnSe with iodine. We present here our preliminary results of iodine doping of MBE ZnSe, using an electrochemical iodine cell.

2 Experimental

MBE ZnSe samples were grown in a Vacuum Generators MB288 system which has been described elsewhere (5). 6N sources of Zn and Se were used and undoped ZnSe layers could be grown which had residual carrier concentrations less than $1x10^{15}$ cm^{-3} . Photoluminescence spectra of undoped samples grown with less than the critical thickness for the generation of mismatch dislocations on GaAs (~1500Å), show only strain split free exciton emission, where the absence of donor bound exciton peaks is an indication of the quality of these layers.

The electrochemical iodine dopant cell was of a design similar to those used previously for the generation of chlorine (6), and was constructed by compressing AgI powder into a pellet of 5mm dia. and placing this in a heated ceramic tube. At temperatures greater than 147°C AgI shows high ionic conduction with a resistance of less than 1Ω for the pellet. Electrical contacts to the pellet were made with silver (cathode) and platinum gauze (anode). Typical currents for the generation of iodine during the growth of ZnSe were in the range 0.1 μA to 1 mA. At higher currents (100 mA) iodine could be detected on the mass spectrometer.

3 Results

The electrochemical iodine cell can be used to dope ZnSe over the full required doping range, to >$1x10^{19}$ cm^{-3}. The electrical carrier concentrations of these layers have been measured by Hall and by electrochemical CV profiling using a Biorad Polaron Plotter. Good agreement is obtained for the values from both techniques for uniformly doped samples. The measured values of carrier concentration as a function of cell current showed a linear behaviour over the entire region of interest up to $1x10^{19}$ cm^{-3}. For the first time CV profiling has been obtained showing that samples grown with a constant cell current are uniformly doped throughout the layer, with a small apparent dip at the interface with the GaAs interface. Details of the material etching conditions will be published elsewhere (7).

Photoluminescence spectra at 4K is dominated by the strain split donor bound excitonic peak at 2.7955 eV which has a half width of 2.8 meV for a carrier concentration of $1x10^{17}$ cm^{-3}, in good agreement with spectra published previously for the MOCVD material (3). At the higher concentrations, the excitonic features broaden and the spectra show typical characteristics of degenerate material and even at the very highest doping levels the spectral features associated with deep levels are observed only on x100 amplification.

One major benefit of the electrochemical cell is the ability to rapidly switch between doping levels, with a time constant of less than one second. This is very fast in comparison with the normal MBE technique which depends on the rate at which a Knudsen cell achieves thermal equilibrium. Hence we have used the iodine cell to grow a structure in which the carrier concentration was decreased in a series of steps as the sample was grown - a normal "staircase" structure. The CV profile shows that the transition between one level and the next is sharp, indicating that the changes in the cell flux are in fact occurring on a time period which is short compared with the time for the growth of one layer (~1s), and also that the iodine does not diffuse or surface segregate in the epilayer.

4 Conclusions

A solid state electrochemical cell has been shown to be a useful source of iodine, which is a good n-type dopant in MBE grown ZnSe. The quality of the material grown using this cell is comparable with that grown by conventional techniques. Electrochemical CV profiles have been obtained for n-type ZnSe for the first time and show the versatility of the iodine source.

5 References

1. T. Yao, J. Crystal Growth 72 (1985) 31

2. H. Kukimoto, in "Growth and Optical Properties of wide bandgap low dimensional semiconductors". Editors: T.C. McGill, C.M. Sotomayor Torres and W. Gebhardt, NATO ASI vol. 200, p119 (Plenum, New York, 1989)

3. A. Yoshikawa, H. Nomura, S. Yamaga and H. Kasai, J. Appl. Phys. 65 (1989) 1223

4. K. Ohkawa, T. Mitsuyu and O. Yamazaki, J. Appl. Phys. 62 (1987) 3216

5. K.A. Prior, J.M. Wallace, J.J. Hunter, S.J.A. Adams, M.J.L.S. Haines, M. Saoudi and B.C. Cavenett, J. Crystal Growth 101 (1990) 176

6. P.J. Goddard and R.M. Lambert, Surface Science 67 (1977) 180

7. F. Harran, K.A. Prior, J. Simpson, J.M. Wallace, H. Stewart and B.C. Cavenett, to be published.

GROWTH AND DOPING OF CdxHg(1-x)Te (111) IN MOLECULAR BEAM EPITAXY.

T.COLIN*, A. MILLION
LETI / Laboratoire Infrarouge
CENG - 85 X - 38041 GRENOBLE CEDEX - FRANCE
Phone : (33).76.88.59.15 - Fax : (33).76.88.51.67

MAIN CHARACTERISTICS OF CdxHg(1-x)Te

CdxHg(1-x)Te (CMT) is a semiconductor material well adapted for infrared optoelectronical applications since its direct bandgap varies almost linearly between the gap of HgTe (-0.116 eV at 300K) and the gap of CdTe (1.529 eV at 300K).Thus it allows to cover a large wavelength range from the near to the mid infrared.

CMT has been extensively studied since the 1950's and, in consideration of its interest for infrared detection, especially in the composition ranges corresponding to the atmospheric transmitting windows : 3-5 µm ($0.30<x<0.39$) and 8-12 µm ($0.20<x<0.24$).

It is only at the beginning of the 1980's that MBE has demonstrated its ability to grow CMT epitaxial layers. Then efforts focused:

first on the control of cristallinity of epitaxial layers

second on the control of compositions which is primordial because of the importance of dEg/dx in CMT (15,875 meV/%).

These aims attained it was possible to consider in-situ electrical doping and realisation of heterojonctions which are favoured by the low lattice mismatch between layers whatever the compositions are ($\Delta a/a$ max= $3\ 10^{-3}$).

GROWTH OF CMT EPITAXIAL LAYERS IN MBE

GROWTH PECULIARITIES

Which is typical of CMT growth is the importance of the equilibrium pressure, especially mercury partial pressure, over the material even at low temperatures. It obliges us, in order to prevent material decomposition, to maintain quite high mercury pressure over the epilayer during growth. This pressure is supplied by a special effusion cell.designed to allow at the same time constant mercury flux and high material consumption (several tens of grams per hour).

Fortunately epitaxial growth of CMT does not require high temperatures - it is the second typical aspect of CMT MBE growth - leading to employ reasonable Hg fluxes (BEP in the 10^{-3} Torr range)

SENSIBILITY OF CRYSTAL PERFECTION

TO THE SUBSTRATE TEMPERATURE

It has been extensively reported that CMT growth control was very difficult especially for the (111) orientation in peculiar because of twinning facility in II-VI materials Nevertheless we select this orientation

first because it is the only one for which quite large substrates of good cristallinity are abundantly available

second because it leads to better surface morphologies (no hillocks) than (100) which is of primordial importance for further technological steps.

But in that case the control of the substrate temperature is of major importance to obtain epilayers of good cristallinity. The evolution of RHEED patterns, crystal quality and surface morphology with temperature will illustrate the need of a stringent control of it.

For technological applications it is therefore imperative to achieve reproducibility and regulation of the substrate temperature at +/-1°C. All commonly used methods appear deficient in reaching such a level. We will present our approach which is compatible with the homogeneization of thicknesses and compositions by substrate rotation.

IN SITU DOPING OF CMT IN MBE

INTRINSIC DOPING

As-grown CMT epilayers present a residual p-type doping which is due to the mercury vacancies present in the material at growth temperatures (for x=0.3 p=1 10^{17} cm^{-3} for LPE layers grown at 475°C and p=1-2 10^{16} cm^{-3} for MBE layers grown at 200°C) The concentration of these vacancies is governed by thermodynamics with a quite rapid kinetics at growth temperatures and beyond. It allows therefore to control p-type doping by short annealings. For example CMT epilayers with x=0.41 doped as-grown at 1.3 10^{15} cm^{-3} (77K) reach 2.1 10^{16} cm^{-3} (77K) after in-situ post-growth annealing at 375°C.

EXTRINSIC DOPING

Principles of substitutional doping in CMT

The principle of substitutional doping is the same in CMT than in other semiconductors and allows to dope the material either n-type or p-type by substitution either on the sites II or on the sites VI. The following table resumes the most encountered situations with general remarks on the behavior of the dopants.

type	substitution on site II	substitution on site VI
n	elements of group III : B, Al, Ga, In element of group IV : Si	elements of group VII : F, Cl, Br, I
p	elements of groups I : Li, Na, K Cu, Ag, Au (fast diffusers)	elements of group V : P?, As, Sb (low efficiency in CMT elaborated in Te-rich conditions)

Electrical doping by Indium

Since as-grown epilayers present a p-type doping we focused, in order to realize in-situ jonctions, on the n-type doping. So we chose In which was one of the n-type dopants the most easier to employ in MBE conditions and was well known to be a slow diffuser in growth and technological conditions.

Experimental (growth and analysis)

CMT layers are doped during growth by means of a standard effusion cell. Dopant incorporation is studied by SIMS and electrical behavior determined by Hall effect.

Physical limitations

We encountered some physical limitations in the study of activation which are mainly:

the residual intrinsic p-type doping

the importance, in SIMS analysis, of the background of CdH molecules which have the same mass as In.

It restricts our analysis of activation to the range of doping above 3-5 $10^{16}.cm^{-3}$

Main results

The main results of our study are:

Incomplete activation of In

The doping efficiency of In is composition dependant and varies between 20% and 50%. It can be increased by anneal under Hg-rich conditions.

Absence of doping memory

No doping memory effect after runs of In doped layers has been observed by Hall Effect in the 10^{14}-$10^{15}cm^{-3}$ range.

Very low diffusion during growth and process

We verified that In does not diffuse during growth and that technological annealings do not alter significantly doping profiles.

REALISATION OF HETEROJONCTIONS

Since growth of CMT layers is well controlled especially in terms of variation of optimal growth temperature with composition and doping, it was so possible to realize heterojunctions. We have succeeded in such a way and we will present I(V) characteristics of MESA diodes realized from CMT heterojunctions.

CONCLUSION

We focused on control of growth parameters of (111) CMT layers whose growth is well known to be very critical but whose orientation is technologically the most interesting too.

Since as-grown layers are p-type we concentrate on n-type doping with Indium which acts as a quasi-ideal dopant in CMT layers.

Progress realized in these ways allows today the growth and the control of heterojunctions and devices whose electro-optical characteristics are very encouraging.

This work is supported by DRET (Ministry of Defense).

MBE GROWTH OF ZINC SELENIDE UNDER INTENSE UV LASER IRRADIATION

J. Simpson, S.J.A. Adams, J.M. Wallace, K.A. Prior* and B.C. Cavenett
Department of Physics, Heriot-Watt University,
Riccarton, Edinburgh EH14 4AS, UK.
Phone: +44(0)31 451 3035
Fax: +44(0)31 451 3088/3136

1 Introduction

Previous work by Matsumura et al. (1-3) on the growth of ZnSe under laser irradiation has shown that it is possible to reduce the growth temperature and the growth rate in areas illuminated by above band-gap radiation at 441.6 nm and 350 nm. However, Ohishi et al. (4) reported an enhancement of the growth rate using the He-Cd UV line at 325 nm. In this work, we present results for multiline UV irradiation from a krypton ion laser (337.5 - 356.4 nm) showing a decrease in the growth rate and almost complete suppression of the growth of ZnSe, together with modification of the material properties at high irradiances and growth temperatures.

2 Experimental

The MBE system has been described elsewhere (5). In this work, the sample was grown at substrate temperatures in the range of less than 100°C to 400°C, with part of the sample irradiated by UV nm) from a krypton laser. Irradiances up to 1W of UV were used, and the laser beam was allowed to expand to a 6mm diameter circle at the sample surface. Changes in the thickness of the grown layer were measured over the irradiated region using a Dektak profilometer. Photoluminescence measurements were obtained from the irradiated and unirradiated areas on each sample.

3 Results

A series of MBE samples has been grown with varying laser powers applied to the illuminated area, up to a maximum of 3.6 Wcm^{-2} at the sample. Typical growth conditions are: growth temperature T_S = 100 - 400°C, growth rate = 0.5μm hr^{-1} and Se/Zn flux ratio = 3:1.

At elevated temperatures (350 - 400°C) and the highest laser powers, deposition of zinc selenide was almost completely suppressed in the centre of the irradiated area, leaving a flat bottomed crater some 3-4 mm across with sloping sides. At high powers and temperatures as low as 100°C, the growth rate is severely reduced in the centre, but is still

finite, confirming that the desorption is a combined photo-thermal effect. The depth profile through the centre of the irradiated area is approximately gaussian with superimposed ripples corresponding to interference patterns from the laser optics.

The photoluminescence spectra from the unirradiated sections of the samples are typical for thick layers showing principally free and donor bound excitons but also the defect related emission referred to as Y_0 and I_V^0 lines (6). In the irradiated area Y_0 is very weak and I_V^0, believed to be related to a Se defect is absent implying that the laser irradiated material is of high quality in agreement with Fukada et al. (2).

It is believed that the action of laser irradiation is to cause the desorption of selenium during growth and so we have examined a series of samples with Se/Zn ratios up to 6:1. This paper will examine and discuss the kinetics of the reduction of growth rate due to laser irradiation with reference to current models (3).

4 References

1. N. Matsumura, T. Kukada, Y. Fukushima and J. Saraie, J. Crystal Growth 101 (1990) 61
2. T. Fukada, N. Matsumura, Y. Fukushima and J. Saraie, Jap. J. Appl. Phys. 29 (1990) L1585
3. N. Matsumura, T. Fukada, K. Senga, Y. Fukushima and J. Saraie, Proceedings of MBE VI, San Diego, 1990.
4. M. Ohishi, H. Saito, H. Okano and K. Ohmori, J. Crystal Growth 95 (1989) 538
5. K.A. Prior, J.M. Wallace, J.J. Hunter, S.J.A. Adams, M.J.L.S. Haines, M. Saoudi and B.C. Cavenett, J. Crystal Growth 101 (1990) 176
6. K. Shahzad, J. Petrazello, D.J. Olego, D.A. Cammack and J.M. Gaines, Appl. Phys. Lett. 57 (1990) 2452.

ASYMMETRIC AZIMUTH ANGLE DEPENDENCE OF X-RAY ROCKING CURVES IN N-ION IMPLANTED ZnSe

K.Imai*, M.Hovinen, E.Kuusisto, J.Lilja and M.Pessa

Department of Physics, Tampere University of Technology, P.O.Box 527, SF-33101 Tampere, Finland. Phone: 358-31-162 548, Fax: 358-31-162 600.

J.Keinonen

Accelerator Laboratory, Helsinki University, SF-00550 Helsinki, Finland. Phone: 358-0-708 4004, Fax: 358-0-708 4042.

ZnSe seems an attractive material to be utilized for blue-light-emitting devices. One of its disadvantages is the difficulty to obtain p-type conduction. Several investigations on p-type ZnSe, however, have been reported using Li, N or O as the acceptor impurities.

Despite the drawback that the crystal is damaged,[1] N ion implantation is a promising method to realize p-type ZnSe.[2] In this paper, we study N implanted, unannealed ZnSe, grown on GaAs by MBE. Cu$K\alpha$ X-ray rocking curves were measured as a function of azimuthal orientation, ϕ, about the growth direction. The full width at half maximum (FWHM) and the position of the diffraction peak for a ZnSe epilayer depend on ϕ, which suggested the presence of a particular interstitial N ion site in the lattice.

The N ions were implanted in the [100] direction of an undoped ZnSe layer of about 3 μm in thickness. The ZnSe layer was grown under usual conditions by MBE[3] on a semi-insulating GaAs (100) surface tilted by 2° towards the [1$\bar{1}$0] direction. The nitrogen isotope $^{15}N^+$ was implanted at an acceleration energy of 6.4 MeV. The dose density was 10^{14} cm^{-2}.

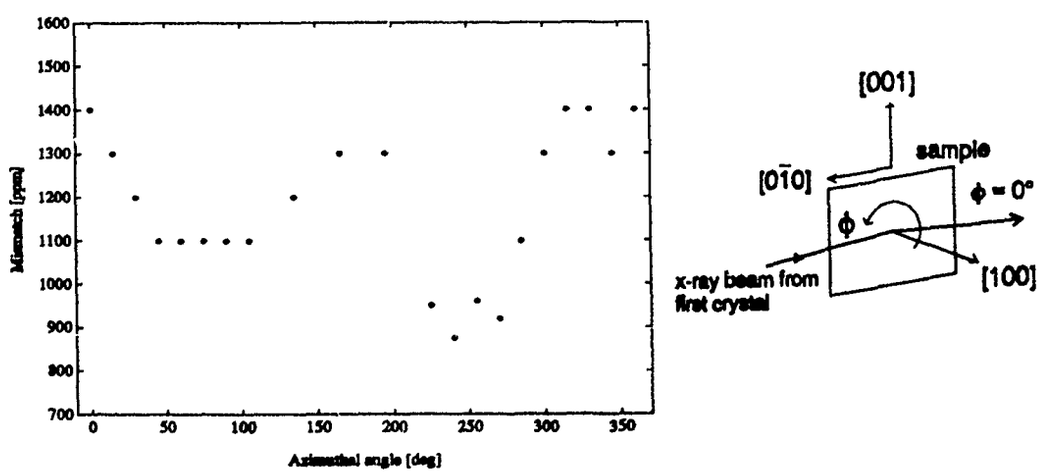

Fig.1 Dependence of lattice mismatch on ϕ.

We analyzed the ϕ dependences of the FWHM value and the lattice mismatch between the epilayer and substrate. The lattice mismatch was obtained from the difference of the (400) peak positions of the epilayer and the substrate. As shown in Fig.1, the lattice mismatch depends on ϕ with a period of π, in contrast to a 2π period of tilted epilayers. The maximum value is about 1400 ppm at $\phi = 0$, where the incident direction of X-ray beam is $[0\bar{1}0]$ of the crystal. At $\phi = 180°$, the mismatch value is about 1300 ppm. At $\phi = 90°$ and 270°, the values are about 1100 and 900 ppm, respectively. On the other hand, FWHM at $\phi = 270°$ is about 450 arc-sec, as shown in Fig.2. At 0°, 90° and 180° the FWHM remains almost constant at about 130 arc-sec. Fig.3 shows that the profile of the ZnSe peak at 270° is asymmetric.

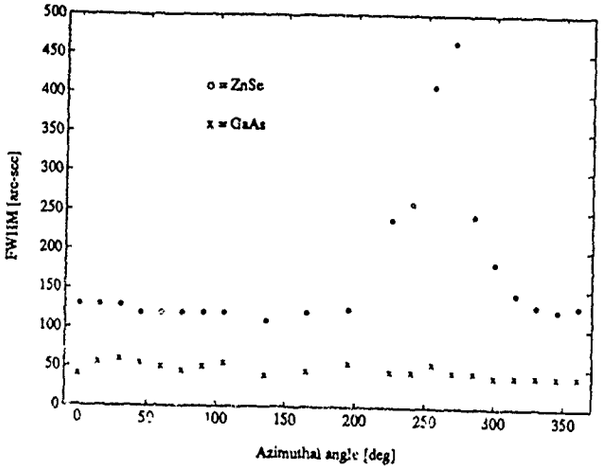

Fig.2 FWHM of ZnSe vs. ϕ.

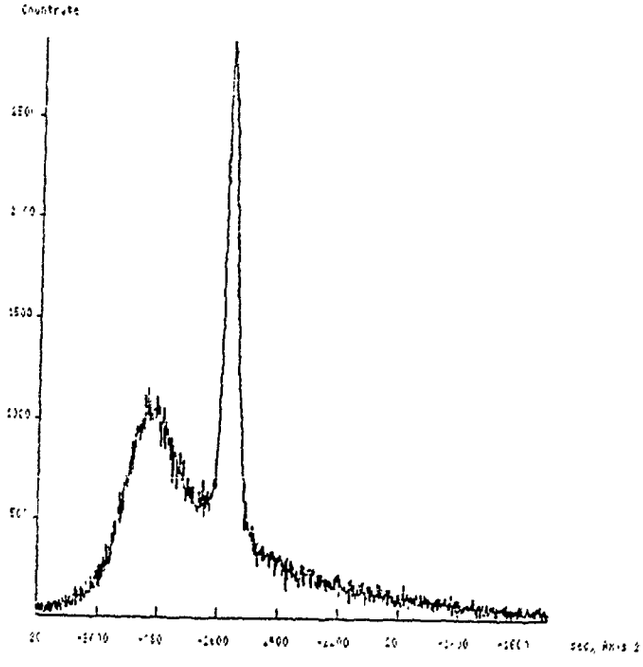

Fig.3 X-ray diffraction rocking curve at $\phi = 270°$.

The N ion implantation causes no effect on the X-ray diffraction profiles at $\phi = 0°$ and 180°. The lattice mismatch reduces at $\phi = 90°$ and 270°. An asymmetry of the profile appears at $\phi = 270°$. These observations suggest that the origin of the ϕ dependence is due to the growth mechanism on the tilted GaAs surface and an anisotropy of the ZnSe crystal. The [011] and [01$\bar{1}$] directions are not equivalent in this crystal structure.

In the case of strained epitaxial layers[4], it seems that the peak position of the epilayer in an X-ray rocking curve depends on ϕ due to an asymmetric density of dislocations along the [011] and [01$\bar{1}$] directions, resulting in the curve of Fig.1. Thus, as a speculation, one can examine a case in which the position of the implanted N atom is at ½,½,½ in the unit cell, i.e. surrounded by 4 Se atoms. The unit cell suffers tension along the [111], [$\bar{1}\bar{1}$1], [$\bar{1}$1$\bar{1}$] and [1$\bar{1}\bar{1}$] directions because of the coulomb interaction between N and Se atoms. Since the N atoms, implanted at an acceleration energy of 6.4 MeV, concentrate at a depth of about 2.2 μm from the ZnSe surface with a deviation of about 0.3 μm, the region most heavily doped is affected by the substrate orientation. Then we can assume that the atomic configuration in the (010) plane including the origin keeps its initial form, because the surface of the substrate tilts towards [1$\bar{1}$0]. Consequently, only the opposite (010) plane is stretched along the [101] direction as shown in Fig.4. It is suggested that this situation results in the observed ϕ dependence. Therefore, we propose that the implanted N atoms occupy the large interstitial site at the center of the unit cell. However, this state of affairs possibly only appears when using large implantation energies.

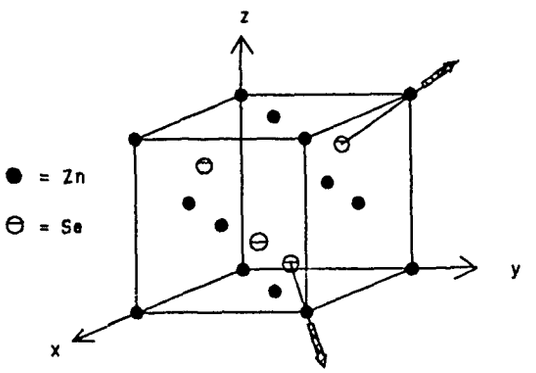

Fig.4 A schematic picture of the strain direction in ZnSe unit cell.

One of the authors (K.I.) acknowledges the Academy of Finland and the Ogasawara Foundation for the Promotion of Science & Engineering (Japan) for their financial support.

References

1) J.S.Vermaak and J.Petruzzello, J.Electronic Mater. **12** (1983) 29.

2) K.Akimoto, T.Miyajima and Y.Mori, Jpn.J.Appl.Phys. **28** (1989) L528.

3) J.Lilja, J.Keskinen, H.Asonen and M.Pessa, J.Cryst.Growth **95** (1989) 522.

4) M.Grundmann, U.Lienert, J.Christen, D.Bimberg, A.Fischer-Colbrie and J.N.Miller, J.Vac.Sci.Technol. **B8** (1990) 751.

DESIGN AND PERFORMANCE OF MULTIWAFER MBE SYSTEM USED IN HEMT PRODUCTION

H. Gotoh and Y. Higuchi
Mitsubishi Kasei Corporation
Research Centre
1000, Higashimamiana
Ushiku-shi, Ibaraki-ken
300-12 Japan
Telephone (81) 298 41-1134
Fax (81) 298 43-3716

V.J. Mifsud and D. Williams *
VG Semicon Limited
The Birches Industrial Estate
Imberhorne Lane
East Grinstead, West Sussex
RH19 1XZ, England
Telephone (44) 342 325011
Fax (44) 342 315800

1. **Introduction** VG Semicon's Model V100 multiwafer MBE system has been installed in Mitsubishi Kasei for a period of twelve months. It has been employed on a continuous production basis for HEMT fabrication. In this paper the design concepts of the V100 system will be described and the achieved results reported.

2. **Design Concepts** The V100 MBE system is designed to maximise throughput and device yield for GaAs/AlGaAs epi-layer device fabrication. It is configured to evaporate simultaneously onto either three 4 inch, or four 3 inch samples. Sample handling is fully automatic and load/unload times are minimised. This ensures that the principal determining factor in throughput is the deposition time.

3. **Installation** The system is installed in a class 1000 production facility with a local area enclosing all sample handling of better than class 10. Two full-time operatives run the system consecutively on a two 8-hour shift basis. These operatives are high-school educated and have received a 2 month MBE training programme. Supervision is by a MBE-experienced scientist, who also does the preliminary layer calibration and analysis.

4. **Throughput** The HEMT structures were grown on Mitsubishi Kasei supplied fabrication-ready wafers. These wafers do not require any in-vacuum outgassing prior to oxide removal in the deposition chamber. Initially the system was operated using 3x3 inch plattens and 6 growths per 18 hour day (ie. eighteen 3 inch wafers). Using the 4x3 inch (or 3x4 inch) capability, automatic pre-calibration and system set-up, this could be increased to 12 growths per day (forty eight 3 inch wafers or thirty six 4 inch wafers).

Multiple large capacity sources allow extended growth periods prior to source-reloading (typically 60 working days on an 18 hour double-shift basis). After air exposure, a 48 hour system bakeout is followed by a 24 hour component and source outgassing period. This is immediately followed by beam calibration, and three preliminary layer-calibration test runs. The first two growths are undoped GaAs. By the second growth, the GaAs material is weak p-type ($1 \times 10^{14} cm^{-3}$) with a room temperature mobility of $300 cm^2 (Vs)^{-1}$. The third run is 2 DEG structure with a 77K sheet carrier density of $(7-9) \times 10^{11} cm^{-2}$ and a corresponding mobility of $(8-10) \times 10^4 cm^2 (Vs)^{-1}$ (see fig 1). After achieving these values, the system is then operated for continuous HEMT fabrication. In this mode the throughput target of 500 4 inch wafers per month can readily be achieved.

5. Uniformities Thickness uniformities measured by stylus profilometer, SEM and CV profiling indicated values of better than $\pm 1\%$ over all wafers for all except the last 5mm edge of the sample (fig 2). Carrier density uniformities measured using CV are better than the measurement error (2-3%). Sheet resistivity measurements indicate uniformities of $\pm 1\%$ (fig 3). The AlGaAs alloy compositional uniformities have been measured by photoluminescence and photovoltage spectroscope measurements, and are less than $\pm 1\%$ (fig 4). All these uniformities are consistent from sample to sample and from run-to-run. To achieve these levels of reproducibility the Ga cell is calibrated using an ionisation gauge on a daily basis. Sheet carrier concentration and Hall mobility measurements have uniformities within 2% at 300K and 5% at 77K.

6. Devices The material is used for DBS (Direct Broadcast via Satellite) applications where the achieved noise specification is better than 0.6 dB at 12 GHz. The material has been supplied to different customers using independent device processing lines where yields are several thousand (3-5) HEMT's per 3 inch wafer.

7. Conclusion The V100 multiwafer MBE system has proven capability of satisfying the high-throughput (500 wafers/month) and high yield requirement for HEMT DBS device fabrication.

Fig.1 Layer Calibration Results.

1. Undoped GaAs

type: weak p

c.c.: $1 \times 10^{14}/cm^3$

μ: 300cm /V•s

2. 2 DEG Mobility

n_s: $9 \times 10^{11}/cm^2$

μ: $1 \times 10^5 cm^2/V \cdot s$ (at 77K)

un - GaAs	100Å
n - $Al_{0.3}Ga_{0.7}As$	c.c. 1E18 800Å
un - $Al_{0.3}Ga_{0.7}As$	60Å
un - GaAs	5000Å
sub.	

2 DEG Structure

Fig.2 Film Thickness.

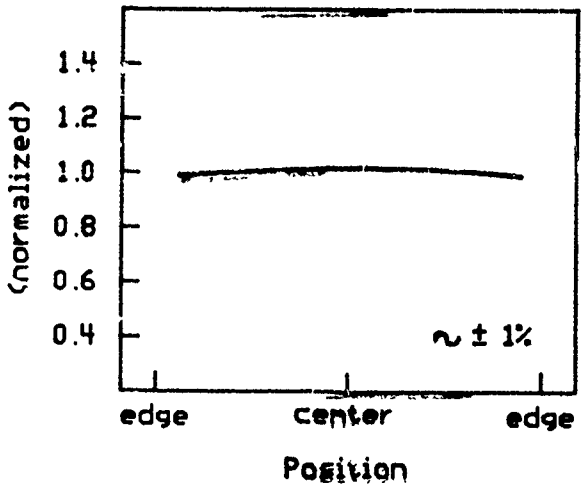

Fig.3 Carrier Concentration (Si doped)

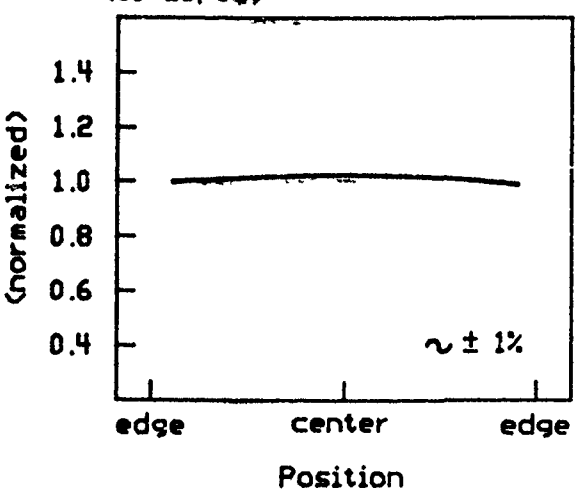

Fig.4 Al Content.

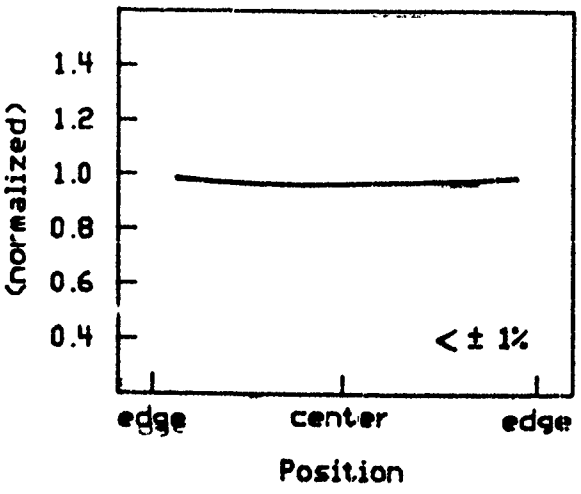

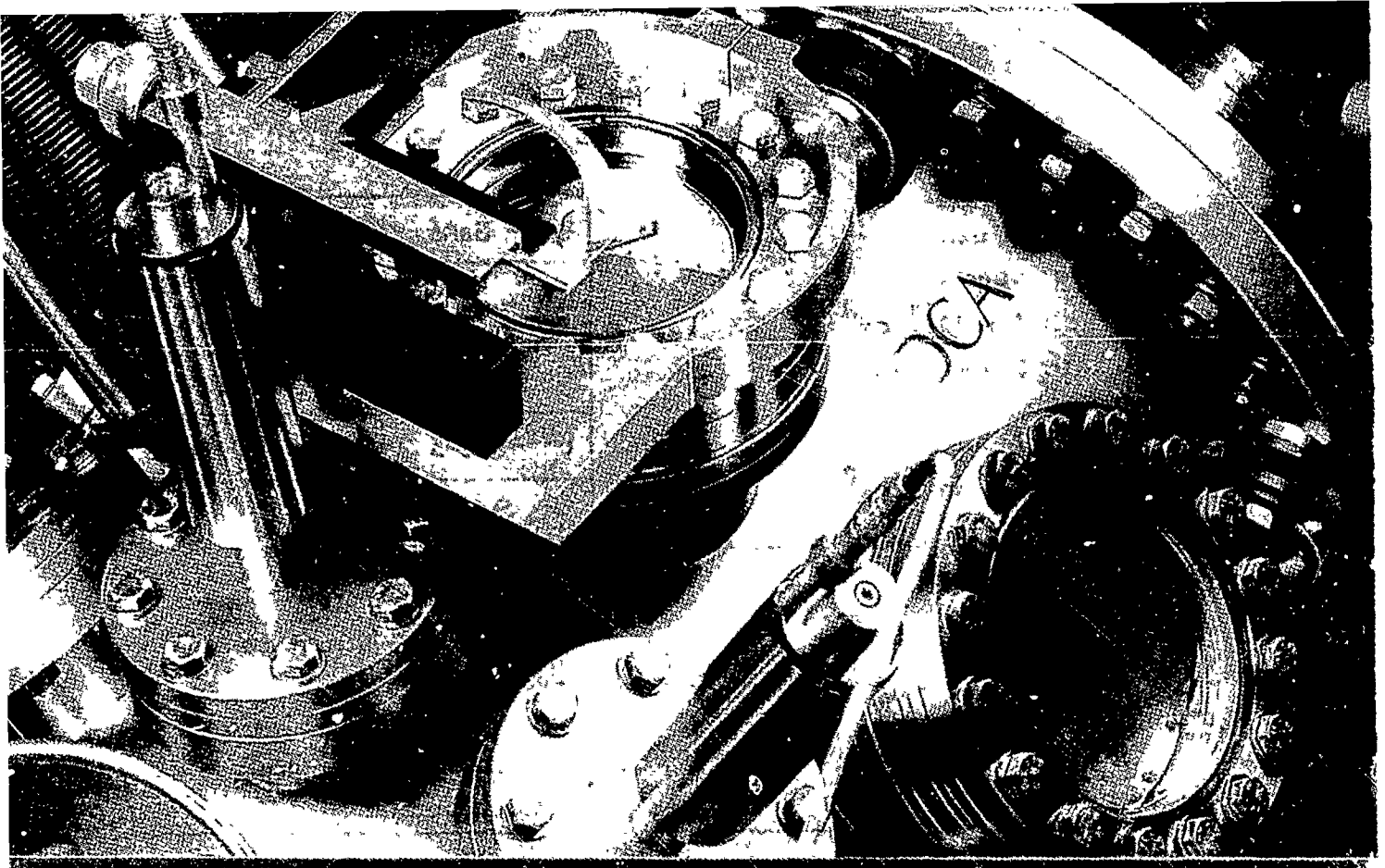

Introducing DCA 350 MBE System

The DCA 350 Molecular Beam Epitaxy System is a new modular MBE system suited mainly for research work and small scale production. The basic system consists of deposition chamber, buffer/preparation chamber and loading module. The deposition chamber is designed for 8 effusion cells and it is equipped with all necessary components for highest quality of epitaxial growth. The buffer/preparation chamber is a true UHV buffer zone

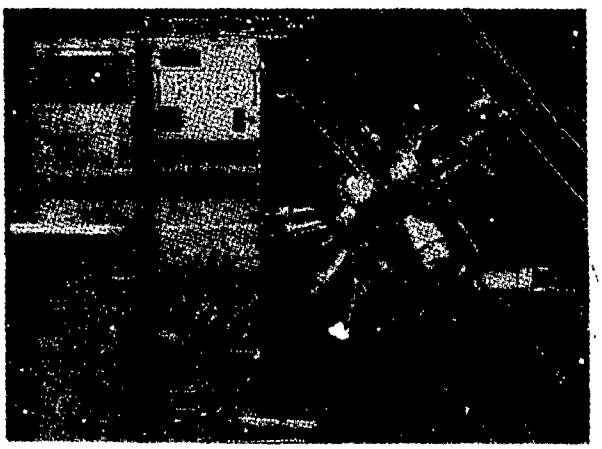

and it has ports for metallization and analytical facilities.

The DCA 350 System allows a total of 8 substrates to be loaded into a loading module and also to be outgassed at the same time. During substrate transport and epitaxial growth substrates are always facing down in order to keep the growth surface free from particles and falling deposits. The deposition chamber system can be installed easily to existing UHV-stations.

FEATURES

GUARANTEED $< 5 \cdot 10^{-11}$ TORR IN THE DEPOSITION CHAMBER • GUARANTEED $< 5 \cdot 10^{-11}$ TORR IN THE BUFFER/PREPARATION CHAMBER • GUARANTEED EPITAXIAL FILM QUALITY • ULTRA CLEAN SOURCES (EFFUSION CELLS, CRACKER CELLS, HYDRIDE CRACKERS, ORGANOMETALLIC SOURCES AND Hg-SOURCES) • FAST-ACTION LINEAR SHUTTERS WITH MICROPROSESSOR CONTROLLED SOFT-MODE OPERATION • CONTAMINATION PROTECTED LINEAR SHUTTER SHAFT MECHANISM WITH ELECTRO-MAGNETIC DRIVE • SUBSTRATE MANIPULATOR WITH CONTAMINATION FREE UNGEARED ROTATION • HIGH TEMPERATURE UNIFORMITY WITH PBN/PG/PBN HEATER ELEMENT • PROVEN SYSTEM DESIGN WITH RELIABLE AND EASY-TO-OPERATE SUBSTRATE TRANSFER • COMPUTER CONTROL OF LINEAR SHUTTERS, TEMPERATURE CONTROLLERS, RGA AND VACUUM GAUGES • UNIQUE CELL LOADING SYSTEM WITH SOURCE MATERIAL DEGASSING WITHOUT CONTAMINATING DEPOSITION CHAMBER OR EFFUSION CELLS • FULLY EXTENDIBLE WITH AUXILIARY PROCESS AND ANALYTICAL INSTRUMENTATION CHAMBERS

ULTRA HIGH VACUUM TECHNOLOGY FOR RESEARCH AND INDUSTRY

DCA Instruments

Address P O Box 111, SF-20521 Turku, Finland, Telephone +358-21-328 131, telefax +358-21-517 220, telex 62004 turku sf

Co2

Indium-free mounting technique retrofit to a 2 inch In bonded wafer substrate holder

Denis Martin,* François Morier-Genoud, F.K. Reinhart.
Institut de Micro et optoélectronique
Ecole Polytechnique Fédérale de Lausanne
CH 1015 Lausanne
Fax: 0041 21 693 44 44, Phone: 0041 693 44 63

Introduction

In-free mounting technique is widly use in new MBE machines. However earlier systems do not have this capability nor does the supplier provide the parts to retrofit these machines with an In-free mounting technique.

Mars and Miller (1) described a solution to change the In-bonded wafer substrate holders into fully In-free mounts by modification of the substrate holder. This solution gives good temperature uniformities when using growth temperature of 600°C and Cr-O doped GaAs wafers. Poor uniformity results with Si doped wafers and for temperatures near or over 700°C, which are needed for obtaining good AlGaAs layers.

In this work 2-inch Si doped GaAs wafers are mounted on a special set-up that consists of various 1mm thick Al2O3 diffusers.Temperature uniformities better than 5°C in the 600°C and 700°C substrate temperature regions are achieved.

Experimental.

A Varian 360 modified for 2 inch wafers is used for this work. The heating station is composed of a square array of four small spiral filaments, 1 cm in diameter with centers located on a 1.5 cm radius circle. The original molybdenum block is opened to allow 51 mm diameter Al2O3 diffusers to be placed as transparent medium over the heating filaments. Each diffuser has one rough surface.

From all the different set ups used in this experiment, three of them are presented in Fig.1. A,D and E. Set ups B and C, not shown,are similar to set up A, but with 2 and 3 Al2O3 diffusers respectively. For each set-up the growth of GaAs layers is undertaken at a substrate temperature between 600°C and 700°C. Temperature variations across the wafer are monitored by an infrared pyrometer IRCON modline-plus V with a spectral response between 0,91-0,97 μm. The probing diameter at the substrate surface was 13 mm.

Results

For the first set up used, type A , the temperature gradient is calculated from the thickness variation due to Ga re-evaporation during the growth of multiquantum well structures grown at 680°C. A gradient of more than 25°C is obtained between the center of the wafer and the position over the filaments.(see Fig. 2, solid dots). By increasing the number of roughened Al2O3 diffuser interfaces as in set up D (see Fig. 2, squares),the temperature gradient is reduced to less than 5°C at the growth temperature of 740°C. However looking through the pyrometer viewport, a 5 mm wide zone shows a color difference at the edge of the wafer indicating a larger temperature gradient near the molybdenum retaining block. A pyrolitic boron nitride (PBN) wafer is used in the set up E, to exploit the anisotropic thermal conductivity (20:1) of PBN (see Fig. 2, crosses). The temperature variation is more than 10°C at 705°C, but the shape of the gradient changed. The hot area over the filaments, found in the previous set ups vanishes,but important heat losses near the edge of the wafer are still observed. A set up similair to D is then used to grow a SQW-GRINSCH laser structure (2).The substrat temperature is maintained at 720°C for the cladding layers and lowered to 680°C during the growth of the graded index layer and the 7.5 nm quantum well. Broad area lasers fabricated with this structure showed threshold currents as low as 200 A/cm^2. This result confirmed the good quality of the layers grown with this In-free modified substrat holder.

Conclusion.

With simple modifications, we showed that In-bonded wafer holders of earlier 2 inch MBE Varian systems can be converted into fully In-free holders capable of operating at temperatures as hight as 740°C with temperature variations less than 5°C inside a diameter of 4 cm.

(1) D.E.Mars, J.N.Miller, J.Vac.Sci.Technol.B4(2), 1986

(2) S.Cao, C.Wüthrich, C.A.Berseth, J.D.Ganière, D.Martin, F.Morier-Genoud, F.K.Reinhart, Helv.phys.Acta 63, 837-838, 1990

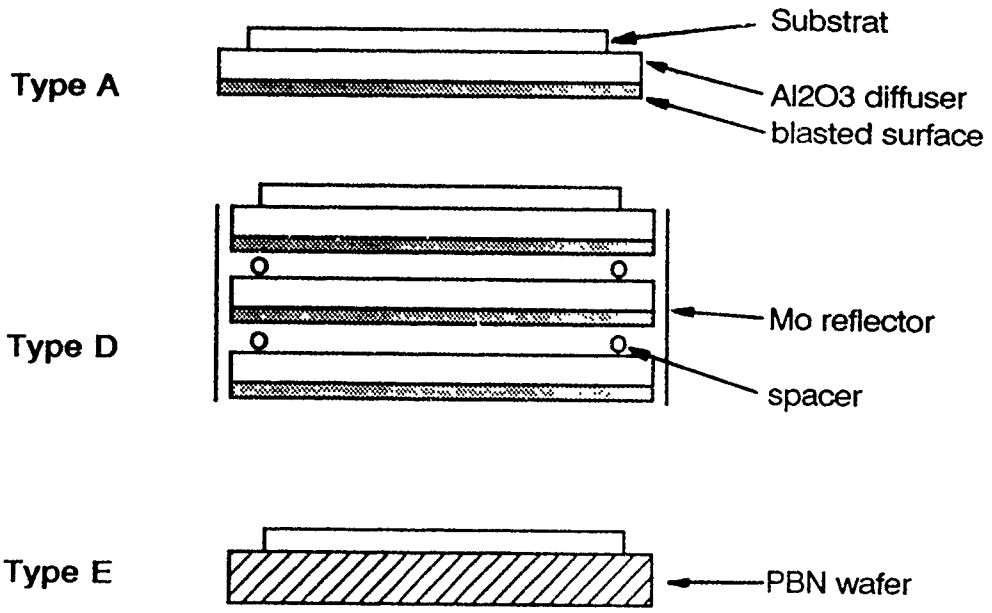

Fig. 1

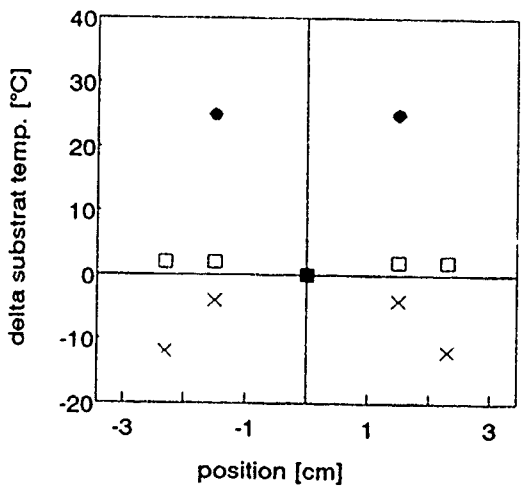

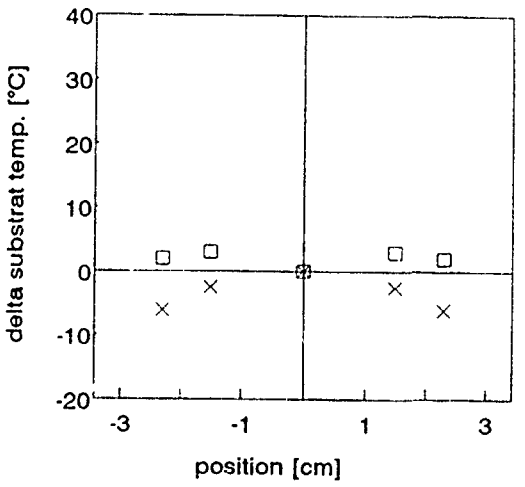

● Type A: Ts=680°C
□ Type D: Ts=740°C
× Type E: Ts=705°C

□ Type D: Ts=627°C
× Type E: Ts=615°C

Fig. 2

Co3

Structure, properties, and purity of pyrolytic boron nitride crucibles for molecular beam epitaxy

Arthur W. Moore
Union Carbide Coatings Service Corporation
12900 Snow Road, Parma, OH 44130, USA
Tel 1-216-676-2217, Fax 1-216-676-2423

A. Introduction

The structure, properties, purity, and chemical inertness of pyrolytic boron nitride (PBN) make it an attractive container material for elemental purification, compounding, and growth of semiconductor crystals. For example, PBN crucibles are widely used for deposition of metals and dopants at high temperatures and ultra-high vacuum by molecular beam epitaxy (MBE). The purity and thermal stability of PBN in this application are very important because even very small amounts of certain impurities, such as carbon in GaAs, can adversely affect device performance. To obtain even greater purity, most customers bake their PBN crucibles at high temperature in ultra-high vacuum before using them in MBE.

The present study was undertaken to compare the structure and purity of PBN crucibles made by the major manufacturers of this material.

B. Structure and morphology

The density, preferred orientation as determined from X-ray (002) rocking curves, interlayer spacing ($c_o/2$), and crystallite size (L_c) of PBN crucibles made by nine different manufacturers were determined. Densities ranged from 2.0-2.2 g/cc. Based on the $c_o/2$ values, these densities are 90-98 % of theoretical for hexagonal BN. Almost all of the crucibles exhibited very broad rocking curves with two or three peaks instead of a single Gaussian peak with a width of about 50^o which is typical of pyrolytic graphite. These peaks indicate the presence of a columnar crystalline component in the PBN.[1] Asymmetry in the (002) diffraction peaks indicated both turbostatic (higher d-spacing) and more crystalline components (lower d-spacing) in most of the crucibles.

C. Thermal stability

Boron nitride does not sublime but decomposes into the elements boron and nitrogen at elevated temperatures. The equilibrium data from the JANAF tables indicate a decomposition temparature of about 2765 K

at 1 atm. A decomposition temperature of about 2500 °C was also indicated from uniaxial hot-pressing experiments to convert PBN into a highly oriented form.[2] Based on equilibrium data, decomposition of PBN might be expected under the most extreme conditions of use, i.e., in an MBE system operating at 10^{-10} Torr at 1600 K, where an equilibrium nitrogen pressure of 5×10^{-5} Torr is indicated.[3] However, vacuum heat-treatment of PBN at temperatures up to 2000 °C yielded results indicating nitrogen pressures at least four orders of magnitude smaller than the equilibrium values.

D. Impurities in PBN MBE crucibles

1. Carbon and oxygen

The carbon and oxygen content of most crucibles averaged around 50 ppmw with a range of 30-80 ppmw. Heating PBN crucibles to 1600 °C for one hour in ultra-high vacuum reduced the carbon content to 5-20 ppmw.[4]

2, Metallic impurities

Table I lists the earlier data for upper limits of metal impurity concentration in PBN as determined by such techniques as atomic absorption, mass spectrometry, and coupled plasma emission spectroscopy. Several of these techniques require methods for getting the PBN into solution so the purity of the added materials becomes an important issue.

Measurements by spark source mass spectroscopy (SSMS) were undertaken in an effort to more accurately determine the concentration of metallic impurities in the PBN. In this method, the PBN is ground to a powder and mixed with high-purity silver to form a solid conducting electrode. A spark is generated and the resulting ions analyzed by mass spectroscopy. Impurities in the silver are also analyzed and subtracted from the total to yield the impurity concentration in the PBN. Results in the last column of Table I show less than 1 ppm of all metallic elements except Si and Ca (< 6 ppma) and Na (< 2 ppma). These values are roughly in agreement with the earlier data, but an order of magnitude lower limit was established for the concentration of the elements Fe, Co, Ni, Cu, and Zn in PBN.

3. Surface impurities

Since surface impurities can be more important than bulk impurities, an attempt was made to determine the level of surface impurities in the PBN crucibles using secondary ion mass spectroscopy (SIMS). Analyses were done using ion beam currents of 10 mA (-20 Å penetration) and 1500 mA (2000-5000 Å penetration). However, quantitative data could

not be obtained because of the lack of a suitable PBN reference standard and the correlation with SSMS data was poor.

E. Conclusions

PBN crucibles made by nine different manufacturers are for the most part similar in structure, properties, and purity.

Spark source mass spectroscopy appears to be an appropriate method for determining very low levels of metallic impurities in PBN

Carbon and oxygen are the most abundant impurities in PBN. The concentration of these and other impuriteis can be reduced by baking at high temperature in ultra-high vacuum.

Thermal decomposition of PBN under MBE use conditions is less than 0.01 % of the equilibrium value for boron nitride.

Table I. Impurities in PBN crucibles

Element	Analytical method	ppma	ppma by SSMS
Na	1	< 1	< 2
Mg	2	< 1	< 0.5
Al	3	< 5	< 1
Si	3	< 5	1-5
K	1	< 1	< 0.3
Ca	3	< 2	0.4-6
Ti	4	< 2	< 0.3
Cr	3	< 2	< 1
Fe	3	< 5	< 0.4
Co	4	< 1	< 0.1
Ni	3	< 3	< 0.1
Cu	3	< 2	< 0.1
Zn	2	< 3	< 0.4

Analytical Methods: (1) Water extraction and atomic absorption; (2) Flame atomic absorption; (3) Alkaline fusion and atomic absorption; (4) Induction coupled plasma emission spectroscopy

References

1. A.W. Moore and S.L. Strong, Ceram. Eng. Sci. Proc. **10** (1989), 846
2. A.W. Moore, Nature **221** (1969), 7133
3. A.W. Moore, J. Crystal Growth **106** (1990), 6
4. F.A. Chambers, G.W. Zajac, and T.H. Fleisch, J. Vac. Sci. Tech. **84** (1986), 1310

Cp1

MBE SYSTEM FOR RESEARCH

M.Láznička*, M.Cukr, J.Krautwurm, P.Svoboda, P.Doubrava, Z.Šourek, I.Gregora, V.Vorlíček, J.Oswald, G.Nachtwei+

Institute of Physics,Czechoslovak Academy of Sciences, CS-162 00 Prague 6, Cukrovarnická 10, Czechoslovakia
+Dept.of Physics,Institute of Solid State Physics, Humboldt University,Invalidenstr.110,D-0-1040 Berlin, Germany

A low cost DCA Instruments MBE system has been installed and tested in Prague. The MBE system consists of 4 chambers: growth chamber, analytical/preparation chamber, buffer chamber and introduction chamber.

The main advantages of the system are:

a) an arbitrary cell position upon request: vertical or quasi-horizontal or horizontal one;
b) growth on indium-free bonded two-inch substrates with continual rotation;
c) growth on both III-V and silicon substrates;
d) the possibility to use up-to-date growth techniques due to very fast acting shutters in combination with RHEED oscillation measurement;
e) utilization of three surface sensitive techniques of LEED, AES and ELS in retarding field analyzer with transparent screen;
f) performing substrate pretreatment and metallization in analytical or in buffer chambers;
g) large computerization of temperature controllers, shutters, rest gas analyzer and RHEED intensity measurement.

The system described was tested by preparing Si doped GaAs layers, GaAs/GaAlAs heterostructures and GaAs/AlAs superlattices as well.

Up to now, the results achieved by faint Si doping of GaAs show rest acceptor level at the beginning of the order of 10^{14} cm^{-3}, compensation ratio $(N_A+N_D)/n$ at higher Si concentrations being 2.

Further we have prepared some normal modulation doped heterostructures GaAs/AlGaAs with 10 nm spacer layer and with superlattice GaAs/AlAs at substrate/buffer layer interface. Fig. 1 shows the results of electron transport measurements on MD structure in a strong magnetic field. Both the longitudinal (ρ_{xx}) and the Hall (ρ_{xy}) resistivity exhibit features characteristic for the quantum Hall devices. Basic parameters of the sample in fig. 1 determined at 4.2 K are $n_{2DEG} = 3.5 \times 10^{11}$ cm^{-2} (concentration) and $\mu_H = 2.2 \times 10^5$ cm^2/Vs (mobility). Well developed Hall plateaus and corresponding minima in $\rho_{xx}(B)$ approaching zero signify the absence of any undesirable parallel conduction channels which makes the samples suitable for metrological applications.

Photoluminescence examination of the same sample measured at 5 K showed two lines corresponding to luminescence from the QW and another two lines which are due to recombination of bound excitons. The latter lines are not observed above 30 K.

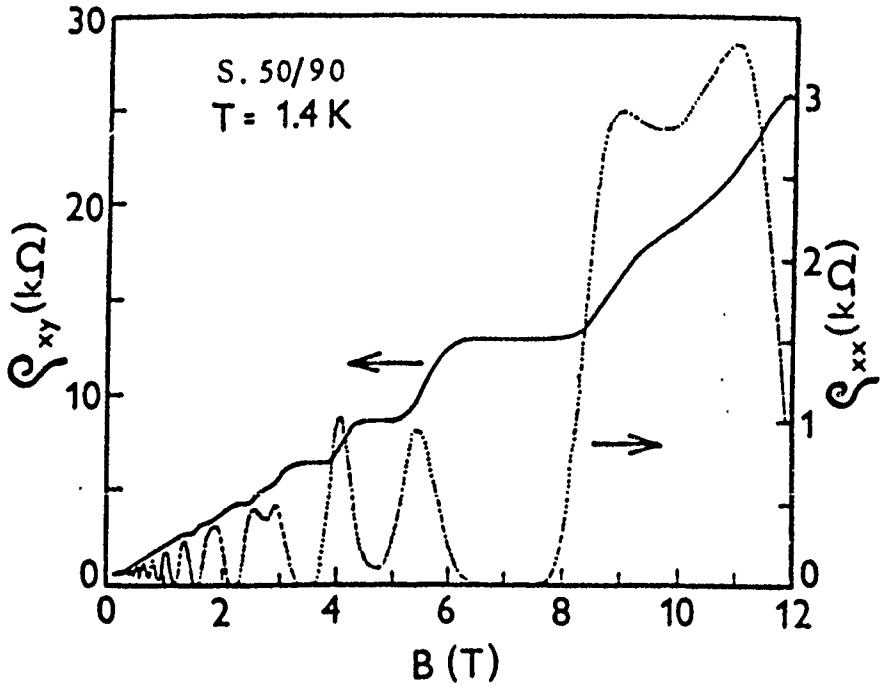

Fig. 1

The superlattices were of GaAs/AlAs type with various number of double layers of GaAs and AlAs, with 100 times repeated period. We used interrupted growth at a temperature which was by about 30 to 50 °C higher than the GaAs oxide desorption temperature.

The superlattices prepared were confirmed by x-ray diffraction and Raman spectroscopy.

The periodicity of the long-period superlattices was determined from the angle distance between the first satellites and the main maximum. Interference bands present on both sides of the main maximum are known from diffraction on very thin and crystallographically perfect crystals.

In the Raman spectra of short-period superlattices, well developed folded acoustical and optical modes confined in the GaAs and AlAs layers, respectively, were found. The measured maxima and well developed structures correspond to the quantum optical phonons which are typical for superlattice periodicity.

The lateral inhomogeneity of prepared layers was also tested and found to be lower than 1 %.

More detailed information about equipment and results achieved will be presented.

On the Accuracy of MBE Cell-Temperature Calibration Investigated by Frequency Domain Analysis of RHEED Intensity Oscillations

J. Kraus*, J. Weyers, W. Prost and F. J. Tegude

Universität-GH-Duisburg, Halbleitertechnik/Halbleitertechnologie, SFB 254
Kommandantenstr. 60, D-4100 Duisburg Tel.: 49-203/3793393 Fax: 49-203/3793400

Abstract

In this work the analysis of Reflection High Energy Electron Diffraction (RHEED) intensity oscillations during the MBE growth of GaAs and AlAs is reported. The frequency of the oscillations is obtained by means of Fast Fourier Transformation (FFT) providing information about incorporation rates, V/III-ratio and the accuracy of the beam fluxes. We will show for both, gallium and aluminium cell, respectively, that the time gradient of the beam fluxes may change the growth rate in the order of 4 %.

For signal recording a specially designed phototransistor and lens system has been developed. The intensity oscillations are sampled at N = 512 data points in variable intervalls. Growth was carried out in a Varian Gen II modular with solid sources. In the case of GaAs the evaluation of the substrate temperature dependent V/III-ratio requires a high precision determination of both group III as well as group V controlled incorporation rates /1/. A typical example of intensity oscillations for GaAs growth under excess gallium conditions is shown in fig. 1. Phase relationships of the oscillations were carefully checked using the criteria of Joyce et al. /2/. In the first part of this curve (I) gallium controlled growth starts on a (2 x 4) reconstruction pattern. Under this condition the evaluation of the growth rate by means of a FFT is easily obtained /3/. Increasing gallium accumulation (part II) results in a change of the reconstruction pattern with exponentionally decreasing signal amplitude. After the gallium shutter is closed the oscillations continue (part III) until the excess gallium is incorporated. A direct spectral analysis of the RHEED oscillations in fig. 1 via the FFT method fails due to the different frequencies of all three parts. The desired frequency ω_V of the oscillations in part II can be extracted using a mean value function together with a filtering HANNING-window with an accuracy of $\Delta f = 0.02$ Hz.

For the growth of quantum well devices with very short well width abrupt changes of material composition are necessary. Therefore beam flux transients due to shutter operation can lead to a remarkable thickness variation. We have

investigated the material system GaAs and AlAs. A package of three blocks each consisting of 10 ML separated by a growth interrupt of 5 sec. were recorded to illustrate the effect of shutter operation on the beam flux. In fig. 2 a typical plot concerning the growth of GaAs in the above described manner is shown. A direct transformation of the whole function of fig. 2 results in a clearly resolved peak splitting of the oscillation frequency shown in fig. 3. The difference between the three peaks is due to beam flux variation. Taking into account that the first oscillation observed after opening the gallium shutter does not correspond to a ful monolayer growth /4/ the resulting frequency variation is 0.039 Hz. This difference can be converted to a growth rate shift of about 4 %. For AlAs the same growth sequence leads only to a broadening of the peak in the frequency spectrum, resulting in a smaller beam flux shift possibly affected by the relative high cell temperature.

References:

/1/ R. Fernandez; J. Vac. Sci. Technol. B6, pp 745 (1988)

/2/ B. A. Joyce, J. Zhang, J. H. Neave, P. J. Dobson; Appl. Phys. A 45, pp 225 (1988)

/3/ G. W. Turner, B. A. Nechag, S. J. Eglash
J. Vac. Sci. Technol. B8, No. 2, pp 283 (1990)

/4/ D. G. Liu, C. P. Lee, K. H. Chang, J. S. Wu, D. C. Liou
Appl. Phys. Lett. 57 (14), pp 1392 1990

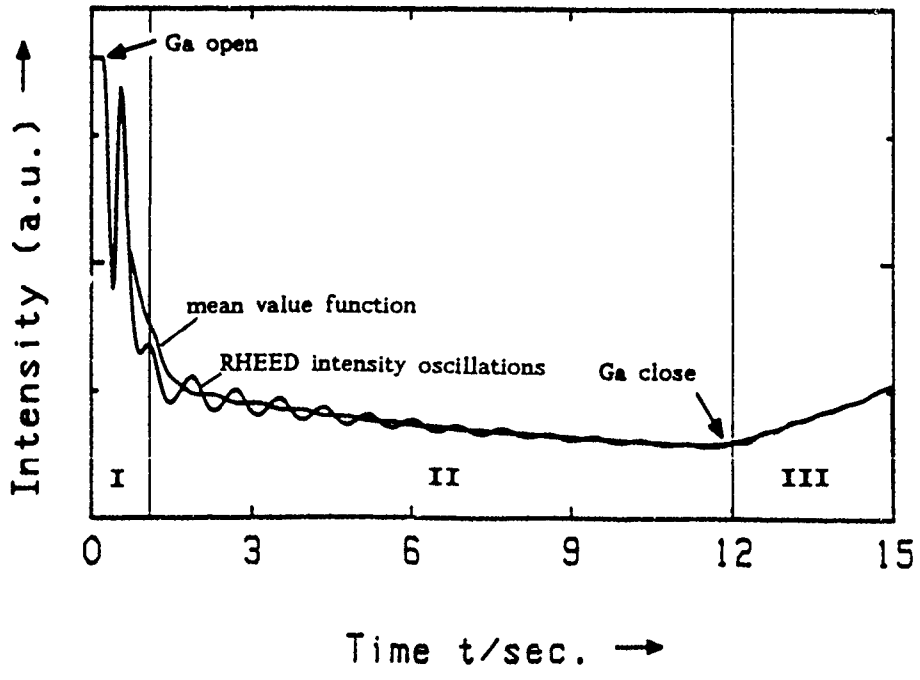

Fig. 1: RHEED Intensity Oscillations for GaAs growth under excess gallium
I: Ga controlled growth; II: As controlled growth; III: Ga shutter closed

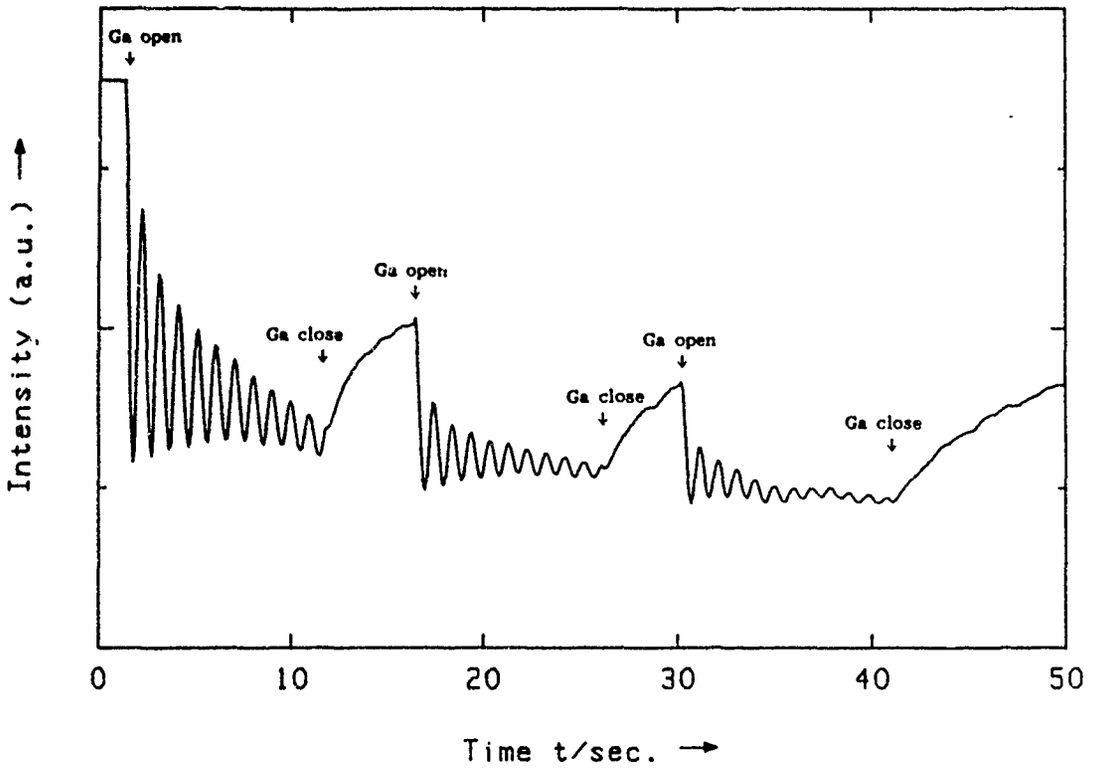

Fig. 2: Sequence for accuracy measurements: 3 blocks of 10 ML GaAs; $T_{Sub} = 595\,^{\circ}C$

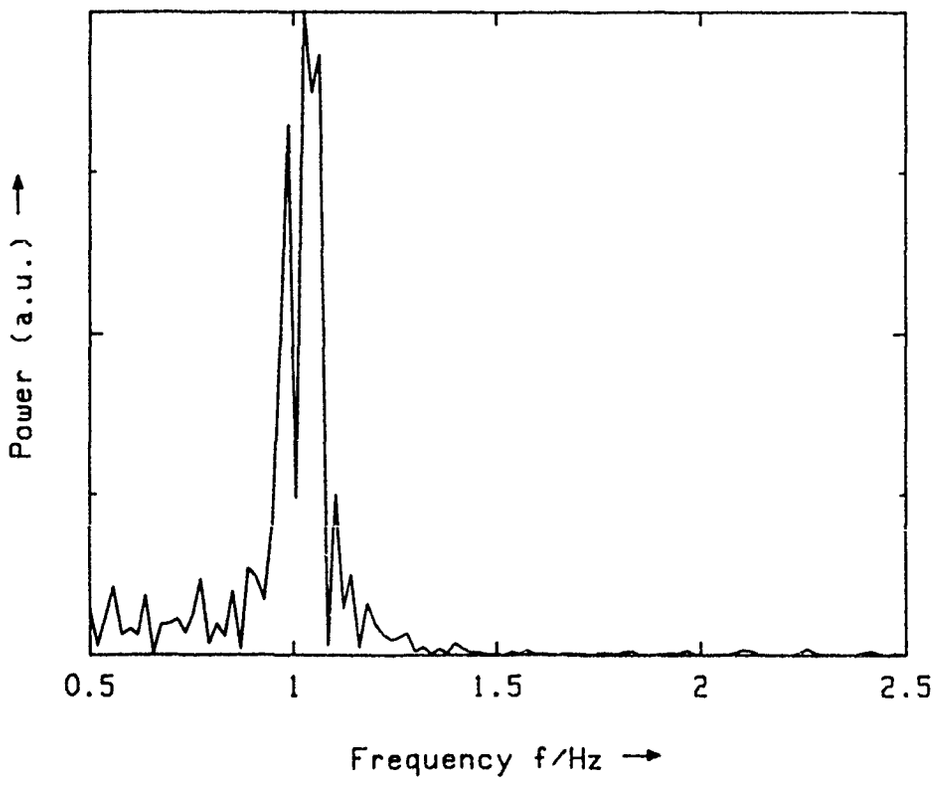

Fig. 3: Frequency spectrum of fig. 2 with splitting into three peaks

OPTICAL SIMULATION OF EFFUSION MOLECULAR BEAM FOR MBE

B. Adamczyk*, L. Michalak and E. Marcinkowska
Institute of Physics, Maria Curie-Skłodowska University, 20-031 Lublin, Poland, phone: 376126, telex: 0643223, fax: /48/81375102

The authors see an analogy between a molecular beam and light beam (Figs.1,2). In a simulation system the light

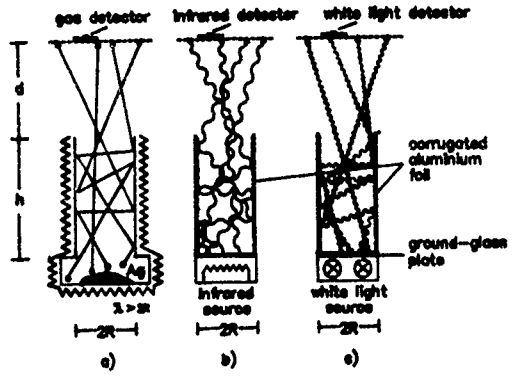

Fig.1. a/Effusion molecular beam formed by the effusion channel. b/"Effusion" infrared beam formed by the modelling tube. c/"Effusion" white light beam formed by the modelling tube

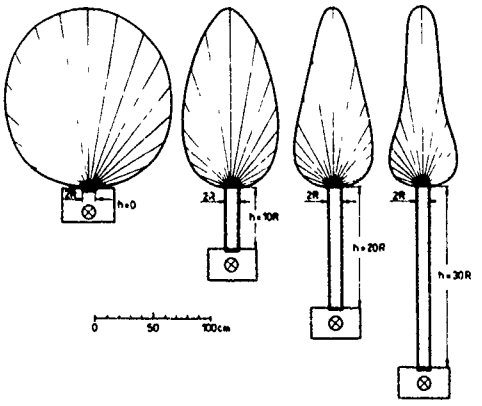

Fig.2. The optical simulation of the molecular beam showing white light beams formed by "effusion" tubes of various lengths. The envelopes marked in the figure indicate the equal light intensity places.

from a bulb was introduced into the channel via a diffusion ground glass plate. The inside of the channel was lined with corrugated aluminium foil with a high reflection coefficient. Due to the corrugation, the light was reflected from the foil in a chaotic way, just like molecules from the wall of the actual channel. The light beam intensity distribution was measured with a photodetector. It means that the high vacuum processes are investigated under normal pressure. Application of infrared radiation instead white light to the modelling of the effusion of a molecular beam gives better information about transverse intensity distributions of a real effusion molecular beams (Fig. 3).

The previous researches of authors dealt mainly with molecular beams crossed by electron beams, which is especially important in mass spectrometry [1-5].

An application of this method in MBE technique [6] is

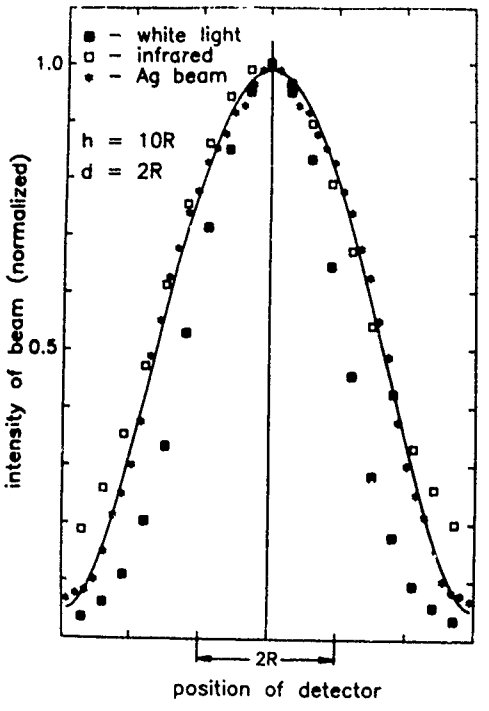

Fig.3. Comparision of the transverse distribution intensity of white light /■/, infrared /□/ and effusion Ag /✳/ beams at the distance d = 2R between outlet of the modelling tubes /or real chanel/ and the detector. Lenght of modelling tubes and the real channel h = 10R.

described by the authors in the previous work [7], where transverse distributions of molecular beams produced by conical effusive cells connected with different cylindrical channels were determined (Fig. 4).

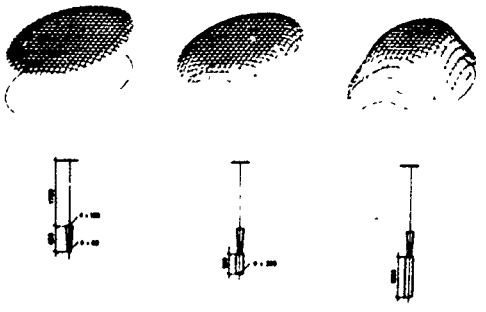

Fig.4. Distributions of white light "effusion" beams generated by three different modelling channels.

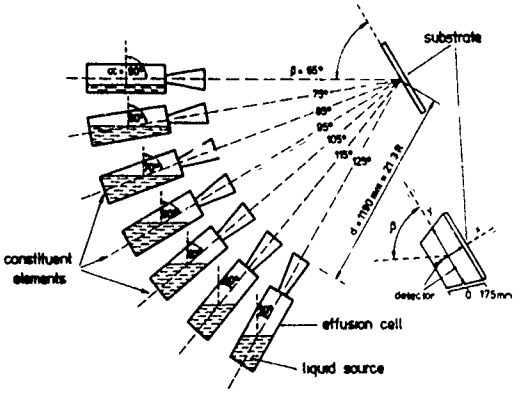

Fig.5. MBE system being an object of the light simulation presented in this report.

The main aim of this work is to use the light simulation method for an evaluation of intensity distributions of molecular beams in an MBE system consisted of seven cells located at different angles to an exposed target (Fig.5). The results of this simulation are presented on the figures

6a and 6b.

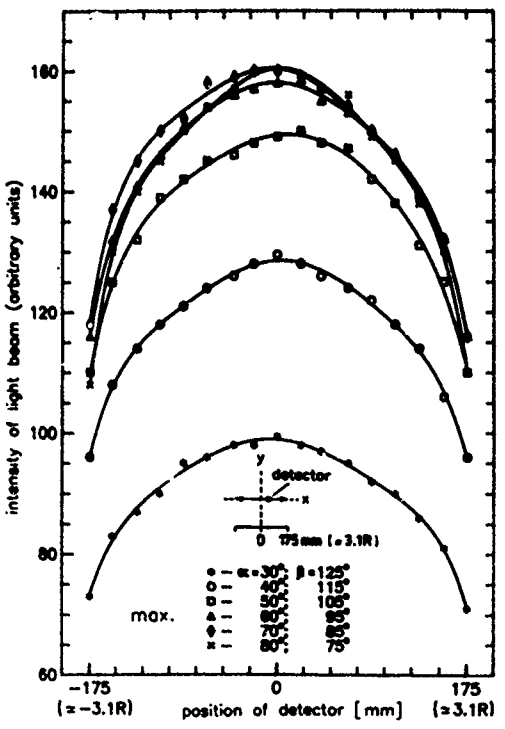

Fig.6a. Intensity distributions of light beams in the exposed torget plane (Fig.5) in direction X at different angles α and β. The simulation corresponds to the maximum level of liquid effusive cell.

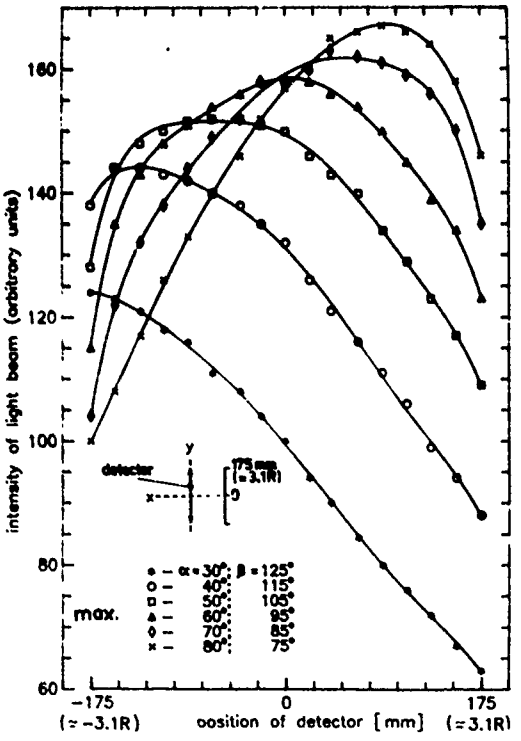

Fig.6b. Intensity distributions of light beams in the exposed torget plane (Fig.5) in direction Y at different angles α and β. The simulation corresponds to the maximum level of liquid effusive cell.

Acknowledgements

The authors wish to thank Prof. M.A. Herman and Prof. J. Marks for their helpful sugestions and cooperation. This work was carried out under the Polish Central Program of Developmental Research CPBR 8.3.6.

References

1 B. Adamczyk and L. Michalak, Int. J. Mass Spectrom. Ion Processes, **69**, 163 (1986).
2 B. Adamczyk and L. Michalak, Int. J. Mass Spectrom. Ion Processes, **71**, 211 (1986).
3 B. Adamczyk and L. Michalak, Int. J. Mass Spectrom. Ion Processes, **74**, 235 (1986).
4 L. Michalak and B. Adamczyk, Int. J. Mass Spectrom. Ion Processes, **85**, 319 (1988).
5 B. Adamczyk, L. Michalak and E. Marcinkowska, Int. J. Mass Spectrom. Ion Processes, **90**, (1991) (in press).
6 M. A. Herman, H. Sitter, Molecular Beam Epitaxy, (springer series in Materials Science) **7** (1988).
7 L. Michalak and B. Adamczyk, Vacuum, (in press).

MATHEMATICAL MODELING OF HEATING AND KNUDSEN FLOW IN EFFUSION CELL FOR MBE TECHNOLOGY

Andris V. Bune, Tariel M. Makhviladze

Modeling Laboratory of Microelectronics Processes
Institute of Physics and Technology,
Academy of Science of the USSR

25a Krasikov Street Moscow 117218 USSR

Phone (70) 95 124 1000 Telex 411598 ANTEX SU

Abstract

The models of temperature field and molecular flow in effusion cell of single-channel type with cylindrical geometry of furnace are presented. The main assumptions are 1) axial symmetry 2) molecular flow of collisionless type 3) equilibrium vapor pressure. The finite-difference method and Monte-Carlo procedure were used. The results of calculation of temperature field in furnace and molecular angular distribution on the effusion cell exit are presented. This model is useful for numerical simulation of MBE technology.

1.Introduction.

Molecular beam epitaxy process (MBE technology) is well known in the silicon technology, in gallium arsenid technology and for preparation of super conducting thin films. In all cases essential of technology is the same. The evaporated material is heated in the effusion cell and after free molecular flow is condensed on the substrate. The problem is to obtain thin film of constant thickness and chemical composition. The aim of the present work is to develop physical and numerical model suitable for simulation and effective control of this process.

2.Models description.

The complete mathematical model includes two separate modulus connected throw the boundary conditions.

2.1 The heat conditions on the effusion surface are defined in the first module. The temperature and directional dependence of the material properties are accounted for. The axial symmetry of effusion cell is assumed. The two dimensional heat equation in cylindrical coordinate systems reads as

$$c_v(r,z,T)\rho(r,z,T)\frac{\partial T}{\partial t} - \frac{1}{r}\frac{\partial}{\partial r}\left[r\, k_r(r,z,T)\frac{\partial T}{\partial r}\right] - \frac{\partial}{\partial z}\left[k_z(r,z,T)\frac{\partial T}{\partial z}\right] = Q(r,z,t,T)$$

Here $T \equiv T(r,z,t)$ - temperature, c_v - specific heat capacity, k_r , k_z - thermal conductivity in r and z directions, ρ - material density, $Q(r,z,t,T)$ - volume heat sources. The finite-difference solution method was used.

2.2 Now let us consider molecular flow model [1]. The main goal on this step is calculation of the number of molecules flights from effusion cell and the angular distribution of it. The total number of molecule is the sum of molecules passed through the cell directly and with a number of collision with cell walls (in our case with walls of cylinder). That is

$$N_{total} = N_d(r) + \int P(\mathrm{r},r)\, N(\mathrm{r})\, d\,\mathrm{r}$$

Here N_d - the fraction of total evaporated molecules N_{ev} that pass through cell without collision with wall. $P(\mathrm{r},r)$- probability, that molecule started from the evaporated surface from the point with coordinate (r,z) will pass from cell at the point with coordinate (r,0).

2.3 For the case $N_{ev} = const$ this problem was solved by P. Clausing [2]. The recent comparison of Clausing solution with experimental data was done in [3,4] and it application for MBE technology can be find in [5]. This model, however, doesn't take into account the temperature distribution on the evaporating surface. From our point of view, this is the main restriction of this analytical approach. In our calculation the test-particle Monte-Carlo method was used [1]. The similar approach was used in the work [6], but the influence of temperature field wasn't taken into account.

3.Results

The numerical calculations of temperature field were done for BN crucible . The BN is very anisotropic material (k_z = 0.0004063 W/m K and k_r = 0.00000956 W/m K). Evaporated material was As.

The calculation was done till stationary temperature regime was obtained. The very high temperature gradients are located in crucible. The calculation of angular diagram was done for various length diameter ratios of empty part of effusion cell. The strong influence of this parameter can be seen on the angular diagram.

The program package for calculation of temperature field in effusion cell and angular diagram is developed.

References

1. G.A.Bird Molecular Gas Dynamics. Oxford University Press 1976.
2. P.Clausing The Flow of Highly Rarefied Gases through Tubes of Arbitrary Length 1971 J. of Vacuum Science and Technology v.8, n.5, p.636-646.(Translated from German [Ann.Physik v.5,n.12.p.961, 1932])
3. S.Adamson, J.F.McGilp Measurement of gas flux distributions from single capillaries using a modified, uhv-compatible ion gauge, and comparison with theory 1986 Vacuum v.36, n.4, p.227-232.
4. H.P.Steinruck, K.D.Rendulic A test of capillary array beam sources for very large knudsen numbers 1986 Vacuum v.36, n.4, p.213-215.
5. J.A.Curless Molecular beam epitaxy beam flux modeling 1985 J.Vac.Sci.Technol. v.B3, n.2, p.531-534.
6. K.Nanbu, Y.Watanabe Thickness distribution of films fabricated by the molecular beam epitaxy technique 1986 Vacuum v.36, n.6, p.349-352.

Do1

A COMPARATIVE STUDY OF InP OXIDE DESORPTION UNDER FLUXES OF As_4 AND P_2

R.Averbeck, H.Riechert*, H.Schlöttere-
Siemens Research Laboratories
p.o.box 830952
D-8000 München 83 , Germany
Tel.: 49-89-636-45230 , Fax.: 49-89-636-3294

G.Weimann
Walter-Schottky-Institut, TU München
D-8046 Garching , Germany

In solid source MBE, the desorption of the surface oxide from InP substrates before epitaxy is commonly carried out under a stabilising pressure of As. This convenient method suffices to prevent the formation of an In-rich surface but is known to change the surface composition significantly[1,2], which should lead to a highly strained overlayer of InAsP.
We studied the oxide desorption process under As and P, determining the surface composition and oxide thickness by X-ray photoemission (XPS) and correlating the results with the observed RHEED patterns[3]. One aim was to compare the practical aspects of the two processes, in order to determine if the effort of introducing phosphorus is outweighed by process advantages and achieved surface quality.

The experiments were performed in a VG V80H MBE system with a large-volume cold-trap backed by a turbomolecular pump. As_4 and P_2 were evaporated from solid sources, utilising a cracker cell for phosphorus. The surface temperature of In-free mounted InP wafers was determined by a narrow-band IR pyrometer, taking the oxide desorption from GaAs (580°C for a standard hydrogen peroxide etched surface) as a calibration point. XPS spectra were taken in a separate chamber

which is connected to the MBE by an all-UHV transfer. The composition of the oxide was calculated from the intensities of the In, P and O signals by a straight-forward model. A chemically shifted P peak allows a separation of the signals from oxide layer and bulk InP.

Chemically treated surfaces (either by H_2O_2:H_2SO_4:H_2O or 10% HF) are found to be covered by an about 1 nm thick, In-rich oxide consisting of 1 part $InPO_4$ and 3 to 5 parts In_2O. The oxide does not desorb at a distinct temperature, but the amount of oxygen on the surface decreases gradually with increasing temperature (see fig.).

Under P_2, the oxide is removed (to less than 0.2% of a monolayer) at 490°C after at most 5 min. A flux of $5 \cdot 10^{14} cm^{-2} sec^{-1}$ is sufficient for the surface stabilisation at this temperature. A (2x1) surface reconstruction is observed by RHEED at about 425°C, which changes to (2x4) when the oxide is completely desorbed. A further increase of the temperature does not lead to a change in surface reconstruction, even if In droplets can be observed. As has been suggested before[4], the In-rich surface does not appear to be thermodynamically stable.

Under As_4 the rate of oxide desorption is significantly lower than under P_2 and a higher temperature (by 40°C) is necessary to remove the oxide (see fig.). XPS reveals a strong incorporation of As, which, according to the observed binding energies must be present in the form of InAs. Thus our results suggest that the slower oxide desorption is caused by the formation of an InAs-rich surface.

The complete removal of the oxide at 520°C requires an As_4 flux of more than $4 \cdot 10^{15} cm^{-2} sec^{-1}$ and results in a 1.2 nm thick InAs overlayer.

From about 400°C up to the limit of thermal stability, RHEED shows (2x1), (2x3) or (2x4) reconstructions. A systemetic dependence on temperature, flux or time could not be found. A (4x2) reconstruction was only observed when heating the substrate rapidly over the stability limit.

The results of these studies confirm that the desorption of the oxide from InP under As_4 poses serious difficulties. Compared to the P_2 stabilisation it requires higher temperatures and therefore higher stabilising fluxes due to the formation of an InAs-rich surface. Furthermore it is not possible to determine by RHEED whether the surface is oxide-free. In contrast to this heating under relatively low P_2 allows a fast and complete removal of the oxide, which can be monitored by RHEED, assuring more reproducible results.

References:

1) K.Y. Cheng et al.,
   J.Appl.Phys.52 (1981) 1015
2) Hollinger et al.,
   J.Vac.Sci.Technol.B8 (1990) 832
3) R. Averbeck,
   Diplom-Thesis ,TU München, 1990
4) M.B. Panish,
   J.Electrochem.Soc.127 (1980) 2729

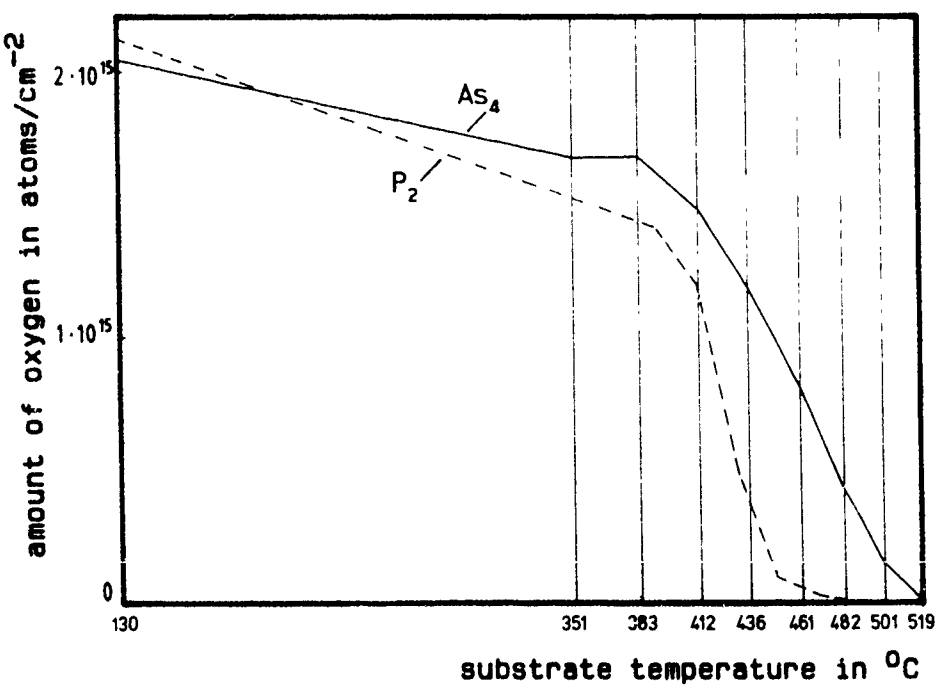

Amount of oxygen under As_4 and P_2 stabilisation versus substrate temperature.

Realization of atomically abrupt InAs/GaAs heterointerfaces by flashoff of the In floating layer

O. BRANDT*,[a] K. PLOOG,[a] L. TAPFER,[a]
M. HOHENSTEIN[b] AND F. PHILLIPP[b]
[a] *Max-Planck-Institut für Festkörperforschung, W-7000 Stuttgart 80, Germany*
[b] *Max-Planck-Institut für Metallforschung, W-7000 Stuttgart 80, Germany*
Phone: 0711/6860-246; Fax: 0711/687371

The synthesis of InAs/GaAs heterostructures is severely affected by the large lattice mismatch existing between the two constituent materials. It has been recognized now that the most serious obstacle for producing well defined InAs/GaAs heterointerfaces is the segregation of In during overgrowth with GaAs. In the initial stage of overgrowth, the In segregates on the growing surface, forming a floating layer which is gradually dissolved during subsequent overgrowth. The incorporation of this floating In layer leads to compositional grading which can extend over 30 nm. This fact has prohibited the realization of InAs/GaAs heterostructures with well defined structural and electronic properties up to now.

Here, we show that the incorporation of the In floating layer can be avoided by its flashoff prior to overgrowth. InAs/GaAs heterostructures synthesized by this technique exhibit an exceptional degree of crystalline perfection. Double-crystal x-ray diffraction patterns of multilayer structures with an InAs thickness of 1 monolayer (ML) and less are essentially undistinguishable from those simulated in the frame of the dynamical diffraction theory for perfect crystals. No broadening can be detected even for the highest order satellites. Exceeding the monolayer coverage creates atomic steps on top of the continuous layer, resulting in thickness fluctuations as manifested in a slight broadening of the satellite peaks. However, as long as the InAs thickness is below the onset of strain relief processes which occur at 2.5 ML, the crystal structure and interface morphology are excellent. As an example, we show the high-resolution lattice image of an InAs film with a thickness of 2.4 ML in the GaAs matrix. Both interfaces are of equivalent abruptness and neither a compositional gradient nor short-range roughness exist on either of the interfaces. The crucial point for obtaining this interface abruptness is the flashoff of the In floating layer. In the following, we therefore focus on the details of our growth technique and explain the reason for its performance.

The samples are synthesized by conventional solid-source molecular beam epitaxy (MBE) on semiinsulating (001) GaAs substrates. The arrival fluxes for GaAs growth are calibrated *in situ* by means of reflection high-energy electron diffraction (RHEED). Temperatures mentioned in the present work refer to the evaporation

of the native oxide at 580°C and the transition from the As-stabilized to the Ga-stabilized regime at 630°C, as observed by monitoring the RHEED pattern during the substrate preparation. The deposition rates for InAs are determined precisely by double-crystal x-ray diffractometry and compared to those obtained by scanning electron micrographs from cleaved edges of bulk InAs layers.

Prior to the growth of the InAs/GaAs heterostructure, a 1 μm thick GaAs buffer layer is deposited at a growth temperature of 580°C. Then, the temperature is lowered to 420°C to initiate InAs deposition. The In and As_4 arrival fluxes used correspond to a deposition rate of 1 ML per 16 s and an As_4/In ratio close to the stochiometric minimum. To minimize the density of atomic steps at the growth surface, growth is stopped after deposition of 0.4 ML and the surface is annealed under an As_4 flux for 120 s at the growth temperature of 420°C. Before heating up again to 540°C for GaAs overgrowth, 3 ML of GaAs are deposited at 420°C on top on the InAs layer. Then, growth is stopped and the temperature is raised to the growth temperature of GaAs (540°C) before GaAs growth is continued.

During this procedure, the growth process is monitored by RHEED. When the temperature is lowered for InAs growth, the (2x4) reconstruction of GaAs changes to the c(4x4) reconstruction, originating from excess As_4 sticking on the surface. After opening the In shutter, a well defined (2x3) reconstruction appears. This type of reconstruction corresponds to As_4-rich conditions, and is caused by adsorbed excess As_4 rather than by the impinging flux. In contrast to bulk InAs, the quality of these ultrathin strained films is not affected by the presence of excess As_4. Probably the long annealing cycles relax the restriction of accurate control of the effective surface stochiometry, which is otherwise only possible by an alternate supply of In and As_4 while monitoring the RHEED pattern during deposition.

The fractional-order streaks of the InAs pattern become sharper while the growth surface is allowed to relax towards equilibrium during the annealing cycle. By opening the Ga shutter, the reconstruction disappears and a (1x1) pattern is observed. This is in striking contrast to the c(4x4) reconstruction usually observed for the GaAs surface at this temperature and As_4 flux. A (1x1) reconstruction is frequently observed when growing AlGaAs in the so-called forbidden temperature range, where a Ga floating layer is present at the surface. Our experimental finding thus suggests the presence of an In floating layer on the surface. During the subsequent heating to 540°C, a well defined (2x4) reconstruction appears at 520°C. Both elementary In on GaAs and InAs on GaAs start to desorb at around 500°C. Thus, the change in reconstruction directly reflects the flashoff of the In floating layer on the surface.

The desorption of a fraction of the delivered In should manifest itself in an apparent change of the growth rate. In fact, growth rates derived from the thickness

of the embedded InAs films are systematically smaller with respect to those obtained from the thickness of bulk InAs. Comparing the thickness of InAs films grown with and without the heating cycle thus provides the direct determination of the amount of In segregating on the surface. Under the growth conditions described above, the thickness of InAs films grown with the heating cycle is about 40% smaller than that of layers grown without, which means that this fraction of In segregates *and* desorbs. On the other hand, the incorporation of the In floating layer in structures grown at a constant temperature leads to a dramatical deterioration of the overall crystal quality.

The amount of segregated In depends strongly on the growth conditions. In particular, an alternate supply of Ga and As_4 during overgrowth is found to result in segregation rates up to 90%. This result is consistent with findings of other authors and with thermodynamic segregation models. From a practical point of view, growth techniques making use of an alternate supply of Ga and As_4 for growing the GaAs are thus less suitable for this material system.

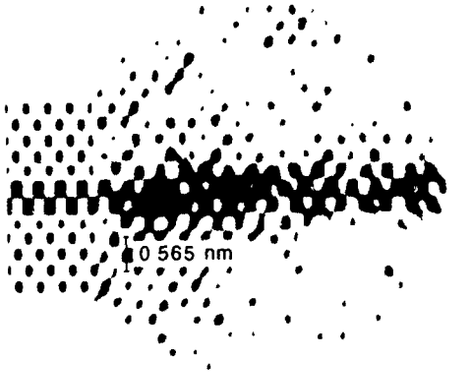

Reconstructed lattice image of an InAs/GaAs heterostructure. On the right, the experimental image is presented. On the left, we show the corresponding image simulation for two InAs monolayers. Both images are Fourier-filtered for reconstruction allowing maximum spatial frequencies of 3.4 nm^{-1}. The position of the dark spots in the images directly reflects the projection of columns of In-As dumbells. The arrow denotes the position of a single-atomic step connecting regions of 2 and 3 ML thickness.

Oral presentation preferred

Do3

THE IMPACT OF THE MBE GROWTH CONDITIONS ON THE $Al_{0.48}In_{0.52}As/Ga_{0.47}In_{0.53}As$ INTERFACE

H. Künzel[x], H.G. Bach, A. Hase, and C. Schramm
Heinrich-Hertz-Institut für Nachrichtentechnik Berlin GmbH
Einsteinufer 37, D-1000 Berlin 10, Germany
Telefon: (030)31002-0, Telefax: (030)31002-213

For InP based optoelectronics the $(Al_xGa_{1-x})_{0.48}In_{0.52}As$ material system (referred to as AlGaInAs) is advantageous compared to the GaInAsP system due to a higher conduction band edge discontinuity. It also meets the requirements of low waveguide absorption losses for long wavelength telecommunication applications. Good interface properties of the AlInAs/GaInAs interface are a stringent requirement for layer sequences within heterostructure devices. Especially, in thin layer structures with multiple heterojunctions device properties may be dominated by the interface quality.

In this work an analysis of CV measurements at AlInAs/GaInAs heterojunctions grown by MBE will be presented. Based on Kroemer's method /1/ the fixed interface state density and the conduction band edge discontinuity are evaluated. In addition, a theoretical fit to the measured data according to Whiteaway /2/ is used to verify the data. A self-consistent Kroemer analysis on the simulated carrier profiles is carried out to confirm our procedure. In all cases, excellent agreement of the calculated data using the different methods is obtained.

To obtain reliable data, especially for the band edge discontinuity, CV measurements on different types of structures are presented. Anisotype p/n junctions in wide-gap emitter HBT structures, isotype n^+/n junctions in HEMT type structures and homogeneously doped n/n junctions are analyzed and are found to deliver almost identical results. Fig. 1 shows the apparent carrier distribution

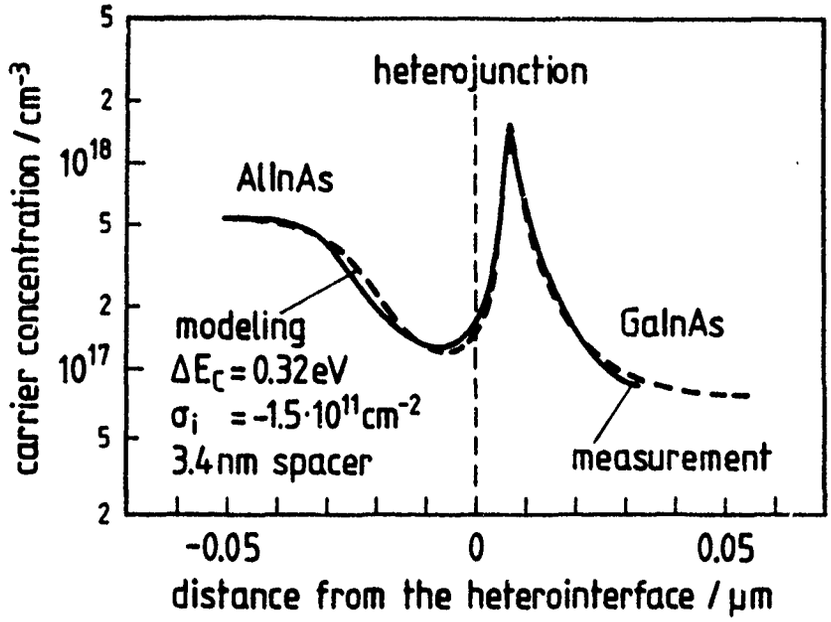

Fig. 1: Measured and modeled carrier profile across a n^+-AlInAs/n-GaInAs interface. (The theoretical fit is calculated according to ref. /2/).

deduced from a CV measurement in conjunction with an optimized simulated profile for a n^+-AlInAs/n-GaInAs junction. Excellent agreement is demonstrated. A conduction band edge discontinuity ΔE_c=0.32 eV is obtained. An interface state density σ_i=-1.5×10^{11} cm^{-2} is deduced /3/ In the case of $(Al_{0.4}Ga_{0.6})$InAs/GaInAs interfaces a density below 1.0×10^{10} cm^{-2} is deduced, demonstrating superior interface quality. This material also shows excellent morphology. For AlInAs/GaInAs the situation is worse which is reflected by an interface density up to 3×10^{11} cm^{-2}. This behaviour can be explained with the reduced morphological and crystalline quality of AlInAs compared to AlGaInAs, which may lead to inferior interfaces.

To optimize the AlInAs/GaInAs interface, the influence of the MBE growth conditions on the fixed interface density are examined. The growth temperature and the growth interruption time at

the interface are systematically varied. Low growth temperatures were found to reduce the interface density in agreement with the influence of the substrate temperature on the quality of AlInAs. In contrast, the influence of the growth interruption time on the heterojunction built-up is not yet clear. The trend observed so far, implies that long interruption times tend to reduce the fixed interface density due to a smoothening of the heterojunction during interruption.

The most dramatic reduction of the fixed interface density is found by suppressing the effusion cell flux transients. Measurements of AlInAs/GaInAs heterostructures with the Al flux transient suppressed by computer control are presented. A reduction of σ_i to values below 3×10^{10} cm^{-2} demonstrates the successful achievement of an improved interface. Consequently, using appropriate growth conditions and suppression of the flux transient will result in optimized AlInAs/GaInAs heterojunctions for interface sensitive devices like HEMTs and MQW lasers. These conditions and their influence on the measured conduction band edge discontinuity will be discussed.

/1/ H. Kroemer and Wu-Yi Chien, J. S. Harris, Jr. and D. D. Edwall:
Appl. Phys. Lett. 36, 295 (1980)

/2/ J. E. A. Whiteaway:
IEE Proceedings, Vol. 130, Pt. I, No. 4, 165 (1983)

/3/ H. G. Bach, in: Proc. Micro System Technol. 90, Ed. H. Reichel
(Springer, Berlin, 1990) p. 205

Si DELTA DIPOLE DOPING TO TUNE AlAs/GaAs HETEROSTRUCTURE BAND OFFSETS

L. Sorba[a,b*], G. Bratina[a], G. Ceccone[a,c], A. Antonini[a], and A.Franciosi[a,c]

[a]Laboratorio TASC dell' INFM, Area di Ricerca di Trieste
Padriciano 99, I-34012 Trieste, Italy
Tel.39-40-37561, FAX 39-40-226767
[b]Istituto di Acustica O.M. Corbino del C.N.R.
Via Cassia 1216, I-00189 Roma, Italy
[c]Department of Chemical Engineering and Materials Science
University of Minnesota, Minneapolis, MN 55455, USA

Tuning heterojunction valence and conduction band offsets has recently been made possible by the use of n^+-p^+ sheets grown in situ some 10nm from the heterojunction by molecular beam epitaxy[1] (MBE), or through electronegativity-induced charge transfer from a single impurity monolayer to the two semiconductors forming the heterojunction to generate a local dipole[2].

An exciting new technique to obtain high stability dipoles that effectively bridges the two other methods described above has been proposed for homojunction by Martin and co-workers[3] based on *ab initio* self consistent total energy calculations which examined the stability and electrostatics of abrupt Ge bilayers at GaAs-GaAs model polar interfaces. The resulting local dipole is expected to induce valence band offsets of 0.7-1.0eV. Since the calculated charge transfer per Ge atom prior to dielectric screening is about -1 electron per atom in the Ge monolayer which "replaces" Ga in the structure, and +1 electron per atom in the Ge monolayer replacing As, the calculations predict that the Ge bilayer will effectively act as a n^+-p^+ dipole layer. The corresponding structure should be more stable against impurity redistribution relative to conventional n^+-p^+ doping dipoles if it can be formed despite kinetic bottlenecks.

We studied the practical fabrication of elemental group IV bilayers within the interface region of AlAs-GaAs heterostructures. We elected to use Si rather than lattice-matched Ge layers because of the extensive literature available on Si δ-doping technology. The use of AlAs-Si-GaAs rather than GaAs-Si-GaAs as a system in which to test the effect predicted in Ref. 3 allowed us a simpler photoemission spectroscopy determination of the valence band offset.

All structures were grown on undoped GaAs(100) wafers. After chemical etching and oxide desorption, a 0.5μm-thick undoped or n-type (Si-doped, $6x10^{17}cm^{-3}$) GaAs buffer layer was grown using the procedure described elsewhere[4]. AlAs-GaAs heterostructures were formed by growing 10-30Å thick AlAs epitaxial overlayers on the GaAs(100) substrate, while GaAs-AlAs heterostructures were fabricated by growing 10-30Å thick epitaxial GaAs overlayers on a 200Å thick undoped AlAs(100) epitaxial substrate grown at 620°C on the GaAs buffer. Si layers were deposited at substrate temperatures in the 240-540°C range with consistent results, under As_4 flux. Si coverages were determined through flux calibrations performed on homogeneously doped GaAs layers[4], and are given here in monolayers (ML), in terms of the GaAs(100) surface atomic density (1ML=$6.25x10^{14}$ atoms/cm^2). During Si growth the RHEED pattern showed an intermediate 2x1 surface reconstruction at low (<0.2 ML) Si coverages,

followed by a sharp 3x1 recostruction troughout the 0.2-2 ML coverage range. Upon completion of the desired Si coverage, the Si shutter was closed, the substrate temperature was raised to the desired overlayer growth temperature, and overlayer growth was started by opening the Ga or Al shutter.

The valence band offset ΔE_V was obtained from the photoemission determined position of the Ga 3d or Al 2p core levels relative to the valence band maximum in the substrate, the position of the cation core levels relative to the valence band maximum in thick (200Å) overlayers, and the energy difference between the Al 2p and Ga 3d core levels at the interface. Using subscripts cl and v for quantities pertaining to the core levels and valence band maxima, respectively, it is:

$$\Delta E_V=[E_{cl}(Ga\ 3d)-E_V(GaAs)]-[E_{cl}(Al\ 2p)-E_V(AlAs)]+\Delta E_{cl}$$

The measured core separation $\Delta E_{cl}=E_{cl}(Al\ 2p)-E_{cl}(Ga\ 3d)$ at the interface is independent of overlayer thickness and can be directly used to monitor the Si-induced change in band offset. The experimental results are summarized in Fig. 1. We observe valence band offsets as low as 0.02eV (0.5ML of Si at the AlAs-GaAs(100) interface) and as high as 0.78eV (0.5ML of Si at the GaAs-AlAs(100) interface). This indicates that a Si induced local dipole of about 0.4eV is subtracted from or added to, respectively, the "intrinsic" heterojunction valence band offset.

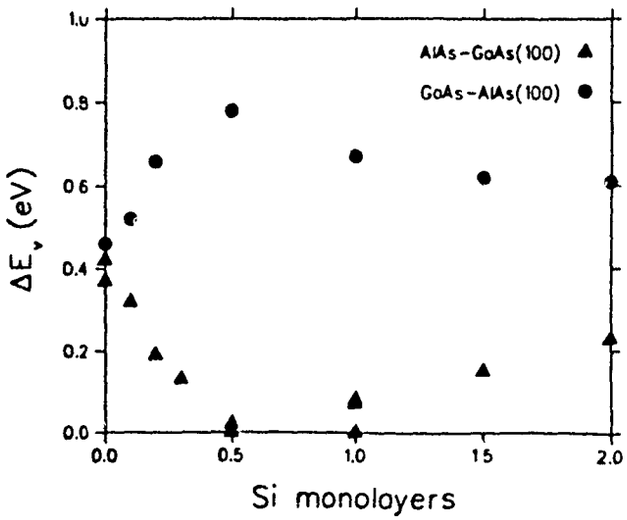

Fig. 1: Measured valence band offset for AlAs-GaAs(100) and GaAs-AlAs(100) in the presence of an interface layer of elemental Si. The Si interface layer thickness is given in monolayers (1ML=6.25×10^{14} cm^{-2}) The resulting Si-induced local dipole is subtracted from or added to, respectevely, the "intrinsic" band offset of 0.40±0.08eV.

Results for the coverage dependence of the Si 2p core intensity suggest that most of the Si atoms remain at the interface in all cases, rather than diffuse in the semiconductor bulk[5]. The direction and order of magnitude of the dipole is consistent with that expected on the basis of the results of Ref. 3, while the Si coverage dependence is not. For Si coverages up to 0.5 ML our results show excellent agreement with new recent calculations by M. Peressi et al.[6], where the variation of the interface dipole with Si coverage was calculated self consistenly using the local density functional approximation. These authors assumed[6] that the Si atoms are uniformly distributed over two consecutive atomic layers to ensure local charge neutrality at all Si coverages. A departure of the measured offset from theoretical predictions at coverages higher than 0.5 ML is attributed to Si diffusion [6].

In conclusion, we have shown that Si layers can be fabricated in the interface region of AlAs-GaAs heterostructures in order to tailor valence and conduction band offsets. Control of the Si coverage, As flux, and growth sequence results in a 0.8eV tunability range of band discontinuities.

This work was supported by the Consorzio Interuniversitario di Fisica della Materia (INFM) and by the Consorzio dell' Area di Ricerca di Trieste. The work at Minnesota was supported by the U.S. Army Research Office under grant No. DAAL03-90-G-0001. One of us (G.C.) would like to thank the Consiglio Nazionale delle Ricerche of Italy for the fellowship that supported his work at Minnesota.

REFERENCES

1)Capasso, F., Ann. Rev. Mater. Sci. 16, 263 (1986).

2)McKinley, J.T., Hwu, Y., Rioux, D., Terrasi, A., Zanini, F., Margaritondo, G., Debska, U., and Furdyna, J.K., J. Vac. Sci. Technol. A8, 1917 (1990), and references therein.

3)Munoz, A., Chetty, N., and Martin, R., Phys. Rev. B41, 2976 (1990).

4)Sorba, L., Bratina, G., Ceccone, G., Antonini, A., Walker, J.F., Micovic, M., and Franciosi, A., Phys. Rev. B (15 January 1991).

5) Ceccone, G., Bratina, G., Sorba, L., Antonini, A., and Franciosi,A., Surf. Sci. in press.

6) Peressi, M., Baroni, S., Resta, R., Baldereschi, A., submitted to Phys. Rev. B

SURFACE STRUCTURES OF EPITAXIAL $CoSi_2$ THIN FILMS GROWN ON Si(111) STUDIED IN-SITU BY SCANNING TUNNELING MICROSCOPY

R. Stalder*, N. Onda, H. Sirringhaus, H. von Känel, Laboratorium für Festkörperphysik, ETH Zürich, CH-8093 Zürich,Switzerland, Phone 01/377 22 78, Fax 41/1/371 59 89

The surface structures of epitaxial $CoSi_2$ films grown on Si(111) have been studied with a scanning tunneling microscope (STM) attached to the UHV environment of a MBE-machine. With the STM both atomic resolution and long range scans up to 4 microns are achieved. The samples used were (111)-oriented Si wafers with 3 inch diameter. The substrate-preparation procedure [1] resulted in smooth surfaces with parallel monolayer steps related to the mis-orientation of the wafer. The silicides were grown by stoichiometric coevaporation [2] of Co and Si at 300K - 400K. After annealing at $T_a > 600K$, continuous $CoSi_2$ films were achieved (about 10Å thick in the first growth step). After growth the samples were transferred under UHV conditions into a dedicated STM-chamber and the measurements were taken at 300K.

With the STM we have detected different reconstructions both on Si-rich and on Co-rich $CoSi_2$(111) surfaces [3]. On most samples unreconstructed areas with the expected hexagonal symmetry (corrugation up to 0.3Å with 50mV sample bias and 1nA current) are present. On Si-rich surfaces (2x1) reconstructed domains with chains perpendicular to the three equivalent ‹11$\bar{2}$› directions in the (111) plane of the fluorite structure of the silicide have frequently been found in addition to the unreconstructed areas. This reconstruction is formed when cooling the Si-rich surface below 470K, as evidenced by a (2x2) RHEED pattern. The measured corrugations were Δz = 1Å perpendicular to the chains and Δz = 0.15Å on top of them. We have performed a detailed analysis of high resolution STM micrographs (Fig. 1b) and propose consistent structure models for the reconstruction of the Si-rich surface at temperatures below 470K Two different types of phase boundaries between rotated (2x1) domains were detected, one being about 1Å higher than the surrounding areas and the other being lower because of point defects. The boundary between (1x1) and (2x1) domains can occur either "in-plane" without difference in height or "out-of-plane" with the (1x1) phase 1Å higher. It is not clear at present whether this 1Å step is due to electronic contrast or due to a combination of electronic and topographic contrast. In the latter case an additional atomic layer of Si atoms on top of the Si-rich surface is one possible explanation.

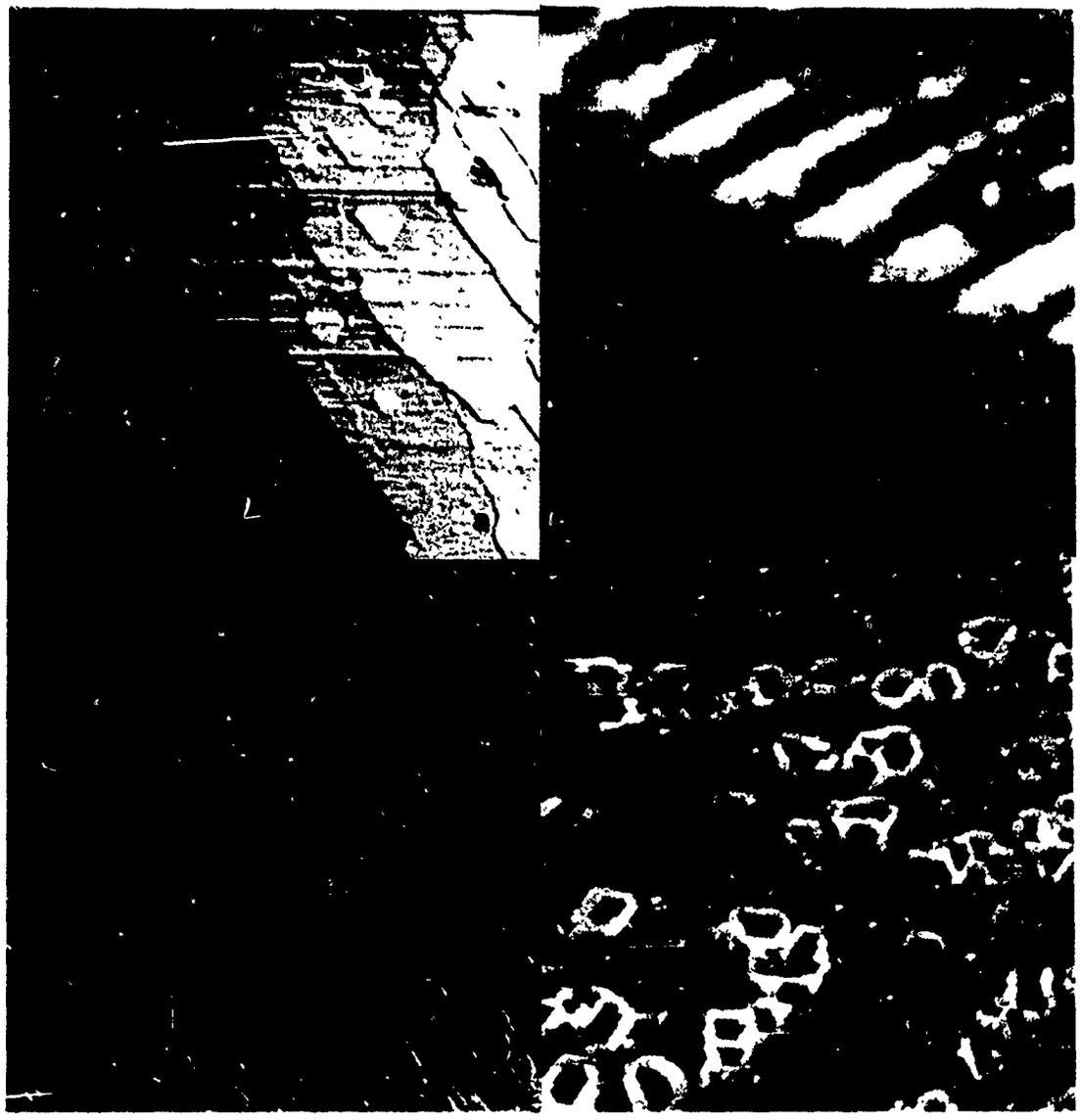

FIG. 1

STM micrographs of various $CoSi_2$(111) surfaces at different scales.

a) 14Å $CoSi_2$, Si-rich annealed at T_a = 800K, monolayer steps due to a misorientation towards [11$\bar{2}$] direction, "out-of-plane" boundaries between (2x1) and (1x1) surface domains are seen as curved lines nearly parallel to the steps. (sample bias V_T = +1V, tunneling current I_T = 1nA, scanning area A = 6000x6000Å^2), **b)** high resolution micrograph of an "in-plane" boundary region between unreconstructed (lower part) and (2x1) reconstructed (upper part) areas, 42 Å $CoSi_2$, Si-rich, T_a = 870K, (V_T = +50mV, I_T = 1nA, A = 60x60Å^2), **c)** 21Å $CoSi_2$, Si-rich, T_a = 800K, parallel monolayer steps (misorientation 0.3 degrees towards [11$\bar{2}$]) and pinholes up to 60Å deep, nucleation of small Si-islands at steps,(V_T = +1V, I_T = 1nA, A = 2x2μm^2), **d)** 21Å $CoSi_2$, Si-rich, T_a = 850K, high density of pinholes (40Å deep) with accumulated ring-structures, (V_T = +1V, I_T = 1nA, A = 4x4μm^2)

Another atomic arrangement was found on Co-rich prepared $CoSi_2$ surfaces. Small areas of (2x2) reconstruction (Δz up to 1.3Å) have been found mostly at steps. In these cases a (2x2) RHEED pattern occurred during annealing at temperatures of about 600K. With STM the surface exhibited unordered areas in coexistence with (2x2) reconstructed domains. We have to infer from this results that the silicide does not come up to a single-domain surface after this weak annealing. The transition from the Co-rich surface to the Si-rich one is a reasonable explanation for the occurrence of the (2x2) domains, as has already been proposed by Hellmann et. al. [4].

With the STM pinholes have been detected on numerous samples. The formation of pinholes in $CoSi_2$ thin films was related to the transformation from the Co-rich surface to the Si-rich one, the necessary Si being supplied by surface diffusion [5]. This is in agreement with the observation of a better stability of the Si-rich surface against pinhole formation during annealing. Another interesting fact is the depth of the pinholes. With the (macroscopically blunt) tips used in STM one can measure a lower limit for the depth of small and deep structures. Nevertheless we often detected the bottom of pinholes to lie underneath the substrate-silicide interface even in films grown under Si excess, exhibiting additional Si-islands. The driving force for Si out-diffusion appears obscure in this case. Evidence for micron-range surface diffusion of Si on Si-rich $CoSi_2$ surface at temperatures as low as 820K has been found, but on many samples an accumulation of material in ring-structures surrounding the pinholes was seen (Fig. 1c, 1d). Annealing 14Å thick $CoSi_2$ films at 820-920K under a weak Si-flux resulted in dewetting and in the formation of an electrically conductive silicide network.

In conclusion the surface of $CoSi_2$ is found to be rather complex, exhibiting sub-monolayer steps and different reconstructions depending on the growth stoichiometry and on the detailed annealing procedure.

[1] H. von Känel, J. Henz, M. Ospelt, J. Hugi, E. Müller, N. Onda, Thin Solid Films 184, 295 (1990)

[2] J. Henz, M. Ospelt, H. von Känel, SolState Common. 63, 445 (1987)

[3] J. Vrijmoeth, A. G. Schins, J. F. van der Veen, Phys. Rev. B 40, 3121 (1989)

[4] F. Hellmann, R. T. Tung, Phys. Rev. B 37, 10786, (1988)

[5] R. T. Tung, J. L. Batstone, Appl. Phys. Lett. 52, 648, (1988)

Dp1

CAPPING AND DECAPPING OF MBE-GROWN GaAs (001) INVESTIGATED WITH ASP, XPS AND RHEED

R.W. Bernstein
Norwegian Telecom Research Institute, P.O.Box 83
N-2007 Kjeller, Norway

B.O. Fimland*, A. Borg, A.P. Grande and J.K. Grepstad
University of Trondheim - NTH, Div. of Physical Electronics
N-7034 Trondheim, Norway
Fax: +47 7 591441

Condensation of a thin layer of elemental arsenic on molecular beam epitaxy (MBE) grown compound semiconductor surfaces has proved a practicable technique for preservation of clean, stoichiometric surfaces upon exposure to atmosphere. Desorption of the protective capping by thermal annealing in ultra-high-vacuum (UHV) environments has been found to produce epilayer surfaces with a low density of bandgap surface states[1-2]. In the present study, arsenic capping of MBE-grown GaAs(001) and decapping by heat treatment in UHV has been investigated with surface sensitive chemical and structural probes, such as Auger sputter depth profiling (ASP), x-ray photoelectron spectroscopy (XPS), and reflection high energy electron diffraction (RHEED). The measured Auger depth profiles show that a protective As capping of 300-400 nm thickness remains intact after exposure to atmosphere for more than 30 days. A thin layer of As-oxide, formed immediately upon exposure of the arsenic capping to air, desorbes after annealing in UHV at 250^{0}C. Subsequent heat treatment at 350-400^{0}C causes desorption of the residual elemental As capping and produces a clean GaAs(001) surface. The corresponding RHEED-patterns (for samples annealed in the MBE growth chamber) unveil a c(4x4) surface reconstruction. This surface superstructure is attributed to an As-terminated surface, with a chemisorbed arsenic overlayer of fractional monolayer coverage[3]. From XPS intensity analysis and the recorded RHEED patterns, we find that the "as grown" As-terminated GaAs(001)-(2x4)/c(2x8) epilayer surfaces is regenerated after annealing at 450^{0}C. A final heat treatment at 600^{0}C causes depletion of arsenic from the topmost

atomic layer an produces the RHEED patterns of a (3x1) surface reconstruction. In conclusion, this work presents a detailed analysis of the As capping technique for preservation and regeneration of clean, stoichiometric GaAs(001) epilayer surfaces. This technique facilitates long-term storage in air and safe transportation of samples between different UHV-systems and laboratories.

1. L.J. Brillson, R.E. Viturro, C. Mailhiot, J.L. Shaw, N. Tache, J. McKinley, G. Margaritondo, J.M. Woodall, P.D. Kirchner, G.D. Pettit, and S.L. Wright, J. Vac. Sci. Technol. B 6,1263 (1988).
2. W.M. Lau, R.N.S. Sodhi, S. Jin, S. Ingrey, N. Puetz, and A. SpringThorpe, J. Appl. Phys. 67, 768 (1990).
3. P.K. Larsen, J.H. Neave, J.F. van der Veen, P.J. Dobson, and B.A. Joyce, Phys. Rev. B 27,4966 (1983).

Dp2

Strain Measurement of Molecular Beam Epitaxially Grown $In_xGa_{1-x}As$ on InP(100) by Double Crystal X-ray Diffraction. The Effect of InAs Interfacial Layers

S A Clark*, J E Macdonald, D I Westwood and R H Williams

University of Wales College of Cardiff
PO Box 913
Cardiff CF1 3TH, Wales, UK
Tel: +44 222874000
Fax: +44 222874056

S J Barnett

Royal Signals Research Establishment
Great Malvern, Worcs WR14 3PS, UK
Tel: +44 684 822733
Fax +44 684 894540

Epitaxial $In_xGa_{1-x}As$ layers have been grown on InP(100) substrates with alloy compositions of x = 54.3% and 50.8% and thickness ranging from 0.04 μm to 5.0 μm. Double Crystal X-ray Diffraction was employed to evaluate strain via epilayer and substrate peak separation in the X-ray rocking curves of symmetric and asymmetric reflections. At first glance this technique appears straightforward, however it has been shown[1] by dynamical simulation that for epilayers of less than 0.5 μm a shift of the epilayer peak towards the substrate peak in the rocking curve is observed. The extent of this shift increases with decreasing thickness. We have carried out dynamical and more straightforward kinematic simulations of $In_xGa_{1-x}As$ to account for this shift in our measurement of strain and find excellent agreement between the two models. X-ray Photoelectron Spectroscopy and X-Ray Photoelectron Diffraction studies[2] of As_4 stabilised thermal deoxidation of InP substrates have revealed that a thin (~2ML) coherent interfacial InAs layer may be present between the InP substrate and the $In_xGa_{1-x}As$ epilayer. Both kinematic and dynamical simulations of the effect of this interfacial layer on

the phase of the interaction of the substrate and epilayer wavefields show an attenuation of the shift for compressively strained layers (x = 54.3%) and a reversal of the direction of the shift to being away from the substrate with decreasing thickness for the tensile strain series (x=50.8%). These factors have been applied to the experimental rocking curves and strain calculated, yielding a dispersion of results for thinner layers.

1. P.F Fewster and C.J. Curling, J. Appl. Phys. p4154 62 (1) 1987.

2. G. Hollinger, D. Gallet, M. Gendry, C. Santinelli and I Viktorovitch, J. Vac. Sci. Technol B8, 832 (1990).

SCATTERING PROPERTIES OF GaAs/AlGaAs Single QUANTUM WELL GROWN BY MBE

Wang Xinghua and Zheng Houzhi
National Lab. for Superlattices and Related Microstructures
and
Institute of Semiconductors, Academia Sinica, P. O. Box 912, Beijing 100083, China

For studying scattering of a two — dimensinal electron system (2DES), two characteristic time parameters — trasport scattering time τ_0 (classical scattering time) and single particle relaxation time τ_q (quantum scattering time) are usually used. The trasport scattering time τ_0 favors large—angle scattering over small—angle scattering and is experimentally determined by the zero—field conductivity:

$$\tau_0 = m^* \sigma_0 / ne^2 \qquad (1)$$

Quantum scattering time τ_q is an evaluation of the broadening of Landau levels. It can be deduced from the analysis of the magnetic field dependence of Shubnikov—de—Haas (SdH) oscillation amplitude at a given temperature and is fitted to the following relation:

$$\frac{\Delta\sigma_{xx}}{\sigma_{xx}} = \frac{2(\omega_0\tau_q)^2}{1+(\omega_0\tau_q)^2} exp(-\frac{\pi}{\omega_0\tau_q}) \frac{\xi}{Sinh\xi} \qquad (2)$$

where $\Delta\sigma_{xx}$ and σ_{xx} are the amplitude of the oscillatory magneto—conductivity and its mean value, respectively. $\xi/Sinh\xi$ is a temperature dependent term. Obviously, the relaxation time is sensitive to all scattering events. In general, τ_q is smaller than or equals to τ_0. The value of τ_0, τ_q and their ratio describe directly a dominant scattering mechanism which limits the mobility of 2DEG.

In present work, the mentioned above two scattering times of 2DES in GaAs/AlGaAs single quantum well (SQW) are studied by the conductivity and Landau level broadening, respectively. The results obtained from SQWs are also compared with those of GaAs/AlGaAs modulation doped heterostructures. The samples used in the study were grown by the molecular beam epitaxy (MBE). Quantum Hall Effect and Shubnikov—de—Haas oscillations were measured at 4. 2K. Basic parameters and two characteristic scattering times calculated by eq. (1), (2) are listed in Table 1. Table 1 shows that the two characteristic scattering times and their ratio are not quite identical for the samples of SQW due to the difference of the dominant scattering mechanism. It is well known that the scattering contributions from ionized— impurities and interface—roughness should be taken into account in a two—dimensional system. In the modulation doped heterostructures , the lattice matches well, the interface is atomically smooth. As a result the interface—rougbness scattering

can be negligible. The dominant scattering contribution is from ionized impurity centers which are spatially separated from 2DEG by an undoped spacer layer. The imputity scattering is a long-range potential and leads to that τ_0 is much greater than τ_q, i. e. $\tau_0/\tau_q \gg 1$.

However, it is much more complex for GaAs/AlGaAs SQW. In low—mobility quantum well such as sample # 47—1, the interfaces were intentionally grown without any attempt to reduce interface—roughness. Roughness scattering is one of the short— range potential and is expected to play an important role. The mobility of 3000 $cm^2/V \cdot s$ and the nearly same value of the two characteristic times were limited by the interface roughness scattering. This is remarkably similar to Si—MOS system where the surface—roughness scattering plays the main role. For the samples # 549 the usual layered structures on the top of GaAs buffer were replaced by undoped, Si — doped and undoped $(GaAs)_4/(AlAs)_2$ superlattices, respectively, so that the interface quality of the main quantum well was greatly improved. Transport scattering time and the ratio of the two characteristic scattering times are obtained for the samples # 549 and are much higher than that for the samples # 47. The results demonstrate that the amplitude of the quantum oscillations was mainly dominated by ionized impurity broadening of Landau level.

In conclusion, the main contribution to scattering in SQW with low mobility is from the interface roughness which is a short—range and results in $\tau_0 = \tau_q$. For SQW with high mobility, the special technology in the epitaxial process was used in order to reduce interface roughness. The ionized impurity scattering plays the dominant role in SQW as well as in modulation doped heterostructures. The two characteristic times are quite deffirent, that is $\tau_0 \gg \tau_q$ due to the scattering from ionized impurity centers.

Table 1. Sample Parameters at 4. 2K

sample number	quantum well				heterostructure	
	#47—1	#47—2	#549—2	#549—1	#43—1	#43—2
n ($\times 10^{11}$ cm^{-2})	12. 5	13. 3	7. 18	7. 18	3. 80	3. 95
μ ($\times 10^3$cm^2/V • S)	3. 0	9. 7	35. 4	35. 7	190	210
spacer width d (Å)	100	100	150	150	120	120
scattering time τ_0(ps)	0. 116	0. 372	1. 34	1. 36	7. 47	8. 30
relaxation time τ_q(ps)	0. 111	0. 121	0. 227	0. 217	1. 46	1. 31
τ_0/τ_q	1. 05	3. 07	5. 90	6. 26	5. 12	6. 34

RHEED Studies of the CdTe Growth Surface and the Orienation Independence of the CdTe-HgTe Valence Band Offset

C.R. Becker *, Y.S. Wu †, A. Waag,
R.N. Bicknell-Tassius and G. Landwehr
Physikalisches Institut der Universität Würzburg
D-8700 Würzburg, Federal Republic of Germany
Telephone: 931/8885776 Fax: 931/706297

The use of light to improve the quality of molecular-beam eptiaxially (MBE) grown II-VI materials and to enhance substitutional doping is one of the recent exciting developements in the growth of compound semiconductors. This will be discussed in detail in an another paper given by A. Waag at this conference. Suffice it to say that photoassisted MBE (PAMBE) greatly improves the structural as well as the electrical properties. Here we report on an investigation of the mechanisms of this process.

Only a few studies of the effect of high energy electrons (HEE) on the surface chemistry have appeared in the literature, even though one of the most widely used in situ surface analysis techniques is reflection high energy electron diffraction (RHEED). In fact, irradiation of the CdTe surface during growth by high energy electrons strongly influences the observed surface reconstruction and therefore the surface stoichiometry. Thus, this brings into question the applicability of RHEED and other such techniques to the investigation of CdTe and perhaps other materials.

---

*presenting the paper

†Institute of Physics, Chinese Academy of Sciences, Beijing

Laser illumination and HEE irradiation

In general, the Te-stabilized surface is smooth and its RHEED pattern displays strong half order reconstruction (HOR) in the [011] azimuth and weaker but clear HOR in the [03$\bar{1}$] azimuth. The Cd-stabilized surface is rougher and the corresponding RHEED patterns in the [010] and [001] display HOR. The stronger HOR in the [011] is always present, even in a Cd environment. Therefore in this work we have used the appearance of HOR in the [010], the first indication of Cd stabilization, to denote the desorption of excess Te. Furthermore we have used the appearance of HOR in the [03$\bar{1}$] as a measure of the desorption time of excess Cd from the Cd-stabilized surface.

Static CdTe Surfaces

Fig. 1 shows the effect of laser illumination and HEE on static CdTe surfaces, i.e., without growth. The time spent on checking RHEED patterns was as short as possible, 2 to 3 s, in order to minimize the effect of HEEs when not desired. It is obvious from Fig. 1 that both laser illumination and HEE irradiation accelerate the desorption of Te, whereby the effect of HEE irradiation is larger.

We found the persistence time of excess Cd on the Cd-stabilized surface at 300°C was 118, 26 and 16 min with HEE irradiation, laser illumination and neither one, respectively. Therefore, it is apparent that laser light and to a greater extent HEE decrease the Cd desorption rate appreciably.

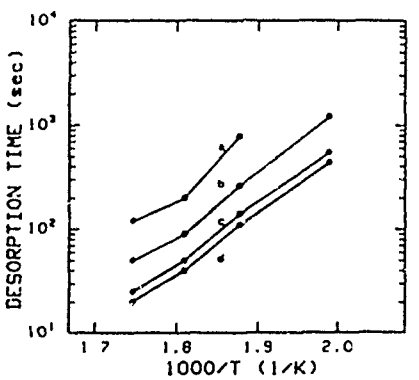

FIG 1 Desorption time of excess Te on the static surface with (a) neither laser nor high-energy electron (HEE) irradiation, (b) laser illumination, (c) HEE irradiation, and (d) both the laser illumination and the HEE irradiation The laser intensity was 45 ± 5 mW/cm²

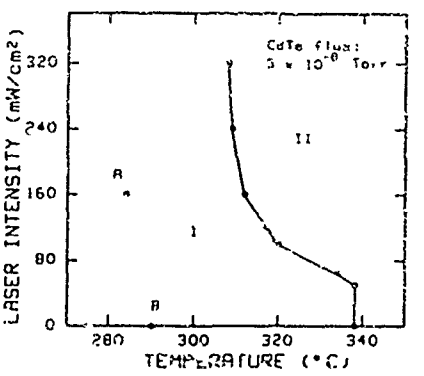

FIG 2 Laser intensity vs substrate temperatures Region I no HOR in the [010] azimuth appeared Region II HOR in the [010] azimuth appeared Points A and B were obtained in HEE irradiation and corresponding laser illumination

Dynamic CdTe growth surfaces

In this experiment the growth rate was approximately 2 monolayers per minute. The substrate temperature was lowered until the HOR in the [010] disappeared, i.e. the substrate was no longer Cd-stabilized, then at a number of temperatures the laser power was increased until HOR in the [010] reappeared.

From the curves in Fig. 2 we can make the following statements: Firstly, there is a laser power threshold, i.e., HOR in the [010] azimuth can not be found if the power density is less than a limiting value. Secondly, laser intensities ranging from 50 to 160 mW/cm^2 can induce large changes in the substrate temperature range over which HOR in the [010] can be observed. Lastly, below a certain temperature HOR in the [010] azimuth can not be observed regardless of laser power, for power densities less than 500 mW/cm^2. These observations are consistent with an optimum power density in the transport data and the photoluminescence spectra of PAMBE grown CdTe epilayers.
Points A and B are with HEE irradiation which again clearly demonstrates the large effect HEE irradiation has on the surface.

CdTe-HgTe Valence Band Offset

The valence band offset (VBO) for an abrupt CdTe-HgTe heterojunction has been determined by a number of X-ray photoelectron spectroscopy (XPS) investigations to be 0.35 ± 0.06 eV at room temperature. In addition the VBO has been shown to be temperature independent. A theoretical study using a self-consistent tight binding model has predicted a significant dependence on orientation, eg. 0.18 eV between the (110) and (100) surfaces. However, we have done XPS experiments on thin epilayers of HgTe, 7 to 40 Å thick, grown on (100), (110) and (111)B CdTe epitaxial layers, and have found the VBO to be orientation independent. In addition the surface structure of the CdTe interface, whether Te-stabilized or not with (1x1) or (2x1) reconstruction, also had no effect on the VBO.

Conclusions and Summary

Both high energy photons and to a larger extent HEE, increase the desorption of Te but decrease the desorption of Cd from (100) CdTe surfaces There is a laser intensity range over which a c(2x2) Cd-stabilized surface can be observed. It is possible that this is related to the optimum laser intensity for the growth of high quality CdTe epitaxial layers. Whether highly conducting CdTe can be grown using HEE is not known, but if it were possible, this effect could have many new and interesting applications. These results should lead anyone using RHEED to characterize growth surfaces to take a careful look to make sure that they are not changing what they are looking at by irradiating with HEE. We have observed no orientation dependence of the VBO in MBE grown CdTe-HgTe heterojunctions.

Acknowledgements

This project was supported by the Bundesministerium für Forschung und Technologie (Bonn) and the Deutsche Forschungsgemeinschaft.

UNION CARBIDE

Advanced Ceramics

PYROLYTIC BORON NITRIDE (PBN) FOR THIN FILM PROCESSES

Molecular beam epitaxy (MBE) and other thin film deposition techniques have become important processes for the growth of epitaxial layers on wafers of III-V and II-VI semiconductor crystals. PBN is the crucible of choice for containing the element or compound to be evaporated in MBE systems because of its purity and thermal and chemical stability. Vacuum baking of the PBN crucibles before use in MBE eliminates surface impurities which could contaminate the epitaxial layers.

PBN is used as a lining material for quartz vapor phase epitaxy reactors and as a coating on machined graphite parts for liquid phase epitaxy and for metalorganic chemical vapor deposition (MOCVD). Resistance heaters machined from a layer of PG deposited on a PBN substrate have now been developed. Power outputs in these heaters can exceed 45 W/cm^2 and heater life is exceptionally tolerant of rapid and frequent thermal cycling. An optional encapsulating layer of PBN can be deposited on the heaters to provide electrical insulation and minimize carbon contamination. These PG/PBN heaters are finding wide-spread use as source heaters for metal evaporation, semiconductor epitaxy, and CVD. There are recent examples describing the use of such heaters in MOCVD reactors for growing epitaxial films on a GaAs substrate.

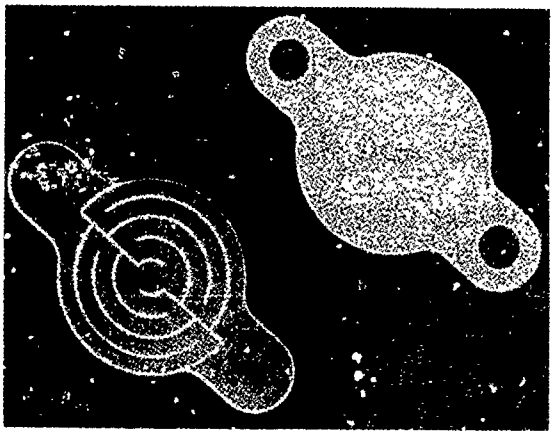

Fig 8. Boralectric™ PG/PBN resistance heaters (a) bare, (b) PBN-encapsulated (Boralectric™ is a trademark of Union Carbide Coatings Service Technology Corporation)

UNION CARBIDE CORPORATION
Advanced Ceramics

P.O. Box 94637, Cleveland, OH 44101
Telephone: (800) 822-4322, In Ohio: (216) 529-3900

INTERNATIONAL AFFILIATES

Tomoe Engineering Co. Ltd.
Daini Maruzen Building
9-2 Nihonbashi 3-Chome
Chuo-Ku, Tokyo 103
Japan
Telephone Tokyo (3) 274-0461

BN Products
Units 5/6 Penmaen, Ind. Est.
Pontllanfraith
Blackwood Gwent NP2 2DQ
Great Britain
Telephone: 0495 222557

SGTi (Societe Generale des Techniques Internationales)
17 Rue de Turbigo
75002 Paris
France
Telephone (4) 2360716

Sintec Keramik GMBH
Romantische Strasse 18
8959 Buching
West Germany
Telephone: (0 83 68) 825

PHOTOLUMINESCENCE CHARACTERIZATION OF STRAINED $Ga_xIn_{1-x}As/Ga_xIn_{1-x}As_yP_{1-y}$ QUANTUM WELLS GROWN BY GAS-SOURCE MOLECULAR BEAM EPITAXY

R. J. Simes*, A. Perales, F. Mollot+, M. Boulou, C. Starck, D. Bonnevie, M. Lambert++ and L. Goldstein

ALCATEL-ALSTHOM RECHERCHE, Route de Nozay,
91460 MARCOUSSIS, FRANCE
Phone: 33-1-6449-1920, Fax: 33-1-6449-0502

Strained $Ga_xIn_{1-x}As/Ga_xIn_{1-x}As_yP_{1-y}$ quantum wells (QWs) are of interest for 1.55 μm lasers because of their potential in reducing threshold current density and waveguide losses [1]. Initial laser results have already been achieved by MOVPE, CBE and GSMBE [2-4]. For MOVPE, dramatic reductions in laser threshold current density were noted for quantum well strains of up to 2.0% [2]. For CBE however, the threshold current density was observed to increase sharply for strains greater than ~1.0%, in contrast to theoretical predictions [3]. The only GSMBE strained quantum well laser [4] reported to date had a small negative strain, -0.35%. In the present work, we discuss the GSMBE growth and PL (4K and 300K) characterization of strained $Ga_{1-x}In_xAs$ QWs with $Ga_{0.2}In_{0.8}As_{0.4}P_{0.6}$, λ=1.18μm ($Q_{1.18\mu m}$) barriers for a wide range of QW strains (0 % to 2.7%). These results demonstrate the capability of GSMBE to produce strained-QW structures with excellent optical properties. The laser properties of samples prepared using different strains will be presented.

The samples for the present work were grown by GSMBE at a substrate temperature of 500°C in a Riber 2300 system. Pure AsH_3 and PH_3 (5-10 sccm for each gas) are introduced into the chamber through a single PBN cracker cell operating at 1050°C. Solid sources are used to supply the column III flux. The well thickness is determined by the deposition time, accounting for the III-flux transients. The QW x-value and thus the strain were determined by the growth of thick, lattice-matched quaternary layers with III fluxes identical to those used for the QW deposition. The values thus determined agreed well with the ones expected from ion-gauge beam flux measurements. The samples grown for PL characterization are similar to the active region of a laser and consist of 0.3 μm of InP, 0.1 μm of $Q_{1.18\mu m}$, the QW(s), 0.1 μm of $Q_{1.18\mu m}$, and a final InP cap layer.

Following the work of Gershoni et *al.*[5], we have calculated the valence band and conduction band energies of $Ga_{1-x}In_xAs$ as a function of x relative to the valence band

energy of InP[5]. These results were used to calculate the transition wavelength for strained quantum wells with $Q_{1.18\mu m}$ barriers using an envelope function approximation. The calculated results for different strains are presented in Fig. 1. In Fig. 1, we also show the experimentally-measured (PL) transition energies for single QW samples with different strains. The experimental agreement with theory is good.

In Fig.2, we present the measured low-temperature PL linewidth for strained (0.6% and 1.2%) and unstrained QWs of similar well width. We also show results for unstrained wells produced in other laboratories. For the 40Å well, the strain does not effect the linewidth. For the 20Å strained well, we observe two (FWHM=10meV) lines separated by ~6.4 meV; such splitting could be attributed to half-monolayer thickness fluctuations in the QW as reported by Thijs [6]. The linewidths observed for the present GSMBE samples are among the lowest ever reported for GaInAsP-GaInAs structures. At 300K, we have furthermore studied the PL efficiency under intense excitation with a 1.06 μm laser. These luminescence results will be compared and contrasted with the observed lasing properties of broad-area lasers samples prepared using similar strains.

We have presented a PL study of strained and unstrained QWs with $Q_{1.18\mu m}$ barrier layers. Our results demonstrate that GSMBE is a technique that can be used to reproducibly and uniformly produce strained QW structures over a wide range of strain. QW lasers with strains of 0.6%, 1.2%, and 2.0% are presently being fabricated, and these results will be presented.

The authors acknowledge J. C. Carballès for encouragement and RACE 1057 for partial funding of the present work. The technical support of R. Vergnaud and J. P. Chardon is gratefully acknowledged.

References

1. A. R. Adams, *Electronics Letters* **22**, 249 (1986).
2. P. J. A. Thijs et *al.*, *J. Crystal Growth* **105**, 339 (1990).
3. W. T. Tsang et *al.*, *Electronics Letters* **26**, 2035 (1990).
4. M. Pessa, "Current state of gas-source molecular beam epitaxy for growth of optoelectronic materials," submitted for publication.
5. D. Gershoni et *al.*, *Physical Review B* **39**, 5531 (1989)
6. P. J. A. Thijs et *al.*, *Appl. Phys. Lett.* **53**, 971 (1988).
7. W. T. Tsang et *al.*, *Appl. Phys. Lett.* **49**, 220 (1986).

+present address: L2M-CNRS, 196 av. H. Ravera, F92220 BAGNEUX, FRANCE
++present address: ALCATEL-CIT, ATC, NOZAY, F91620 LA VILLE DU BOIS, FRANCE

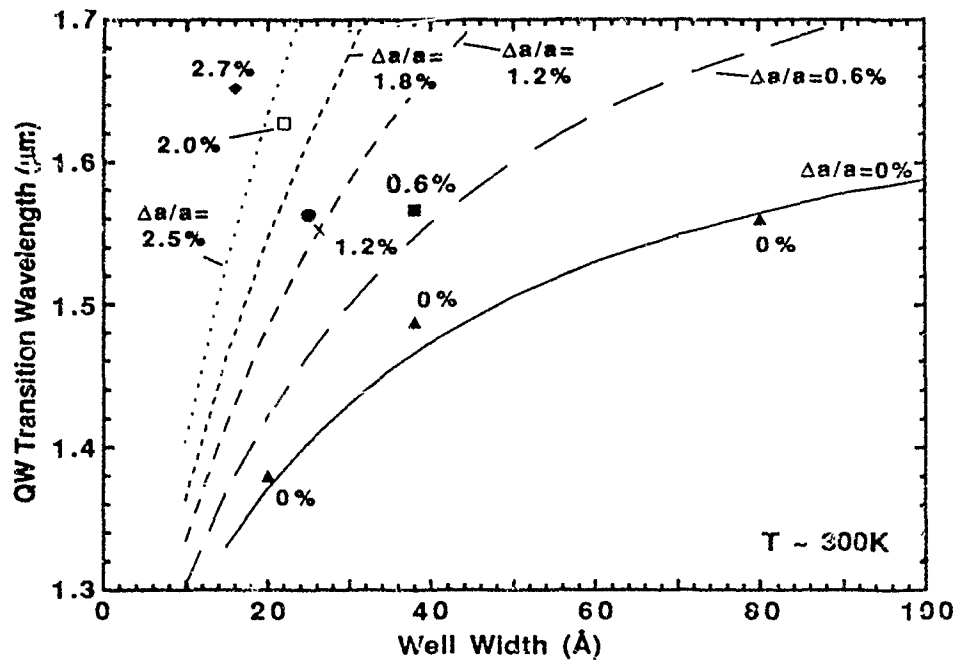

Fig. 1: Calculated QW transition energies for GaInAs wells with $Q_{1.18\mu m}$ barriers as a function of strain (0%, 0.6%, 1.2%, 1.8%, and 2.5%) and well thickness. Measured PL peak wavelength for wells of different thickness and strain.

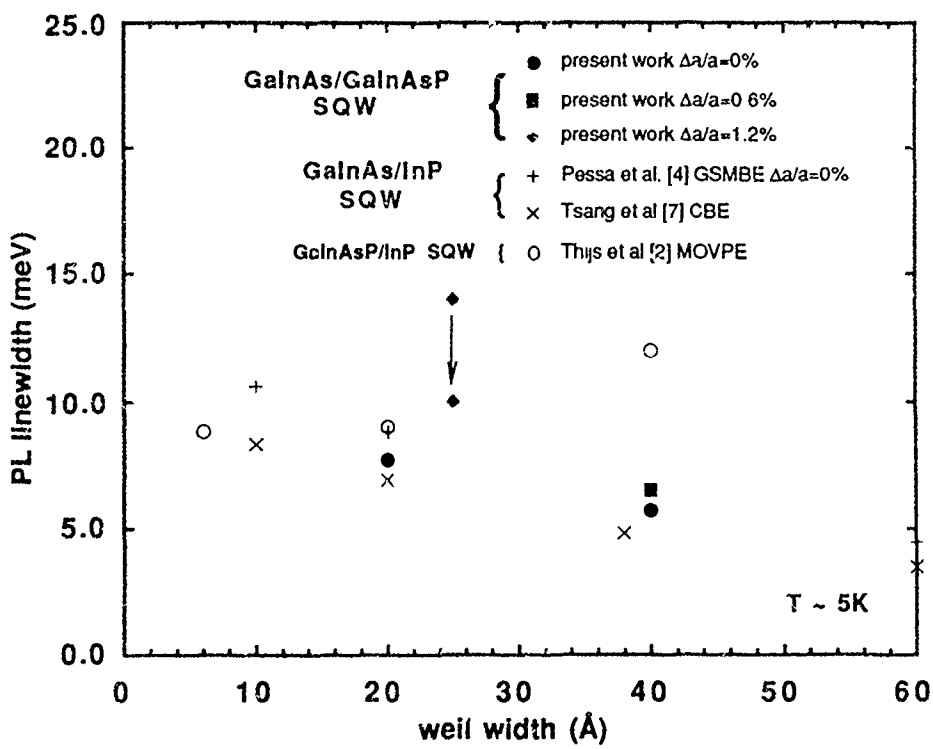

Fig. 2: Low-temperature PL linewidth vs. well width for strained and unstrained InGaAs/GaInAsP single QWs from the present work. Also presented are narrowest linewidths for unstrained QWs prepared in other laboratories by GSMBE, CBE, and MOVPE. The luminescence from the 25Å, 1.2%-strained well is the combination of two 10 meV lines.

The temperature dependence of the critical layer thickness in $In_{0.36}Ga_{0.64}As/GaAs$ single quantum wells grown by molecular beam epitaxy.

M. J. Ekenstedt, S. M. Wang and T. G. Andersson.
Department of Physics,
Chalmers University of Technology,
S-412 96 Göteborg. Sweden.
Tel. 031-723328, Fax 031-165176

ABSTRACT.

The critical layer thickness (CLT) for $In_{0.36}Ga_{0.64}As/GaAs$ single quantum wells has been studied by both reflection high energy electron diffraction (RHEED) and photoluminescence (PL) and found to be strongly dependent on the growth temperature. Thus for layers grown between 470 °C to 590 °C the CLT ranged from 55 Å to 15 Å respectively.

INTRODUCTION.

The problem of growing lattice mismatch materials has attracted interest the last decade not least due to the prospect of growing dislocation free GaAs on Si-surfaces. A number of groups have studied the strained growth of $In_xGa_{1-x}As$ on GaAs and especially the CLT by various techniques such as PL, X-ray double crystal diffraction (XRD), Hall effect, transmission electron microscopy (TEM), RHEED[1-5] and cathodoluminescence (CL). Theoretical models of the CLT exist only in terms of dislocation generation exemplified by the Matthews and Blakeslee (MB) model which have been capable of fitting calculations to many experimental results.

EXPRIMENTAL.

The growth of the samples was accomplished in a modified Varian 360 system, equipped with a growth chamber, preparation chamber and load lock. As in all MBE-systems with rotating substrate holders a correct reading of the substrate temperature is difficult to accomplish since the substrate thermocouple is not in direct contact with the substrate. For systems equipped with a pyrometer this is normally not a problem for temperatures above 500 °C but for temperatures below 500 °C the reading becomes uncertain. For this reason we developed a temperature probe working in a non growth position capable of giving correct temperature measurements from 375 °C to 530 °C with a reproducibility of ±2 °C[6-7].

The structures examined by PL were grown with a 1.0 μm buffer layer before depositing the $In_{0.36}Ga_{0.64}As$ quantum wells. Each sample contained a series of $In_{0.36}Ga_{0.64}As$ SQW's, grown without interruption, each QW with increasing thickness and separated by 500 Å GaAs layers. The samples analyzed during growth by RHEED at 10 kV, were grown with a 0.5 μm GaAs buffer layer before depositing the $In_{0.36}Ga_{0.64}As$ film. The in situ RHEED-pattern was recorded by a Panasonic VHS camera. This diffraction pattern was later analyzed by a Teragon 4000 image processing system to determine the change in lattice parameter with increasing film thickness.

RESULTS AND DISCUSSION.

Our result using both RHEED and PL measurements showed a strong growth temperature dependence for the CLT. In figures 1a and 1b, the results from the RHEED measurements are presented. A dramatic change of the lattice parameter can be seen as the layer thickness increases, indicating a relaxation of the lattice. The RHEED pattern also became spotty in the regime where the lattice parameter changed, due to a change in growth mode from two dimensional (2D) to three dimensional (3D) growth.

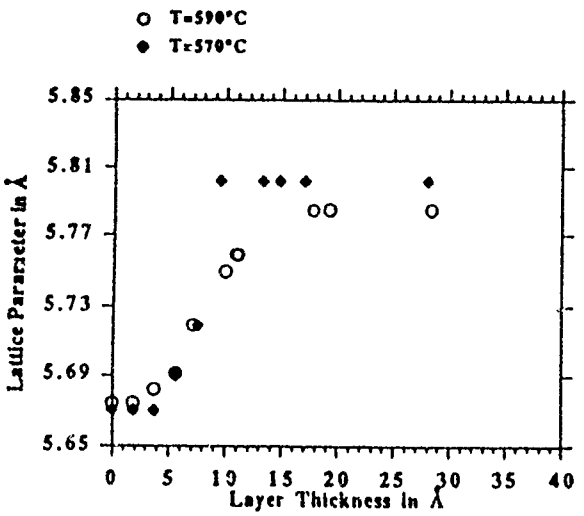

Fig 1a.

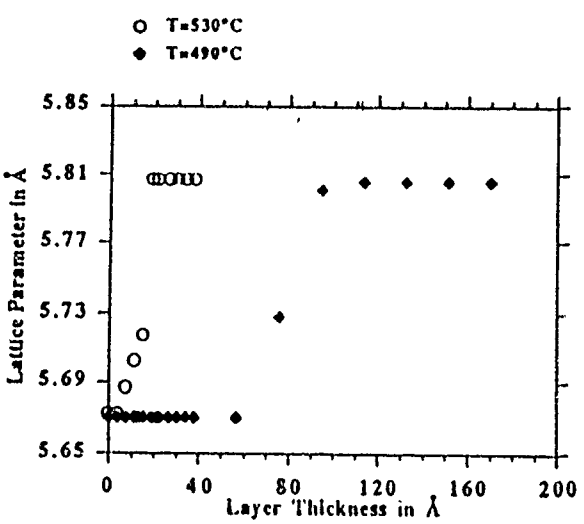

Fig1b

The lattice constant of $In_xGa_{1-x}As$ has been studied earlier[3-5] in the temperature regime up to 520 °C by RHEED and these results indicated a temperature dependent CLT. A change in growth kinetics when the CLT was reached was suggested by Whaley and Cohen[3,4]. This change has theoretical support by a model by Berger et. al.[5] which, based on thermodynamic consideration, argue that the minimum free energy surface changes from 2D to 3D in a strained system.

The results from PL-measurements are shown in figure 2 were the critical layer thickness as a function of growth temperature is shown. The CLT is here determined by the onset of 3D growth in which PL is shown as a broad low intensity peak becoming blue shifted with increasing excitation intensity. The blue shift can be explained in terms of the presence of two growth modes. Because of the island growth the surface is not flat and the thickness will vary over the surface. Part of the quantum wells, grown in a 3D mode are thicker and will have lower confined energy levels than the quantum wells grown in the 2D mode. At low excitation the carriers occupy only the lower energy levels. As the excitation increases the lower energy levels saturate and the recombination process is shifted towards the higher confined energy levels, hence the observed blue shift. Samples were grown from 410 °C to 590 °C but samples grown below 470 °C provided no PL-emission. The sample grown at 590 °C shows a larger CLT than the sample grown at 570 °C which is due to a decrease in the In incorporation rate at high temperatures.

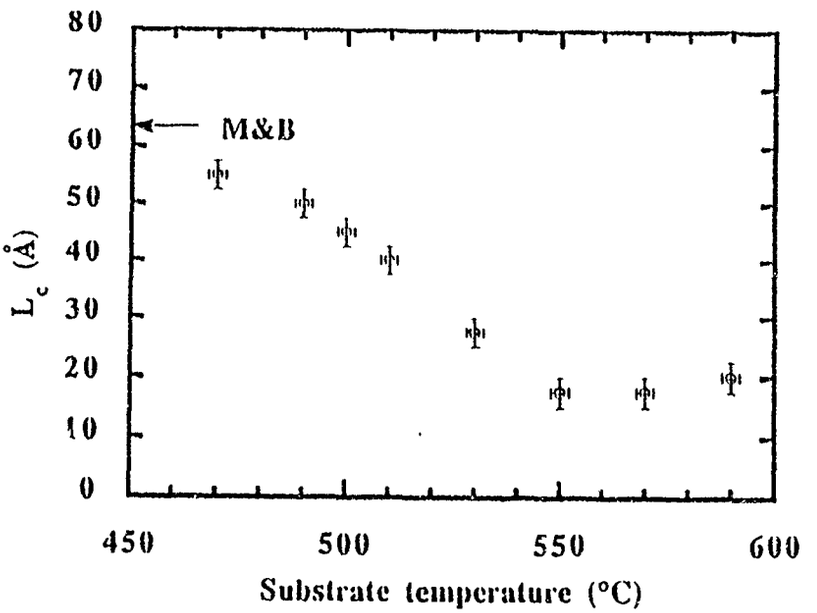

Fig 2.

References.

1) G. L. Price, Appl. Phys. Lett. 53, 1288,(1988)

2) B. Elman, E. S. Koteles, P. Melman, C. Jagannath, Johnson Lee, and D. Dugger, Appl. Phys. Lett. 55, 1659 (1989)

3) G. J. Whaley and P. I. Cohen, J. Vac. Sci. Technol. B6, 625 (1988).

4) G. J. Whaley and P. I. Cohen, Appl. Phys. Lett. 57, 144 (1990)

5) P. R. Berger, K. Chang, P. Bhattacharya, and J. Singh, Appl. Phys. Lett. 53, 684 (1988)

6) M. J. Ekenstedt, T. G. Andersson and H. Millqvist, Proc. of the 14th Nordic Semicond. meeting, Århus, Denmark, 47 (1990)

7) M. J. Ekenstedt and T. G. Andersson, unpublished.

OBSERVATION OF TYPE-I TO TYPE-II TRANSITION IN STRAINED $In_{0.22}Al_yGa_{0.78-y}As/GaAs$ QUANTUM WELLS GROWN BY MBE

S M Wang, T G Andersson, M J Ekenstedt and V D Kulakovskii

Department of Physics, Chalmers University of Technology

S-41296 Göteborg, Sweden

Quantum well (QW) structures of quaternary semiconductor alloys become progressively more interesting. Devices like quantum well lasers, photodiodes and optical modulators based on $In_xAl_yGa_{1-x-y}As$ related heterostructures have been demonstrated but the physics behind such materials is still in the initial stage[1-3]. Here we present photoluminescence (PL) measurements from an $In_{0.22}Al_yGa_{0.78-x-y}As/GaAs$ ($0 \le y \le 0.12$) multiple QW structure. The dependence of PL excitonic emission upon the Al concentration y has been studied and a transition from type-I to type-II band edge alignment was found for $0.09 < y < 0.12$.

The sample was grown on a (001)-oriented semi-insulating GaAs substrate using a modified Varian MBE-360 system. Figure 1 shows the structure in which six 100 Å thick quaternary alloy layers, with different Al concentration y (y= 0, 0.03, 0.06, 0.09 and 0.12) but fixed In concentration x=0.22, are sandwiched by GaAs cladding layers. One $GaAs/In_{0.22}Al_{0.12}Ga_{0.66}As/GaAs$ sequence is further cladded by two $Al_{0.15}Ga_{0.85}As$ barriers. To assign the emission peaks reliably, the structure was etched QW by QW using a solution of H_2SO_4:H_2O_2:H_2O (1:8:80) and the etching depth was then checked by a surface profiler (α-step). Photoluminescence measurements were performed at 77 K with a 40 mW He-Ne laser as an excitation source. The PL signal was dispersed by a Spex 1704 monochromator and detected with a cooled S-1 photomultiplier, a conventional lock-in amplifier and a PC for data acquisition.

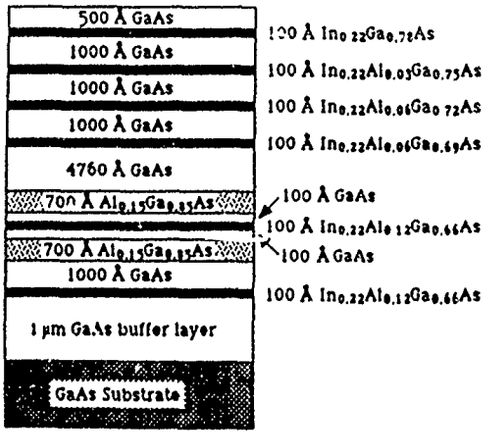

Figure 1. The sample structure.

Figure 2 shows the PL spectra in which spectrum 1 is from the whole structure and spectra 2-6 are taken after selective etching one-by-one of the first five QW's. The 1.505 eV peak observed in all spectra corresponds to free exciton emission from bulk

GaAs while the other four well pronounced excitonic peaks at $h\nu$=1.317, 1.365, 1.4165 and 1.4645 eV in spectrum 1 are associated with the QW's. After subsequent removal of the QW's, they are assigned to excitonic emission from layers with y=0, 0.03, 0.06 and 0.09, respectively. The emission from the QW with y=0.12 becomes pronounced only when the deep QW's with smaller Al content are removed, as illustrated by spectra 4-6. It is seen from spectrum 5 that the structure, containing two extra $Al_{0.15}Ga_{0.85}As$ barriers, reveals a PL peak at 1.481 eV, which also appears in spectrum 4 as a weak shoulder at the high energy side of the excitonic peak from the y=0.09 QW under high excitation density. However, this is not the case for the further etched structure without the $Al_{0.15}Ga_{0.85}As$ barriers. No emission related to this quaternary alloy layer has been found even under high power density, see spectrum 6. The weak emission peak at 1.49 eV is associated with impurities (carbon) in bulk GaAs.

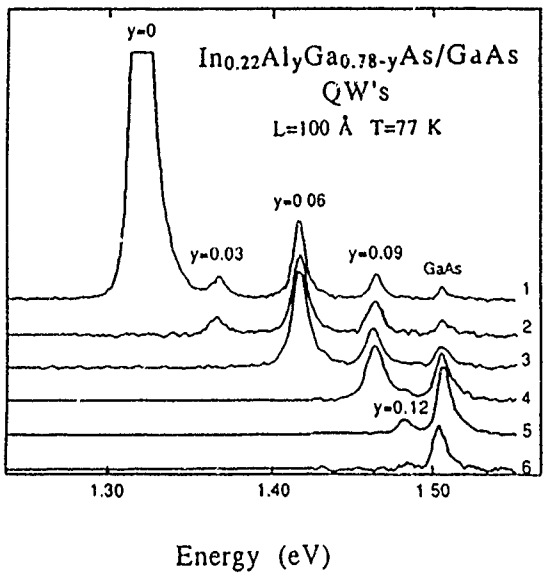

Figure 2. Photoluminescence spectra of the $In_{0.22}Al_yGa_{0.78-y}As/GaAs$ multiple QW structure at 77 K. The spectra 2 to 6 are recorded when the QW's with smaller Al concentration are subsequently removed by etching.

The observed behaviour of the PL emission in spectra 4-6 indicates a type-II band edge alignment for the $In_{0.22}Al_{0.12}Ga_{0.66}As/GaAs$ heterostructure. For the structure without the $Al_{0.15}Ga_{0.85}As$ barriers, either electrons or holes lose confinement and move away from the interfaces, resulting in a low spatial overlaps of electron and hole wavefunctions and thus strongly reducing the PL intensity (c.f. spectrum 6). When the two $Al_{0.15}Ga_{0.85}As$ layers are present they act as barriers to block carriers and a type-II QW structure is formed. In this case the wavefunctions of electron and hole near the interfaces have certain overlaps causing carrier recombination and thus PL emission stronger than the former case.

We corrected the PL peaks for the exciton effect by adding an exciton binding energy of 8 meV, measured by Hou et. al.[4] on 100 Å thick $In_{0.13}Ga_{0.87}As/GaAs$ QW's. The obtained transition energy, $E_{PL}(y)$, was found to follow a straight line for $y \leq 0.09$.

The $E_{PL}(y)$ can also be expressed as $E_{PL}(y)=E_e(y)+E_{hh}(y)+E_g^s(0.22,y)$, where $E_e(y)$ and $E_{hh}(y)$ are quantized energies of electrons in the conduction band and heavy holes in the valence band respectively and $E_g^s(0.22,y)$ is the strained band gap. The influence from the band edge offset is small. For the barrier height less than 250 meV, a variation from 0.9 to 0.5 in the conduction band edge offset results in a change of $E_e(y)+E_{hh}(y)$ by less than 4 meV. Based on this and the results of $E_{PL}(y)$, we calculated $E_g^s(0.22,y)$ and found

$$E_g^s(0.22,y)=1288+1814y \qquad (\pm 2 \text{ meV}) \qquad (1)$$

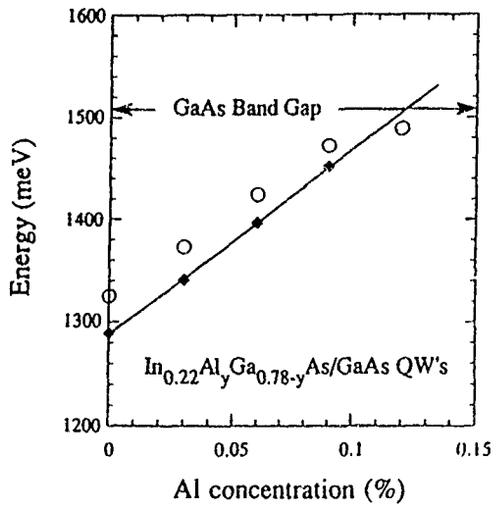

Figure 3. The measured energy of the PL peaks after correction for the exciton effect, $E_{PL}(y)$ (open circles), and the strained energy band gap of the $In_{0.22}Al_yGa_{0.78-y}As$ alloy, $E_g^s(0.22,y)$ (solid squares), as a function of the Al concentration y.

The value 1288±2 meV at y=0 allows us to check the real In concentration giving x=0.214±0.002, which is in very good agreement with the nominal value, x=0.22. Equation (1) together with $E_{PL}(y)$ are represented in Fig. 3. The extrapolation of the $E_g^s(0.22,y)$ to y=0.12 results in a value 1.506 eV, which is 25 meV larger than the observed PL emission energy. Correction for the exciton in a type-II QW is not expected to account for this large difference. A type-I band line-up with the quaternary alloy as barriers is also excluded because that causes an emission energy higher than that of bulk GaAs (1.508 eV) which contradicts our result. Therefore the only possibility is a type-II band edge line-up. We believe that such a transition from type-I to type-II occurs for $0.09<y<0.12$. A final comment is that MBE allows a highly controlled growth of lattice mismatched quaternary compounds.

References:

1 E. P. O'Reily and G. P. Witchlow, Solid State Commun. **62**, 653 (1987)
2 G. P. Kothiyal, S. Hong, N. Debbar, P. K. Bhattacharya, and J. Singh, Appl. Phys. Lett. **51**, 1091 (1987)
3 J. M. Gerard, J. Y. Marzin, C. d'Antertoches, B. Soucail, and P. Voisin, Appl. Phys. Lett. **55**, 559 (1989)
4 H. Q. Hou, Y. Segawa, Y. Aoyagi, S. Namba, and J. M. Zhou, Phys. Rev. B**42**, 1284 (1990)

STRAINED LAYER DEVICES FOR OPTICAL COMPUTING APPLICATIONS.

R. Grey*, P. A. Claxton, J. Woodhead, A. S. Pabla, M. H. Moloney+.

Dept. of Electronic and Electrical Engineering,
The University of Sheffield,
Mappin St.,
Sheffield.
S1 3JD
U.K. Tel. (0742) 768555 Fax. (0742) 726391

+Optronics Ireland Research Centre,
Dept. of Pure and Applied Physics,
The University of Dublin,
Trinity College,
Dublin 2,
Ireland. Tel. +353-1-772941 Fax. +353-1-6798412

Much interest is being shown in the effects of strain in III-V semiconductor devices and the possible benefits which may be obtained by the incorporation of materials of different lattice parameters in Low Dimensional Device (LDD) structures. Such benefits include greater flexibility in design of device structures, a larger bandgap range and useful novel properties due to the strain itself.

In particular we have been investigating the InGaAs/(Al)GaAs system with the intention of producing a range of device structures in which these benefits are expected to provide useful improvements in device performance. The types of device structure we have grown include p channel MODFET's, MQW pin's for APD and modulator devices, AFPM's and VCSEL's. In this paper we review work that we have done to optimise the growth conditions involved in the growth of these structures and constraints that are known to exist.

A particular aim of the work that we are carrying out in the InGaAs/(Al)GaAs system is to provide devices for optical computing-neural network applications. For this purpose this material system has the advantage of a transparent substrate allowing

flexibility in the interconnection methods used. It is a lower cost alternative to the lattice matched InGaAs/InP system which, in MBE, suffers from problems of As/P incorporation control.

We have been able to grow high quality material in this system e.g. a 9nm SQW $In_{.11}Ga_{.89}As$/GaAs having a PL FWHM of 1.2meV @ 4K. InGaAs/GaAs MQW pin's with various In fractions up to .3, which have applications for optical modulation at wavelengths around 1μm, have been grown with low leakage currents although they have low contrast ratios. Significant improvements in performance have been obtained by changing to an AFPM structure where an AlAs/GaAs Bragg reflector is used beneath the resonant cavity. We have grown such a structure from which devices have been produced in the normally off mode with an on/off ratio of 5.7dB at a low applied voltage of 4V. The same structure has also been tested in an all optical switching and modulation mode. A significant improvement in contrast ratio to 15:1 was obtained in this mode together with a low insertion loss of 1.25dB. Further optimisation is expected to lead to improvements and suggests that this device is likely to be very useful for all optical computing systems.

In producing this device it was discovered that the layer thicknesses varied across the 2" wafer so as to vary the resonant wavelength of the cavity while the InGaAs quantum well emission remained relatively constant being mainly controlled by the In fraction in the structure we had chosen. This would make such a wafer useless for a large array of such devices. To counter this, steps have been taken to improve the uniformity. Initial results on test structures, (AlAs/GaAs Bragg reflector stacks) indicate a much improved uniformity with thickness variations over the whole wafer of less than 1.7% as measured by double crystal X-ray diffraction and SEM. We have yet to repeat the growth of an AFPM but confidently expect a significantly improved result.

MBE Growth of Doped CdTe Thin Films and CdTe-CdMnTe-Quantum Wells and their Characterization

A.Waag *, S.Schmeusser, R.N. Bicknell- Tassius, Y.S. Wu†
T. Kuhn, B. Schmied, D.Yakovlev ‡, W. Ossau and G. Landwehr
Physikalisches Institut der Universität Würzburg
D-8700 Würzburg, FRG

Phone 0049-931-888-5779 Fax 0049-931-706297

1 Doping of CdTe films and the compensation mechanism

The II-VI semiconductors feature bandgaps ranging from the near ultraviolet to the far infrared. As a consequence, these materials could be used in a wide variety of electronic and especially optoelectronic devices [1,2]. However, their use in device applications has been severely limited because of the problem of controlling their electrical properties through substitutional doping [3].

---

*presenting the paper

†Institute of Physics, Chinese Academy of Science, Beijing

‡Ioffe Physico-Technical Institute, Leningrad

Substitutional doping of CdTe and other II-VI semiconductors has been a longstanding problem. The strong tendency towards self-compensation in these materials is the reason for the generally poor activation of dopants. The introduction of dopants is generally accompanied by the formation of dopant-defect complexes which provide the compensation mechanism [7,8]. Nonequilibrium thin film growth techniques may provide a means to reduce the formation of the compensating centers. In particular, the photoassisted MBE technique appears to greatly reduce the density of the self-compensating centers. During the photoassisted MBE growth, the growth surface is illuminated by photons with energies usually well above the band gap of the growing semiconductor [4,5,6].
These photons can influence the growth mechanism in different ways, including enhancement of surface migration of constituent atoms, modification of surface bonding, conversion of surface molecules into atoms, and modification of surface potentials through generation of photoexcited electron-hole pairs.
In the first part of this contribution, the influence of different growth parameters including power density and additional Cd-flux on the self- compensation of CdTe epitaxial films is investigated in detail. The results give insight in the compensation mechanism as well as the Photoassisted MBE mechanism.
Photoassisted MBE and growth under additional Cd-flux have been found to have very similiar influence on the photoluminescence spectrum, transport properties and surface reconstruction, respectively. These facts lead us to the conclusion that laser illumination during growth changes the surface stoichiometry to a more Cd-rich surface which then suppresses the self- compensation of the CdTe material. This shows that the compensation mechanism of (in our case) indium donors obviously is provided via Cd vacancies. The magnitude of compensation in doped CdTe thin films is derived by transport and photoluminescence measurements. As a result the In-doped CdTe films grown by conventional MBE are highly compensated, wheras the PAMBE-grown In-doped CdTe films are less than 20 % compensated.

2 Growth and Characterization of CdTe-CdMnTe single quantum wells

The second part of this contribution deals with the growth and characterization of CdTe-CdMnTe single quantum wells. Such dilute magnetic semiconductor (DMS) materials like CdMnTe show very interesting (magnetic) properties including a giant Faraday rotation, enhanced effective g-factor and the formation of magnetic polarons, which are generated by the magnetic moment of the Manganese ions and its interaction with the conduction electrons [9].

In particular, a magnetic polaron is an exciton, which has polarized the manganese spins sitting inside its exciton Bohr radius and therefore experienced an energy decrease.
We report results of photoluminescence (PL) and reflection measurements on thin CdTe-CdMnTe single quantum wells with well thicknesses ranging from 6Å to 60Å. The PL line widths are in general smaller than what one would expect from a one monolayer thickness fluctuation of the quantum well. We conclude that the interface is rough on a scale smaller than the exciton radius. Laser illumination during growth doubles the linewidths, indicating that photoassisted MBE enhances the quality of the interface.
From reflexion measurements we find an increasing longitudinal-transverse exciton splitting with decreasing well thickness for single quantum wells as thin as 6Å. The photoluminescence spectra of such single quantum wells show very narrow (3meV) peaks, if a resonant excitation energy for the incoming photons is chosen. In this case excitons are excited into localized states. The narrowing of the PL features makes it possible to detect for the first time free magnetic polarons in quantum well structures. In the photoluminescence spectrum the free magnetic polaron is identified by its temperature as well as magnetic field dependence.

3 Acknowledgements

This project was supported by the Bundesministerium für Forschung und Technologie (Bonn).

References

[1] F.V. Wald, Rev. Phys Appl. **12, 277(1977).**

[2] R.O. Bell, Rev. Phys. Appl. **12**, 391(1977).

[3] Y. Marfaing, Rev. Phys. Appl. **12**, 211 (1977).

[4] R.N. Bicknell, N.C. Giles, J.F. Schetzina, Appl. Phys. Lett. **45**, 1095(1986).

[5] R.N. Bicknell, N.C. Giles, J.F. Schetzina, Appl. Phys. Lett. **49**, 1735(1986).

[6] R. N. Bicknell-Tassius, A. Waag, Y. S. Wu, T. A. Kuhn, W. Ossau, J. Crystal Growth **101**,33(1990).

[7] D.Wegener, E.A.Meyer, J.Phys.:Condensed Matter **1**,5403(1989).

[8] R.Kalish, M.Delcher, G.Schatz, J.Appl.Phys **53** ,4793(1982).

[9] J.K.Furdyna, J.Appl.Phys **64**,R29(1988).

Large Piezoelectric Fields in (111) CdTe-CdZnTe Quantum Wells

J.Cibert*, R.André, C.Deshayes, Le Si Dang, S.Tatarenko
Laboratoire de Spectrométrie Physique
Université Joseph Fourier Grenoble France
G.Feuillet, P.H.Jouneau, R.Mallard, K.Saminadayar
Département de Recherche Fondamentale
Centre d'Etudes Nucléaires Grenoble France
Mail: DRF-SPh-PSC, CENG, 85X, 38041-Grenoble, France
Phone: 76 88 34 95 Fax: 76 88 51 53

Strained heterostructures grown along a polar axis may exhibit very peculiar optical properties due to the existence of a strong piezoelectric field which completely modifies the band configuration. This specificity was pointed out theoretically in 1985 [1]. Experimental evidences first in GaAs-GaInAs are much more recent[2] but rapidly spreading to other materials such as CdS-CdSe, GaSb-AlSb or CdTe-CdZnTe. In the last case the elimination of twins during the growth and at the mismatched interfaces allows to grow heterostructures with good optical properties. Thus we could obtain a direct measure of the built-in electric field from samples associating on the same CdZnTe buffer layer several quantum wells with different thicknesses. In Photoluminescence and in Photoreflectance the transition energy exhibits a large redshift almost linear in the QW thickness, with a slope equal to the built-in field. The variation of the field with the buffer alloy composition is also described.

Samples are grown by Molecular Beam Epitaxy on (001) GaAs substrates. In order to avoid the formation of twins during the growth of (111) CdTe slightly misoriented substrates are used. When the CdTe layer is 500-1000 angstroem thick we switch to ZnTe or CdZnTe to grow a 2μm thick buffer layer. This layer is almost completely relaxed at the temperature of growth and it suffers only a weak residual strain at room temperature or lower due to the difference in thermal expansion between the II-VI layer and the substrate. As will be seen below twins are formed to accommodate the mismatch and the growth conditions have to be chosen to avoid them propagating across the entire sample. Before the growth of the active heterostructure the

ZnTe or CdZnTe surface is smoothed so that a c(8x4) or a (2V3x2V3) reconstruction is seen: these surfaces are those where clear RHEED intensity oscillations are recorded on non-tilted substrates[3].

We first tried to grow CdTe-ZnTe QWs along (111). The mismatch is high (6%) and the critical thickness is expected to be low: for CdTe on (001) ZnTe we measured h_c=5 monolayers, and since CdTe is slightly harder along (111) we could expect a slightly smaller critical thickness along (111). However a strong variation of the RHEED specular intensity is observed around 2ML (on nominally (001) substrates), and we could not observe Photoluminescence from QWs thicker than 2ML while thinner QWs nicely luminesce. Transmission Electron Microscopy confirms the relaxation of the thicker QWs in the form of a dense array of twins at the interface[4].

Thicker QWs can be grown with CdZnTe barriers. In order to get a clear evidence of the built-in field we grew samples including on the same $Cd_{1-x}Zn_xTe$ buffer layer several CdTe- $Cd_{1-x}Zn_xTe$ QWs with different thicknesses[5]. Figure 1 displays low temperature Photoluminescence and Photoreflectance spectra for a sample featuring four QWs.

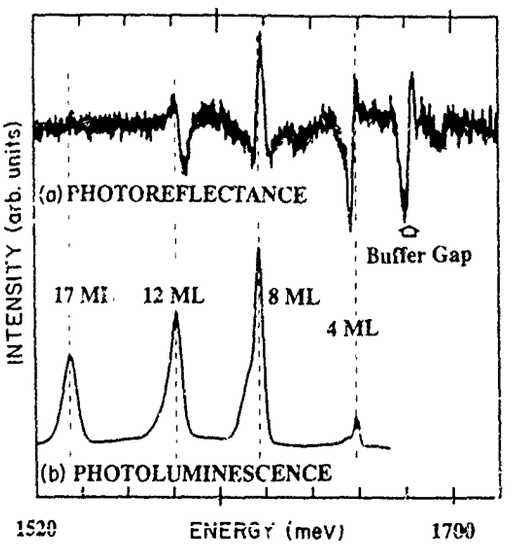

FIG.1: Photoluminescence and Photoreflectance spectra of a sample with four CdTe-CdZnTe QWs

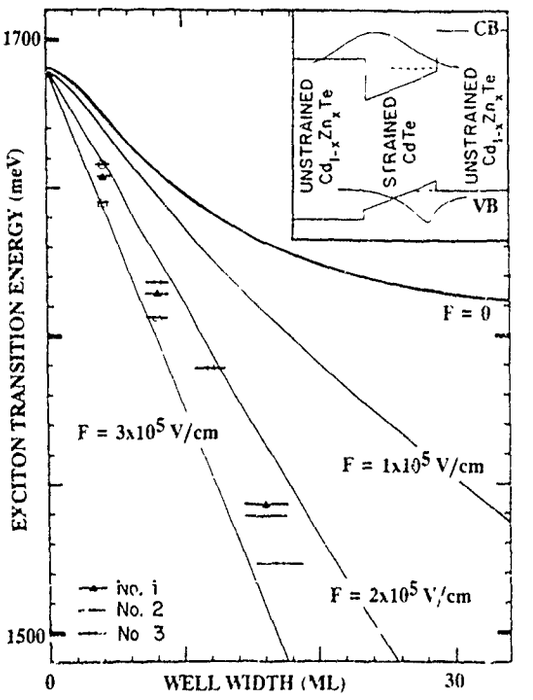

FIG.2: Transition energy versus the QW thickness

The alloy composition is given by the exciton energy as x=.17. The four other lines correspond to the four QWs. The decrease of the oscillator strength in Photoreflectance reveals an increasing spatial separation of electrons and holes when the QW thickness increases. Meanwhile the transition energy almost linearly shifts to the red. These characteristics are well explained when the polar character of the growth axis is taken into account in the band configuration. The buffer layer and the barriers are practically strain free and the conduction and valence bands are flat. The CdTe in the QW suffers a compressive strain within the (111) plane. This strain induces a polarisation and an electric field in the <111> direction, localized within the QW. Then it is straighforward to calculate the electron and hole energies within the band configuration depicted in Fig.2, using for the wavefunctions Airy functions in the QW and decreasing exponentials in the barriers. The result is indeed a quasi-linear shift of the transition energy as a function of the QW thickness, with a slope equal to the built-in electric field. In fact the electrons are confined in the triangular well close to one barrier while the holes are pushed away to the opposite barrier. Hence the transition energy includes a term equal to the potential drop across the QW. We thus have a direct measurement of the built-in field.

The strain within the QW is well known since it corresponds to the mismatch with the strain free CdZnTe buffer layer. Using published data for the piezoelectric coefficient we can calculate the corresponding electric field. We find a close agreement for structures involving an alloy with a low Zn content, while the measured built-in field is systematically larger for structures with higher Zn contents.

References

1 References in: D.L.SMITH and C.MAILHIOT, Rev.Mod.Phys. 62 (1990) 173

2 B.K.LAURICH, K.ELCESS, C.G.FONSTADT, J.G.BEERY, C.MAILHIOT and D.L.SMITH, Phys.Rev.Lett. 62 (1989) 649

3 S.TATARENKO et al. this conference

4 G.FEUILLET et al. to be published

5 R.ANDRE, C.DESHAYES, J.CIBERT, LE SI DANG, S.TATARENKO and K.SAMINADAYAR Phys.Rev.B 42 (1990) 11392

ENHANCED EXCITONIC TRANSITIONS AND ELECTRO-OPTICAL BISTABILITY IN STRAINED $In_xGa_{1-x}As/Al_{0.15}Ga_{0.85}As$ MULTIPLE QUANTUM WELLS

Kenzo Fujiwara,* Kenji Kawashima, and Kikuo Kobayashi
ATR Optical and Radio Communications Research Laboratories,
Seika-cho, Soraku-gun, Kyoto 619-02, Japan
TEL.No.+81/7749/5/1511 TELEFAX No.+81/7749/5/1508
and
Naokatsu Sano
Department of Physics, School of Science,
Kwansei Gakuin University, Nishinomiya 662, Japan

Recently strained $In_xGa_{1-x}As$ heterostructures grown on the GaAs substrate have received a great deal of attention.[1] This is because the strained systems provide additional freedom for the material design and many advantages to opto-electronic device applications. In this paper, we report on optical absorption properties of strained $In_xGa_{1-x}As/Al_{0.15}Ga_{0.85}As$ multiple quantum wells (MQW) by photocurrent (PC) spectroscopy. By virtue of the stronger quantum confinement by $Al_{0.15}Ga_{0.85}As$ barriers, distinct exciton resonances are observed up to the 2nd order even at room temperature. A theoretical analysis is given to explain all the energies of both parity allowed and forbidden transitions, taking the strain effects into account. Using the merit of the substrate transparency at the exciton resonance, a novel electro-optic bistable device is proposed and demonstrated without removal of the GaAs substrate.

$In_xGa_{1-x}As/Al_{0.15}Ga_{0.85}As$ MQW samples with different In contents x were grown on n^+-type GaAs (100) substrates by molecular beam epitaxy.[2] Five periods of nominally undoped $In_xGa_{1-x}As$ quantum wells with a width of L_Z=100 A and L_B=250 A thick $Al_{0.15}Ga_{0.85}As$ barriers in between were grown at 470℃. They are confined by undoped 500 A $Al_{0.15}Ga_{0.85}As$ and 0.1 μm $Al_{0.3}Ga_{0.7}As$ layers and further by n- and p-type $Al_{0.3}Ga_{0.7}As$ clad layers grown at 520℃ to form p-i-n structures. A schematic diagram of the p-i-n diodes with gold-ring windowed electrodes is illustrated in Fig. 1.

Figure 2 shows PC spectra of the MQW p-i-n diodes at room temperature. The spectra were taken with the bias voltage Vb=0 (which is nearly equal to the flat band conditions). Assignment of the transitions is also indicated in Fig. 2. Here we use the notation ijH (ijL) for the heavy-hole (light-hole) exciton transition between the i-th electron and the j-th heavy-hole (light-hole) subband. Sharp exciton resonances are clearly seen up to the 2nd order. Linewidth of the 1H transition in Fig. 2 is as low as 14 meV. This demonstrates excellent quality of our strained epitaxial layers and homogeneous layer thickness and In distribution in the well layers. In Fig. 2, we note that the 1L exciton transition is clearly seen. This results from the fact that the lowest light-hole

subband is certainly bounded in the well because of the use of $Al_{0.15}Ga_{0.85}As$ barrier. The energy separation ΔE_{LH} of the 1IL and 1IH transitions is found to be 27, 47, and 72 meV, increasing with the In content in the well. This gives direct evidence for the strain induced effect on the valence band splitting and cannot be explained by the quantum confinement alone.

In order to quantitatively explain the transition energies, we have calculated subband energies of the strained MQW. In the calculation we assume that the lattice-mismatch is accommodated by the elastic strain given by the tensor $\tilde{\varepsilon}_{ij}$ ($\varepsilon_{xx}=\varepsilon_{yy}=\varepsilon=(a_L-a_S)/a_L$, $\varepsilon_{zz}=-2C_{12}/C_{11}*\varepsilon$) with the lattice constants a_L and a_S of the unstrained ternary $In_xGa_{1-x}As$ layer and of the substrate, respectively. We further assume that valence-band offsets between unstrained $In_xGa_{1-x}As$ and $Al_{0.15}Ga_{0.85}As$ are calculated by a simple summation of the offset values for the $In_xGa_{1-x}As/GaAs$ and $GaAs/Al_{0.15}Ga_{0.85}As$ heterointerfaces using a linear interpolation scheme.[3] Our calculation shows that the transition energy changes from that of bulk unstrained $In_xGa_{1-x}As$ by two effects of strain and quantum confinement. We find that the ΔE_{LH} is mostly determined by the valence-band axial deformation potential b_v. This is because the hydrostatic strain component δH moves the H and L valence band edges by the same amount. Therefore, the measured ΔE_{LH} allows us to determine the x value in the well accurately and self-consistently, as indicated in Fig. 2. We should point out that the precise determination of the x value is particularly important because of its sensitivity to the transition energy. In Fig. 2, the calculated results are also indicated by vertical bars, assuming an exciton binding energy of 7 meV.[4] Excellent agreement between theory and experiment is obtained.

The results presented above indicate an interesting possibility for applications to vertical-beam optical devices since the exciton resonance can occur at energy below the bandgap of the GaAs substrate.[2] Figure 3 demonstrates operation of optical bistable devices based on the self-electro-optic effect device (SEED) principle by connecting a load resistor (R), a constant bias (V_0) and a LED in series to the sample. Importance of the results in Fig. 3 is twofold:(1) the bistable operation is achievable without removing the substrate since the substrate is transparent;(2)optical switching and hysterisis loop of the optical output power versus the input power are demonstrated at two different wavelengths λ_1 and λ_2. This result suggests important implication for a vertically integrated-type asymmetric SEED devive that uses two wavelengths and one pixel instead of using one wavelength and two pixels like a symmetric SEED.[5] This type of integration is possible when at least one of the wavelengths is transparent to the substrate with the use of strained $In_xGa_{1-x}As$ layers.

References

1)R.G.Waters and J.J.Coleman, Conference on Lasers and Electro-Optics 1990 Technical Digest Series, Vol.7 (Optical Society of America, Washignton, DC 1990) pp.32-33 and other papers therein.

2)K. Fujiwara, K. Kawashima, K. Kobayashi, and N. Sano, Appl. Phys. Lett. 57, 2234 (1990).
3)D. Gershoni, J. M. Vandenberg, S. N. G. Chu, H. Temkin, T. Tanbun-Ek, and R. A. Logan, Phys. Rev. B40, 10017 (1989)
4)J.-P. Reithmaier, R. Höger, H. Riechert, A. Heberle, G. Abstreiter, and G. Weimann, Appl. Phys. Lett. 56, 536 (1990).
5)A. L. Lentine, H. S. Hinton, D. A. B. Miller, J. H. Henry, J. E. Cunningham, and L. M. F. Chirovsky, Appl. Phys. Lett. 52, 1419 (1988).

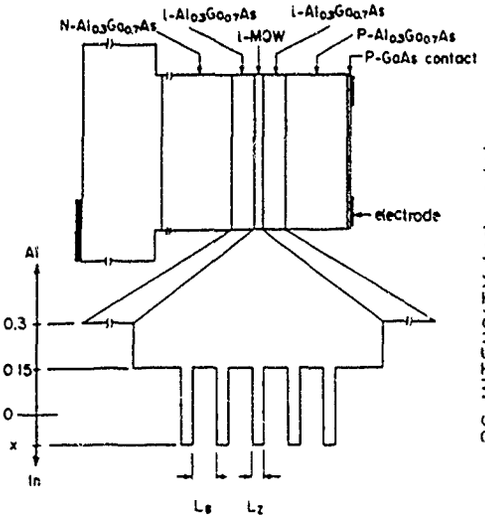

Figure 1
Schematic diagram of the sample structure.

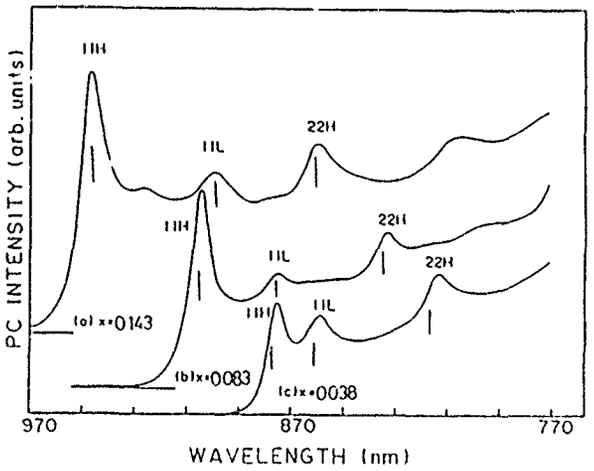

Figure 2
Photocurrent spectra of the MQW samples (L_z=100 A) with Vb=0. Calculated wavelengths for the hh(i) exciton transitions are indicated by vertical bars.

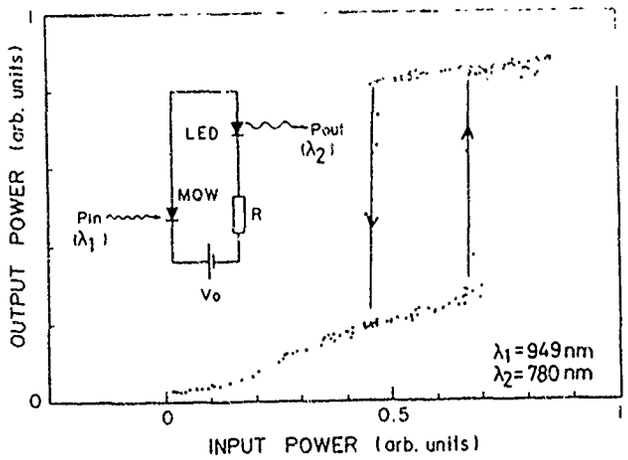

Figure 3
Optical output versus input power for a LED biased SEED device at wavelength λ_1=949 nm and λ_2=780 nm. The arrows refer to the direction of the increase and decrease of the optical power. The inset shows the configuration of the device circuit (R=1 M Ω, V_o=12 V).

Ep2

MBE GROWTH AND RELAXATION OF STRAINED $In_xGa_{1-x}As$ LAYERS ($0.53 < x \leq 1.$) ON InP

M. Gendry*, V. Drouot, J.L. Duvault, D. Gallet,
C. Santinelli, and G. Hollinger
Laboratoire d'électronique, UA, CNRS 848,
Ecole Centrale de Lyon, 69131 Ecully Cedex,France.

Lattice matched InAlAs/InGaAs/InAlAs heterostructures grown on InP are promising combinations for producing high-electron-mobility-transitors (HEMT). These systems are well suited for microwave and optoelectronic applications. Significant improvements of their electronic properties (electron mobility and sheet carrier density) are expected if compressively strained (In-rich) InGaAs layers are used in the channel region. Therefore, there is a strong interest to define growth conditions for strained InGaAs layers with the highest thickness for a given In content.

In this work, we have studied the pseudomorphic growth and the relaxation of $In_xGa_{1-x}As$ ($0.53 < x \leq 1.$) layers on InP(100) substrates and on InGaAs buffer layers, lattice matched to InP. To characterize the strain relaxation and to evaluate critical thicknesses, the surface lattice parameter of $In_xGa_{1-x}As$ was determined from streak spacing in reflection high energy electron diffraction (RHEED) patterns.

The experiments were performed using a Riber 2300 MBE system connected to a VSW surface analysis chamber. During growth the RHEED patterns can be recorded using a CCD camera and a tape recorder. Digitalized RHEED oscillation curves and RHEED patterns can be analyzed simultaneously The lattice parameter was determined within 0.02 Å. Oxidized "ready to use" InP(100) substrates from SUMITOMO and METAUX SPECIAUX were deoxidized at 570°C. The growth rate was 0.8 μm/h. The V/III beam equivalent pressure ratio was equal to 25, and the substrate temperature ranged from 450 to 525°C. The $In_xGa_{1-x}As$ alloy composition ,for the strained layers ,was defined by extrapolating In/Ga pressure ratio values used for growing lattice matched InGaAs layers (checked by DDX), and assuming the same In and Ga incorporation coefficients. The validity of this calibration procedure was ckecked by measuring XPS Ga 3d and In 4d core level intensity ratios. (Fig. 1).

The strain dependence of the relaxation is shown in fig. 2 where the measured surface lattice parameter of $In_xGa_{1-x}As$ is plotted versus film thickness for different In compositions and different growth conditions. Two sets of experiments are presented. First, $In_xGa_{1-x}As$ layers have been grown at 525°C on InP substrates with x= 0.58, 0.65, 0.82, 1. . Second, $In_{0.82}Ga_{0.18}As$ layers have been grown, at 450 and 525°C, on InGaAs lattice matched to InP . The main results can be summarized as follows:

i) The onset of relaxation (critical thickness) was detected at 750, 75, 21, and 11 Å for $In_xGa_{1-x}As$ layers grown on InP substrates with x = 0.58, 0.65, 0.82, 1. ,respectively. For $In_{0.82}Ga_{0.18}As$ the critical thickness increases to 110 and 220 Å when the growth is performed on InGaAs buffer layers at 525 and 450°C, respectively.

ii) A layer by layer growth mode is observed for pseudomorphic layers. The onset of relaxation is simultaneous with the apparition of three dimensional (3D) island formation

iii) The apparent lattice relaxation,as detected by RHEED, strongly depends on the growth conditions. The oscillations detected in fig. 2 are indicative of different competing nucleation processes and of inhomogeneous relaxation ,previously detected by TEM (*P.Ferret and M.Pitaval -to be published-*).

In summary,the strain relaxation cf $In_xGa_{1-x}As$ layers during growth is mismatch dependent as well as substrate dependent and temperature dependent. Thick pseudomorphic layers can be grown by decreasing the growth temperature. Critical thicknesses range between values predicted by Matthews and Blaskeslee force balance model and People and Bean energy balance model. The applicability of the thickest strained layers to fabricate HEMT devices will depend on their electronic quality and stability and to what extent the growth conditions are compatible with device fabrication.

ACKNOWLEDGEMENTS : This work was supported by the Economic European Community under contract ESPRIT BRA N° 3086

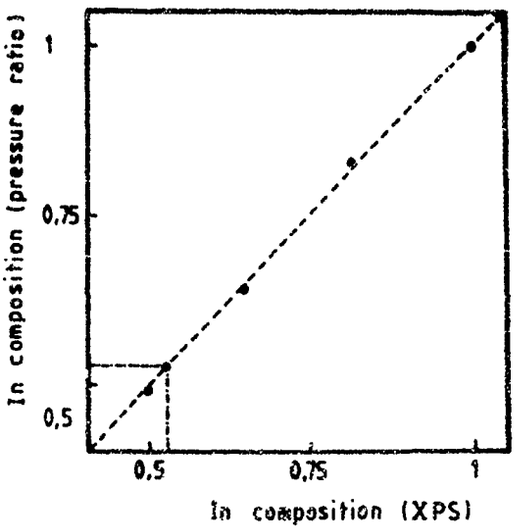

fig.1. Correlation between In concentrations defined from In/Ga beam equivalent pressure ratios and In concentrations determined from XPS In 4d and Ga 3d core level intensity ratios.

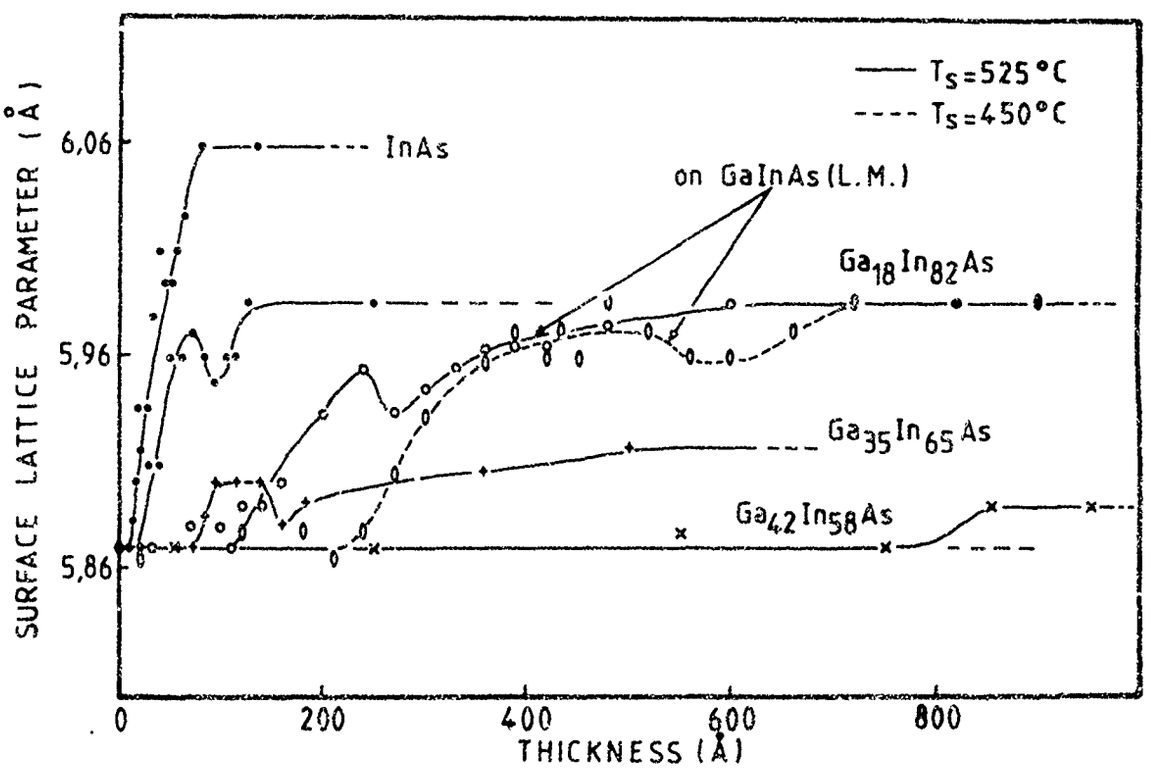

fig. 2. Measured surface lattice parameter during growth of $In_xGa_{1-x}As$ for different compositions and growth conditions.

MBE grown MQW in the InGaAlAs/InGaAs system: Non-radiative lifetime monitoring

M. Quillec, K. Satzke, and B. Sermage
Centre National d'Etudes des Telecommunications
196 Avenue Henri Ravera, 92220 Bagneux, France
Tel 33 1 45 295 441, Fax 33 1 45 295 405

MBE has been successfully used for demonstrating 1500 nm multi-quantum well lasers[1,2,3] and modulators[4] for telecommunications. One promising feature of these devices is their good high frequency behaviour. In order to improve the intrinsic limitation for fast operation of the modulators, the idea is to slightly decrease the non-radiative lifetime of injected carriers in the active region. By reducing the growth temperature and arsenic flux, we show that this result is obtained, while keeping a good quality to the crystalline structure and to the electronic band structure. Time resolved photoluminescence was performed on undoped graded refractive index MQW structures obtained at different temperatures in the InGaAlAs/InGaAs system. Non-radiative lifetimes ware varied from 10 ns in the optimized growth conditions to less than 100 ps at low growth temperatures. X-ray characterization shows the good overall structural quality of the structures. Faster operation is also expected with lasers using p-type doping of the active layer. We will show how this affects the carriers' lifetime; consequences on laser operation will be discussed.

This work was partly supported by EEC through the RACE programme (RACE 1057).

References

1. M. Quillec, M. Allovon, F. Brillouet, A. Gloukhian, J.P. Praseuth, and B. Sermage, Electron. Lett. **25**, 1731 (1989)
2. M. Blez, C. Karmierski, M. Quillec, D. Robein, M. Allovon, A. Gloukhian, and B. Sermage, Electron. Lett. **27**, 93 (1991)
3. C. Karmierski, M. Blez, M. Quillec, M. Allovon, and B. Sermage, Electron. Lett. **26**, 889 (1990)
4. E. Bigan, M. Allovon, M. Carre, and A. Carenco, Electron. Lett. **26**, 355 (1990).

THE APPLICATION OF FLUX VARIATIONS FOR THE MBE GROWTH OF LATERALLY GRADED GaAs/AlGaAs QUANTUM WELL STRUCTURES

V.M. Airaksinen* and R. Salo

Electron Physics Laboratory, Helsinki University of Technology, Otakaari 7A, 02150 Espoo, Finland

Tel: +358 0 4512329, Fax: + 358 0 460 224

U. Gyllenberg

Semiconductor Laboratory, Technical Research Centre of Finland, Otakaari 7B, 02150 Espoo, Finland

H. Lipsanen

Optoelectronics Laboratory, Helsinki University of Technology, Otakaari 1, 02150 Espoo, Finland

Tel: +358 0 4513123, Fax: + 358 0 465 077

1. Introduction

The energy band structure and (in the case of strained layer superlattices) the crystal quality of a quantum well structure are strongly influenced by the thicknesses of the individual layers in the heterostructure. By using quantum well structures with different layer thicknesses, but otherwise identical properties, for instance band offsets or critical layer thicknesses can be determined. For such studies it would be convenient if the layers could be grown with areas of different thicknesses on the same substrate. This would reduce the amount of work required for the preparation of multiple samples and also reduce the possibility of sample-to-sample variations due to different growth temperatures, group III and V fluxes, doping levels etc. In this paper we show that it is possible to have large lateral variations of the Ga and Al growth rates over a 75mm wafer and still achieve an excellent compositional uniformity of the AlGaAs alloy. Examples of the optical spectroscopy of the band structure on such laterally graded GaAs/AlGaAs superlattices are shown.

2. Experiment

The samples were prepared in a commercial MBE system[1] capable of using wafers up to 75mm in diameter. Ga and Al fluxes from the standard 40cm^3 K-cells were calibrated using RHEED intensity oscillations. GaAs/AlGaAs superlattices and multiple quantum well structures were grown using a substrate rotation rate of 6rad/s at both on In-free 75mm (100)-oriented GaAs wafers and on smaller GaAs wafers mounted on a 90mm molybdenum block with indium. The growth temperatures of 580-590°C were measured with an optical pyrometer. The superlattice layer thicknesses and compositions were determined from the comparison of calculated and experimental X-ray diffraction rocking curves. The superlattice band structure was investigated with photoreflectance[2] measurements using a standard experimental setup[3].

3. Results and discussion

Figure 1 shows the normalised well and barrier layer thicknesses in a 25 period GaAs/AlGaAs superlattice as a function of the distance from the centre of the 75mm wafer. The layer thicknesses are approximately constant in the central area of about 15mm in diameter. Outside this area, however, both the GaAs wells and the AlGaAs barriers become thinner towards the edges of the wafer, the reduction in thickness being quite steep (about 1%/mm). We have found that the central area of constant thickness is increased slightly if the Ga and Al cells are nearly full. The total thickness reduction, however, is not affected much.

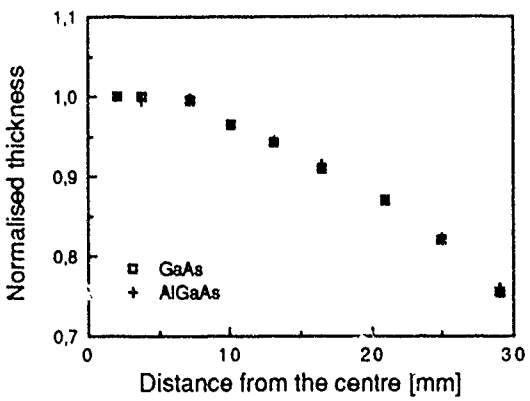

Figure 1. The normalised thickness of GaAs wells and AlGaAs barriers vs. distance from the centre of the wafer Thicknesses at the centre are 178Å (GaAs) and 293Å (AlGaAs).

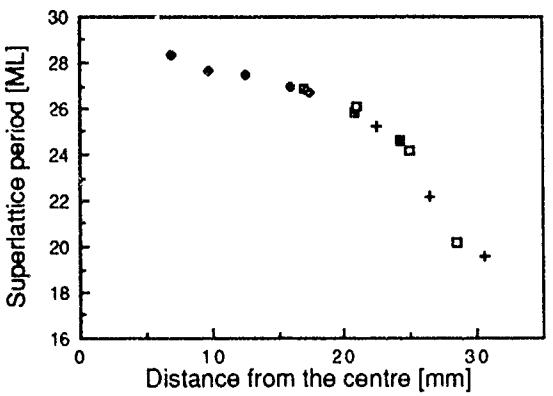

Figure 2. Thickness variation vs distance from the centre of rotation in a GaAs/AlAs superlattice.

The important feature shown of Figure 1 is that the Al and Ga fluxes decrease at the same rate towards the edges of the wafer. Therefore, the composition of the $Al_xGa_{1-x}As$ barrier layers in this superlattice remains constant at x=0.231 +/- 0.004 in spite of the total thickness reduction of 24% from the value at the centre. A similar compositional uniformity has been confirmed in several different samples and allows the growth of quantum well structures with variable well and barrier thicknesses whilst the barrier composition is maintained at a constant value. Also, the ratio of the well and barrier thicknesses remains constant. This feature has been utilised for the simultaneous growth of $(GaAs)_n/(AlAs)_n$ superlattices with n=9-14 . Figure 2 shows the thickness variation in such a superlattice of 40 periods grown on indium mounted substrates.

The band structure of laterally graded superlattices was characterised using optical modulation spectroscopy at 294K. In figure 3 the evolution of the various transition

energies is shown as a function of the well thickness for the GaAs/AlGaAs superlattice. The transitions (labelled nHm or nLm) between the n-th electron energy level and the m-th heavy hole (H) or light hole (L) level can be identified by comparison with the values calculated using Bastard's model[4]. The agreement between theory and experiment is very good. Figure 4 shows the energies of the two lowest transitions observed in the $(GaAs)_n/(AlAs)_n$ superlattice. In this thin layer structure the direct band gap increases as the period decreases until n=10 when the Γ-minimum of the GaAs well moves above the X-minimum of the AlAs barriers and the superlattice becomes spatially indirect. This value of n for the direct-indirect transition is in good agreement with the recent work of Fujimoto et al.[5]

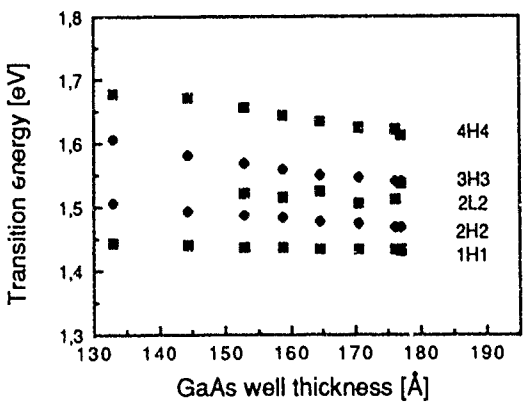

Figure 3. Optical transitions in the GaAs/AlGaAs superlattice measured by photoreflectance at 294K

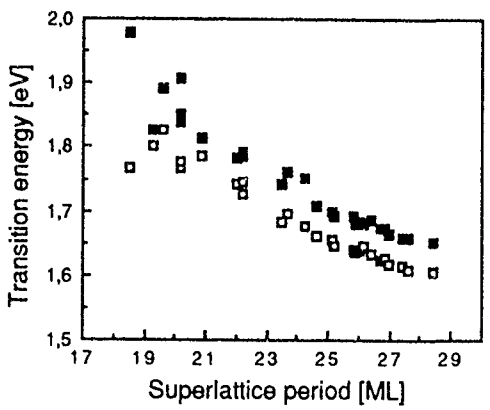

Figure 4. The energies of the two lowest optical transitions in the GaAs/AlAs superlattice vs. the superlattice period.

In conclusion, GaAs/AlGaAs superlattices of excellent compositional uniformity with laterally graded layer thicknesses have been grown by MBE. The energy band structure of such superlattices has been studied with photoreflectance spectroscopy.

4. References

1. VG Semicon V80H.

2. See for instance: O.J. Glembocki, SPIE Proceedings 1286 (1990) 2-30.

3. V.M. Airaksinen, H.K. Lipsanen, P. Ravila, T. Tuomi and P.A. Claxton, SPIE Proceedings 1286 (1990) 238-243.

4. G. Bastard, J.A. Brum, IEEE J. Quantum Electron. QE-22 (1986) 1625.

5. H. Fujimoto, C. Hamaguchi, T. Nakazawa, K. Taniguchi and K. Imanishi, Phys. Rev. B41 (1990) 7593-7601.

MEE GROWTH AND CHARACTERIZATION OF STRAINED GaSb LAYERS ON GaAs(100) FOR GaSb/InAs/GaSb QW STRUCTURES

S.V.Ivanov*, A.A.Budza, A.A.Dzamashvili, P.S.Kop'ev
B.Ya.Meltser, V.M.Ustinov, S.V.Shaposhnikov
A.F.Ioffe Physico-Technical Inst., USSR Academy of Sciences
Politekhnicheskaya 26, Leningrad 194021, USSR

GaSb/InAs/GaSb quantum well structures seem to be very promising for high speed microelectronics [1,2]. Using the improved structure of such type with 10Å InAs prewell allowed us to obtain routinely heterostructures with 2D electron mobility higher than 10^5 cm^2/Vs (4.2K) and room temperature conductivity at least an order of magnitude higher than the traditional AlGaAs/GaAs modulation doped structures can show [3]. However, the growth of rather thin ($\leq 2\mu m$) high quality GaSb layers with low dislocation density on strongly lattice mismatched GaAs semi-insulating substrates ($\Delta a/a \simeq 6,8\%$) is the main problem which is to be solved to improve the GaSb/InAs/GaSb structure parameters for their device applications.

In this paper we present the attempt of thermodynamic description of strained layer GaSb/GaAs(100) growth based on the model previously reported for the lattice matched III-V compound growth [4,5], compare it with experimental results, and discuss the methods of the dislocation density decrease.

The investigated GaSb layers were grown in a three-chamber MBE machine (u.p. ~ 10^{-10} Torr) on GaAs(100) S.I. substrates. The experimental conditions and procedures were published elsewhere [6]. The growth temperature varied within 500-550°C, the growth rate was about 0.7μm/h, Sb/Ga ratios were 1-15. Usually 1.2μm GaSb layer were grown on a buffer layer consisting of both GaSb layers (0.2-0.5μm) and their different combinations with AlGaSb/GaSb and AlSb/GaSb strained-layer short-period superlattices (SL SPS). It was shown that the increase of growth temperature resulted in better GaSb electrical and optical properties. However to obtain good surface morphology at 530-540°C one should rise the Sb/Ga ratio by 8-9 times compared to that

corresponding to the transition to the (3×2) Ga-stabilized RHEED pattern at 500°C.

In the case of lattice matched MBE growth of GaSb on GaSb substrate:

$$Ga(g) + 1/2Sb_2(g) = GaSb(s) \qquad (1)$$

with the respective equation of acting masses [4]

$$P_{Ga}P_{Sb_2}^{1/2} = K_{GaSb} = 3{,}97\times10^{10}\exp(-4.54/kT), \qquad (2)$$

where P_{Ga} and P_{Sb_2} are the equilibrium partial pressures of gallium and antimony molecules over the GaSb surface (in atm), K_{GaSb} is the equilibrium constant, kT is in eV. The solid curves in fig.1 show the gallium ($P_{Ga}^{Ga_L}$) and antimony ($P_{Sb_2}^{Ga_L}$, $P_{Sb_4}^{Ga_L}$) equilibrium partial pressures along the Ga-Sb-GaSb liquidus calculated according [7], using (2) and taking into account that $P_{Ga}^{Ga_L}$ is the same as for GaAs [7] (dashed line). Dotted line corresponds to the minimum possible antimony pressure in the incident beam at a given growth rate. As is seen from fig.1, the $P_{Sb_2}^{Ga_L}$ variation in the range of 500-600°C is negligible compared to $P^{o}_{Sb_2,min}$. In the case of strained layer growth one should take into considerarion the additive strain Gibbs free energy [8] which is maximum during growth of first several monolayers before the GaSb film relaxes with formation of high (~ 10^{8}-10^{9} cm^{-2}) dislocation density. The broken line in fig.1 shows the $(P_{Sb_2}^{Ga_L})_s$ temperature dependence at the maximum strain calculated according to [8,9] assuming that $(P_{Ga}^{Ga_L})_s \simeq P_{Ga}^{Ga_L}$:

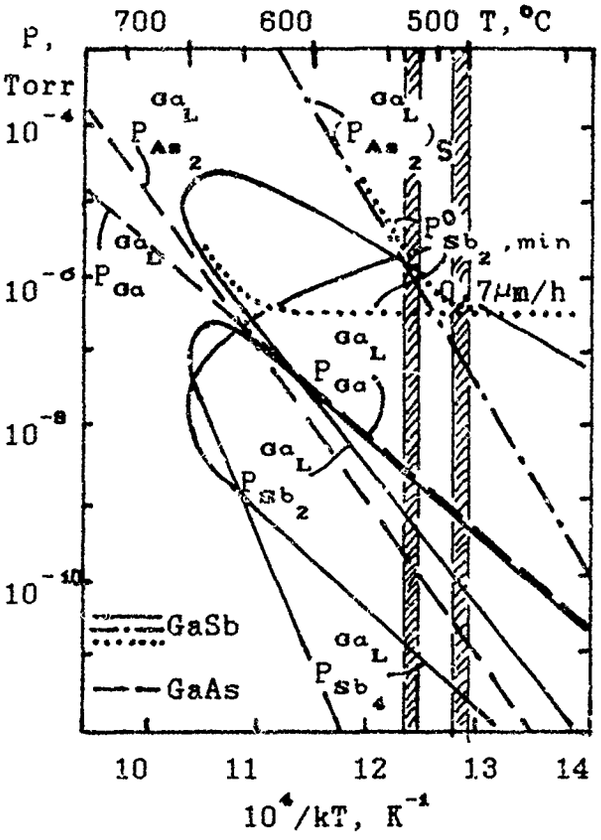

Fig.1

$$(P_{Sb_2}^{Ga_L})^{1/2} = 3{,}0\times10^{10}\exp(-4.78/kT) \qquad (3)$$

It is clearly seen from fig.1 that in the case of GaSb/GaAs growth the temperature dependence of antimony equilibrium pressure over the Ga-GaSb liquidus is much more steep compared to the unstrained growth. Further, the increase of T_{sub} from 500°C to 540°C results in the $(P_{Sb_2}^{Ga_L})_s$ increase by factor ~ 40 and requires the $P^{o}_{Sb_2,min}$ increase by factor ~ 7-8 at given growth rate (0.7μm/h) to compensate the antimony evaporation from the surface and to prevent Ga droplets appearance. This conclusion is in a good agreement with experimental data.

Optimization of growth parameters: the antimony excess pressure $P_{Sb_2,exc}$ [5] and the substrate temperature according to this consideration allowed us to grow GaSb layers (1.2μm) with $p=1.5\text{-}5\times10^{16}cm^{-3}$ and $\mu\simeq700cm^2/Vs$ (300K) and $p=4\text{-}15\times10^{15}cm^{-3}$ and $\mu=4000cm^2/Vs$ (77K), but with very weak photoluminescence (PL) intensity robably caused by high dislocation density. The introduction of 20-period 50Å-GaSb /50Å-AlSb SL SPS after 0.5μm-GaSb buffer layer, as a way to decrease the dislocation density in the upper 1.2μm-GaSb layer, led to more than 3 times increase of PL intensity with clearly observed excitonic luminescence and the increase of μ_{77K} up to $4500cm^2/Vs$, which is comparable with 7μm-GaSb MBE layers grown on GaAs(100) [10]. The isoelectronic doping of GaSb with In (0.15-0.2 at.%) was also shown to result in nearly the same effect on PL intensity.

REFERENCES

1. H.Munekata et al., J.Vac.Sci.Technol.B 5(1987)809.
2. L.F.Luo et al., Appl.Phys.Lett. 55(1989)789.
3. S.V.Ivanov et al., phys.stat.sol.(a) 118(1990)169.
4. P.S Kop'ev et al., Sov.Phys.Semicond. 22(1988)1093.
5. S.V.Ivanov et al., J.Crystal Growth 104(1990)345.
6. P.S.Kop'ev et al., J.Crystal Growth 96(1989)533.
7. D.T.J.Hurle, J.Phys.Chem.Solids 40(1979)613.
8. F.Turko et al., J.Cryst.Growth 88(1988)282.
9. R.E.Nahory et al., J.Electrochem.Soc. 125(1978)1053.
10. G.R.Jonson et al.,Semicond.Sci.Technol. 3(1988)1157.

Ep6

On the growth of InGaAs/InP QW structures by CBE.

Antolini A., Campi D., Gastaldi G., Genova F., Iori M., Lamberti C.[1], Morello G. and Rigo C.*

CSELT Centro Studi E Laboratori Telecomunicazioni

Via G. Reiss Romoli 274, 10148 TORINO (I)

Tel. ++39 11 2169510, Fax. ++39 11 2169695

[1]Dottorato di Ricerca Universita` di Torino and INFN Sez. Torino

CBE (Chemical Beam Epitaxy) is becoming a competitive growth technique for the preparation, with extreme reproducibility and uniformity, of very sophisticated device structures in the InGaAsP material system, and seems the most suitable to grow InGaAs/InP and InGaAs/InGaAsP QW structures.

High quality Single and Multi QW growth have been successfully reported using this technique and very abrupt interfaces at either the well edges have been obtained; however till now, to our knowledge, a discussion on the quality of the QW's and of their interfaces in relation with the growth conditions and of the gas-system set-up is lacking. Problems with InGaAsP thin layer formation at the interfaces and the eventual presence of As in the InP barrier have been extensively discussed in MOVPE and GSMBE QW's growth, but not in CBE. Nevertheless these effects, also present in CBE QW's, are strongly dependent on the growth conditions and in some case can contribute to enhance the optical quality as it will be reported in this work.

More in general the conditions for the growth of high quality single and multiple QW will be extensively discussed in this work and those will be correlated with Fourier Transform Photo-Luminescence (FTPL), High Resolution X-ray Diffraction (HRXRD), Absorption Photo-Absorption and Photo-Current (in PIN structures) measurements.

The growth apparatus is a standard diffusion pumped VG-80H MBE, connected to a pressure controlled gas system. While the group V gas line and furnace are standard, the group III introduction system has been entirely designed from the authors, with the aim to test simplified gas-lines, while maintaining flux stability and reproducibility at satisfactory levels and fast switching operations. All the metalorganic sources (TEGa, TMIn) were kept at constant temperature, using thermostatic baths. The fluxes were controlled by means of a variable automatic leak valve with a feedback control to maintain a constant pressure in the line connecting this valve to the effusion cell. No carrier gas has been employed. The effusion cell, common to all the four group III lines have been specially designed in order to assure a correct premixing of the m.o. reactants.

QW's were grown at different condition of rates (.5 μm/h and 1μm/h), and of arsine and phosphine pressures, while the temperature has been kept in the range of 500-520 °C. In order to verify the effect of growth interruption on QW abruptness, several combination of interruption at both the interfaces were compared using PL, Absorption and HRXRD measurements on very thin single and multi QW. The effect of a purge in arsine of InP and in phosphine of InGaAs has been also studied and will be discussed in detail.

In some particular growth conditions incorporation of As in the barriers and formation of InGaAsP at the interfaces has been clearly demonstrated even using a very fast flux switching system. However the conditions for growing very high quality QW's have been also determined, and the very good results obtained on PIN structures are a clear demonstration.

In fig. 1 is shown the PL spectra of single QW's of nominally 2 monolayers (0.58 and 1.46 nm) grown using different growth interruption times. Narrow (< 20 meV) and very intense multiple PL peaks were observed for the 2 and 5 ml single QW's, demonstrating very abrupt interfaces, even with a growth interruption time of only 1 second at each interface. Multiple peaks are presents and the mean island size (evaluated following the ref. 1 modified for InGaAs/InP QW's) is larger than 6 nm. This evaluation is based also on data from thicker QW's.

In addition, a detailed discussion of the 60 and 40 period MQW of nominally 7.6/8.0 nm InGaAs/InP will be presented. Absorption (fig. 2), HRXRD (fig 3), and Photo-current (fig.4) spectra have been evaluated and compared with the help of theoretical simulations.

The high optical quality of the MQW structures is demonstrated by the sharp and intense excitonic features of the 300 K absorption spectra and from their marked bias dependence in electro-optic characterizations The absorption spectrum shows an outstanding 7500 cm^{-1} exciton peak (placed at 1.55 μm), probably the largest value reported so far. Measurements on PIN show dark currents lower than 0.5 nA at -20 V on 165 μm mesa diameter devices.

Remarkable structural quality is demonstrated by the presence of up to 8 orders of satellite peaks in the HRXRD spectra.

The results of all these characterizations will be compared and discussed in detail.

We would like to thank C. Coriasso for Absorption , P. J. Bradley for Photo-Current and C. Cacciatore for Photo-Absorption measurements.

Ref. 1 J. Singh et Al : Appl. Phys. Lett. **44** (1984) 805.

Fig.1 4 K FTPL spectra of a nominally 2 monolayer InGaAs/InP single QW grown with an interruption time of 1, 2.5, 4, 10, 20 seconds respectively at each interface.

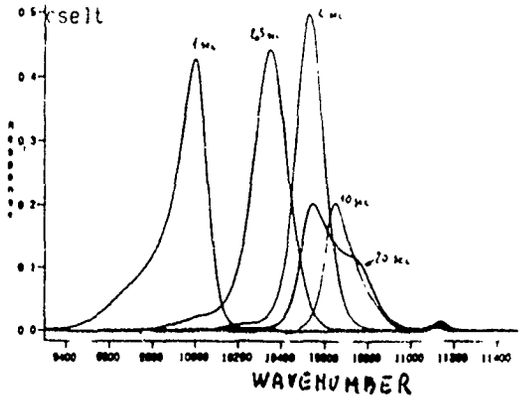

Fig 2 Absorption spectrum of a CBE InGaAs/InP 7.6/8.0 nm sample, 60 periods (dashed line). The exciton feature corresponding to the first electron-heavy hole transition is sharp and intense. The solid line represents the result of a computer simulation of the absorption spectrum.

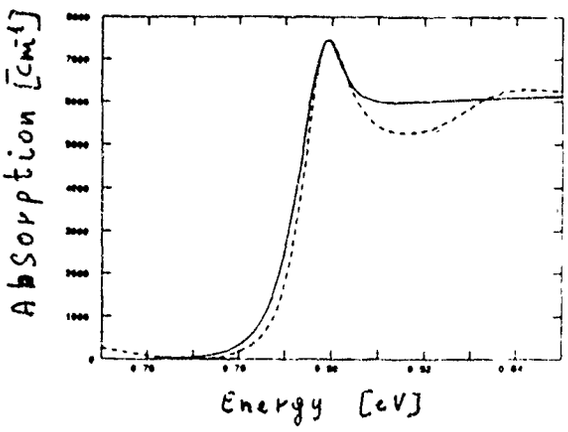

Fig. 3 High Resolution X-Ray Diffraction spectrum of a 40 periods MQW with the same nominally well and barrier widths as fig.3 sample in the (400) symmetric reflection configuration.

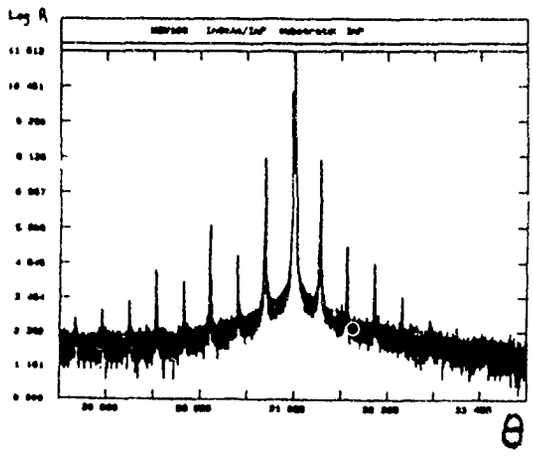

Fig.4 Photo-current response for different bias of a PIN structure containing a 40 period InGaAs/InP (nominally 7.5/8 nm) MQW in the active layer. The response was made quantitative by comparison with absorption measurements. The interruption time is less than 1 second in the samples of fig. 2, 3, 4.

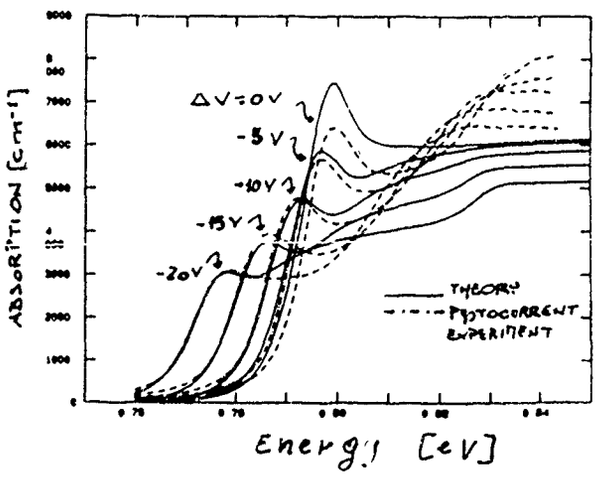

Ep7

Molecular Beam Epitaxy of PbSe/$Pb_{1-x}Mn_xSe$ Multiquantum Wells

N. Frank*, E. Koppensteiner, and G. Bauer

Institut für Halbleiterphysik, Johannes Kepler Universität Linz, A-4040 Linz/Auhof
Phone: 0042732 2468 9600
FAX: 0043732 2468 10

Dilute magnetic quantum wells are of interest for their unique magnetic properties as well as the potential of tuning band offsets by external magnetic fields. We report here on the first succesful growth of PbSe/$Pb_{1-x}Mn_xSe$ structures. Bulk $Pb_{1-x}Mn_xSe$ has been grown previously by polish and russian groups. The system PbSe/$Pb_{1-x}Mn_xSe$ has among the IV-VI heterostructures the adventage that the constituents PbSe ($a_1 = 6.128$Å) and MnSe ($a_2 = 5.451$Å) crystalize both in the NaCl-structure. In comparison to the PbSe/$Pb_{1-x}Eu_xSe$ heterostructures which have been studied extensively because of possible applications as infrared lasers [1], the PbSe/$Pb_{1-x}Mn_xSe$ system is adventageous since the exchange interactions between mobile carriers and the Mn-3d-electrons are much stronger than those involving the 4f-electrons in the Eu-case.

The MBE-system used has been described previously [2], an Se-effusion cell has been used with a special orifice construction for stabilizing the Se partial pressure. No cracker cell attachement has been employed so far. In Fig.1 the partial pressure of PbSe, Mn and Se are shown together with the mole fraction of the Se-compounds present in the Se-vapour. All shaded areas indicate the range of temperatures used for the PbSe-cell (520-560°C), the Mn-cell (590-680°C), as well as the Se-cell (165-210°C).

Layers of both n- as well as p-type PbSe and $Pb_{1-x}Mn_xSe$ were deposited on cleaved BaF_2 substrates. Their structural perfection was checked by X-ray diffractometry as well as electron channeling patterns. Electron and hole mobilities were determined as a function of temperature. With increasing Mn-content the mobility drops appreciably decreasing from $10^5 cm^2/Vs$ to about $10^4 cm^2/Vs$ (20K) for Mn-contents of $x = 3\%$. For electrons a similar behaviour was found with 77K mobilities as high as $32000 cm^2/Vs$ for PbSe.

It turned out that the Mn-content in the $Pb_{1-x}Mn_xSe$-layers is determined mainly by the Mn-effusion cell temperature. In contrast to the $Pb_{1-x}Mn_xTe$-case, the group VI element partial pressure is of minor importance for the Mn-content in the $Pb_{1-x}Mn_xSe$-case. Whereas for the $Pb_{1-x}Mn_xTe$-case the Te-sublimation leads entirely to Te_2, for the Se-case the concentration of rings consisting of five and six Se-atomes is appreciably higher than that of Se_2 molecules which most probably determine the incorporation of Mn into the $Pb_{1-x}Mn_xSe$ (Fig.1).

Multi Quantum Well structures (MQW) were grown using either PbSe- or $Pb_{1-x}Mn_xSe$-buffer layers with thicknesses in the order of 1μm. In the first case the $Pb_{1-x}Mn_xSe$-layers within the MQW experience a biaxial tensile strain and beyond a total critical thickness the whole structure is unstable towards misfit dislocation formation. On the other hand, strain symmetrized structures $PbSe/Pb_{1-x}Mn_xSe$ were grown on a $Pb_{1-y}Mn_ySe$-buffer, where the PbSe-layers are under biaxial compressive strain and the $Pb_{1-x}Mn_xSe$-layers under biaxial tensile strain. Typical x-values ranged from 1 to 3%, the thicknesses from 40 to 500 Å. A strain analysis was performed by using X-ray diffraction on lattice planes parallel to the substrate surface (222) as well as inclined to it (246). In Fig.2 (MQW65) the countrate of the (222)-Bragg-reflexion is shown vs 2Θ for a strain symmetrized MQW (65) sample of 10 double layers ($d_1 = d_2 = 140$Å, $x \approx 2.5\%$) deposited on a 1μm thick $Pb_{1-y}Mn_ySe$ buffer layer ($y \approx 1.2\%$). In the same figure we show in the lower panel a similar sample (MQW57, $d_1 = d_2 = 140$Å, $x \approx 1.9\%$, 10 double layers) deposited on a PbSe-buffer, where the corresponding PbSe Bragg peak is clearly separated from the $i = 0$ superlattice peak. The differences in composition and strain are apparent from the comparison of the upper and lower panel. The period of both samples turns out to be identical, as evidenced by the sattelite peak separations. In order to seperate the influence of the elastic strain, "oblique" Bragg reflections like the (246) one have to be investigated. In Fig.3 a comparison of the (222) Bragg reflection with a (246) rocking curve is presented from which, using an elaborated numerical analysis, the strain status can be extracted on the basis of the elastic constants. The components of the elastic strain tensor are determined to be:

$\varepsilon_{xx} = \varepsilon_{yy} = +4*10^{-4}$, $\varepsilon_{zz} = -4.6*10^{-4}$ for $Pb_{1-x}Mn_xSe$,

$\varepsilon_{xx} = \varepsilon_{yy} = -1.6*10^{-4}$, $\varepsilon_{zz} = +1.8*10^{-4}$ for PbSe.

From the X-ray data it is apparent that the control over the structural perfection (growth rates, composition) has been achieved on this system.

We thank H. Krenn for helpful discussions and A. Pesek for the rocking curves.

Work supported by Jubiläumsfonds der österreichischen Nationalbank, No. 3735.

[1]: M. Tacke, B. Spanger, A. Lambrecht, P. R. Norton, H. Böttner, Appl. Phys. Lett. **53**, 2260 (1988).

[2]: N. Frank et. al., J. Cryst. Growth, submitted.

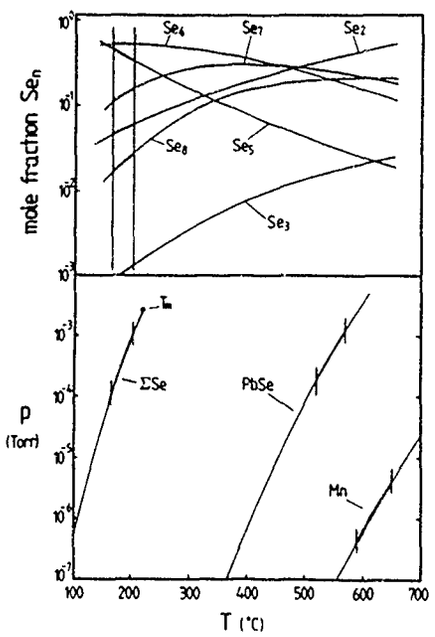

Fig.1: Mole fraction of several Se-complexes as a function of temperature and partial pressure of PbSe, Mn and Se vs T. Shaded areas denote range used for MBE growth.

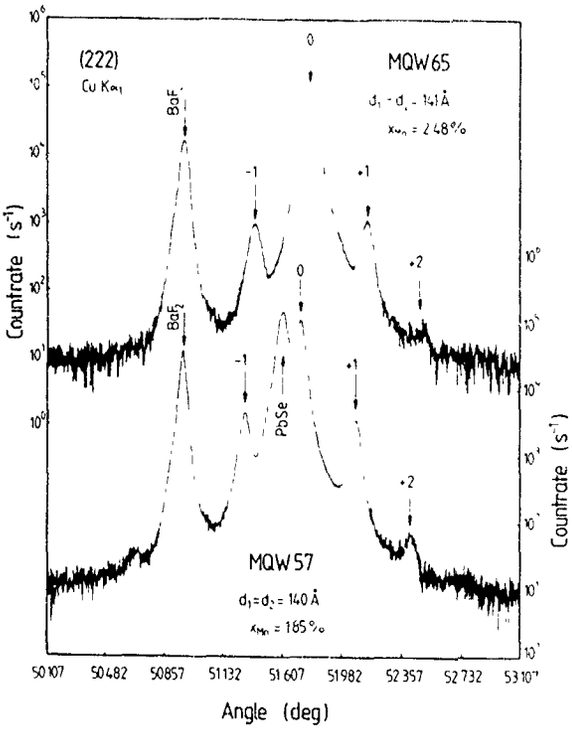

Fig.2: Θ-2Θ scan of symmetric (222) Bragg reflexions of PbSe/$Pb_{1-x}Mn_xSe$ MQW structures.
Upper panel: MQW65 deposited on strain symmetrized $Pb_{1-y}Mn_ySe$ buffer.
Lower panel: MQW57 deposited on PbSe buffer, which is clearly separated from the i = 0 SL peak.
Period ($d_1 + d_2 = 280$Å) is identical for both samples.

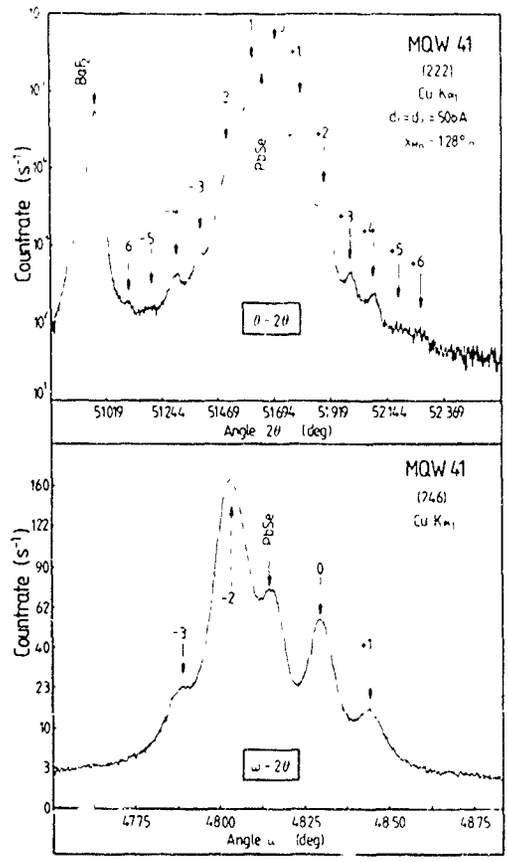

Fig.3: Symmetric (222)(upper panel, Bragg reflexion) and asymmetric (246) (lower panel, rocking curve) diffraction patterns showing sattelite structure for PbSe/$Pb_{1-x}Mn_xSe$ MQW41 sample.

High resolution x-ray diffractometry

- *State-of-the-art HR diffractometer for structural characterisation of epitaxial layers*
- *Unique 4-crystal Bartels monochromator delivers ultimate optical performance*
- *Automated x-y stage allows wafer area mapping*
- *Bond's method permits high-accuracy lattice parameter measurement*
- *All Bragg reflections accessible for strain/relaxation determination*
- *PC software covers data collection and display, plus on-line analysis of mismatch, composition and layer thickness*
- *Dynamical scattering simulation program aids in-depth data interpretation*
- *Systems supported by Philips' world-wide service organisation*

For more information:
Philips Analytical
Lelyweg 1, 7602 EA Almelo,
The Netherlands
Tel: (05490) 39911
Fax: (05490) 39598

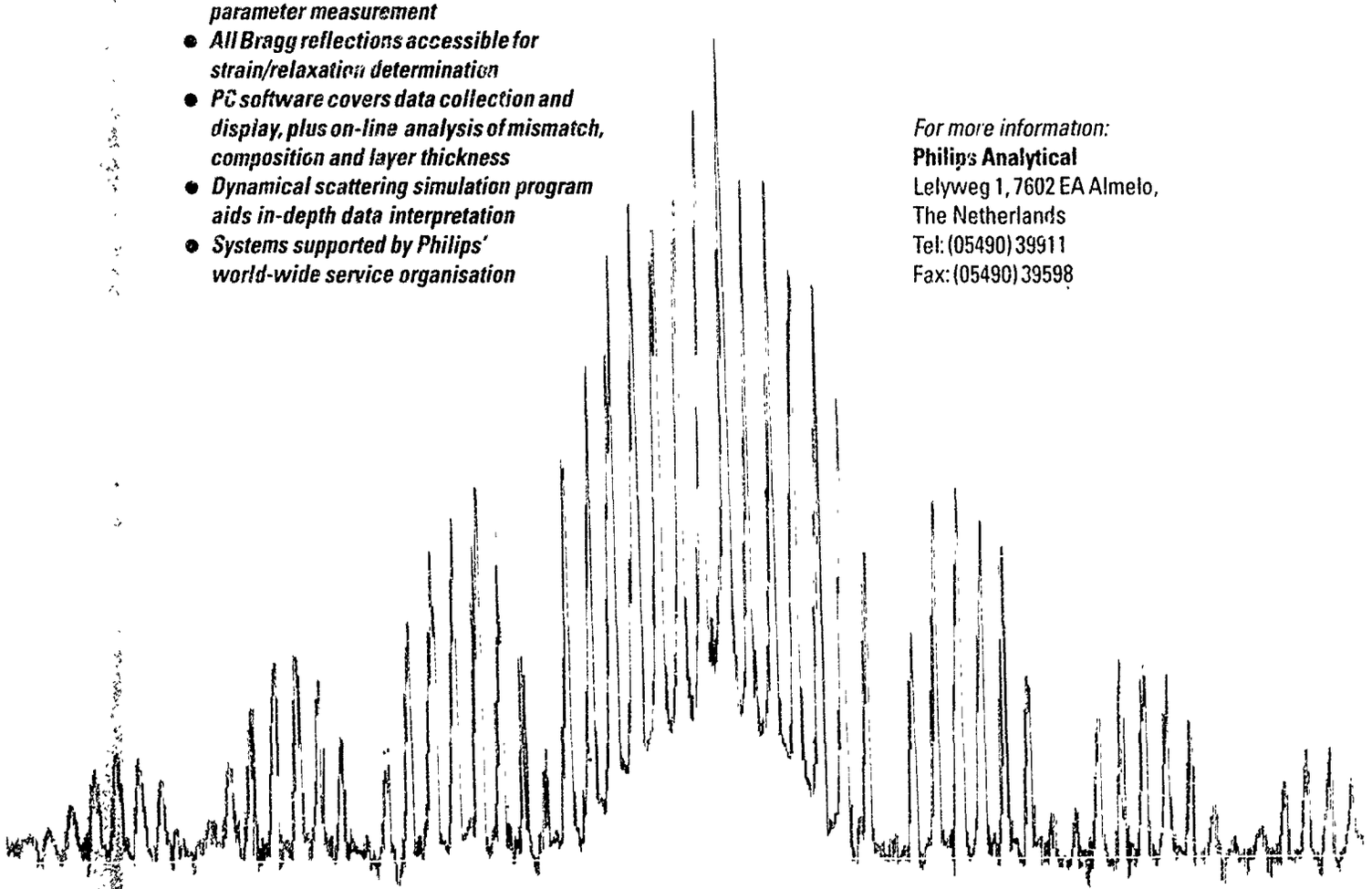

PHILIPS

PHILIPS

Defect Self-Annihilation in Surfactant-Mediated Hetero Epitaxial Growth

M. Horn-von Hoegen, F. K. LeGoues*, M. Copel* and R. M. Tromp*

Institut für Festkörperphysik, Universität Hannover,
Appelstr. 2, 3000 Hannover 1 , Federal Republik of Germany
phone: (511)-762-4820, fax: (511)-762-4877
*(IBM Research Division, Thomas J. Watson Research Center,
P.O. Box 218, Yorktown Heights, NY 10598, USA)

PACS: 61.16.Fk; 68.35.Bs; 68.55.-a

Islanding and misfit related defect formation are the two most outstanding obstacles for growth of high quality heteroepitaxial films. We show that surfactants may be used not only to inhibit islanding, but also to control defect structure. Growth of Ge films on Si(111) at 600°C was mediated by a monolayer of Sb floating on the surface. Exceeding the critical thickness, partial Shockley dislocations are initially found to thread to the surface. The threading defects are self-annihilating, acting as a nucleation site for a complementary partial dislocation which slides down to the interface, leaving behind a fully relaxed, defect free epitaxial Ge film. Thus, the seemingly incompatible goals of strain relief and defect free growth can be accommodated by a surfactant modified growth front.

The driving force for the formation of dislocations and islanding is the strain energy built up by the lattice mismatch between the substrate and overlayer. In the Si/Ge system the initial small islands are dislocation free, but with increasing thickness, dislocations are introduced from the edges of the islands. For thick films, where the islands coalesce, many defects thread up to the surface and cannot be overgrown.

Experimental results were obtained by in situ examination with medium-energy ion scattering (MEIS), low energy electron diffraction (LEED), by ex situ high resolution cross-sectional transmission electron microscopy (TEM) and Raman scattering. The samples were prepared under ultra high vacuum conditions in a MBE (molecular beam epitaxy) chamber directly coupled to the MEIS chamber.

Initial studies were done without the surfactant. In fig.1.(a) we show backscattering spectra after deposition of 10 ML Ge at 600°C. The random spectrum (dotted line) shows a peak at 187 keV, due to the 3 ML thick continous Ge film (Stransky-Krastanov layer) covering the whole surface. The long low energy tail is caused by Ge islands with an average height of about 50 ML, covering ~15 % of the surface.

Ge films grown with an Sb saturated surface at the same temperature show an altogether different behavior. In fig.1(b-d) we show backscattering spectra for 18 ML, 30 ML and 100 ML thick Ge films on Si(111). The random spectra always show a compact trapezoidal shape for the Ge yield, reflecting a continuous, uniformly thick film. The channeling spectra show two features: the Ge surface peak at 187 keV, and another peak at the low energy edge of the Ge signal (the Si-Ge interface), found in films grown past the critical thickness for defect introduction. The integral yield of the interface peak corresponds to 2 ML of Ge, independent of film thickness. The

peak does, however, broaden with increasing film thickness, as a result of the energy straggling of the ions.

For the thick Ge films the angular positions of the blocking minima are the same for the Ge film and for the Si substrate, indicating that the Ge is fully strain relieved. Raman scattering measurements show an unshifted Ge phonon, characteristic of unstrained Ge, without any intermixing with Si. The peak broadening of 3 cm^{-1} of this phonon is the same as expected for a Ge(111) crystal with a doping concentration of $\cong 3 \cdot 10^{19}/cm^3$. Based on ion scattering data we estimate an upper limit of incorporation of $\cong 4 \cdot 10^{19}$ Sb/cm^3.

Low energy electron diffraction of the (2x1) reconstructed Ge surface also reflects excellent epitaxial quality of the Ge films. We observe sharp, brilliant spots with a low background, indicating large superstructure domains, no terraces (within the resolution limit of 100Å terrace size) and a low point defect density.

TEM was used to determine the nature, structure and location of the strain relieving defects as a function of film thickness. The strain relief occurs in two stages. First, a Shockley partial dislocation15 glides at a Ge film thickness of 8-10 ML from the surface to the interface. A stacking fault extends along the interface, then threads through the Ge layer, linking the Shockley partial dislocation to the surface. The second stage of strain relief, seen for thicker films, involves the nucleation of a second Shockley partial dislocation where the stacking fault intersects the surface. The second Shockley partial glides from the surface to the interface along the pre-existing stacking fault, fortuitously eliminating the portion of the stacking fault that threads through the epilayer and leaves a full, but split dislocation at the interface.

Fig. 2 shows a 100 ML film. The bulk of the film is now perfect, since no threading dislocations are present. Dissociated dislocations are located at the Si/Ge interface. On the avera- one dislocation is observed every 25 lattice fringes, thus relieving the misfit completely. Since the misfit is entirely relieved by Shockley partials, the interface is composed alternately of faulted and unfaulted regions, which is clearly seen on the micrograph. The annihilation of the threading portion of the dislocation is an extremely efficient process. It has been observed in a large number of cross-sectional samples, with a total absence of threading defects. In contrast, defect densities for structures grown by conventional procedures suffer from defect densities as high as $10^{12}/cm^2$. In addition, the dislocation network is remarkably abrupt in the growth direction. If we neglect the strain fields, the dislocations are localized to within a few atomic planes of the interface.

Epitaxial growth of non-lattice matched structures is a struggle to simultaneously control film morphology, strain relief and defect structure. Conventional growth strategies may include the use of thick buffer layers and even superlattices to relieve lattice mismatch and to exclude defects from the active regions. Control of surface free energy with a surfactant eliminates islanding. Simultaneously, it strongly modifies defect nucleation. For Ge/Si(111), the defect microstructure is self-annihilating, since each thread contains the seeds of its own destruction. The result is an ideal heterostructure, consisting of two perfect, fully relaxed crystals joined at an atomically abrupt interface.

Figure 1. Ion backscatter spectra for Ge films grown at 600°C.
(a) Growth without surfactant results in islanding.
(b-d) Ge films grown with Sb as a surfactant show no sign of islanding. The channeling spectra show the peak due to dislocations at the Ge-Si interface.

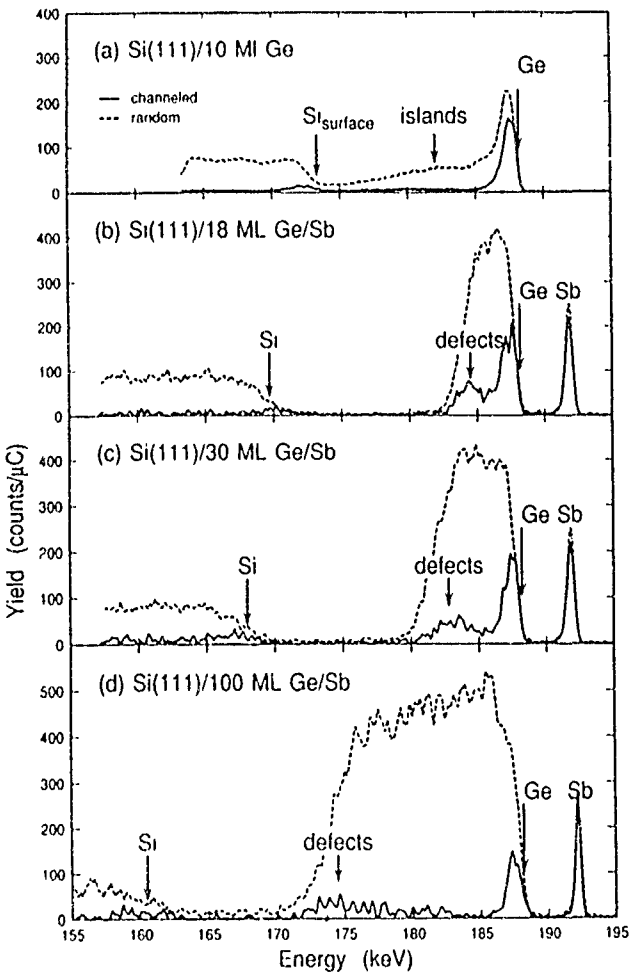

Figure 2. Cross-sectional transmission electron micrographs of Ge/Si(111).A 100 ML Ge film with fully evolved microstructure. The interface (I) contains a network of Shockley partial dislocations, (D1) and (D2). The partials have 1/6 (211) and 1/6 (112) burgers vectors, respectively. Threading dislocations are completely absent from the bulk of the Ge film.

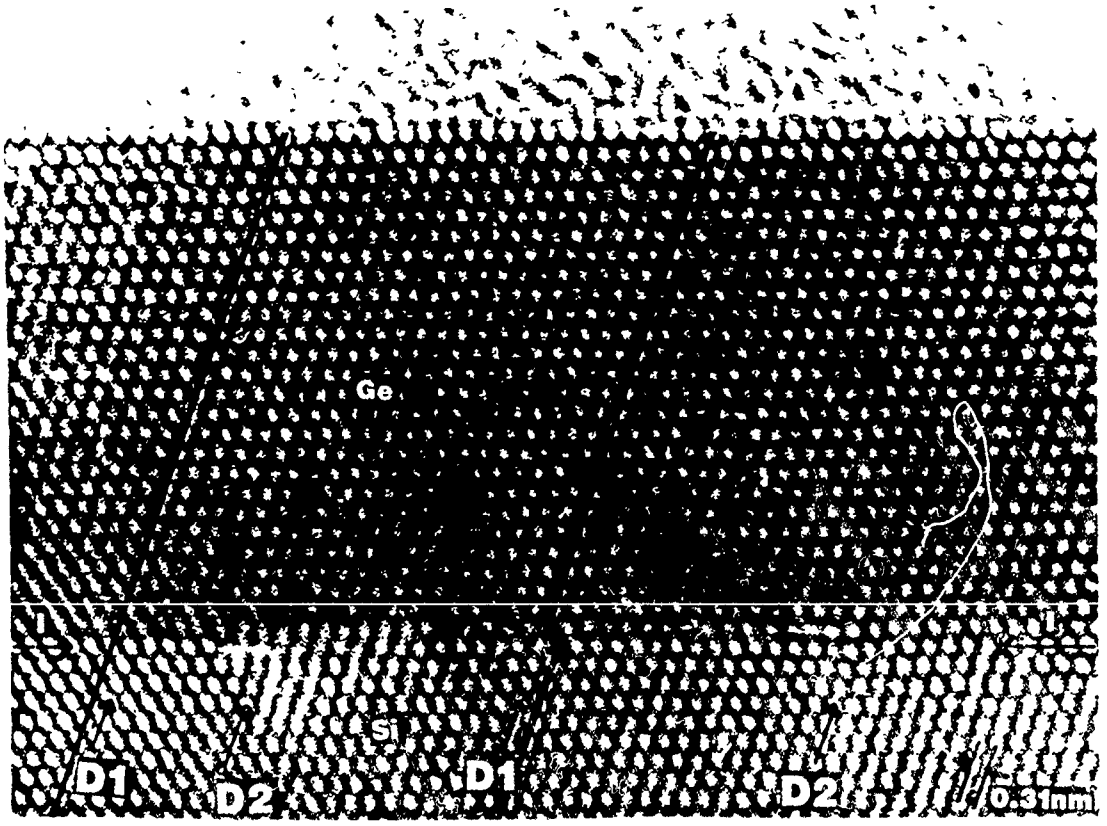

LOW TEMPERATURE PROCESS OF GaAs/AlAs HETEROSTRUCTURES ON Si BY ATOMIC LAYER MOLECULAR BEAM EPITAXY

Y. González*, L. González and F. Briones
Centro Nacional de Microelectrónica,
Serrano 144, 28006 Madrid (Spain).
Phone: 34-1-2625311 or 2625356, FAX: 34-1-4117651

In the past years a great effort has been made in order to get high quality GaAs on Si layers. Although very important advances have been achieved, its compatibility with conventional Si technologies has not been got yet. In order to solve this problem it is necessary to reduce the temperature of Si substrates preparation as well as the temperature of epitaxial growth. With this aim we have used a low temperature (400°C < Ts < 550°C)[1] Si substrates process based in HF vapour exposure before introducing the samples in the ultra high vacuum prechamber. This method produces hydrogen passivation layer adsorbed in the Si surface which is thermally desorbed at substrate temperature, Ts, below 550°C, leaving clean, 2x1 reconstructed Si surface ready for epitaxial growth.

On the other hand epitaxial growth at low Ts is achieved by ıg Atomic Layer Molecular Beam Epitaxy (ALMBE), a new development of MBE carried out in our laboratory, that has demonstrated to be very useful in epitaxial growth of a good quality mismatched systems[2].

Test structures consisting in a 50 Å thick GaAs QW confined by 0.1 μm thick GaAs/AlAs short period superlattices grown by ALMBE at Ts = 300°C on a thin (1.2 μm) GaAs buffer layer showing excellent optical properties (see fig. 1). This 1.2 μm thick GaAs buffer layers consists of 2000 Å thick grown by ALMBE at Ts = 300°C directly grown on Si substrates, followed by conventional MBE growth of 1 μm thick

GaAs at Ts = 585°C. The Si substrates were prepared by a conventional high temperature (800°C) process. We want to point that during the first layer grown by ALMBE a single domain growth front is achieved when only 500 Å have been grown[3].

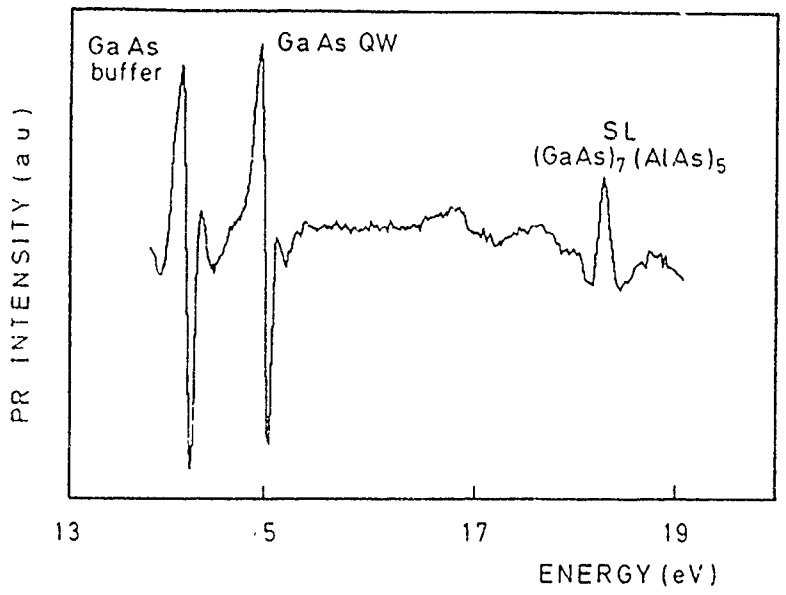

Fig. 1: Photoreflectance spectra of GaAs QW confined by 0.1 μm AlAs/GaAs short period superlattices ALMBE grown at low temperature on conventional prepared Si substrates.

We have extended this work to the low temperature growth of GaAs/AlAs MQW on Si substrates also prepared at low temperature in order to get a full low temperature process. These structures were made on variable thick GaAs buffer layers ($0.2 < d < 0.7$ μm) grown by ALMBE at Ts = 300°C on Si substrates processed at $400°C \leq T \leq 550°C$.

All these layers exhibit an excellent morphology and good absorption properties (see fig. 2). Data will be presented on the influence of these new starting Si surfaces on the kinetics of antiphase domains annihilation process as well as its influence on the absorption properties in these layers.

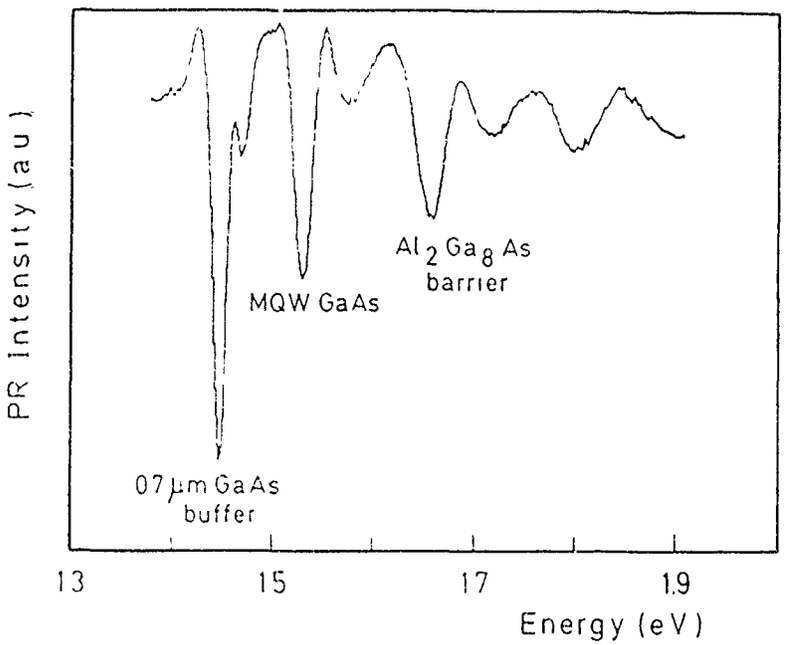

Fig. 2: Photoreflectance spectra of GaAs/Al_2Ga_8As MQW ALMBE grown at low temperature on Si substrates prepared at low temperature.

Acknowledgements:

The authors wish to thank to J. M. Rodríguez for the PR characterization. This work has been supported by the Commission of the European Communities under ESPRIT II Project 2289 (Optical Interconnections for VLSI and Electronic Systems).

References:

(1) S. S. Iyer, M. Arienzo and E. de Fresart, Appl. Phys. Lett. 57 (1990) 893.

(2) F. Briones, L. González and A. Ruiz, Appl. Phys. A 49 (1989) 729.

(3) Y. González, L. González and F. Briones, Jpn. J. Appl. Phys. 30, No. 2B (1991) (In press).

FIRST STAGES OF THE MOLECULAR BEAM EPITAXY GROWTH OF ZnTe ON GaAs(001) STUDIED BY GRAZING INCIDENCE X-RAY DIFFRACTION

by V.H. Etgens*, R.Pinchaux[a], M. Sauvage-Simkin[b], J. Massies[c], N. Jedrecy[b], A. Waldhauer[d] , S.Tatarenko[e] P.H. Jouneau[f]

LURE, CNRS-CEA-MENJS, Bat. 209d, Centre Universitaire, 91405-Orsay-Cedex (France)

and

(a) Université P. et M. Curie

(b) Laboratoire de Minéralogie-Cristallographie, 4 Place Jussieu, 75252 Paris-Cedex 05 (France)

(c) LPSES, rue B. Gregory, 06560 Valbonne (France)

(d) DSM/ DPhG/ SPAS- Bat 462 CEN-Saclay-91191 Gif sur Yvete-Cedex (France).

(e) Laboratoire de Spectrométrie Physique, Université Joseph Fourier-CNRS, Grenoble (France)

(f) CEN-Grenoble, DRF/SPh-PSC, BP 85X, 34041 Grenoble Cedex (France).

When a material with a lattice constant a_L is grown epitaxially on a substrate with a slightly different parameter a_S, it first produces an elastically strained layer which then suffers plastic deformation when the energy stored in the epilayer (proportional to its thickness) is sufficient to create dislocations in the system. The relative lattice parameter difference ($\Delta a/a = a_S - a_L/a_S$) occuring of usual heterostructures in III-V devices are classically smaller than 10^{-3} , however in the last few years work has been done to understand how systems like GaAs/Si[1], Ge/Si (001)[2], CdTe/GaAs(001)[3], ZnTe/GaAs(001)[4] with a mismatch larger than 10^{-2} accomodate the epitaxial strain. In our study we have analyzed the first stages of the growth of ZnTe on GaAs(001) using grazing incidence X-ray diffraction (GIXD) and high resolution electron microscopy (HREM).

The X-ray measurements were performed in a ultra-high vacuum (UHV) compatible 4-circle diffractometer coupled to a molecular beam epitaxy (MBE) chamber[5], at the LURE (Orsay-FR) synchrotron radiation facility. A GaAs(001) substrate "ready for epitaxy" was cleaned with methanol and ethanol prior to introduction in the MBE chamber. A GaAs buffer layer was grown to improve the surface smoothness. The ZnTe was supplied by an effusion cell. Typical growth rates of 0.1 to 0.3 monolayer(ML)/s were used with the substrate temperature close to 320 C. The ZnTe was deposited in successive steps starting on clean reconstructed GaAs(001) c(4x4), up to a total of 13 ML. The sample was transferred each time from the MBE to the diffractometer under UHV, without any new surface cleaning or air exposure. The sample surface state was controlled with reflection high energy electron diffraction

(RHEED) before transfer to the diffractometer. The ZnTe growth on GaAs(001) c(4x4) starts with a 2-D mode up to 4-6 ML, where it presents a transition to a 3-D growth[6]. The 2-D growth mode recovers after a few hundred layers.

The evolution of the (200) reflection profile of the heterostructure with respect to the thickness of the ZnTe layer is presented in Fig. 1. The first evidence of a ZnTe relaxed layer is observed after 4 ML. Before that we observe a perfect elastically accomodated layer. In table I we present the variation of the in plane lattice mismatch vs. layer thickness. Plastic deformation of the layer starts around 4 to 5 ML, which can be considered as the critical thickness value in this system. Grazing incidence geometry is well suited for such a study ofthe earliest stages of growth since for incident angles lower than α_c (critical angle), total reflection occurs and the transmitted wave in the crystal becomes evanescent, enhancing the epilayer signal with respect to that from the substrate. In Fig. 2 we show the variation of the Bragg angle shift directly related to the mismatch ($\Delta\theta = -\Delta a/a \tan\theta$) as a function of the grazing incidence angle for the 13 ML sample. We observe that the layer is more strained near the interface, and that the misfit near the surface is very close to ZnTe/GaAs bulk mismatch (see table II).

In order to verify that the growth by steps did not change the quality of our results and that we did not have a decomposition of our layer during the X-ray measurements, two directly grown layers of 4ML and 6ML were prepared on two different substrates using the same procedures. The results were identical to the previous ones obtained with step-growth. For the HREM cross section experiments the ZnTe/GaAs samples were protected by a 100 Angstrom GaAs amorphous layer. This was shown not to introduce any spurious strain in the layers and provided a suitable protection. The HREM indicated the onset of plastic deformation between 4-6 ML, in agreement with GIXD and RHEED data. Our calibration of thickness was determined by HREM data.

[1]- N. Jedrecy, M. Sauvage-Simkin, R. Pinchaux, J. Massies, N. Greiser & V. H. Etgens. J. Cryst. Growth,**102**:293, (1990).

[2]- J.E. Macdonald, A.A. Williams, R. van Silfhout, J.F. van der Veen, M.S. Finney, A.D. Johnson & C. Norris, Proceedings of the NATO advanced (1989).

[3]- H. A Mar, N. Salansky & K.T. Chee. Appl. Phys. Lett., **44**: 898, (1984).

[4]- S. Tatarenko, K. Seminadayar, J. Cibert. Appl. Phys. Lett., **51**:1690, (1987).

[5]- P. Claverie, J. Massies, R. Pinchaux, M. Sauvage-Simkin, J. Frouin, J. Bonnet & N. Jedrecy. Rev. Sci. Instr., **60**:2369, (1989).

[6]- J. Cibert, R. Andre, C. Deshayes, G. Feuillet, P. H. Jouneau, L. S. Dang, R. Mallard, A. Nahmani, K. Saminadayar, S. Tatarenko. Presented at 5th Int. Conference on Supperlattices and Microstructures, Berlin, (1990).

-TABLE I-

Thickness (ML)	Mismatch (%)
3	--
5	4.9
6	5.6
8	5.9
13	6.2

-TABLE II-

$\alpha/\alpha c$	Penetration Depht (A)	Mismatch (%)
1.0	103	5.7
0.5	26	6.3
0.3	23	7.0

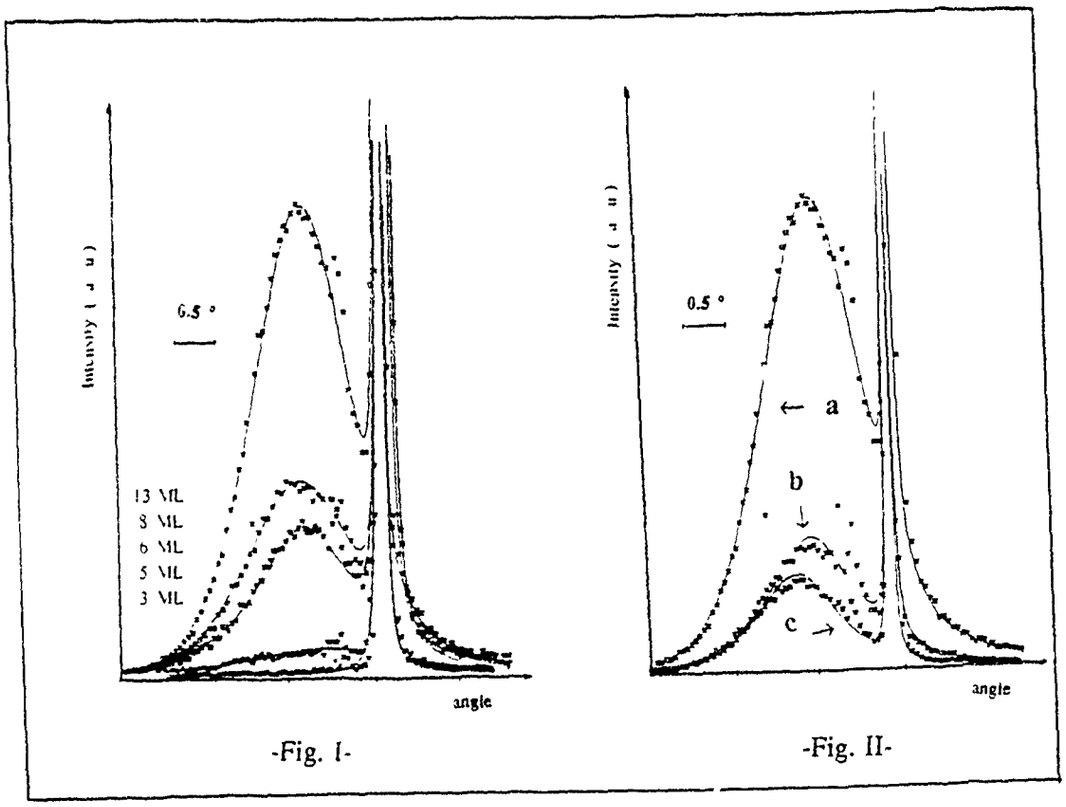

-Fig. I-

-Fig. II-

Fig. I- Evolution of the (200) reflection for the different thicknesses of ZnTe. Just the lower part of the GaAs peak is taken for the representation.

Fig. II- Evolution of the (200) reflection for the 13 ML sample at different incidence angles: a) α_c ; b) 0.5 α_c and c) 0.3 α_c.

GROWTH OF InP ON GaAs BY GAS-SOURCE MBE

K. Rakennus*, T. Hakkarainen, K. Tappura and M. Pessa

Department of Physics, Tampere University of Technology
P. O. Box 527, SF-33101 Tampere, Finland
Tel (358)-(31)-162111, Fax (358)-(31)-162600

The work reported here describes our preliminary results on growth of InP on GaAs, using gas-source molecular beam epitaxy. In particular, we shall study the effects of buffer layers on the quality of InP.

The samples were grown in a VG 80H MBE reactor equipped with two AsH_3 and two PH_3 gas injection manifolds and a high-pressure cracking cell [1]. The substrate was semi-insulating GaAs (001) deliberately misoriented by 2° toward (011) plane. A standard surface treatment procedure of the substrate was performed prior to growth of the buffer layer [2].

Three different types of buffer layers were prepared. In the simplest case, a single InP layer of 17 - 100 nm in thickness was deposited on GaAs at 400 °C, and then annealed at 520 °C for 2 minutes. On this layer, a 2-μm device layer of InP was grown at 490 °C, with the top region of 1 μm doped with Si.

The other buffer layers prepared in this work were more complicated and contained superlattices (SL). One of them was a thermal InP superlattice [3] which was deposited onto an initial 33-nm InP buffer layer (described above). This SL was made by growing a 100-nm InP layer at 490 °C, followed by annealing at 540 °C for 2 minutes, and then growing another 100-nm InP layer at 490 °C. Such a growth and ramp-up period was repeated 10 times, yielding the total SL thickness of 1 μm. Finally, a 1-μm device layer of InP (doped with Si) was grown at 490 °C.

The third type of buffer layer applied here was a compositional strained-layer superlattices (SLS). It consisted of a pair of 2-nm $Ga_xIn_{1-x}P$ and 2-nm InP layers, repeated 50 times. The SLS was grown on 50-nm buffer layer of InP (deposited at 400 °C) upon which another 200-nm layer of InP was grown (at 490 °C). Growth temperature for the SLS and the successive 2-μm device layer was 490 °C and, again, the surface region of 1 μm was doped with Si.

Growth was monitored by observing reflection high-energy electron diffraction patterns. In all cases, the device layer exhibited a P-stabilized (2×4) reconstructed surface, similar to that of high quality homoepitaxial InP grown under closely identical conditions.

Surface morphology of InP on GaAs was essentially the same as that of homoepitaxial InP, as deduced from Nomarski micrographs.

At the time of writing this paper only crystalline structure of the InP/GaAs system has been examined in detail, using X-ray diffraction technique. The Table below lists the full width at half maximum (FWHM) of the rocking curve of CuKα X-ray diffraction from the samples prepared. The smallest FWHM of 350 arc sec was achieved when compositional SLS's with x = 0.2 - 0.3 were used as buffer layers. This FWHM value is about 20 times larger than the FWHM for homoepitaxial InP, due to the poor InP/GaAs interface region. Crystal structure of the film appears to be very sensitive to composition of the SLS. This is clearly seen for composition x = 0.4 for which the FWHM amounted to 730 arc sec, indicating that strong relaxation of strain took place in this SLS by the formation of misfit dislocations.

The net carrier concentration (n) and the Hall mobility at room temperature (μ_{300K}) for sample InP3 were 3.7×10^{15} cm^{-3} and 2395 cm^2/Vs, respectively. For TSL, they were n = 3.0×10^{15} cm^{-3} and μ_{300K} = 2940 cm^2/Vs, and for SLS3 n = 2.7×10^{15} cm^{-3} and μ_{300K} = 2780 cm^2/Vs. The Hall mobility for our homoepitaxial InP with the same thickness and same carrier concentration is typically 3200 cm^2/Vs [4]. This comparison implies that the electrical properties of the top region (1 μm) of InP on GaAs are reasonably good.

In conclusion, we have shown that epitaxial growth of InP on GaAs is feasible by gas-source MBE. InP/GaAs heteroepitaxy may provide an acceptable alternative to homoepitaxial layer growth on more fragile and expensive InP substrate, in particular, for applications where large-area films are desired [5]. Although further studies must be carried out to assess the quality of InP on GaAs in a greater detail it is conceivable that good InP could even be grown on silicon, using an optimized intermediate GaAs layer, and this approach would be very interesting when fabricating InP solar cells for space applications.

Table. Full width at half maximum of the (004) rocking curve of CuKα X-ray diffraction from InP (001) grown by gas-source MBE on GaAs (001). The total thickness of the overlayer was 2.0 - 2.1 μm for InP1 - InP5 and TSL, and 2.4 μm for SLS1 - SLS4. The growth rate was 1 μm/h in all cases.

Sample	Buffer layer thickness (nm)	Thermal SL	Compositional SLS		FWHM (arc sec)
			x	Thickness	
InP1	17	-	-	-	495
InP2	33	-	-	-	475
InP3	50	-	-	-	445
InP4	75	-	-	-	450
InP5	100	-	-	-	490
TSL	33	×	-	-	375
SLS1	50 at 400°C + 200 at 490°C	-	0.1	0.2 μm	375
SLS2	− " −	-	0.2	− " −	350
SLS3	− " −	-	0.3	− " −	350
SLS4	− " −	-	0.4	− " −	730

References:

1. H. Asonen, K. Rakennus, K. Tappura, M. Hovinen and M. Pessa, J. Cryst. Growth 93, 101 (1990).

2. K. Tappura, A. Salokatve, K. Rakennus, H. Asonen and M. Pessa, Appl. Phys. Lett. 57 (1990) 2313.

3. J.W. Lee, Inst. Phys. Conf. Ser. No. 83: Chapter 3., Paper presented at Int. Symp. GaAs and Related Compounds, Las Vegas, Nevada, 1986.

4. K. Rakennus, K. Tappura, T. Hakkarainen, H. Asonen, R. Laiho, S.J. Rolfe and J.J. Dubowski, to be published in J. Cryst. Growth 1991.

5. M. Razeghi : The MOCVD challenge, Vol.1: A survey of GaInAsP-InP for photonic and electronic applications. Bristol, Adam Hilger, 1989, p. 290-320.

Fp1

MOLECULAR BEAM EPITAXY OF III-VI LAYERED COMPOUNDS InSe AND GaSe

J-Y. EMERY*, L. BRAHIM-OTSMANE

Laboratoire de Physique des Solides, associé au CNRS (UA 154)Université Pierre et Marie Curie,4 Place Jussieu, T13-2, 75252 Paris Cedex 05, France

A.CHEVY

Laboratoire de Physique des Milieux Condensés, associé au CNRS (UA 782)Université Pierre et Marie Curie4 Place Jussieu, T13-4, 75252 Paris Cedex 05, France

Abstract : InSe and GaSe III-VI layered compounds semiconductors thin films have been grown through coevaporation of In, Ga and Se elements for substrates temperatures T_s ranging from 300°C to 470°C. In situ RHEED analysis shows that InSe and GaSe do grow on amorphous substrate in a two dimensional process and grow epitaxially when InSe (00.1) and GaSe (00.1) substrates are used. Smooth surfaces with low growth defect density are observed for InSe epilayers grown on InSe (00.1) substrate. Worse surface morphologyare observed fo for InSe epilayer on GaSe (00.1) and GaSe epilayer on InSe (00.1) because of lack of a GaSe buffe layer in the first case and a low substrate temperature used in the second case.

I.Introduction

In the part few years, growing of lamellar compounds heterostructures by mean of Molecular Beam Epitaxy (MBE) has been reported [1-3]. Lamelllar compounds are structurally very anisotropic : their building blocks are layers of saturated covalence bonds between atoms and therefore no dangling bonds are avalaible at their surface. Thus, dangling bonds cannot be invoqued to interprete epitaxial growth of these materials and one speaks of van der Waals epitaxy. at least, large lattice mismatches are expected to be relaxed between layers due to the weakness of the van der Waals forces [1-3].

InSe and GaSe are III-VI semiconductors which crystallize with a lamellar structure. In the hexagonal description, the layer is built up from covalent bonds in the sequence VI-III-III-VI along the c-axis. The lattice mismatch between the two semiconductors is $\Delta a/a = 7$ % in the (00.1) plane. The electronic band structure of InSe and GaSe in the Brillouin zone center is quite flat ; the reduced electron-hole mass is three to five times larger than that of GaAs. Therefore, the exciton binding energy at 4K is 13 meV for InSe (Eg = 1.35 eV) and 20 meV for GaSe (Eg = 2.15 eV). The width of the exciton at room temperature is of the order of 10 meV, so that it is easily observed in an optical transmission experiment. Recently, optical gating using GaSe bulk material have been demonstrated [4, 5] using this property which is more currently found in multiple quantum well structure because of electronic confinement effects.

The III-VI films were grown in a MBE 2300 Riber chamber as discribed elsewhere [6,7]. The equivalent partial pressure, read at the gauge controller, were $P_{In} = 2.15 \times 10^{-7}$ Torr for $T_{In} = 770$°C, $P_{Ga} = 1.2 \times 10^{-7}$ Torr for $T_{Ga} = 860$°C and $P_{Se} = 5.4 \times 10^{-7}$ for $T_{Se} = 155$°C. Pyrex and intrinsic

InSe and GaSe substrates [8] of 1 x 1 cm^2 were hela onto a molybdenum substrate holder. The lamellar substrates were peeled just before their introduction in the load lock chamber.

II. Results and discussion

The growth of InSe is rigorously controlled by the equivalent partial pressure ratio R = P_{Se}/P_{In} because of the In_4Se_3 and γ-In_2Se_3 phases which are also formed by Molecular Beam Deposition (MBD) [6, 7]. GaSe is less difficult than InSe to realize by MBD. In the substrate temperature ranging from T_s = 250°C to 470°C only GaSe is formed though Ga_2Se_3 is also present in the Ga-Se phase diagram. In our experimental conditions, InSe thin films are grown for equivalent partial pressure ratio ranging from R = 2 to R = 3 while GaSe is obtain under Se-rich condition for R ≥ 4. InSe and GaSe thin films deposited on amorphous substrates have their c axis perpendicular to the substrate plane but are randomly oriented in the a x b plane of the layers. RHEED diagrams observed during the growth of InSe are streaky patterns typical of a two dimensional growth mode which are made of a superposition of diagrams obtained for the InSe hexagonal reciprocal lattice shown on fig. 1a-b. The two dimensional growth mode of InSe is observed in the substrate range temperature 225°C ≤ T_s ≤ 345°C. Above T_s = 345°C the streaky pattern changes into a ring pattern indicating a disorientation of the c axis. We did aiso observe these features for GaSe thin films for substrate temperature ranging from 250°C to 450°C which is the upper limit for the GaSe twodimensional growth.

Fig. 1 shows RHEED patterns observed during the growth at T_s = 330°C of an InSe buffer layer (fig. 1d-f) on InSe (00.1) substrate followed by a GaSe heteroepitaxy (fig. 1g-l). In the course of InSe homoepitaxy (fig. 1d-f), the RHEED diagram of the InSe (00.1) surface is observed as early as the growth occurs until deposition of 300 nm thick. The GaSe epilayer is grown under an equivalent partial pressure ratio of R = 4.6. As the growth occurs, no drastic intensity decrease of the RHEED pattern is observed and the six fold symetry of the GaSe (00.1) surface is found after the GaSe epilayer reaches a thickness of 250 nm(fig. 1j-l).

Fig. 2 reports the surface morphology of InSe and GaSe epilayers grown on InSe (00.1) and GaSe (00.1) substrates. The InSe layer grown on InSe (fig. 2a) exhibits a smooth surface with few growth defects of 200 nm in diameter. InSe epilayer grown directly on GaSe substrate (fig. 2b) is very disturbed with large grain appearing in a quite smooth surface. The final aspect of the surface reflects perturbations in the film nucleation process during the growth which could come from the lack of a GaSe buffer layer. The GaSe epilayer grown on a InSe buffer layer exhibits a surface morphology (fig. 2c, 1g-l) quite different of the InSe epilayer shown on figure 2b. This surface (fig. 2c) presents a high density of unknown growth defects with some holes appearing on an orange skin surface morphology. From our results on amorphous substrate the optimal substrate temperature for GaSe should be near T_s = 400°C. Thus, the orange skin reflects a small size grain in the plane because of the non optimal substrate temperature used in this study.

References

[1] A Koma and K. Yoshimura, Surface Sci. 174 (1986) 556.

[2] K. Saiki, K. Ueno, T. Shimida and A. Koma, J. Cryst Growth 95 (1989) 603.

[3] K. Ueno, T. Shimada, K. Saiki and A. Koma, Appl. Phys. Lett. 56, 4 (1990) 327.

[4] C. Hirlimann and J.F. Morhange, Proceedings of the International Congress on Optical Science and Engineering, March 12-15, 1990, The Hague, The Netherland.

[5] Y. Iwamura, M. Moriyama and W. Watanabe, Extended Abstracts of the 22nd, International Conference on Solid States Devices and Materials, Sendai, 1990, 617.

[6] J.Y. Emery, L. Brahim-Otsmane, to be published.

[7] J.Y. Emery, L. Brahim-Otsmane, M. Jouanne, C. Julien and M. BalkanskMaterials Science and Engineering B 3 (1989) 13.

[8] A. Chevy, J. Cryst. Growth 51 (1981) 157.

Figure 1 : RHEED patterns of InSe buffer layer and GaSe thin film grown on InSe (00.1) substrate at T_s = 330°C. (a)-(c) InSe (00.1) surface at room temperature(d)-(f) InSe buffer layer, V_{InSe}=300 nm/h (0.15monolayer /s); (d) t = 30", (e) t = 10', (f) t=60'. (g)-(i) GaSe growwth: V_{GaSe}=230 nm/h (0.08 monolayer /s);(g) t = 30", (h) t = 10', (i) t = 50'.(j)-(l after one hour of GaSe growth .

Figure 2. Surface morphology of InSe and GaSe thin films : (a) InSe epilayer of 300 nm thick on InSe (00.1) (T_s=300°C); (b) InSe epilayer of 300 nm thick on GaSe (00.1) (T_s=300°C); (c) GaSe epilayer of 250 nm thick on InSe buffer layer (fig.1)

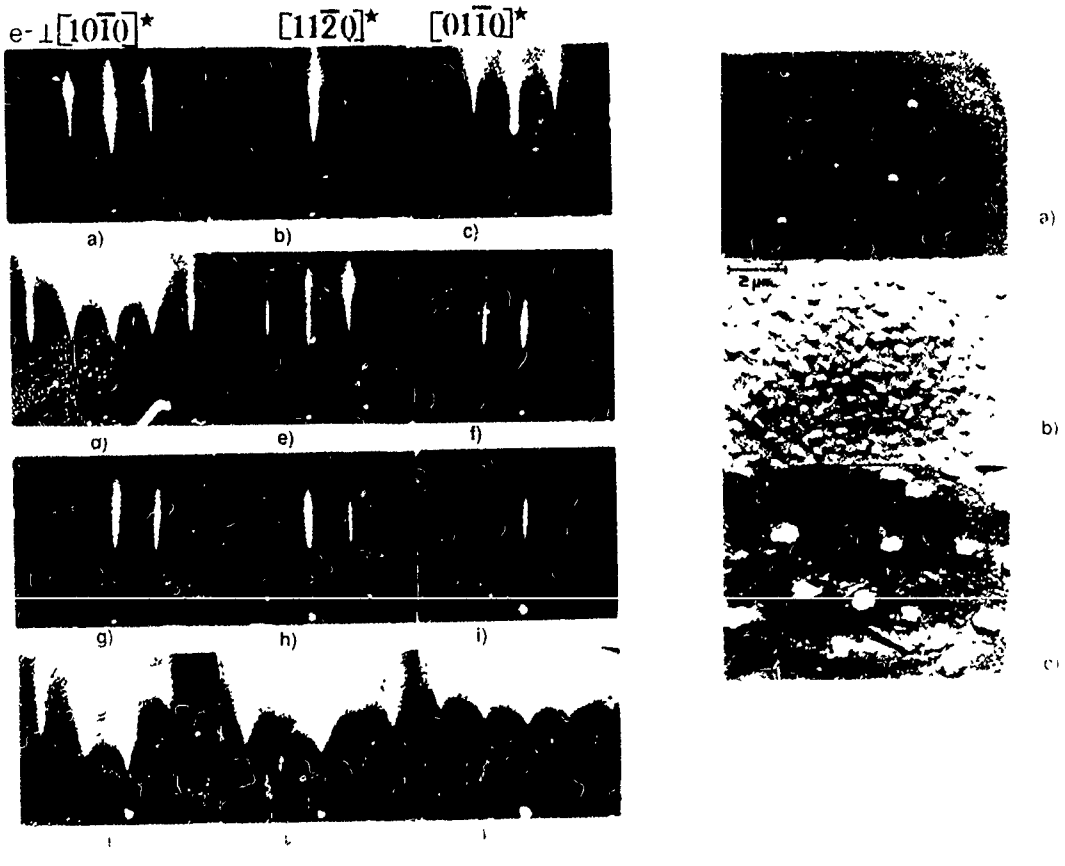

Fp2

MBE-Growth of InSb Bulk-Layers on GaAs Substrates and Observation of Resonant Tunneling in InSb/AlInSb Double-Barrier Structures

J.R. Söderström*, M.M. Cumming, J.Y. Yao and T.G. Andersson

Department of Physics, Chalmers University of Technology

S-412 96 Göteborg, Sweden

Introduction

The scope of this work has been to examine the material system of InSb and $Al_xIn_{1-x}Sb$ for use in heterostructure devices. The lattice mismatch (5.3 % in a InSb/AlSb heterojunction) requires the AlInSb grown on the InSb buffer layer to be below the critical thickness. This InSb layer in turn is grown on a GaAs substrate with a lattice mismatch of 14.6%. This creates a large number of threading dislocations in the InSb epilayer emanating from the heavily mismatched interface. The study is divided into two parts; first the MBE-growth of bulk InSb on GaAs substrates is examined and second InSb/AlInSb double-barrier resonant tunneling structures are investigated.

InSb epilayers on GaAs-substrates

The InSb layers were grown on semi-insulating (100) GaAs substrates in a modified Varian 360 MBE-system. Cracker sources (Epi-systems) were used for the evaporation of the As and Sb materials resulting in dimers (As_2 and Sb_2) in the molecular beams. The beam flux ratio, J_{Sb}/J_{In}, was measured to be about 1.4 for "normal" growth. The growth rate is set to about 1 µm/h. The "pseudo" (1X3) reconstruction was the preferred reconstruction for the InSb growth.

The room-temperature Hall mobility (electrons) was studied as a function of substrate temperature and Sb/In flux ratios with the InSb epilayer thickness kept constant at 2 µm. The highest mobility, 55000 cm^2/Vs, was obtained for a substrate temperature of 420 °C and a flux ratio of 1.4.

The TEM investigation revealed a large amount of crystal defects (treading dislocations and microtwins) in the epilayer. Most of the dislocations were confined to the vicinity of the interface.

Samples with different InSb layer thicknesses were also fabricated and studied with temperature-dependent Hall-measurements. The van der Pauw method works well only when either hole or electron conduction dominate. When more than one type of carrier is present, compensation of the Hall voltage, and consequently the Hall constant R_H, occurs. This problem is evident in these samples. This can be seen in Fig. 1a where the "measured carrier concentration" for an 8 μm-thick sample is shown as a function of the temperature. The two singularities are due to transitions from p-type to n-type conduction. In a 2 μm-thick sample no singularities were observed as seen in Fig. 1c. The proposed reasons for these observations are that there is an electron accumulation layer in the surface of InSb and a background acceptor level in the bulk of the InSb and that the light-mass intrinsic electrons dominate at higher temperatures.

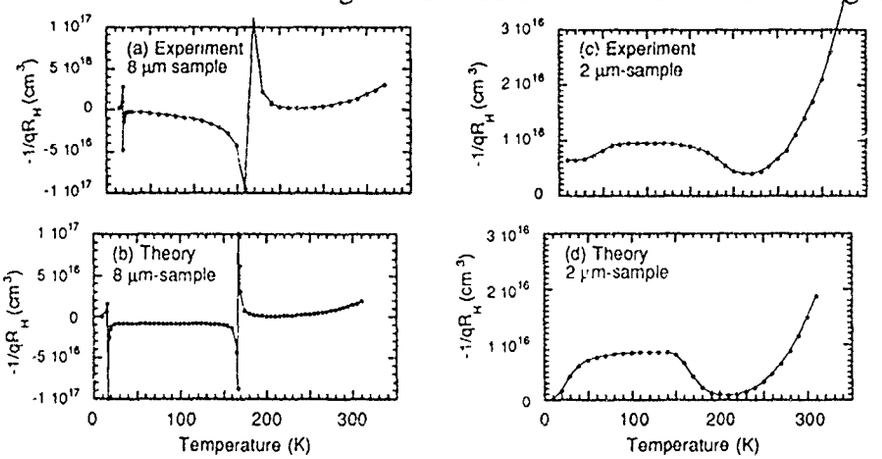

Figure 1. Measured and calculated carrier concentrations (as given by $-1/qR_H$) for an 8μm-thick InSb epilayer (a and b) and a 2 μm-thick InSb epilayer (c and d).

We developed a simple theory for calculation of the Hall-constant to validate these assumptions taking into account (i) intrinsic holes and electrons, (ii) extrinsic holes due to an acceptor background level and (iii) an accumulation layer of electrons in the InSb surface. In Figs. 1b and 1d are shown the calculated curves corresponding to the measured samples above. The agreement between theory and experiments is good. This validates the assumption that the InSb has a p-type background and an electron accumulation region in the surface. The absence of singularities in the 2 μm sample is because the surface electrons prevents the Hall constant to go down to zero as the temperature is lowered from room temperature.

The problem of compensation is further illuminated when the samples are intentionally doped n-type with silicon as shown in Fig. 2.

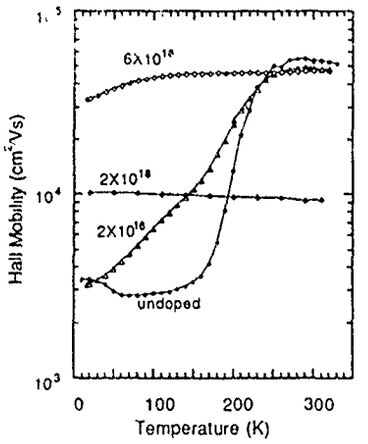

Figure 2. Measured mobility for 2 μm thick InSb epilayers with different intentional n-type Si-doping level. The low values obtained at low temperatures for the undoped and lightly doped samples are due to compensation and do not represent the true electron mobility.

InSb/AlInSb double-barrier structures

We report the first observation of resonant tunneling in the InSb/$Al_xIn_{1-x}Sb$ material system. Five samples with InSb quantum well thicknesses ranging from 70 Å to 110 Å and $Al_{0.5}In_{0.5}Sb$ barrier thicknesses ranging from 22 Å to 36 Å were grown by molecular beam epitaxy on GaAs (100) substrates at a temperature of 420 °C. The best sample, which had 22 Å-thick barriers and a 110 Å-thick quantum well, displayed a peak-to-valley current ratio of 1.4 (3.9) at room temperature (77 K) with a corresponding peak current density of $3.6X10^4$ A/cm^2. The sample layout and the current-voltage characteristic are shown in Fig. 4

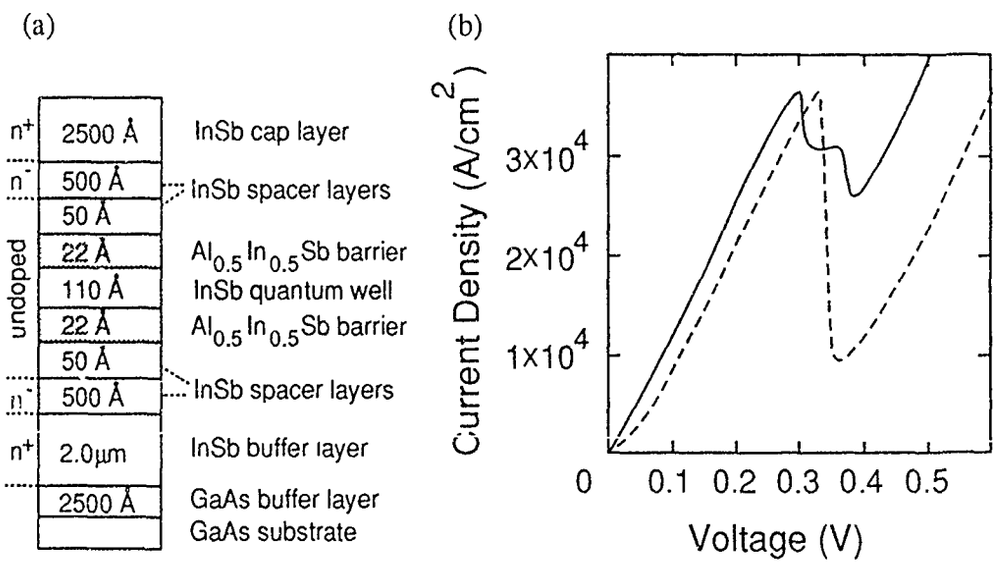

Figure 3. The sample layout of an InSb AlInSb double-barrier structure (a) and the measured current-voltage curve for this sample (b).

Fp3

MBE GROWTH OF $In_xGa_{1-x}As$ (x≈0.53) ON SILICON

A. Georgakilas, M. Lagadas, J. Stoemenos[a] and A. Christou[b]

Foundation for Research and Technology-Hellas
Institute of Electronic Structure and Laser
P.O. Box 1527, 711 10 Heraklion, Crete, Greece. TELEFAX: 30-81-239735

[a]University of Thessaloniki, Physics Department
540 06 Thessaloniki, Greece. TELEFAX: 30-31-206138

[b]University of Maryland, Department of Electrical Engineering
College Park, 20742 Maryland, USA. TELEFAX: 001-301-3149281

Optoelectronic applications favor the development of epitaxial $In_xGa_{1-x}As$ layers (with x around 0.53) on Si substrates[1,2]. However, a large misfit equal to -0.075 occurs between $In_{0.53}Ga_{0.47}As$ and Si which is about double of the -0.039 misfit between GaAs and Si. The higher misfit imposes more difficulties for the heteroepitaxy of InGaAs on Si, beyond the known problems which exist in GaAs on Si (misfit, polar on nonpolar). We have undertaken a systematic study of the $In_{0.53}Ga_{0.47}As$ heteroepitaxy on Si.

Like in the GaAs on Si case we found that the use of Si substrates misoriented from (001) towards a <110> direction is the necessary condition to avoid Antiphase Domains (APDs) formation which results in electrical and optical properties degradation and bad surface morphologies. On Si substrates oriented 3^0-4^0 off (001) we have examined different growth conditions and InGaAs structures. A GaAs intermediate layer with thickness from 30nm to 1.5μm as well the direct deposition of InGaAs on Si have been investigated. In some cases a Si growth chamber connected to the III-V MBE was used to deposit a 0.9μm thick Si buffer layer. Abruptly or continuously graded InGaAs buffer layers and InAs/GaAs short period superlattices were also studied.

Double crystal X-ray diffractometry (DDX) showed that the InGaAs structural quality was almost independent from the growth temperature in a range of 50 ^{0}C around 500 ^{0}C, while the higher growth temperatures rather deteriorated the crystal quality For the InGaAs/GaAs/Si samples the optimum InGaAs and GaAs thicknesses were estimated to be 3.5μm and 30nm, respectively. The typical (400) FWHM was 1100-1200 arc seconds for 3.0-4.0μm InGaAs while the lowest value of 900 arc secs was obtained for a 30nm thick GaAs intermediate layer. The FWHMs did not differ significantly in the other structures and values around 1200 arc secs were

measured using graded InGaAs buffers.

Concerning the InGaAs surface morphology it was found impossible to obtain smooth surfaces like in GaAs on Si. The best results were obtained using an As prelayer (As_4 beam) at 350 ^oC and then depositing InGaAs directly on Si but this result was not reproducible. Electron Channeling Patterns (ECPs) were not adequately fine indicating an inferior crystal quality. Planar and cross-sectional transmission electron microscopy (TEM, XTEM) observations showed that the main defects in InGaAs on Si were dislocations, low angle grain boundaries, stacking faults and spinodal decomposition. The dislocation density in the surface layers of various structures was found between 3 - $8x10^9$ cm^{-2}, the stacking fault density $3x10^6$ - $5x10^7$ cm^{-2} and the grain boundaries density $6x10^6$ - $5x10^7$ cm^{-2}. The dislocation density in the interfacial region was higher, approaching 10^{11} cm^{-2}. From the investigated samples the better results were obtained using a 1.5μm thick intermediate GaAs layer instead of the direct InGaAs deposition on Si, graded InGaAs buffer or InAs/GaAs short period superlattices. These results are attributed to the quality of the InGaAs in the early stages of growth on Si or GaAs/Si, because of a three dimensional island growth mechanism Additonally, in contrast to GaAs on Si a 3-D growth mode seems to happen during the whole growth and this is consisted to the worse surface morphologies and the observation of stacking faults[3]. Although the misfit between

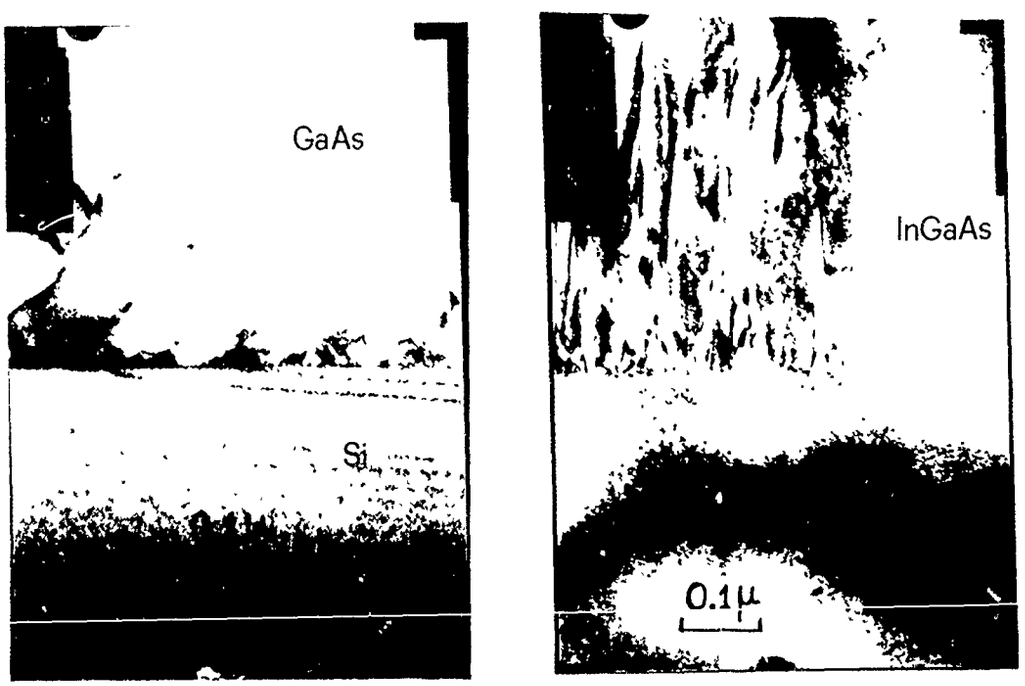

a) b)

Fig. 1. XTEM micrographs showing a) the GaAs/Si and b) the InGaAs/GaAs interfaces, in a InGaAs/GaAs/Si structure.

GaAs and Si is higher than that between $In_xGa_{1-x}As$ ($x \approx 0.53$) and Si, the InGaAs/GaAs interfacial region (Fig. 1b) is highly defected compared to GaAs/Si (Fig. 1a).

The strained layers do not prevent the dislocation propagation since the great majority of them is perperdincular to the (001) plane and hence non glissille.

Finally, a fine (10nm) or a coarse (0.1μm) spinodal decomposition contrast was observed in the InGaAs on Si samples. The spinodal decomposition occured only along the vicinal <110> direction and the contrast was maximum when the reflection g was perpendicular to the direction of the lines. On InP substrates it is known that InGaAs spinodal decomposition occurs along the [100] and [010] crystallographic directions parallel to the substrate, forming a basket weave contrast when is viewed along the [001] direction. Thus the inhomogeneous strain due to tilted Si substrate probably is responsible for the preferential decomposition along the vicinal direction

In conclusion, although we have advanced significantly our understanding of the InGaAs on Si heteroepitaxy, further work is needed to clarify the material aspects and possibly find improvements by affecting the growth process.

References

[1] A. Georgakilas, Z. Hatzopoulos, A A. Iliadis, A. Christou, Mat. Lett. 7, 456 (1989).

[2] A. Christou, N. Flevaris, A. Georgakilas, A.A. Iliadis, Mater Lett. 8, 109 (1989).

[3] L.J. Schowalter, E.L. Hall, N. Lewis, A.S. Hashimoto, presented in: Mater Res. Soc. Symp. C: "Thin Films", Fall Meeting 1988, Boston, USA.

[4] P. Pirouz, F. Ernst, T.T. Cheng, Mater. Res. Soc. Symp. Proc. 116, 57 (1988).

Fp4

MBE GROWTH OF GaAs ON Si WITH A Si BUFFER LAYER

A. Georgakilas, J. Stoemenos[a], P. Panayotatos[b] and A. Christou[c]

Foundation for Research and Technology-Hellas
Institute of Electronic Structure and Laser
P.O. Box 1527, 711 10 Heraklion, Crete, Greece. TELEFAX: 0030-81-239735

[a]University of Thessaloniki, Physics Department
540 06 Thessaloniki, Greece. TELEFAX: 0030-31-206138

[b]Rutgers University, Department of Electrical and Computer Engineering
P.O.Box 909, Piscataway, NJ 08855-0909, USA. TELEFAX: 001-201-9325313

[c]University of Maryland, Department of Electrical Engineering
College Park, 20742 Maryland, USA. TELEFAX: 001-301-3149281

We have used a combined GaAs and Si Molecular Beam Epitaxy (MBE) system for the introduction of Si buffer layers in the growth of GaAs on Si. A common preparation chamber is shared by two separate growth chambers for III-Vs and silicon, respectively. So, the samples can be transferred from one chamber to the other without breaking the vacuum. We found that using the Si source the deoxidation heat treatment can be limited at around 750 ^{o}C, while a thin Si buffer results in overal GaAs quality improvement, by optimizing the Si surfaces and affecting the GaAs nucleation. The Si buffers have indeed resulted in excellent MESFETs performance[1].

The Si substrates were misoriented from (001) by 3-4^{o} towards <110>. A typical chemical preparation was followed[2] which results in the formation of a thin volatile oxide. Oxide desorption took place in the Si MBE. The procedure is consisted by 10-20 min heating at less than 750 ^{o}C, 10min under a low Si flux[3] at the same temperature and 10min while heating the Si E-gun source for higher deposition rate. RHEED observations showed that the impingement of the Si beam resulted in a clear double domain 2x1 pattern in less than 1min.

The Si buffers were grown at a growth rate of 0.4μm/hour and growth temperature of 680 ^{o}C. Following Si deposition, the RHEED pattern still showed a double domain surface while splitted streaks appeared when the beam was incident along the <110> azimuth parallel to the step edges. This indicates the formation of a periodic step array and the ellimination of the facets which are known to form after the thermal desorption of a chemically grown oxide on Si[4].

Following the deposition of 0.2-1.0μm Si the wafers were transferred to the III-V chamber where the GaAs deposition was accomplished using a two step growth process. A 30nm thick nucleation layer was deposited at 350 ^{o}C with a growth rate of 0.35μm/h, while the growth was continued for the rest structure at 600 ^{o}C with 1.0μm/h. An As prelayer (As_4 beam) on the Si surface at 350 ^{o}C was always used before the GaAs deposition, since it results in GaAs oriented with the [110] azimuth parallel to the Si<110> misorientation direction and to a 2-D growth mode.

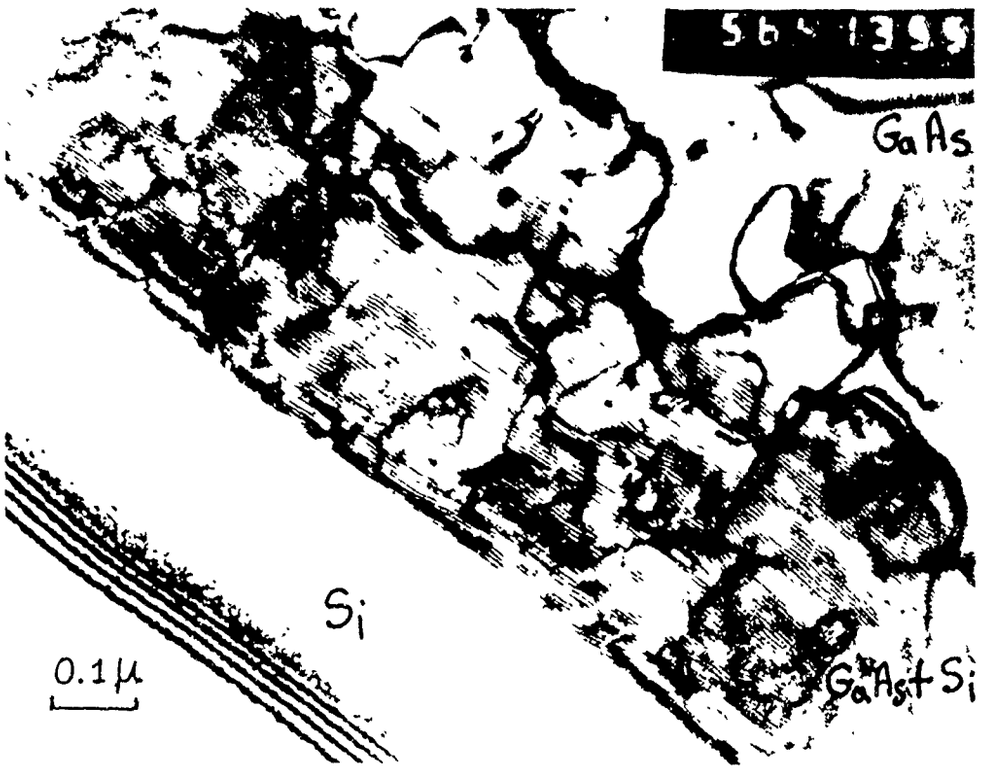

Fig. 1 TEM micrograph for the GaAs/Si interfacial region of a GaAs/Si/Si sample indicating a regular moire pattern (220 reflection).

SEM micrographs showed that absolutely smooth GaAs surfaces were obtained Cross-sectional and planar transmission electron microscopy (XTEM, TEM) observations showed the complete absence of any planar faults and an overally improved GaAs crystal quality. The TEM micrograph of Fig. 1 was taken from the GaAs/Si interfacial region, using a 220 reflection, to see the evolution of defects from the top Si buffer, the GaAs/Si interface and the first GaAs layers. In one area there was only Si, in the middle area there were both GaAs and Si and in the next area there was only GaAs. A perfect Si buffer is shown In the GaAs/Si part of the specimen, moire fringes of translation type parallel to <110> are shown which form a very regular pattern, in large areas, with spacing 4.8nm. It is noted that the moire

patterns are very sensitive to any local strain or nucleus misorientation. All the above observations indicate that a two-dimensional growth mode was followed from the very early stages of growth. It seems that the suppresion of defects on the Si surface enhanced the uniform GaAs nucleation resulting very soon in a 2-D growth mode. However, the dislocation density near the interface was 10^{10} cm^{-2} and decreased to 10^{8} cm^{-2} in the GaAs surface.

Double Crystal X-rays Diffractometry gave a (400) FWHM of 255 arc seconds for 1μm GaAs epilayer which is the best value ever reported for such thickness However, the FWHM decreases only to 212 and 205 arc secs for 2μm and 3μm GaAs epilayers respectively, indicating a saturation in the material quality The dislocation density for 2μm GaAs was estimated to be around 10^{8} cm^{-2} even for this improved material in agreement with other investigators reporting optimized material by thermal cycling[5]. Finally, the XTEM observations indicate that the Si buffer seems to affect the stress relaxation mechanisms, since an unexpected (energetically unfavorable) dislocation reaction was often observed in the GaAs layers. A threading dislocation with burgers vector parallel to the interface was split to two dislocations with burgers vectors inclined to the interface.

References

[1] A. Georgakilas, J. Stoemenos, C. Berge, C. Michelakis, C. Cason, M. Lagadas, Z. Hatzopoulos, A. Christou, presented in: 17th Int. Symp. on GaAs and Rel. Comp., Jersey, U.K. September 24-27, 1990.

[2] P. Panayotatos, A. Georgakilas, J-L. Mourrain, A. Christou, SPIE Int Conf. on Physical Concepts of Materials for Novel Optoel. Dev Applications, Aachen, FRG, Oct. 28 - Nov. 2, 1990.

[3] L. Kugimiya, Y. Hirofuji, N. Matsuo, Jpn. J. Appl. Phys. 24, 564 (1985).

[4] R. Hull, A. Fischer-Colbrie, S.J. Rosner, Appl. Phys. Lett 51, 1723 (1987).

[5] N. Chand, F. Ren, A.T. Macrander, J.P. van der Ziel, A.M. Sergent, R. Hull, S.N.G. Chu, Y.K. Chen, D.V. Lang, J. Appl. Phys. 67, 2343 1989).

Fp5

MBE PROCESS COMPATIBLE PLASMA ENHANCED GROWTH OF SILICON-BASED DIELECTRIC FILMS

I. Eisele, H. Lorenz, Institut für Physik, Fakultät für Elektrotechnik, W-8014 Neubiberg, Germany
J. Ramm, E. Beck and A. Züger, Balzers AG, FL-9496 Balzers

Tel.: UniBwM - 089/6004-3519
Fax: UniBwM - 089/6004-3560

The synthesis of silicon-based dielectric films at low substrate temperatures is of great interest for the development of new semiconductor devices as well as for their higher integration. Low process temperatures help to reduce interface reactions and segregation of dopants if sharp transitions or delta doping profiles are required. However, they increase also the sticking probability for the residual gas components. To obtain the desired film synthesis the processes are often plasma enhanced. This again increases the reactivity of the residual gases. Therefore, it is advantageous to develop process sequences which are compatible with UHV environment and can be carried out in-situ in combination with MBE.

The described plasma enhanced evaporation (PEE) of silicon under Ar/O_2 and Ar/N_2 plasma to obtain SiO_2 and Si_3N_4 films, respectively, is suited for this purpose.

Silicon is evaporated in a conventional MBE system by an electron beam evaporator from a copper crucible insulated from ground. For the growth of dielectrics this crucible simultaneously functions as anode for the electrons from a non-self-maintained gas discharge. The cathode for this discharge is a heated filament placed in a separate cavity. With the power supply between the crucible and the heated filament electron currents of about 100 A can be obtained for applied voltages of about 100 V. These low voltage electrons have high ionisation probabilities for the evaporated material as well as for gases. Therefore, an intense plasma is created during deposition. The current density of the electrons in this plasma is much higher than that of the ions. Insulating

substrates placed in this plasma are charged negatively and maintain a negative potential (typically 20 V) with respect to the plasma. The ions of the plasma are accelerated towards the substrate and increase the reactivity of the process.

With this PEE process SiO_2 and Si_3N_4 films are synthesized at temperatures between 100° C and 400° C. The films are stoichiometric and have hydrogen contents below 1 at %. For the electrical characterisation metal-insulator-semiconductor diodes were fabricated and investigated before and after annealing in H_2/N_2 atmosphere at 430° C. Ellipsometric and capacitance-voltage measurements yield the dielectric constants which agree well with the theoretical values. From conductance-voltage characteristics the silicon-insulator interface state densitiy D_{it} was determined. After annealing D_{it} amounts to 5×10^{10} $eV^{-1}cm^{-2}$ for SiO_2. In addition the bulk resistivity and the surface resistivity of the deposited films were measured and compared with the values for film grown by conventional high temperature processes.

In a second process step the above described gas discharge is used for a plasma oxidation of silicon wafers at low temperatures. The discharge parameters (low voltage and high electron currents) in comparison with other methods of plasma generation are expected to accelerate the oxidation. The process and rate measurements are under investigation.

Fp6

Initial Stage of epitaxially grown ZnSe on GaAs:Experiment and Theory

D.Schikora,J.Griesche,A.Josiek,R.Enderlein

Department of Physics,Humboldt-University Berlin,
Federal Republic of Germany

The initial stage of epitaxial growth of ZnSe on GaAs is studied. GaAs substrates of different orientations ((001),(111),(110)) are considered.
Atomic arrangements of Zn,Se and ZnSe layers are investigated by means of tight binding total energy calculations. In the case of Ga-terminated (100)- substrate surfaces it is found,that the first Se -monolayer is partially dimerized, and shows a (2x1) reconstruction.In the case of a Zn monolayer on As-terminated GaAs, c(2x2) or (2x1) reconstructions are found to be favoured. If more Se and Zn monolayers are deposited,the reconstruction alternates between (2x1) for Se-rich and c(2x2) for Zn-rich surfaces,in agreement with experiments /1/. We present new RHEED data, which claerly demonstrate this reconstruction behavior.
The question is studied if this behaviour represents a bulk property of ZnSe or is due to the influence of the GaAs/ZnSe interface. It is demonstrated that a ZnSe/GaAs monolayer is instable against partial exchange of Zn and Ga atoms ,and against the formation of Ga vacancies. We consider these processes to be the initial steps of the formation of a Ga_2Se_3 interregion which has been found experimentally /2/. It is speculated, how this knowledge could be used to avoid the Ga_2Se_3 formation, for instance by applying a definite sequence of Zn-and Se-pulses during the growth of the first three monolayers. We have extended our growth experiments to (111) and (110) substrate orientations.
RHEED measurements have been performed showing two different reconstructions. Assuming complete Ga or As coverage of the (111) surface, Se,Zn and ZnSe monolayers are calculated with respect to their total energies. Reconstructions are found in accordance with experiment. It is shown that the formation of Ga vacancies is not favourable at this interface,thus Ga_2Se_3 should not be formed. This is found to be true also for the (110) interface.

/1/ M.C.Tamargo, J.L. deMiguel, D.M.Hwang and H.H.Farrel
J.Vac.Sci.Technol. B 6,784 (1988)
/2/D.W.Tu and A.Kahn
J.Vac.Sci.Technol. A 3,922 (1985)

STRUCTURAL PROPERTIES OF MBE GROWN BaF_2/CaF_2 BILAYERS ON BOTH Si(111) AND Si(100)

F. Nguyen-Van-Dau*, V. Mathet, J. Siejka[a], P. Galtier and D.G. Crété
THOMSON CSF - LCR, 91404 Orsay Cedex FRANCE
Phone number: (1)60.19.7454 - FAX: (1)60.19.7829
[a]permanent address: G.P.S.E.N.S., Univ. Paris 6, 2 place Jussieu, 75252 Paris Cedex 05 - FRANCE

Recently, there has been a growing interest in the heteroepitaxy of large mismatched compound semiconductors onto silicon substrates. This interest is partly due to the possibility of a monolithic integration between specific functions (e.g. detection, optoelectronic, etc...) and silicon circuits. Among the various systems that have been studied, it has been shown[1] that high quality heteroepitaxy of lead salts compounds (LSC) on Si(111) can be achieved using $(Ba,Ca)F_2$ buffer layers in order to overcome the important difference between lattice parameters (typically 12-15%) as well as thermal expansion coefficients (a factor of 8 between LSC and Si). However, the understanding of detailed structural features of the fluoride layers such as defects in the layers, interface microstructure is still an opened question.

In this contribution, we will present results concerning the growth by molecular beam epitaxy (MBE) and structural characterizations of BaF_2/CaF_2 layers on both Si(111) and Si(100).

a) Growth on Si(111)

It is well known that a (111) orientation of the Si substrates strongly favours a two dimensional growth of the fluoride layers[2] due to surface energies considerations. Our fluoride structures consist of ≈100Å CaF_2 grown at 650°C followed by 2000-4500Å BaF_2 grown at ≈420°C. The reduction of temperature from 650°C to 420°C is performed either before or during the BaF_2 nucleation.

The cristallinity of the BaF_2 layer is characterized both "in situ" by Reflection High Energy Electron Diffraction (RHEED) and "ex situ by Rutherford Backscattering Spectroscopy (RBS) in channeling geometry. We obtain streaky RHEED patterns all along the growth. Moreover. a bulk BaF_2 RHEED pattern is formed within the first few monolayers of growth indicating a non-pseudomorphic mode of growth. From RBS

measurements, we obtain $\chi_{min.}$ as low as 5% (Ba edge) indicating a good crystalline quality of the BaF_2 layers.

We have developped a chemical etching technique in order to characterize the defects density of our samples. The best results are obtained with HCl(2.5-7%):H_20 or HNO_3(2.5-7%):CH_3OH baths. Typical etching rates are 80 Å.s^{-1}. Defects densities as low as 10^4 cm^{-2} have been measured on 4100Å BaF_2/100Å CaF_2//Si(111) samples using this technique. Figure 1 shows defect densities measured on the same sample with the two baths for different etched thicknesses. These very low densities suggest that a large majority of defects coming from the lattice mismatch between BaF_2 and CaF_2 (≈14%) stay confined at the BaF_2/CaF_2 interface. An additional point on figure 1 indicate that, from scanning electron microscopy observations, the final BaF_2 surfaces are essentially defect-free, even with magnifications as high as 20000. The lowest defect densities are obtained for BaF_2 layers whose nucleation is operated at 420°C. It is worth noting that when this nucleation occurs at 650°C, the samples exhibit defect densities that are higher by almost two orders of magnitude.

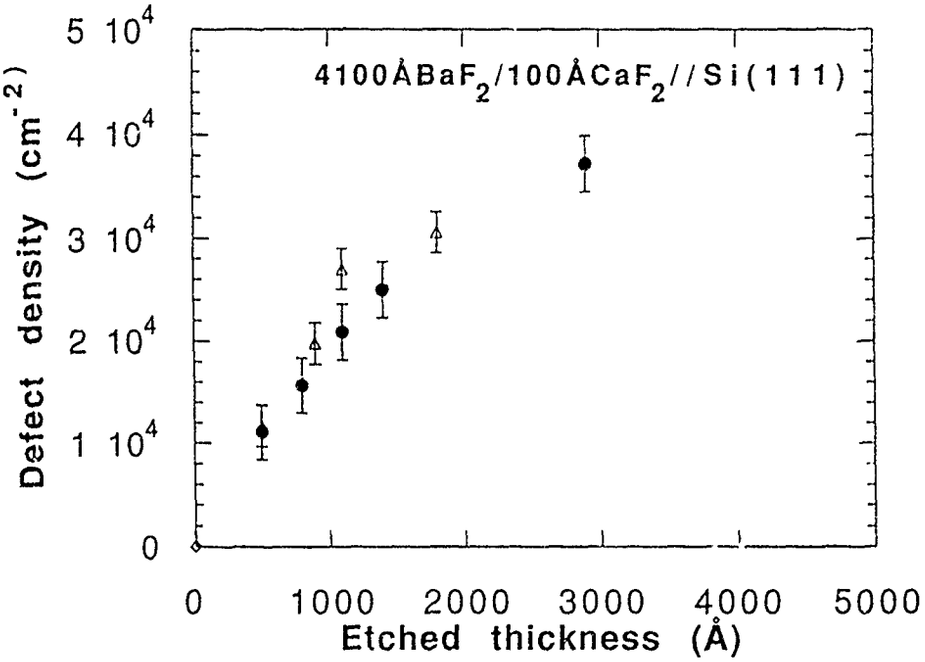

Figure 1: Defect densities measured with a etching chemical technique (• = HCl bath; Δ = HNO3 bath; ◊ = SEM observation)

An attempt was made to understand the microstructure of the BaF_2/CaF_2 interface by growing BaF_2/CaF_2 superlattices on Si(111). Typical structures are (BaF_2 50Å/CaF_2 100Å)$_{10}$. These samples were characterized by X-rays diffraction in the θ-2θ configuration. The observation of several satellite peaks around Bragg peak indicate that the BaF_2/CaF_2 interfaces are sharp. Preliminary observations by scanning transmission electron microscopy will be presented. They confirm that all the interfaces are well defined and that there is no significant intermixing between the layers. Furthermore, electron microdiffraction experiments on these samples reveal that each fluoride layer have taken a bulk lattice parameter. These results are interpreted in terms of non-pseudomorphic mode of growth and incoherent nature of the BaF_2/CaF_2 interfaces. Transmission electron microscopy experiments are currently in progress in our laboratory in order to correlate this interpretation. However, it shall be noted that a non-pseudomorphic mode of growth is in good agreement with the obtention of very low defect densities as far as in such case, there is no defect generation through mismatch stress relaxation.

b) Growth on Si(100):

For the same surface energies considerations as above, fluoric hs on Si(100) lead to three dimensional growth modes. We will present preliminary results concerning the growth of BaF_2/CaF_2 layers on nominal and viscinal (3° off) Si(100) substrates. Optimized growth conditions allow to determine the role played by surface diffusion in the fluoride growth mechanisms.

Acknoledgements: The authors would like to thank S. Lequien for X-rays diffraction experiments. C. Chenu, F. Lemaire, M. Magis and A. Peugnet are greatly acknoledged for their technical assistance.

1 H. Zogg *et al.*, Thin Solid Films, 184, 247 (1990)

2 S. Blunier *et al.*, Mater. Res. Soc., Vol. 116, 425 (1988).

Fp8

RHEED INTENSITY OSCILLATIONS DURING CaF_2 AND SrF_2 MBE GROWTH ON Si(111) AND GaAs(111)B

S.V.Novikov, N.S.Sokolov†, N.L.Yakovlev
A.F.Ioffe Physico-Technical Institute, 194021, Leningrad
USSR, phone (7)-(812)-2478188, fax (7)-(812)-2478640

Dynamic RHEED studies proved to be a powerful tool for exploration of MBE growth processes and *in situ* precise thickness measurements of growing semiconductor epitaxial layers. A lot of extensive investigations in this field have been carried out [1,2]. However there is only a few reports [3,4] on the successful application of this technique for investigation and monitoring of fluorides epitaxial growth on semiconductors. These crystalline insulator layers have a lot of promising applications in opto- and microelectronics [5].

Our RHEED experiments were conducted in two separate UHV chambers (for MBE of fluoride/Si and fluoride/GaAs heterostructures), equipped with electron guns and phosphorescent screens. The intensity of specular beam (00-spot) during fluoride deposition was measured with optical fiber and a photomultiplier. The incidence angle was about 30' (close to the so called off-Bragg condition at 15 KeV electron energy).

After the conventional chemical etching and thermal cleaning of silicon substrates RHEED pattern showed 7x7 superstructure usual for Si(111) clean surface. GaAs(111)B substrates were etched and thermally cleaned at 580° under arsenic beam. Then 50-100 nm GaAs buffer layer was grown by means of migration enhanced epitaxy [6]. RHEED pattern taken from this layer under As-beam exhibited As-stabilized 2x2 superstructure. Fluoride molecular beams were produced by sublimation of fluoride crystals in graphite crucibles. Fluoride growth temperature was from 100°C to 700°C.

Figures 1 and 2 show the dependences of specular beam intensity on the time of fluoride deposition. The layer/substrate materials and the growth temperatures are signed at the curves, the electron beam azimuth is [11$\bar{2}$]. All the

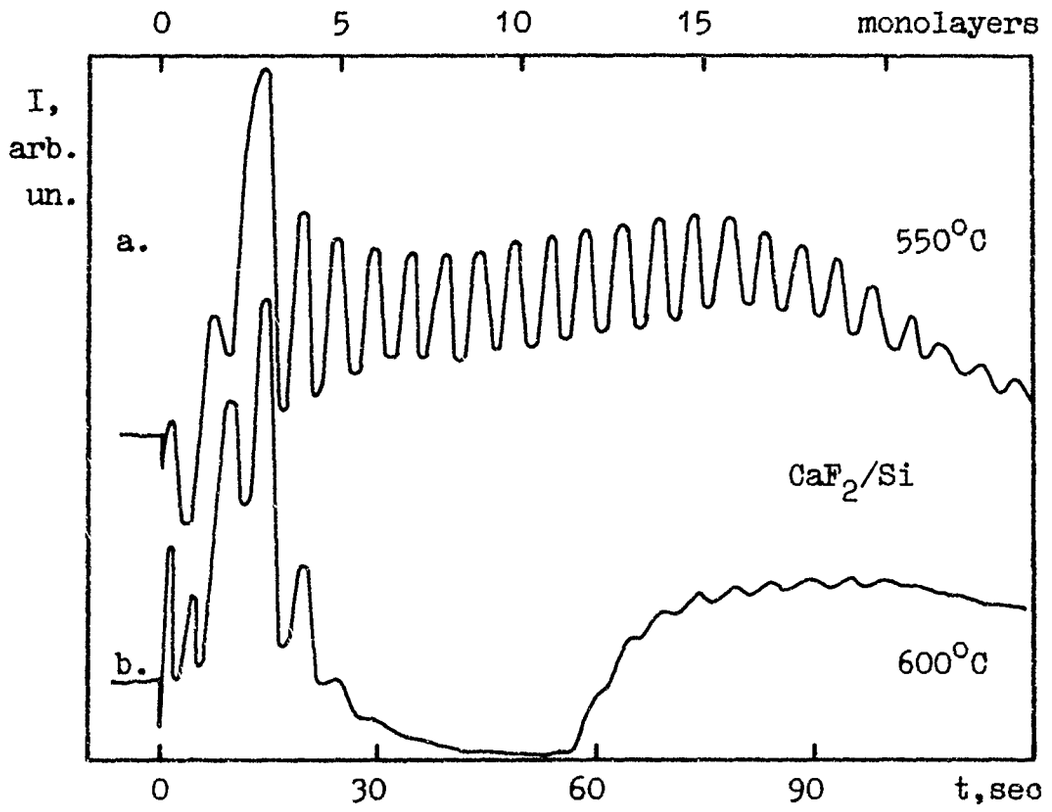

Figure 1.

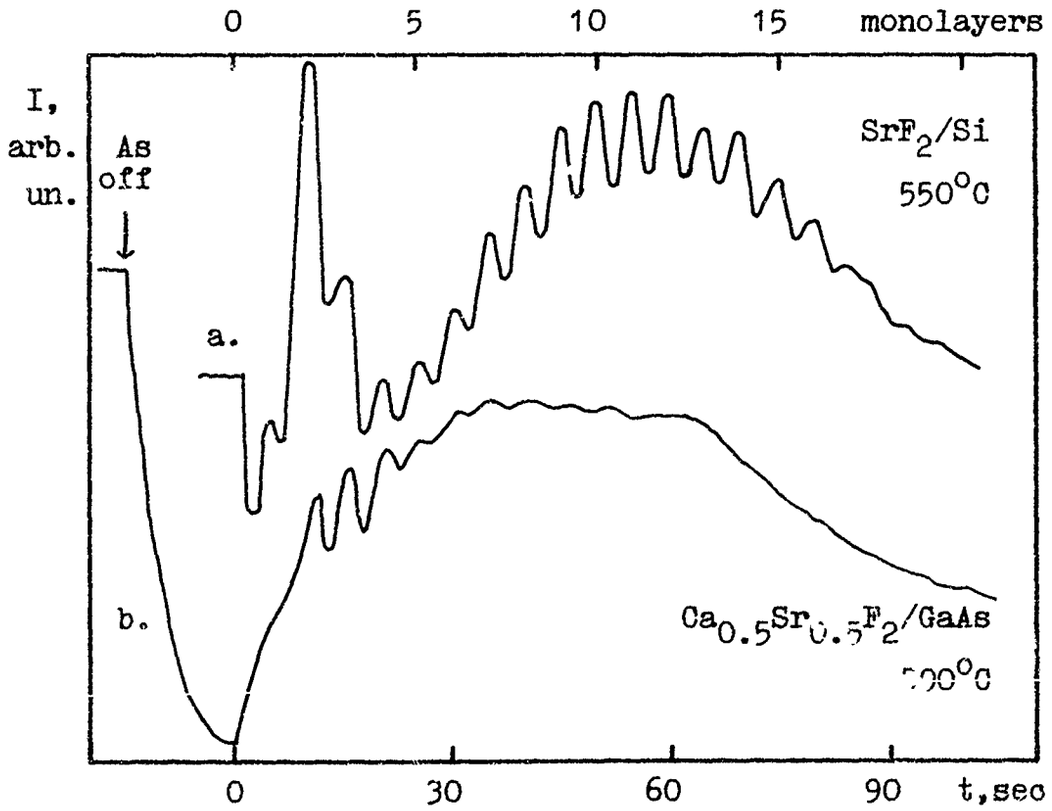

Figure 2.

curves exhibit oscillating periodic component with the period corresponding to the growth of one triple F-Ca-F layer of 0.315 nm thickness. This observation convincingly proves 2-D layer-by-layer growth mode of fluorides on (111) semiconductor face.

The observed complicated oscillation shape at the early stages of fluoride epitaxy (up to 3 monolayers) is easily reproducible, yet its origin remains so far unclear. One of the reasonable explanations of this nonperiodic structure is the difference of electron scattering by the silicon substrate and growing fluoride layer. Different diffusion of fluoride molecules on the substrate and the film surface, perhaps, may also contribute in it.

The slow average intensity variations on the later stages of fluoride epitaxy could be caused by structural transformations of growing film. The decrease after the growth of 3 layers in fig.1b, 2a and 14 layers on fig.2b is probably caused by the breakdown of pseudomorphic growth mode [4,7]. The rise of the intensity can be due to the flattening of the growing surface after misfit stress relaxation.

The authors are indebted to J.Carlos and E.Martynenko for the assistance during MBE-growth.

1) Neave J.H., Joyce B.A., Dobson P.J., Norton N. J.Appl.Phys. A31(1), 1 (1983)

2) Sakamoto T., Kawai N.J., Nakagawa T., Ohta K., Kojima T. Appl. Phys. Lett. 47(6), 617 (1985)

3) Novikov S.V., Sokolov N.S., Yakovlev N.L. Zh.tekh.Fiz., Pisma, 13(23), 1442 (1987) (Sov.Tech.Phys. Lett. 13(12), 603 (1987))

4) Sokolov N.S., Yakovlev N.L., Almeida J. Solid State Commun. 76(7), 883 (1990)

5) Schowalter L.J., Fathauer R.W. J. Vac. Sci. Technol. A4(3), 1026 (1986)

6) Takano Y., Kanaya Y., Torihata T., Pak K., Yonezu H. J.Crystal Growth 102, 341 (1990)

7) Berger P.R., Chang K., Bhattacharya P.K., Singh J. J.Vac.Sci.Technol. B5(4), 1162 (1987)

Abstract submitted to the European MBE Workshop 1991

Fp9

LAYER BY LAYER MOLECULAR BEAM EPITAXY OF BiSrCaCuO: STUDY OF THE BISMUTH INCORPORATION

M. Laguës, L. Ranno, M. Viret and X.Z. Xu
Laboratoire de Physique Quantique, CNRS URA421,
ESPCI, 10 rue Vauquelin 75231 Paris, France

J.P. Contour* and P. Bernstein
Laboratoire de Physique du Solide, ESPCI, 10 rue Vauquelin 75231 Paris, France

In situ deposition of good quality films of BiSrCaCuO is not presently achieved by MBE in a temperature range consistent with microelectronics multilayer processing ($T < 600^{\circ}C$), while good quality films of YBaCuO are currently prepared in this range. Among the difficulties encountered in depositing BiSrCaCuO films, the stoechiometric incorporation of bismuth is the first one. Elemental Bi, Sr and Ca are evaporated from Knudsen cells , while copper is evaporated from an electron gun. We present both coevaporation and layer by layer MBE results under both molecular and atomic oxygen flux. The growth is continuously followed by RHEED, while the intensity of the main spots and of the background is recorded. The films are characterized by X ray diffraction, RBS spectometry, SEM and EDX. We show that bismuth incorporation is strongly related to the elements which are deposited simultaneously (for instance O_2, O, Sr ...) and to the composition of the uppermost layer of the growth interface.

Phone number: 33 -1 - 4337 1528 Fax: 33 -1 - 4331 4222

EUROMBE-91 Tampere, Finland April 21-24, 1991

Fp10

EPITAXIAL GROWTH OF LATTICE MATCHED $Sc_{0.2}Yb_{0.8}As$/(001)GaAs AND GaAs/$Sc_{0.2}Yb_{0.8}As$/(001) and (111)GaAs HETEROSTRUCTURES

V. DUREL, J. CAULET, Y. BALLINI, M. MINIER, B. GUENAIS, G. DUPAS and A. GUIVARC'H*

CNET - LAB/OCM/MPA Route de Trégastel BP40 F22301 LANNION France

Telephone +33 96 05 38 68 Fax +33 96 05 32 39

New materials structures incorporating epitaxial metallic layers within semiconductors have the potential of opening up new classes of electronic and optoelectronic devices (for a very recent review article, see the paper of T. Sands et al [1]). Up to now, two classes of metallic materials have been studied : the transition-metal gallides and aluminides with the CsCl structure as NiGa [2-5] and NiAl [6] and the rare-earth monopnictides with the NaCl structure (RE-V) as YbAs [7] and ErAs [8,9]. For this last classe of materials, it was shown that exact lattice matching with the III-V semiconductor substrates could be achieved by forming ternary RE-V alloys [10,11] for instance in the case of $ErP_{0.4}As_{0.6}$/GaAs [12-14] and $Sc_{0.38}Er_{0.68}As$/GaAs [15] heterostructures. The approach of the present paper is to combine ScAs (-3.3% mismatch) and YbAs (+0.9% mismatch) to produce $Sc_{0.2}Yb_{0.8}As$, an alloy that is lattice matched to GaAs.

The samples were fabricated in a RIBER 2300 molecular beam epitaxy system. A 500nm n-GaAs (2 10^{16} Si/cm^3) buffer layer was grown on GaAs substrates at 600°C. Prior to $Sc_{1-x}Yb_xAs$ growths ($0 \leq x \leq 1$) at a deposition rate equal to 0.01-0.02 nm/s, the substrate block was cooled to 450°C in an As_4 flux. On the top of some $Sc_{0.2}Yb_{0.8}As$ samples, a 200nm thick GaAs layer was grown at a rate of 0.5μm/h and 550°C sample temperature. The samples were characterized, in situ, by RHEED, UPS and XPS and, ex situ, by X-ray diffraction, RBS, TEM and I-V. The effects of the thickness of the $Sc_{0.2}Yb_{0.8}As$ layer (2 and 40nm) and of the GaAs substrate orientation ((001), (001) 4° off toward the (111) Ga plane and (111)) on the quality of the buried heterostructures was particularly studied.

$Sc_{1-x}Yb_xAs$/(001)GaAs heterostructures :

The ScAs and YbAs alloys appeared to be completely miscible and, as predicted by Vegard's law, the lattice matching to GaAs was observed for an approximate composition of $Sc_{0.2}Yb_{0.8}As$ (fig. 1). On RBS spectra the large amount of dechanneling at the YbAs/(001)GaAs and ScAs/(001)GaAs interfaces for the GaAs signal is greatly reduced in the case of the lattice matched $Sc_{0.2}Yb_{0.8}As$/(001)GaAs system. This reduction betokens an improvement of the quality of the heterostructure at this level.

The Schottky barrier heights were determined from I-V measurements on diodes fabricated from $Sc_{1-x}Yb_xAs$/n-GaAs samples. These diodes yielded excellent I-V characteristics with the ideality factors and barrier heights reported in table I. Unlike what is observed in the case of the $Sc_{1-x}Er_xAs$/GaAs structures [1], we did not found a greater barrier for the lattice matched contact, than for the mismatched ones.

The UPS spectra ($He_{II\alpha}$) of fig. 2 point out that for YbAs and $Sc_{0.2}Yb_{0.8}As$ the main contribution is due to the Yb_{4f} levels, near the valence-band. The details of these contributions confirm the model presented in ref. 7 to explain the X.P.S spectrum of YbAs. For $Sc_{0.2}Yb_{0.8}As$, the modifications resulting from the presence of Sc become visible as shoulders into the valence-band, between the Yb_{4f} levels and the Fermi level (arrows). At last, for all these semimetals with resistivity in the 50-100 $\mu\Omega$cm range, the density of states at the Fermi level is weak.

GaAs/$Sc_{0.2}Yb_{0.8}As$/GaAs heterostructures :

For heterostructures with the thin $Sc_{0.2}Yb_{0.8}As$ metallic layers ($\approx$ 2nm), RBS spectra of figure 3 and χ_{min} of table II point out the effects of GaAs substrate orientation on the structural properties of the systems. The 4° misorientation of (001)GaAs leads to an improvement of the epitaxial overlayer due to a decrease in the density of defects (mainly twins and stacking faults) observed by TEM in the case of (001) oriented substrates. With (111)GaAs, in spite of the crystalline imperfections which introduce a dechanneling at the depth of the $Sc_{0.2}Yb_{0.8}As$ layer (i.e. between B and C), the GaAs overlayer is nearly perfect for the RBS technique.

For thick metallic layers ($\approx$ 40nm) a similar effect of the substrate orientation was noticed but the GaAs overlayers present a higher defect density (table II).

As a conclusion, our study shows that good quality lattice matched $Sc_{0.2}Yb_{0.8}As$/n-GaAs Schottky diodes can be grown by MBE and the use of vicinal surfaces leads to an improvement of the GaAs overlayer quality in the GaAs/$Sc_{0.2}Yb_{0.8}As$/GaAs heterostructures.

References :

1 T.Sands et al, Mater. Science Reports 5 (1990) 99.
2 A. Guivarc'h et al, Electron. Letters 52 (1987) 1004.
3 Y. Ballini et al, Rev.Phys.Appl. 24 (1989) 71.
4 B. Guenais et al, J. Crystal Growth 102 (1990) 925.
5 V. Durel et al, Inst. Phys. Conf. Ser. N° 112 (1990) 129.
6 J.P. Harbison et al, Appl. Phys. Lett. 53 (1988) 1717.
7 H.J. Richter et al, Appl. Phys. Lett. 53 (1988) 99.
8 C.J. Palmstrom et al, Appl. Phys. Lett. 53 (1988) 2608.
9 J.D. Ralston et al, J. Electron Mater. 19 (1990) 555.
10 A. Le Corre et al, French patent N° 89, 04 899.
11 A. Guivarc'h et al, Electron. Letters 25 (1989) 1051.
12 A. Le Corre et al, Appl. Phys. Lett. 55 (1989) 2298.
13 J. Caulet et al, J. Crystal Growth 102 (1990) 309.
14 A. Le Corre et al, J. Crystal Growth 105 (1990) 234.
15 C.J. Palmstrom et al, Appl. Phys. Lett. 56 (1990) 382.

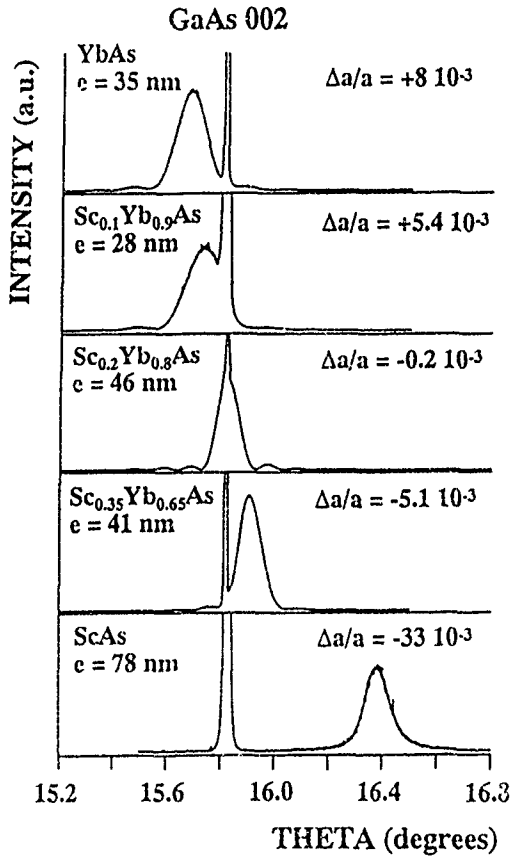

Fig. 1 : X-ray $CuK_{\alpha 1}$ patterns of the 002 reflections of various $Sc_{1-x}Yb_xAs/GaAs(001)$ systems.

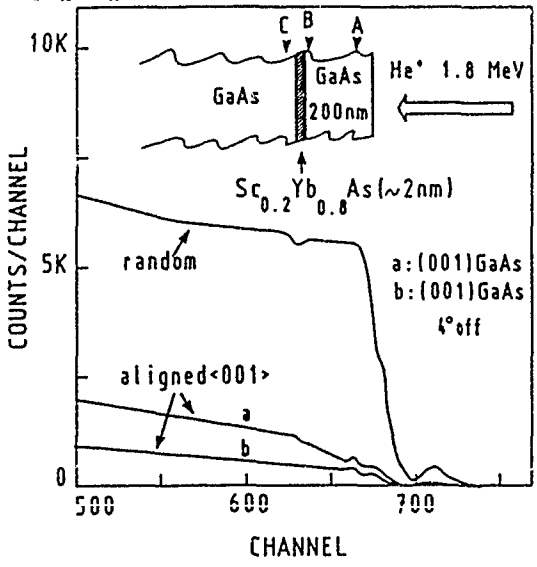

Fig. 3 : RBS/channeling spectra from buried GaAs/(2nm) $Sc_{0.2}Yb_{0.8}As/GaAs$ heterostructures for (001) and (001) 4°off substrates. The two random spectra are quite similar.

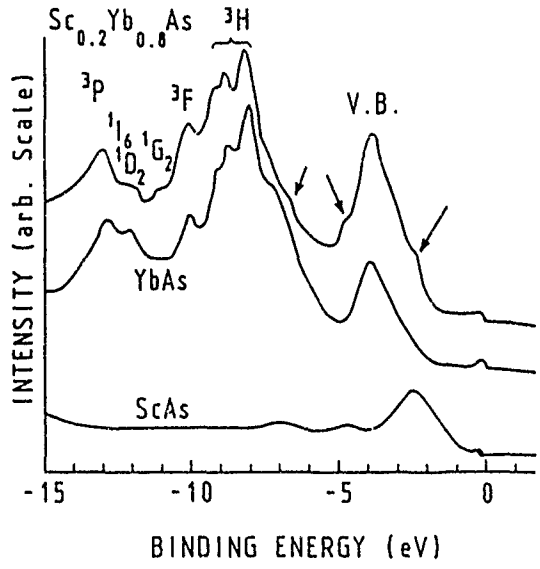

Fig. 2 : UPS spectra taken on $Sc_{0.2}Yb_{0.8}As$, YbAs and ScAs epitaxial surfaces with $He_{II\alpha}$.

Table I
Schottky barrier heights and ideality coefficients of YbAs, $Sc_{0.2}Yb_{0.8}As$ and ScAs/n-GaAs diodes.

	ϕ_{bn}(eV)	n
ScAs	0.75	1.06
$Sc_{0.2}Yb_{0.8}As$	0.84	1.05
YbAs	0.89	1.08

Table II
χ_{min} values (%) at the three typical depths A, B & C reported in fig. 3 for the various $GaAs/Sc_{0.2}Yb_{0.8}As/GaAs$ heterostructures.

$Sc_{0.2}Yb_{0.8}As$	GaAs	A	B	C
≈2nm	(001)	10	20	20
	4°off	5	8	8
	(111)	5	6	11
≈40nm	(001)	26	46	50
	4°off	15	30	33
	(111)	5	11	18

Monitor and protect your ion pump system with DIGITEL™ "intelligent" power supplies.

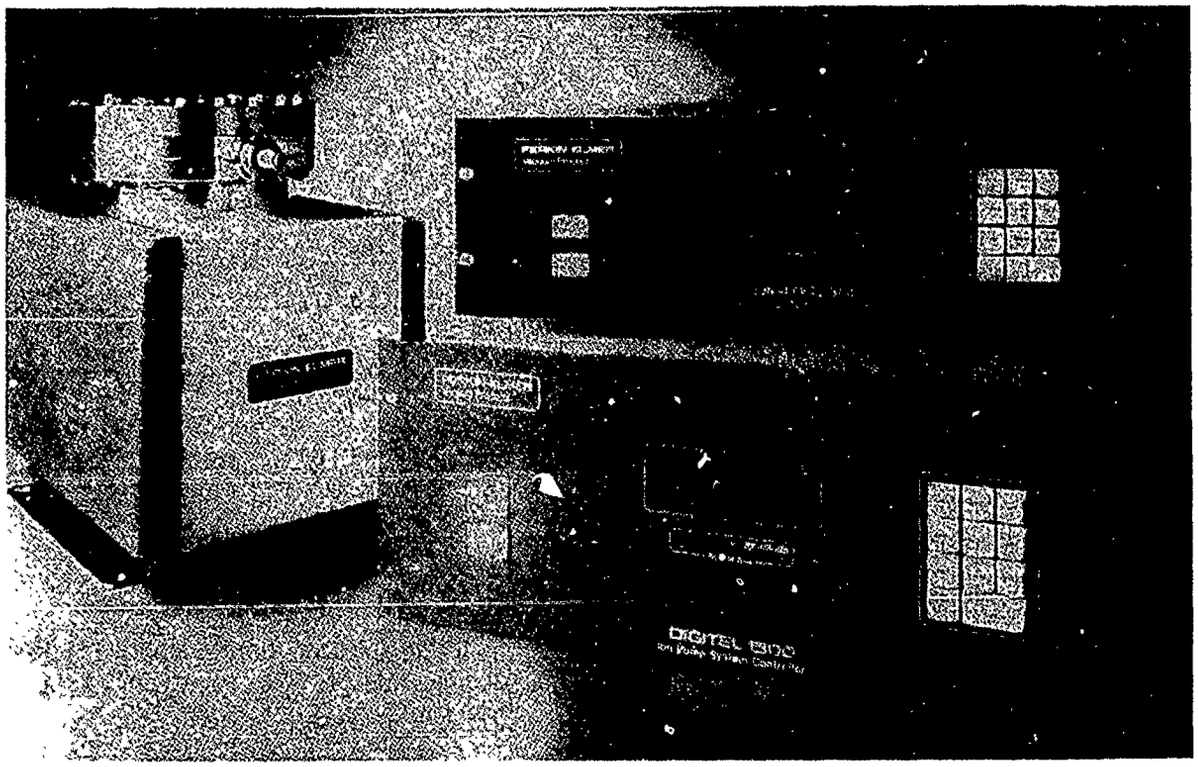

Providing power is just the beginning.

The DIGITEL does much more than supply power. It performs all start-up, control and monitoring functions. It is truly a system controller that works as well with a single ion pump as it does a complete system, adapting to your needs as they evolve.

The DIGITEL's powerful microprocessor is designed to take full advantage of progressive technology, such as digital readout, non-volatile memory, retrofittable options and programmable capabilities.

Operate pumps from 20 l/s to 500 l/s in size.

The DIGITEL is now available in two models to accommodate both large or small ion pump requirements. The DIGITEL 500 is ideal for starting and operating pumps from 20 l/s to 220 l/s. The new, more powerful DIGITEL 1500 provides ample current to control pumps ranging in size from 120 l/s to 500 l/s.

Innovative features and options.

- "Autorun" frees the operator from supervising the pump while starting or during operation.
- Digital display of pump voltage, current and pressure (in Torr or Pascal).
- Rate of rise bar graph shows pressure trends at a glance. Also useful for leak detection.
- IEEE 488 or RS-232 computer interface option allows on-line data handling and remote control from an external computer.
- Set point option provides two digital set points to initiate pressure related processes.
- Bakeout option provides programmable, automatic bakeout control

Unique design, exceptional value.

The DIGITEL is different from ion pump power supplies in every way... except price. For approximately the same price you pay now, you can step up to maximum flexibility and protection for your system. If all your present power supply does is supply power, you're not getting your money's worth. For complete information, simply write "DIGITEL" on the back of your business card and send it to us.

Bruckmannring 6
8042 Oberschleißheim
(Munich) W. Germany
Telefon (089) 315 7170
Telefax (089) 315 3117 Sales
(089) 315 4316 Service
Telex 5216219

PERKIN-ELMER

Growth of GaInAs and GaInAsP by CBE

**A. Rudra*, J.F. Carlin, M. Gailhanou,
J.L. Staehli†, P. Ruterana and M. Ilegems**

Institute for Micro- and Optoelectronics, †Institute for applied physics,
Ecole Polytechnique Fédérale de Lausanne,
CH 1015 Lausanne, Switzerland
Phone - 41 21 6934533 Fax - 41 21 6934444

This paper describes the structural, optical and transport properties of GaInAs and GaInAsP (λ = 1.3 μm) bulk materials and heterostructures obtained by Chemical Beam Epitaxy (CBE).

All layers were grown using Trimethylindium, Triethylgallium, Arsine and Phosphine with a pressure regulated gas manifold and no carrier gas. The hydrides were decomposed between 300 and 1000 Torr inside a cracker cell usually kept at 885 °C.

Undoped GaInAs layers show residual electron concentration of 2 10^{15} cm^{-3} and 77 K bulk mobilities of 37'000 $cm^2v^{-1}s^{-1}$. An unintentionally doped InP buffer layer enhances the 77K mobility to 65'000 $cm^2v^{-1}s^{-1}$ by introducing a two dimensional transport evidenced by the observation of Shubnikov-de-Haas oscillations. For similar growth conditions, the run-to-run reproducibility in the layer mismatch is 2 10^{-4} and over 11 months of operation, the standard deviation in $\Delta a/a$ is still better than 5.10^{-4}.

Below 470°C and above 490°C in growth temperature, $\Delta a/a$ respectively decreases and increases by at least 6 10^{-5} $°C^{-1}$. When the substrate temperature is carefully stabilized, the (004) Bragg reflection for a 2 μm thick layer shows a FWHM as low as 14 arc seconds, which is the best published value for layers of similar thickness[1-10], with a lateral mismatch variation of 1.3 10^{-4} accross a quarter of a 2" wafer.

The substrate temperature dependance is much stronger in GaInAsP than in GaInAs (fig.1). Under our optimized growth conditions, the In incorporation coefficient is found to be constant whether InP, GaInAs or GaInAsP are grown. In contrast, the incorporation coefficient of Ga is about 30% lower in InGaAs and 40% lower in InGaAsP as compared to GaAs. This suggests that TEGa (rather than TMIn) decomposition and desorption are the controlling factors in the growth kinetics.

Under continuous pyrometer control, GaInAsP layers, with an (004) Bragg reflection FWHM of 30" for a 0.6 µm-thick layer (fig.2), a lateral mismatch variation of 8 10^{-4} and a wavelength spread lower than 5 nm over a quarter of a 2" wafer are grown with a reproducibility of a few nanometers.

InP/GaInAs/InP and GaInAsP/GaInAs/GaInAsP quantum wells 30 to 90 Å thick were succesfully grown, as evidenced by wedge transmisson electron microscopy. In the first system, a 45 Å QW showed a 4K photoluminescence linewidth of 5.2 meV, one of the best values published so far[11,12]; with quaternary cladding layers, a 30 Å-thick well showed a PL linewidth of 17 meV.

Present work involves the continued investigation of the influence of the growth parameters and the gas transients on the structural and optical properties of the quantum wells.

References

1. Y. Kawagushi, H. Asahi and H. Nagai, extended abstracts of the 18th Conference on Solid State Devices and Materials, Tokyo 1986, 619-622
2. W.T. Tsang, A.H. Dayem, T.H. Chiu, J.E. Cunningham, E.F. Shubert, J.A. Ditzenberger, J. Shah, J.L. Zyskind and N. Tabatabaie, Appl. Phys. Lett. 49 (3) 1986, 170-172
3. C. Ferrari, P. Franzosi, L. Gastaldi and F. Taiarol, J. Appl. Phys. 63 (8) 1988, 2628-2632
4. Y. Matsiu, H. Hayashi, K. Kikushi, S. Igushi and K. Yoshida, J. Vac. Sci. Technol. B3 (2) 1985, 528-530
5. S.J. Bass, S.J. Barnett, G.T. Brown, N.G. Chew, A.G. Cullis, A.D. Pitt and M.S. Skolnick, J. Crystal Growth 79 (1986) 378-385
6. I.C. Bassignana, C.J. Miner and N. Puetz, J. Appl. Phys. 65 (11) 1989, 4299-4301
7. M. Razeghi, "The MOCVD challenge", Vol. 1, Ed. Adam Hilger, ISBN 0-85274-161-8
8. K.H. Goetz, D. Bimberg, H. Jürgensen, J. Selders, A.V. Solomonov, G.F. Glinskii and M. Razeghi, J. Appl. Phys. 54 (8) 1983, 4543-4552
9. A.T. Macrander and V. Swaminathan, J. Electrochem. Soc., Vol.134, No. 5
10. H. Heinecke, B. Baur, R. Höger and A. Miklis, in: Proceedings of the 5th International Conference on MOVPE and related techniques, Aachen, June1990, to be published in J. Crystal Growth 107 (1991)
11. W.T. Tsang and E.F. Shubert, Appl. Phys. Letters 49 (4) 1986, 220-222
12. M. Gailhanou, L. Goldstein, M. Lambert, M. Boulou, C. Stark and L. Le Gouezigou, in: Proceedings of the 19th European Solid State Device Research Conference, Berlin 1989, p.495, A. Heuberger, H. Ryssel & P. Lange eds., Springer-Verlag.

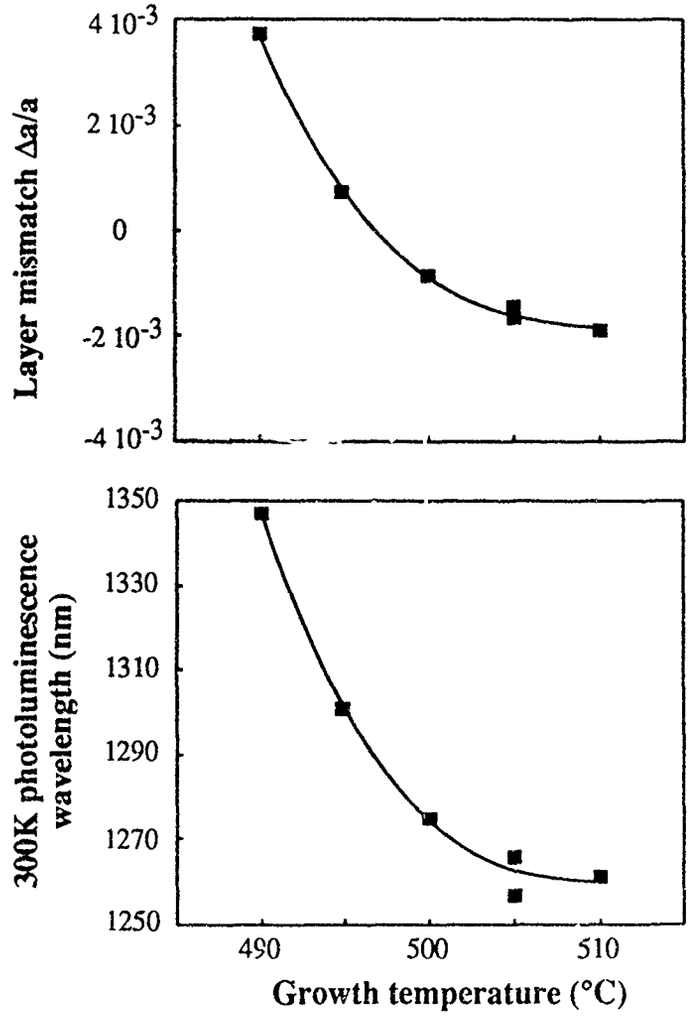

Figure 1:
Effect of the growth temperature on the GaInAsP composition

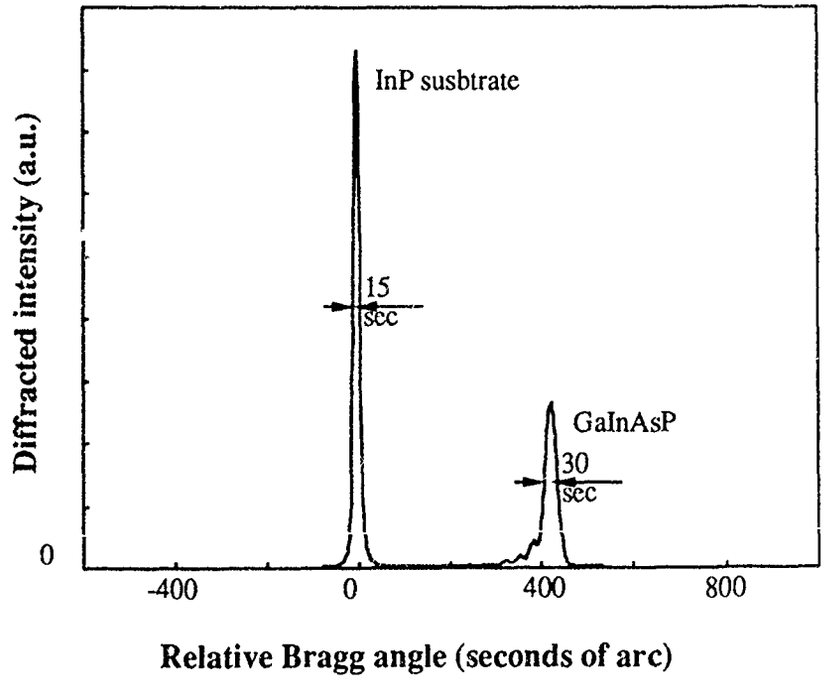

Figure 2:
X ray rocking curve (004 reflection) measured on a 0.6 µm thick, 1.3 µm wavelength , GaInAsP layer.

GROWTH OF InP/InGaAs MULTIPLE QUANTUM WELL STRUCTURES WITH EXCEPTIONAL LATERAL UNIFORMITY BY CHEMICAL BEAM EPITAXY

P J Skevington*, S J Amin and G J Davies
British Telecom Research Laboratories
Martlesham Heath, Ipswich, IP5 7RE, UK
Tel: +44 473 646808 Fax: +44 473 646885

The use of gas sources in chemical beam epitaxy (CBE) leads to the possibility of growing crystal structures with extremely high lateral uniformity in both thickness and alloy composition.

We have investigated the lateral uniformity achievable in our modified VG V80H CBE system. A 2" S-doped InP wafer was mounted in an In-free holder and rotated during growth. The test structure consisted of 0.35 μm $In_{0.53}Ga_{0.47}As$ on a 0.30 μm InP buffer. Uniformity of the sample was characterised by double crystal X-ray diffraction. Layer thicknesses for both layers were derived from Fourier transforms of the X-ray interference fringes [1].

Fig. 1 shows the thickness uniformity data for a 9-point scan along a radius of the wafer. Individual layer thicknesses had an error of ±0.003 μm (about ±1%). InGaAs measurements within a 15 mm radius of the centre were all 0.349 ± 0.003 μm. There was a slight fall to 0.344 ± 0.003 μm for the two measurements at radii of 17.5 and 20 mm. InP measurements were all in the range 0.288-0.308 μm, with a mean value of 0.301 ± 0.005 μm (±1.8%).

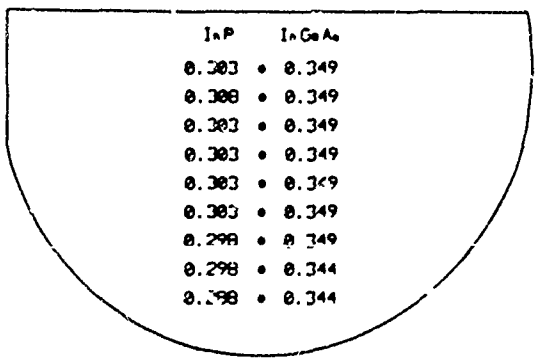

Fig. 1. InP and InGaAs thickness uniformity data along a radius of a 2 inch wafer. Thicknesses in μm.

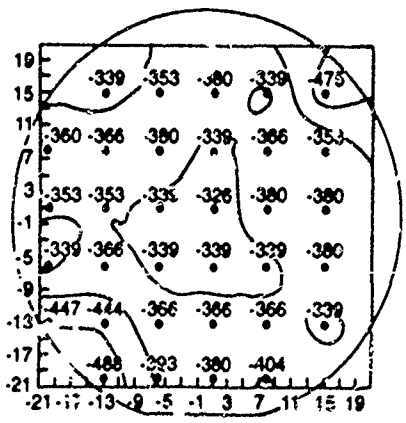

Fig. 2. Contour map of InGaAs mismatch (ppm) across a 2 inch wafer.

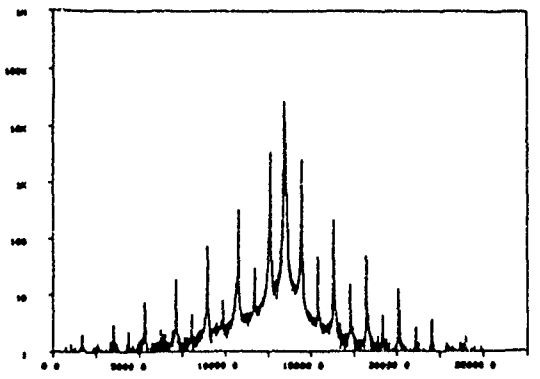

Fig. 3. X-ray rocking curve for 50 period MQW.

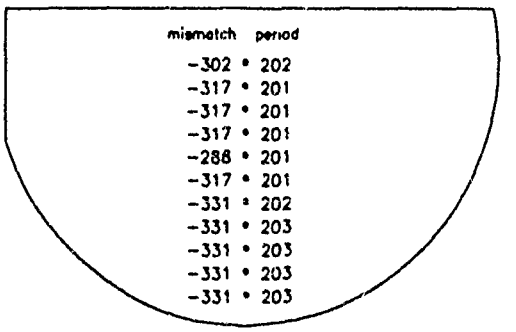

Fig. 4. MQW period (Å) and mismatch (ppm) uniformity data along a radius of a 2 inch wafer.

InGaAs compositional uniformity was measured for a 7 x 7 point array covering the entire sample. Lattice mismatch variations across the wafer are shown in fig. 2. There is no clear trend in mismatch from middle to edge. The mean mismatch across the central region of the wafer (27 readings) is -373 ± 19 ppm. This corresponds to an In content of 52.6 ± 0.03 atom%, or an uncertainty in bandgap wavelength of ±0.69 nm. Note that the residual error in the measurements is ±7 ppm (from the step length of 3.5 arc sec).

The lateral uniformity of InP/InGaAs multiple quantum well (MQW) structures has also been studied. A 50 period MQW of nominally 100 Å InP / 100 Å InGaAs exhibited 13 orders of satellite peaks (fig. 3). X-ray simulation showed that the barrier and well widths were equal and that the interfaces were sharp. X-ray data from an 11 point radial scan were used to determine the lateral uniformity of the MQW period and mismatch (fig. 4). The period was measured as 202 ± 1 Å across the 2" wafer, whilst the lattice mismatch was -318 ± 13 ppm. Fourier transform infra-red spectroscopy was used to measure the absorption edge for the same points (fig. 5). The edge was constant to ±0.5 nm wavelength between the centre of the wafer and 18 mm radius, with a maximum wavelength shift of 7 nm at the edge of the wafer. These properties suggest that CBE has great potential for the growth of quantum confined Stark effect modulators in large area arrays.

The lateral uniformity achieved in CBE is dependent on a number of factors. To a first approximation, compositional uniformity is determined by mixing in the gas manifolds, whilst thickness uniformity is determined by the design of the group III injector. However, substrate temperature and group V overpressure (V:III ratio) [2] also have significant effects on the growth. In our work, the substrate was mounted in an annular Mo holder with a sapphire backing plate, and radiatively heated by a standard VG Ta foil heater. We measured InGaAs lattice mismatch as a function of substrate temperature for both the centre and edge (20 mm radius) of 2" wafers (fig. 6). From this data, lateral variations in our system were estimated as 3°C in temperature and 8% in V:III ratio across a 2" wafer.

[1] S J Amin and M A G Halliwell, presented at British Crystallographic Assoc. Conference, Exeter, 1990.

[2] P J Skevington, G J Davies, A T S Wee, C L French and J S Foord, submitted to Appl. Phys. Letters.

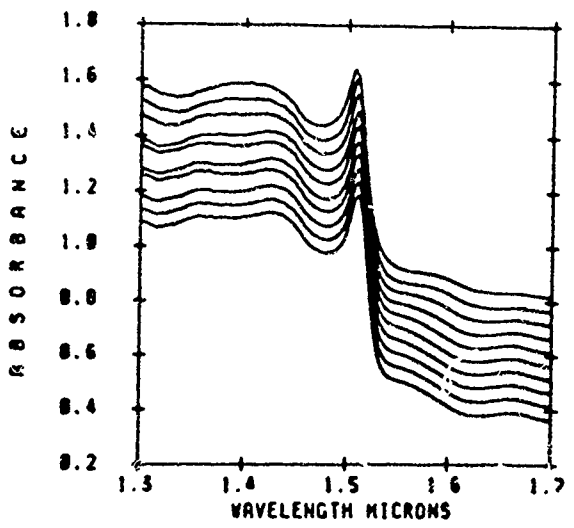

Fig. 5. MQW absorption edges for 10 points measured at 2 mm intervals along the radius of a 2 inch wafer (offset for clarity).

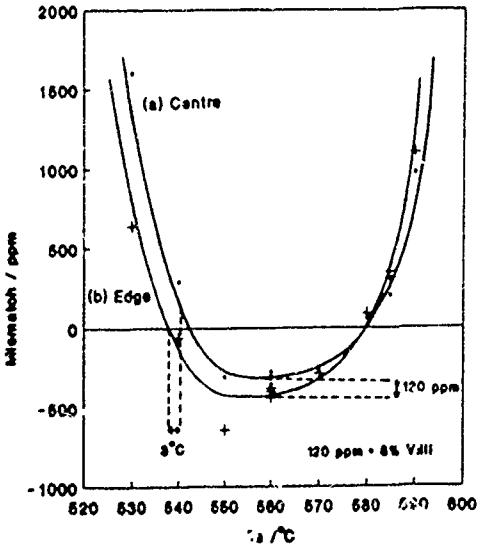

Fig. 6. InGaAs lattice mismatch as a function of measured growth temperature for points at (a) the centre and (b) the edge of 2 inch wafers.

Carbon incorporation in MOMBE grown $Ga_xIn_{1-x}P$ layers.

Ph. MAUREL*, J.C. GARCIA, Ph. BOVE, C. GRATTEPAIN, J.P. HIRTZ

THOMSON-CSF/ Laboratoire Central de Recherches, Domaine de Corbeville
91401 Orsay Cedex, FRANCE. Phone:(33) 60 19 77 13, Fax: (33) 60 19 78 29

Carbon is the main impurity detected in all Metalorganic Molecular Beam Epitaxy (MOMBE) grown materials [1,5,7]. However, the acceptor or donor character of carbon depends on the host material. As an example, whereas carbon acts as an acceptor in GaAs, it acts as a donor in InAs [1]. Consequently, carbon to some extent could exhibit in ternaries alloys an amphoteric behaviour as already demonstrated in $Ga_{0.47}In_{0.53}As$ [1] . We present in this paper such a comparative study for carbon incorporation in InP and $Ga_{0.5}In_{0.5}P$ grown by MOMBE. Triethylgallium (TEGa) and trimethylindium (TMIn) have been used as group III element sources, phosphine (PH_3) as group V element source . The net carrier concentration (N_D-N_A) in the layers were determined by both C-V profiles and Hall measurements. The 77K mobilities were used to determine the compensation ratios (N_A/N_D) in InP layers [2]. The carbon concentrations were measured by Secondary Ion Mass Spectroscopy (SIMS).

Undoped InP bulk layers have been grown in the temperatures range 450 to 530°C. Growth rate has been fixed to 1µm/h. Figure 1 exhibits the [C] concentration detected by SIMS as a function of the inverse of growth temperature, as well as the total impurity concentration N_d+N_a derived from Hall measurements by taking into account the compensation ratio deduced from the 77 K mobilities of the layers. The phosphine flow rate is kept constant to 7 sccm. Carbon concentrations and N_d+N_a data are in fairly good agreement, indicating that carbon is the main impurity incorporated in the layers. The n-type conductivity shows that it preferentially acts as a donor in MOMBE grown InP layers using TMIn and PH_3. The carbon concentration increases on increasing V/III ratio (at a fixed temperature (470°C) increasing the PH_3 flow rate from 7 sccm up to 10 sccm increases the carbon contamination from 4.10^{16} cm^{-3} up to 8.10^{16} cm^{-3}) and decreases as the growth temperature increases [3,4]. An activation energy of about 55 kcal/mol is deduced for this latter process. This value is too high to be related to an incomplete pyrolisis of the TMIn molecule, leading to carbon contamination from undecomposed III-CH_n radicals like in MOMBE grown GaAs layers using TMGa [5]. It can therefore be suggested that a more stable molecule is involved in the process for carbon incorporation. It should be noticed that this type of conductivity is also observed in MOMBE grown InP using triethylindium (TEIn) and PH_3 [6,7,8] and in Gas Source MBE (GSMBE) grown InP using solid In and PH_3 [8,9]. The donor character of carbon in InP layers indicates that carbon favourably binds to phosphorus atoms if compared to indium atoms. In the case of TMIn, the formation of intermediate species such as methylphosphorus with high C-P binding energies [10] could lead to the high activation energy experimentally derived. The formation of such molecules should be favoured by the increase of the phosphine flow rate, leading to the experimentally observed increase in carbon contaminatio for high phosphine flow rates. Additional modulated mass beam spectrometry work is in progress in order to clarify the chemical nature of the various species involved in the growth process.

In the case of MOMBE and GSMBE grown GaP layers, the acceptor role of carbon has already been clearly demonstrated [11]. Nevertheless, intentional carbon doping of $Ga_{0.5}In_{0.5}P$ layers lattice matched to GaAs has led to marginal n or p type conduction, depending on the carbon source used [11] We have investigated its behaviour on nominally undoped $Ga_{0.5}In_{0.5}P$

layers. SIMS profiles have been performed (see figure 2) establishing that carbon is still the main impurity detected. All of the epilayers exhibited carbon concentrations in excess of 10^{16} cm^{-3}, while C-V profiles showed residual doping levels in the low 10^{14} cm^{-3} range. At the same time, most of the epilayers had too high a resistivity to provide any valuable Hall data, in agreement with the results reported by Osaza et al [12]. A marginal n-type conduction has been found on some samples grown with high phosphine flow rates (10 sccm or more), exhibiting a carrier concentration in the low 10^{14} cm^{-3} range, in agreement with C-V data, two orders of magnitude lower than the carbon concentrations detected on SIMS profiles. While carbon preferentially acts as a donor in InP and as an acceptor in GaP, it shows an amphoteric behaviour in the ternary alloy where both binaries are mixed in equal proportions. The same medium tendancy is thus found for $Ga_{0.5}In_{0.5}P$ and for $Ga_{0.47}In_{0.53}As$[1]. Carbon contamination can be reduced in GaInP by both increasing the growth temperature and decreasing the V/III ratio, so that the tendancies are qualitatively comparable to what happens in InP. By increasing the growth temperature from 510 up to 535°C and keeping the V/III ratio constant, a decrease in carbon contamination with an associated activation energy for the process of about 35 kcal/mol is observed. The effect of the V/III ratio on carbon incorporation is clear as well. Figure 2 shows the carbon concentration performed on the SIMS profile of a $Ga_{0.5}In_{0.5}P$ thick layer with three values of the V/III ratio by varying the phosphine flow rate between 2 and 15 sccm and keeping constant the TEGa and TMIn input flow rates . The carbon concentrations are lowered by one decade (from 2.10^{17} cm^{-3} down to 2.10^{16} cm^{-3}) when PH_3 flow rate is decreased from 15 sccm down to 2 sccm.

In summary, carbon incorporation in MOMBE grown $Ga_xIn_{1-x}P$ layers is presented. Carbon is shown to have an amphoteric behaviour in the ternary alloy $Ga_{0.5}In_{0.5}P$. This has been correlated with the corresponding behaviour in the two binaries GaP and InP where it respectively acts as an acceptor and as a donor.

The authors would like to thank D. Le Guen for excellent technical assistance. This work has been supported by EEC under ESPRIT contract n° 5031.

References.

1) M. Kamp, R. Contini, K. Werner, H. Heinecke, M. Weyers, H. Luth, P. Balk, J. Cryst. Growth 95, 154, 1989.

2) W. Walukiewicz, J. Lagowski, L. Jastrzebski, P. Rava, M. Lichtensteiger, C.H. Gatos, H.C. Gatos, J. Appl. Phys. 51, 2659, 1980.

3) A. Rudra, J.F. Carlin, M. Proctor, M. Illegems, Proceedings of 6th Int. Conf. on MBE, San Diego 1990.

4) H. Heinecke, B. Baur, R. Hoger, A. Miklis, J. Cryst. Growth 105, 143, 1990.

5) N. Putz, H. Heinecke, M. Heyen, P. Balk, M. Weyers, H. Luth, J. Cryst. Growth 74, 292, 1986.

6) Y. Kawaguchi, H. Asaki, H. Nagai, Inst. Phys. Conf. Ser. n°79, Chap. 2, 1985.

7) J.L. Benchimol, F. Alaoui, Y. Gao, G. Le Roux, E.V.K. Rao, F. Alexandre, J. Cryst. Growth 105, 135, 1990.

8) D.A. Andrews, S.T. Davey, C.G. Tuppen, B. Wakefield, G.J. Davies, Appl. Phys. Lett. 52, 816, 1988

9) M. Lambert, A. Péralès, R. Vergnaud, C. Starck, J. Cryst. Growth 105, 97, 1990

10) G.B. Stringfellow, "OMVPE: Theory and practice", Academic press 1989.

11) T.J. de Lyon, N.I. Buchan, P.D. Kirchner, J.M. Woodall, D.T. Mc Inturff, G.J. Scilla, F. Cardone, Proceedings of 6th Int. Conf. on MBE, San Diego 1990.

12) K. Osaza. M. Yuri, S. Tanaka, H. Matsunami, J. Appl. Phys. 65, 2711, 1989.

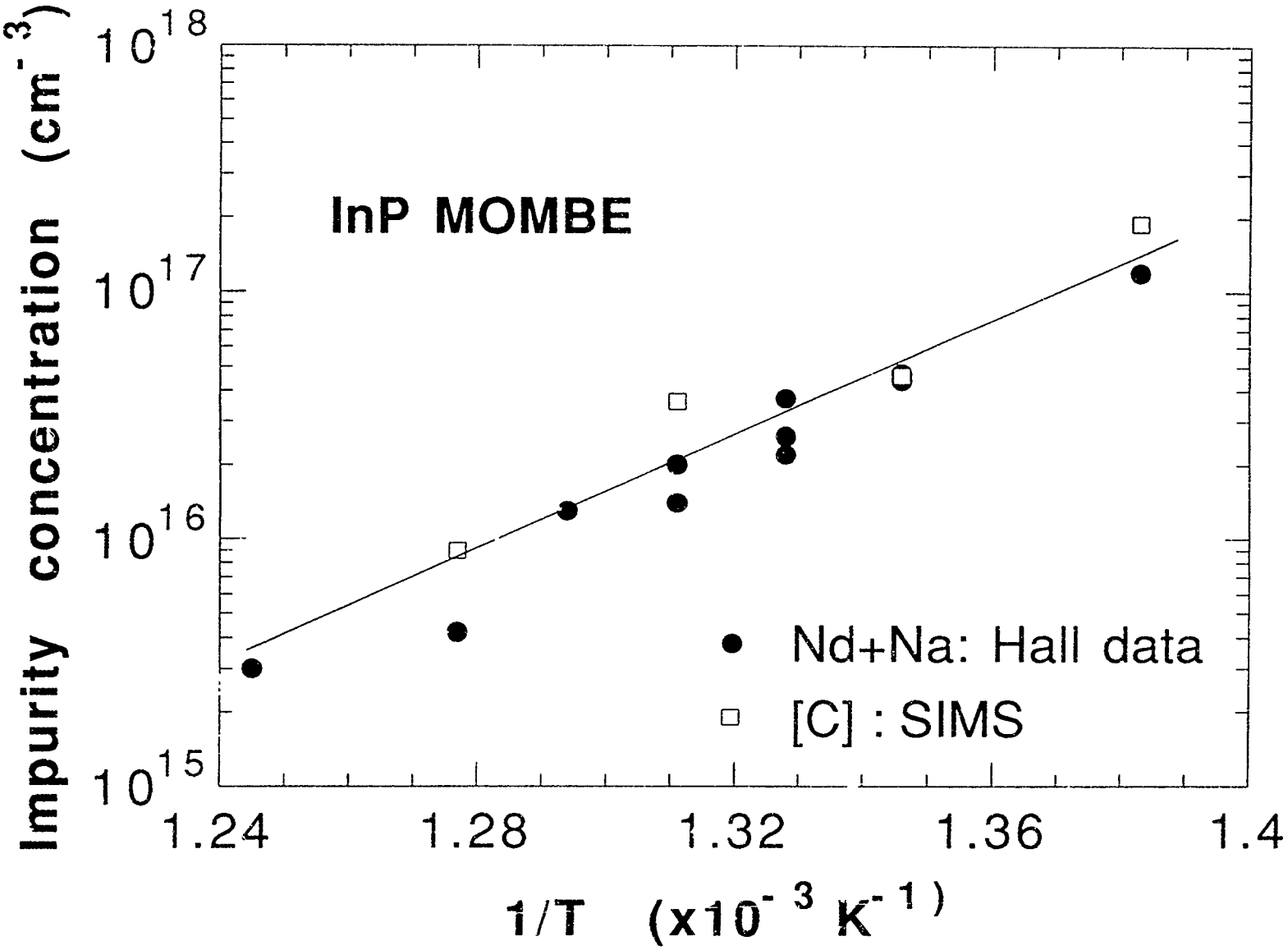

Figure 1: Carbon and total impurity concentrations in MOMBE grown InP

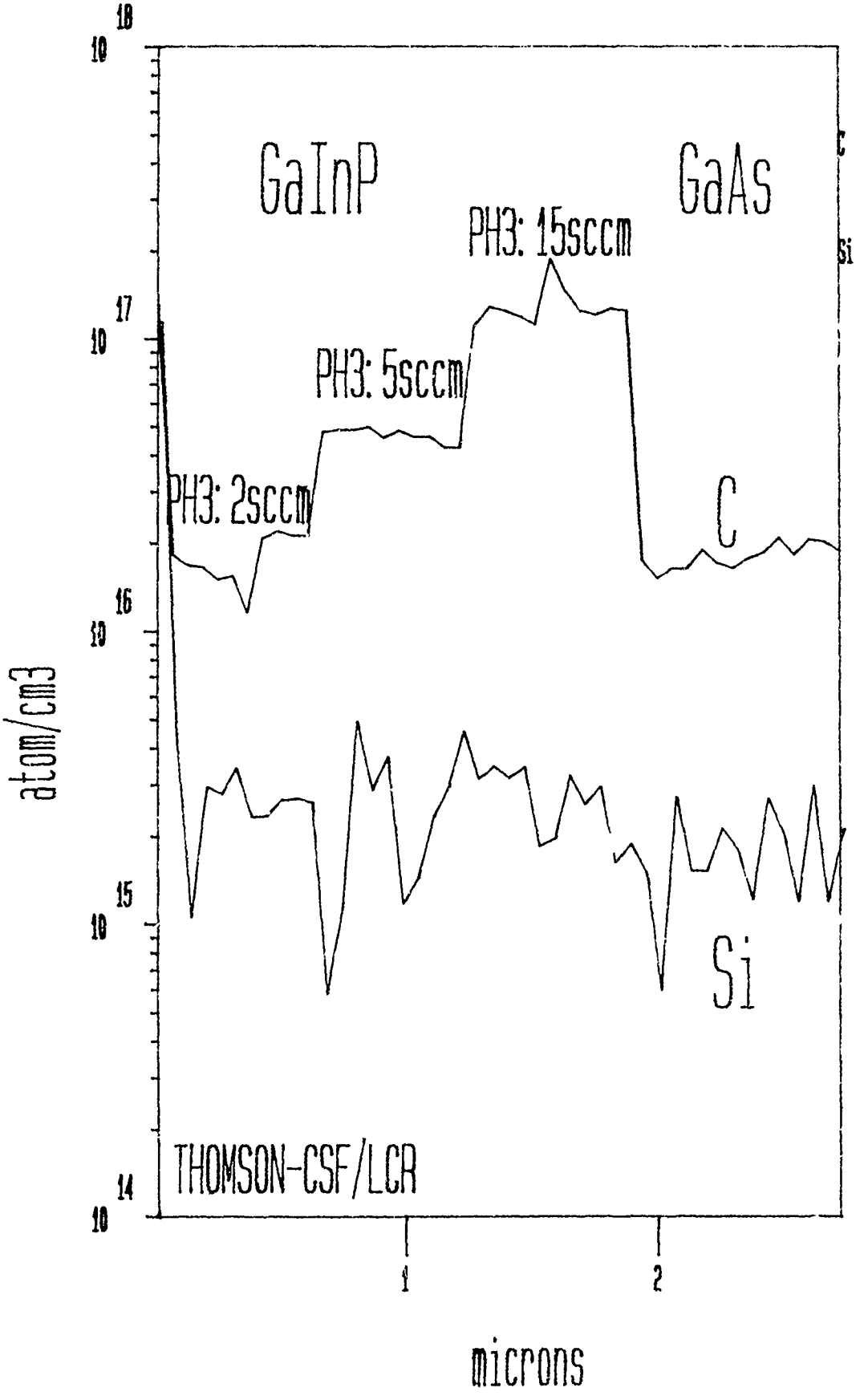
GaInP
GaAs
PH3: 15sccm
PH3: 5sccm
PH3: 2sccm
C
Si
THOMSON-CSF/LCR
atom/cm3
microns
1
2

APAH - A COORDINATIVELY SATURATED ALUMINIUM PRECURSOR FOR MOMBE

M. Kamp*, F. König, G. Mörsch and H. Lüth
Institut für Schicht- und Ionentechnik,
Forschungszentrum Jülich, P.O.Box 1913, D-5170 Jülich, FRG
Phone : -49-2461-612340 Fax : -49-2461-612333

L. Pohl and M. Hostalek
E.Merck, Frankfurter Str.250 , D - 6100 Darmstadt, FRG
Phone : -49-6151-722784 Fax : -49-6151-723119

1. Introduction

While growth techniques dealing with gaseous precursors, especially MOVPE and MOMBE, are well established for epitaxy of phosphorous based III - V semiconductors, the growth of aluminium containing materials still suffers from the insufficient purity and suitability of gaseous precursors and is therefore still dominated by solid source MBE.

The chemical structure of the conventional metalorganic trialkyls (TEGa , TMAl ,...) make them highly reactive towards electron-pair-donors such as oxygen. Therefore these metalorganic alkyls tend to form alkoxy groups which unfortunately have vapour pressures comparable to the precursor itself. Since oxygen contamination during production is hardly to be avoided, alkoxy groups were found in almost all trialkyls [1], but only for Al containing materials this becomes a strong evidence due to the distinct affinity of aluminium to oxygen .

However, there are approaches for new or modified precursors which are most promising for the growth of Al containing semiconductors in MOVPE and MOMBE [2,3]. To reduce the affinity of the precursor towards oxygen, there are two basic ideas. On one hand an adduct can be formed with an intermolecular saturation, an example is TEG - TMN adduct, and on the other hand an intramolecular saturation can be established [4].

1-(3-DimethylAminoPropyl)-1-Ala-cycloHexan, abbreviated APAH (Fig.1), is a representative of such a non-pyrophoric intramolecularly saturated precursor where the fourfold coordination of the aluminium is achieved by the free electron pair of the nitrogen [5].

APAH is a stable precursor up to 370 K, the vapour pressure is approx. p = 1 Pa at 300 K and approx. p = 60 Pa at 370 K, respectively.

While APAH has already been tested in MOVPE with reasonable results [2], we report on the first use of this precursor under UHV conditions in MOMBE.

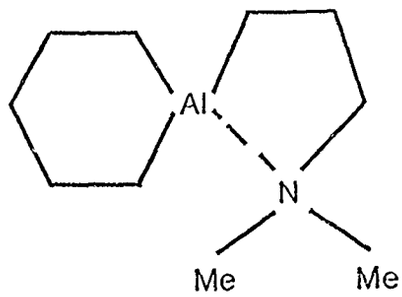

Fig 1. Structural formula of APAH.

2. Experimental

The experiments were carried out in a slightly modified Varian GEN II MOMBE system. Substrates were exactly oriented (100) GaAs wafers which were etched with $H_2SO_4 : H_2O_2 : H_2O$ (10 : 1 : 1) for 1 min. and rinsed in DI - water before being mounted on In-free substrate holders and loaded into the system. After heating the substrates to 900 K for 15 min, growth was initiated with the deposition of a 0.1 µm GaAs buffer followed by the AlGaAs layer and subsequent deposition of a 15 nm GaAs cap layer. Growth temperature was determined by an infrared pyrometer.

Since the vapour pressure of the APAH is rather low, the design of the gas inlet system required the use of a carrier gas (H_2, Pd purified) to achieve reasonable growth rates, whereas the other precursors (TEG and AsH_3) were used by direct destillation.

3. Results and Discussion

With APAH reasonable growth rates could only be achieved at higher vapour pressures, which necessitated a heating of both, bubbler and gas system. At bubbler temperatures below 340 K the Al - content of the deposited layers is directly related to the predicted vapour pressure of the APAH, whereas at higher bubbler temperatures a reduced Al content was found, which may be due to condensation within the gas system. Therefore, AlAs growth rates above 0.1 µm/h could not be achieved without exceeding a background pressure of $p = 5x10^{-3}$ Pa in the growth system.

Fig. 2 shows the temperature dependence of the AlAs growth rate and the resulting Al content in AlGaAs, which also depends on GaAs growth rate. Beside the temperature dependence the Al incorporation rate was found to depend on the supply of TEG, too. The AlAs growth rate calculated from $Al_{0.05}Ga_{0.95}As$ deposition is two times lower than in pure AlAs, this is most likely due to different surface diffusion rates of the particular decomposed species.

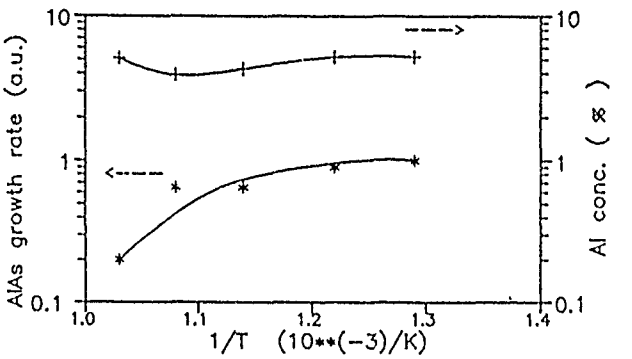

Fig. 2. Al content and AlAs growth rate versus inverse growth temperature.

SEM micrographs demonstrate that the morphology of the mirrorlike $Al_xGa_{1-x}As$ layers is excellent and smooth even at high Al content and under higher magnification (50.000x). Layers grown around 850 K show an excellent crystalline quality as is proven by XRD measurements ($Al_{0.12}Ga_{0.88}As$, FWHM = 20 arcsec for (004) bragg peak).

Hall measurements at 300 K reveal always p-type doping with hole mobilities comparable to data from literature [6]. The Hole concentration is plotted versus growth temperature for different Al concentrations in fig. 3. The data reveal carrier concentrations higher than in MOVPE layers grown under comparable growth conditions [2]. This suggests that the decomposition of the APAH is incomplete in MOMBE, due to lower growth temperature and reduced pressure. A contribution of an alkyl transfer, between TEG and APAH, to the obtained carrier concentrations seems unlikely as this would result in $Al(C_2H_5)_x$ species where the Al - C bonding strength is lower than in APAH. Secondary Ion Mass Spectroscopy (SIMS) measurements identify carbon as the main residual impurity, whereas nitrogen was not observed above the detection limit of approx. [N] = 10^{18} cm^{-3}.

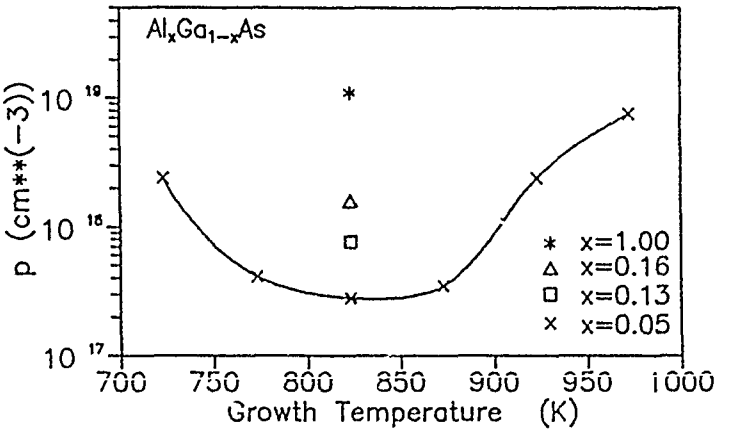

Fig. 3. Dependence of hole concentration at 300 K on growth temperature and Al content.

Photoluminescence measurements provided the data shown in fig. 4. The diagram reveals an optimized growth temperature of approx. 850 K. Highest PL intensities and narrowest line widths as well as lowest carrier concentrations (see fig. 3) could be achieved at this considerably low temperature.

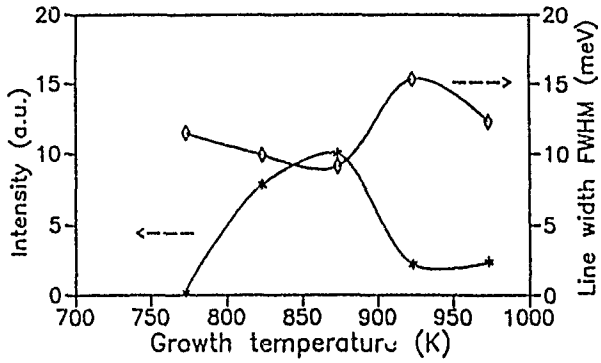

Fig. 4. Linewidth and relative intensity versus growth temperature obtained from 4.2 K PL measurements on $Al_{0.05}Ga_{0.95}As$.

Preliminary results of quantum well structures reveal the suitability of the precursor for the growth of heterostructures. PL measurements at 4.2 K show good reproducibility and remarkable linewidths of less than 8 meV for a 100 A SQW and 17 meV for a 30 A SQW, respectively.

4. Conclusions

APAH is a coordinatively saturated precursor for the growth of AlGaAs with high optical and crystalline quality even at considerably low growth temperatures, which suggests a strong reduction of oxygen contamination. Under UHV growth conditions a reasonable carbon incorporation limits the suitability of APAH to applications where p-type carrier concentrations above 10^{17} cm^{-3} are acceptable or required. Interaction between GaAs and AlAs growth rates in AlGaAs indicates competing incorporation mechanisms of the group III precursors on the surface.

References

[1] M. Hata, N. Fukuhara, Y. Zempo, M. Isemura, T. Yako and T. Maeda, J. Crystal Growth 93 (1988) 543.

[2] V. Frese, G. K. Regel, H. Hardtdegen, A. Brauers, P. Balk, M. Hostalek, M. Lokai, L. Pohl, A. Miklis and K. Werner, J. Electron. Mater. 19 (1990) 305.

[3] C. R. Abernathy, A. S. Jordan, S. J. Pearton, W. S. Hobson, D. A. Bohling and G. T. Muhr, Appl. Phys. Lett. 56 (1990) 2654.

[4] H. Schumann, U. Hartmann, A. Dietrich and J. Pickardt, Angew. Chem. 100 (1988) 1119.

[5] M. Hostalek, L. Pohl, A. Brauers, P. Balk, V. Frese, H. Hardtdegen, R. Hövel, G. K. Regel, A. Molassioti, M. Moser, F. Scholz and A. Stapor, Thin Solid Films 174 (1989) 1.

[6] M. Ilegems in "The Technology and Physics of Molecular Beam Epitaxy", ed. E. H. C. Parker (Plenum Press, New York, 1985) p. 134.

OBSERVATION OF ELECTRO-OPTICAL EFFECTS IN InGaAsP/InP QUANTUM WELLS AND SUPERLATTICE GROWN BY GSMBE

F. MOLLOT†*, M. BOULOU, C. STARCK
ALCATEL ALSTHOM RECHERCHE, Route de Nozay - 91460 MARCOUSSIS (France)
Phone : 33 (1) 64 49 10 00 - Fax : 33 (1) 64 49 05 02

Quantum well structures exhibiting electro-optic effects are of growing interest for new optoelectronic devices. For instance, absorption modulators made with MQW or superlattice structures will permit fast (multigigabit) transmission with very low chirp effects.

In this report we have studied the ability of Gas Source Molecular Beam Epitaxy (GSMBE) to grow high quality quantum well and superlattice structures in the GaInAs/GaInAsP/InP system. Two kinds of electro-optic effects have been investigated :

- The Quantum Confined Stark Excitonic effect [1] (QCSE) with a red shift energy under applied electric fields $\vec{E}$.

- The Wannier Stark effect [2] with strongly coupled wells which exhibits a blue shift energy with $\vec{E}$.

The transition energies under electric field are calculated for both systems using envelop function and transfer matrix techniques. This approach enables a prediction of the effects and further optimization of the structure.

The QCSE is very sensitive to well width and it is shown that a maximum shift of excitonic energy level is expected for well thicknesses of ~ 100 Å. For this reason we have studied quaternary GaInAsP wells/InP barriers to keep the well width at 100 Å and energy transitions at the desired wavelength simultaneously .

The WS effect consists of a field induced blue shift of the absorption edge of a strongly coupled superlattice. The staggering of adjacent wells states induced by the electric field prevents resonance between the wells. With field, the superlattice minibands then change into localized excitonic levels. The energy blue shift is roughly half the miniband width. Further, other optical transitions between neighbouring wells occurs at intermediate electric field. One of these transitions is red shifted relative to the absorption edge and can then be used for modulation purposes [3]. A typical WS structure has been designed as a

superlattice with 45 Å InGaAs wells and 25 Å InP barriers. Both the QCSE or WS effect have been studied by inserting the structures in the undoped region of a pin InP diode.

The optical quality investigated by PL has been shown very sensitive to the growth procedure at the interfaces. Best results have been obtained using growth interruptions and purges of the gas lines. The electro-optic effects have been characterized by photocurrent spectroscopy. The QCSE sample exhibits well shaped excitonic transitions at room temperature (figure 1). The Stark red shift has been observed as a 15 meV displacement of the excitonic peak under 40 kV/cm. This corresponds to a 2 V reverse bias voltage.

Photocurrent spectra of WS sample are shown on figure 2. All features of WS effect are clearly observed under applied electric field : blue shift of the absorption edge, emergence of excitonic peak, and a low energy red-shifted crossed transition. It has to be noted that the last transition vanishes at high electric field. For further applications, i.e. absorption modulator, both effects (blue shift and low energy transition) can be separately used by applying a selected bias voltage.

In conclusion we demonstrate that high quality ternary or quaternary QW and superlattices can be grown by GSMBE. These structures show electro-optical effects predicted by theory and are attractive for modulation purposes in optical communications.

REFERENCES

[1] E.E. MENDEZ, G. BASTARD, L.L. CHANG, L. ESAKI, Phys. Rev. B26, 7101, (1982)

[2] J. BLEUSE, G. BASTARD, P. VOISIN, Phys. Rev. Lett. 60, 220, (1988)

[3] E. BIGAN, M. ALLOVON, M. CARRE, P. VOISIN, Appl. Phys. Lett. 57, 327, (1990)

† Present address : L2M, CNRS, 196 Avenue Henri Ravera - 92220 BAGNEUX (France)

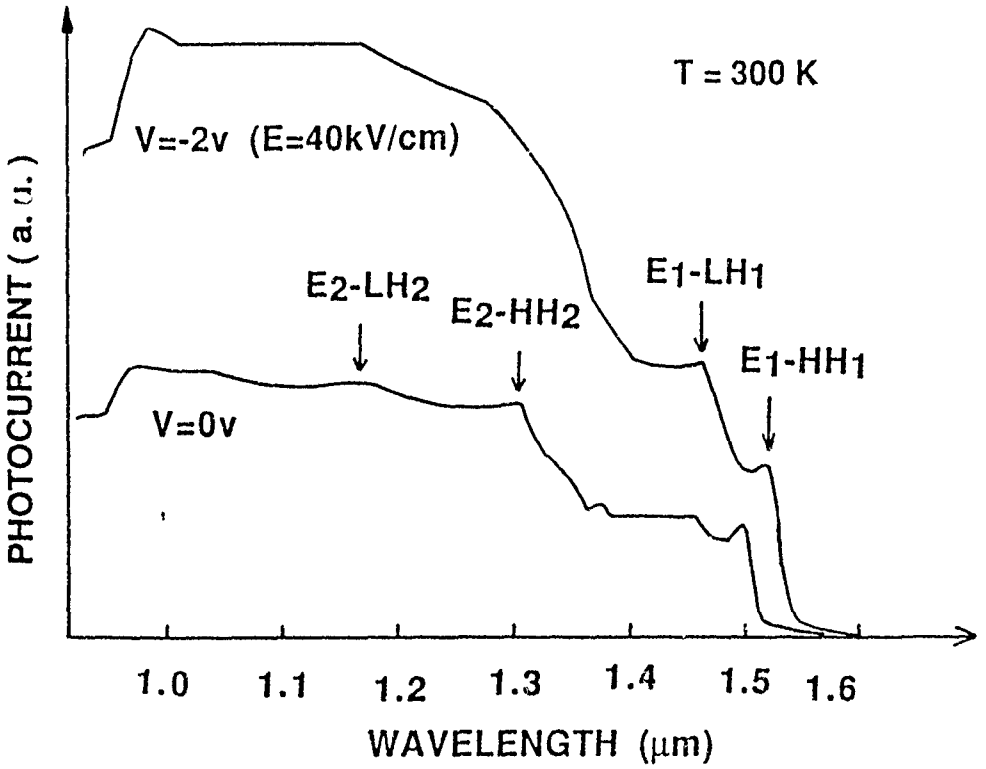

Figure 1 Photocurrent spectra of the QCSE sample. Arrows correspond to calculated wavelengths.

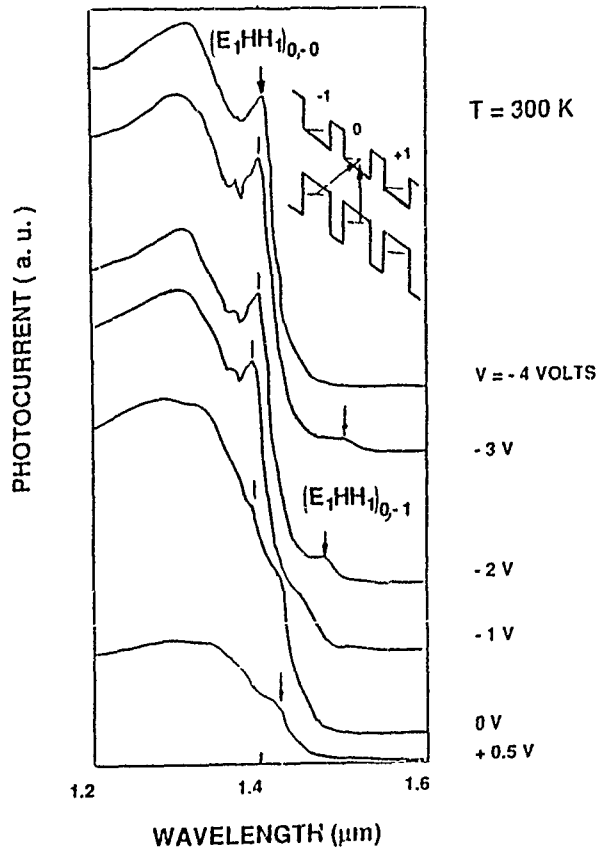

Figure 2 Photocurrent spectra of the Wannier-Stark sample.

GROWTH OF PBH LASER BY GSMBE

D. BONNEVIE, J-L. LIEVIN, C. STARCK, F. POINGT, D. SIGOGNE, L. GOLDSTEIN*
ALCATEL ALSTHOM RECHERCHE, Route de Nozay - 91460 MARCOUSSIS (France)
Phone : 33 (1) 64 49 10 00 - Fax : 33 (1) 64 49 05 02

INTRODUCTION

During the last few years, it has been shown that Gas Source Molecular Beam Epitaxy (GSMBE) is of particular interest for the growth of InP and GaInAsP compounds [1]. Double heterojunctions with bulk quaternary material or multiquantum well (MQW) structure active layers exhibit low threshold current densities [2], [3]. However the realization of optimized laser such as Planar Buried Heterostructure (PBH) is required for devices exhibiting low leakage current and good optical confinement. This will result in improved characteristics such as power emission or L-I linearity. Liquid phase epitaxy which is widely used as a regrowth technique to bury the active layer suffers from limitations due to inhomogeneous growth rate or small epitaxial substrate surface. In this communication we show the realization of PBH - MQW laser using three independent GSMBE epitaxial steps. To our knowledge this is the first report of a BH laser grown by MBE.

EXPERIMENTS

The first step of epitaxy consists of the growth of an active layer (MQW structure) with barrier of GaInAsP (λ = 1.18 µm) and 5, 80 Å GaInAs wells. Then a p type layer of InP (1 µm) is grown on the top of the MQW structure followed by 0.3 µm of GaInAs. After the first epitaxy, a mesa structure of 2 µm depth is defined by wet etching using bromine methanol. The width of the mesa at the active layer is about 2 µm.

The regrowth of InP for the p - n lateral blocking layer is done by GSMBE. The growth conditions are similar to those described elsewhere [2] at substrate temperature of Ts = 500 °C. The InP layers are deposited on both the side and the top of the mesa. The In flux being normal to the substrate there is no lateral growth of InP along the vertical wall of the mesa. Careful control of the thickness of regrowth layers permits to buried the active layer without deposition of InP on the side of the upper GaInAs layer. A detailed description of the regrowth process from a cristallographic point of view will be presented.

The GaInAs upper layer as well as InP regrown layers on the top of the mesa are lifted-off by selective etching. Then the p type layer of InP is deposited in the third epitaxial step as well the GaInAs contact layer by GSMBE. For comparison the last epitaxial step can also be done by LPE. Preliminary laser characteristics show threshold current in the range of I = 30 to 70 mA. The quantum efficiency is about $\eta = 19$ %. As expected the L-I characteristics show a small leakage current. In summary we have demonstrated the growth of BH laser by GSMBE for the first time using a non selective regrowth technique. Preliminary lasers characteristics show promising behaviour. The authors would like to thank F. Brillouet and P. Doussière for helpful discussions.

REFERENCES

[1] M.B. PANISH, Annual Rev. Mater. Sci. 1989, **19** : 209 - 29

[2] L.G. GOLDSTEIN, J. of Crystal Growth, 1990, **105**, 93

[3] A. PERALES, L. GOLDSTEIN, A. ACCARD, B. FERNIER, F. LEBLOND, C. GOURDAIN and P. BROSSON, Electron. Lett., 1990, 26, p. 236

Strained GRIN-MQW lasers for λ = 1.5 μm grown by gas-source MBE

H. Asonen, J. Keskinen, J. Näppi, M. Korteoja, K. Tappura,
K. Rakennus, T. Hakkarainen, and M. Pessa

Department of Physics, Tampere University of Technology,
P.O. Box 527,SF-33101 Tampere, Finland
Tel: (358)-(31)-162111, Fax: (358)-(31)-162600

Strained-layer graded-index multi quantum well (GRIN-MQW) lasers of InGaAs(P) have become very important both as light sources for pumping Er-doped optical fiber amplifiers (λ = 1.48 μm) and for optical telecommunication systems (λ = 1.55 μm) /1-4/.

In this paper we describe the effects of GRIN structure of the InGaAsP confinement layer and strain of the InGaAs active layer on the threshold current, J_{th}, of the quantum well lasers. All layers were grown by gas-source molecular beam epitaxy using solid sources for the group-III elements and hydrides for the group-V elements /5/.

To study the effect of quantum well thickness on J_{th} we grew two strained GRIN quantum well lasers containing four quantum wells whose thickness was 4.5 nm for laser A and 6.2 nm for laser B (Fig. 1). Table I lists J_{th} of these lasers. The values of J_{th} appear to be same for both lasers, suggesting that the thickness of the active layer does not influence J_{th} if lattice mismatch is not relieved via misfit dislocations.

Compressive strain is preferred over tensile strain in the quantum wells because the light hole moves upward in energy, as compressive strain increases, reducing the heavy hole-conduction band recombination. To examine the effects of compressive and

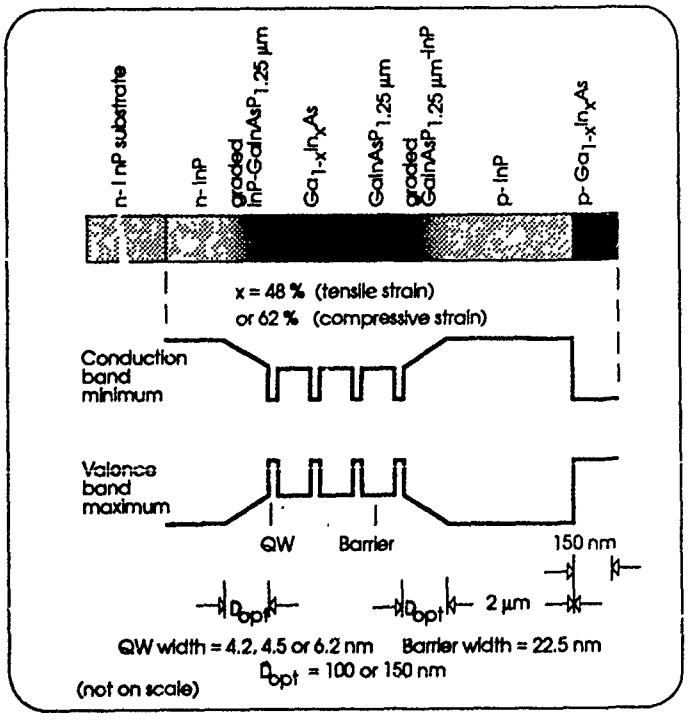

Figure 1. *Real space band structure of a strained multi quantum well laser containing lattice-matched graded-index optical confinement layers, grown by gas-source MBE.*

tensile strains on J_{th} we prepared two GRIN MQW lasers (labelled B and C) with the opposite signs of strain, caused by a difference in indium concentration: 62 % and 48 %, respectively. As shown in Table I, compressive strain yields lower J_{th} than tensile strain does, in accordance with the results of Tsang *et al.* /1/.

Moreover, we studied the dependence of the optical confinement factor, Γ, on GRIN structure and prepared two GRIN MQW lasers (labelled C and D) with different confinement layer widths. Theoretically, laser D should exhibit higher Γ and, hence, lower J_{th} /6/. The measured values of J_{th} were systematically smaller for laser D than laser C at all cavity lengths studied, lending qualitative support to this theoretical prediction. The very low threshold current density of 500 A/cm^2 achieved further demonstrates that gas-source MBE is capable of producing state-of-the-art lasers with complex layer structures.

Table I. *Summary of the study of threshold current densities J_{th} of strained multi quantum well InGaAs/InGaAsP/InP lasers with lattice-matched graded-index optical confinement layers. The longest GRIN structure and cavity length, and compressive strain in the well region yield the lowest J_{th}.*

Laser	GRIN layer thickness (nm)	Active layer thickness/strain (nm)/%	Threshold current density J_{th} (A/cm^2) L_{opt} = 0.6 mm	L_{opt} = 0.8 mm	L_{opt} = 1.0 mm
A	100	4.5 / -0.35	950	900	780
B	100	6.2 / -0.35	970	900	750
C	100	4.2 / +0.65	830	650	600
D	150	4.2 / +0.65	660	590	500

1. W.T. Tsang, M.C. Wu, L. Yang, Y.K. Chen, and A.M. Sergent, *Electronic Letters* **26**, 2035 (1990)
2. H. Temkin, N.K. Dutta, T. Tanbun-Ek, R.A. Logan, and A.M. Sergent, *Appl. Phys. Lett.* **57**, 1610 (1990)
3. T. Tanbun-Ek, R.A. Logan, N.A. Olsson, H. Temkin, A.M. Sergent, and K.W. Wecht, *Appl. Phys. Lett.* **57**, 224 (1990)
4. M.J. Ludowise, T.R. Ranganath, and A. Fisher-Colbrie, *Appl. Phys. Lett.* **57**, 1493 (1990)
5. M. Pessa, T. Hakkarainen, J. Keskinen, K. Rakennus, A. Salokatve, G. Zhang, and H. Asonen, *SPIE's Int. Conf. on Physical Concepts for Novel Optoelectronic Device Applications*, 28 Oct.-2 Nov., 1990, Aachen , Germany
6. B. Sermage, M. Blez, C. Kazmierski, A. Ougazzaden, A. Mircea, and J.C. Bouley, *SPIE's Int. Conf. on Physical Concepts for Novel Optoelectronic Device Applications*, 28 Oct.-2 Nov., 1990, Aachen, Germany.

HIGH POWER AlGaAs-SQW-SCH-LASERS AND LASER ARRAYS PREPARED BY MOLECULAR BEAM EPITAXY

V.P.Chalyi, S.Yu.Karpov, Yu.V.Kovalchuck, V.E.Myachin*,
A.Yu.Ostrovski, A.P.Shkurko, N.A.Strugov, A.L.Ter-Martirosyan
A.F.IOFFE PHYSICO-TECHNICAL INSTITUTE
Polytekhnicheskaya 26 , 194021 Leningrad , USSR
Phone: (812)-247-99-89 Telex: 121453 FTIAN SU

As a rule, heterostructures required for the fabrication of highpower semiconductor lasers are produced by MOCVD [1-3] or LPE [4] methods. In this abstract we present the results of investigation of high-power AlGaAs/GaAs-semiconductor heterolasers and laser arrays prepared by molecular beam epitaxy

After optimization the base heterostructure which allows to obtain high radiation power preserving rather high differential efficiency was chosed (zone diagram of the structure is shown in the insertion of fig.1). As an active layer was used the low level n-type doped 150 Å-width single quantum well.

For the preliminary control four-cleaved laser diodes have been fabricated on the basis of the grown structure. Threshold current density in such lasers didn't depend on their size and was 250÷300 A/cm^2. Mesa-stripe lasers with additional oxide isolation (stripe width - 100 and 200 μm) have been produced from other part of the structure. In this case threshold current density was about 300 A/cm^2 according to resonator length L=1,2 mm . Differential quantum efficiency η_d didn't depend on the stripe width and was up to 75-80% in short resonator lasers.

Measured dependence of threshold current density and differential quantum efficiency on resonator length have allowed to determine the optimal value L provided maximum light output power. For the power mesurements the samples with L≅ 1 mm and W= 100 μm soldered with indium on copper heat sink were used. The measurements have been made both in puise oscillation mode (pumping pulse duration - 400 ns, frequency - 25 kHz) and at continuous wave generation (in last case the temperature of the heat sink has been kept constant). The maximum light output power of lasers without additional coatings obtained at continuous wave generation and in pulse oscillation mode was 0.9 W

and 4.5 W respectively. It was limited by active area heating up at continuous wave generation and by catastrophic damage of resonator mirrors in a pulse oscillation mode.

Laser arrays with 10÷15 stripes (W = 100 μm , interval between stripes - 100 μm) have been fabricated using the base heterostructure. The multilayer coating with 85%-reflectivity has been deposited by sputering on a rear mirror. The testing of the laser array has been made in a quasi-cw regime (pumping pulse duration - 200 μs , frequency - 50 Hz. The heat sink temperature was maintained 15^{o}C . Near field pattern measurements (fig.2) have shown that under pumping current exceeding twice threshold current the power emited by single stripe differed from another stripe one not more than on 15% . Fig.3 presents a power-current characteristic of the array. The differential efficiency about 52% and the maximum light output power about 25W for the array of 15 lasers were achieved. The width of emission spectrum at FWHM was estimated ~ 5 nm and far field divergency in the direction parallel and perpendicular to p-n-junction plane was obtained 12^{o} and 50^{o} respectively.

[1] D.V.Welch,B.Chan,W.Streifer,D.R.Scifres // Electron.Lett., 24 , 1.5 (1988)

[2] M.Sakamoto,D.F.Welch,J.G.Endriz,D.R.Scifres,W.Streifer // Appl.Phys.Lett., 54 , 2299 (1989)

[3] H.Yamanaka,K.Iwamoto,N.Yamaguchi,K.Honda,T.Mamine,C.Kojima // Proc.Conf.on Laser & Electro-Optics, 468 (1990)

[4] D.Z.Garbuzov,A.B.Gulaskov,A.V.Kochergin,A.P.Shkurko,N.A.Strugov,A.G.Ter-Martirosyan,V.P.Chalyi // Proc.Conf.on Laser & Electro-Optics, 468 (1990)

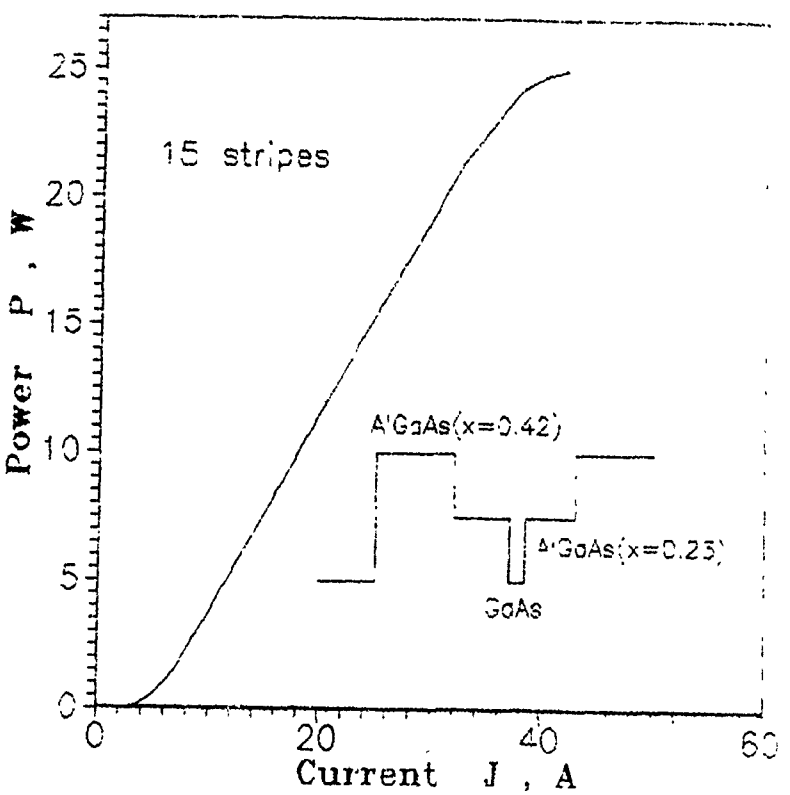
15 stripes
Power P , W
Current J , A
0
5
10
15
20
25
0
20
40
60
AlGaAs(x=0.42)
AlGaAs(x=0.23)
GaAs

Fig.1

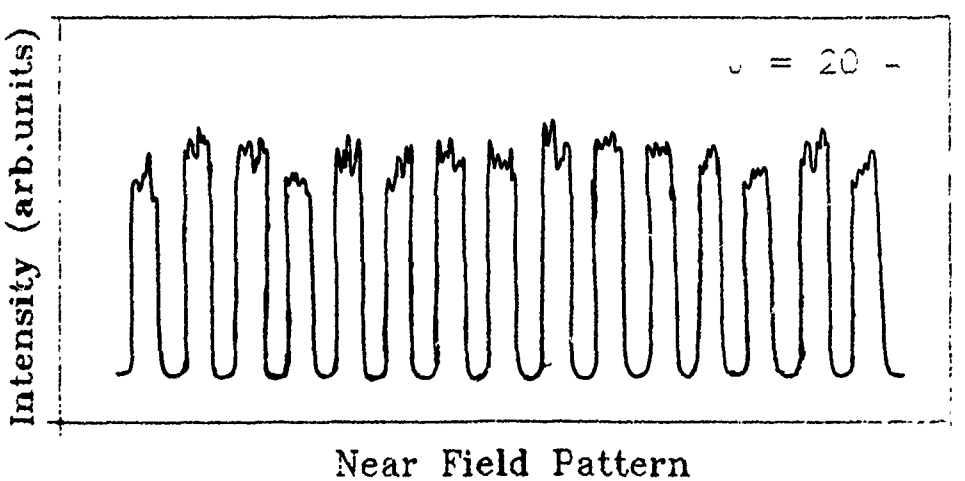
Intensity (arb.units)
Near Field Pattern

Fig.2

IMPROVED M.B.E. GROWTH OF HEAVILY DOPED GaAs(Be)/GaAlAs HBTs WITH HIGH DEVICE PERFORMANCES AND HIGH THERMAL STABILITY.

N.Jourdan, F.Alexandre*, C.Dubon-chevallier, J.Dangla, Y.Gao, A.C.Papadopoulo
Centre National d'études des Télécommunications
196 Av. Henri Ravera, 92220 Bagneux, France, (Phone: 45 29 54 10, Fax: 45 29 54 05)

Heavy Be doping of GaAs in excess of $10^{20}cm^{-3}$ have been easily achieved by Molecular Beam Epitaxy (MBE) [1]. This capability is very attractive for the obtention of high frequency performances of GaAs(Be)/GaAlAs Heterojunction Bipolar Transistor (HBT) by decreasing the base sheet resistance. However the distribution of the base dopant has to be controlled very precisely during the MBE growth (500-600°C) and during the technological process of the device such as an implanted technology, which offers potential advantages versus standard double mesa technology and which requires high temperature annealing (800°C). Such thermal treatment can induce important Be diffusion towards the emitter layer which has drastic effect on device performances since it decreases dramatically the emitter injection efficiency.

Previous studies have shown that a decrease of the growth temperature [2] and an increase of the V/III flux ratio [3] can minimize Be during the MBE growth of GaAs. In the present study, we investigate directly for the first time the influence of these growth parameters on the HBTs electrical characteristics.

For that purpose two sequences of four 1µm thick GaAs(Be) layers and of three HBT structures have been grown with different V/III flux ratio in the range 20 to 80. The Be doping level for the GaAs epilayers and for the 100 nm thick HBT base is $5\ 10^{19}cm^{-3}$, which corresponds to a measured base sheet resistance as low as 145Ω/□. The samples have been characterized by SIMS, electroluminescence, cathodoluminescence and electrical measurements. The experimental results obtained demonstrate that an increase of the V/III flux ratio leads to:

1. an improvement of the minority carriers diffusion length in GaAs(Be)

2. a related increase of almost one order of magnitude of the current gain of HBT devices. For the optimized growth conditions a record maximum current gain value of 70 for a 145Ω/□ base sheet resistance has been obtained on devices processed by a conventional double mesa technology.

3. a drastic reduction of Be diffusion during post-growth annealing at high temperature (800°C), leading to the first operational heavily doped base HBTs processed with an implanted technology.

These results can be attributed to a reduction of the concentration of Be incorporated in interstitial position, inducing high material quality and low dopant diffusion even at high temperature. The high thermal stability of HBT structure obtained by an optimization the MBE growth is very promising for the future realization of integrated circuits with self-aligned technology and for an improved reliability of HBT devices.

[1] J.L.Liévin, F Alexandre, Electronics Lett. 21,10,413 (1985)

[2] J.L.Liévin, C.Dubon-Chevallier, F.Alexandre, G.Leroux, J.Dangla, D.Ankri, IEEE Electron Device Lett., 7,2 (1986)

[3] Y.C.Pao, J.Franklin, J.S.Harris, Proc. of MBE V (Sapporo,Japan),415 (1988)

INFLUENCE OF MBE GROWTH TEMPERATURE ON THE DEVICE PERFORMANCE OF AlGaAs/GaAs HBT's AND THEIR CHARACTERIZATION BY PHOTOLUMINESCENCE

C. Wölk*, H. Leier, F.J. Berlec

DAIMLER BENZ AG Research Center Ulm
P.O.Box 2360, Wilhelm-Runge-Straße 11, D-7900 Ulm, Germany
Tel.: (+731) 505 2088, Fax: (+731) 505 4102

The precise control of the pn-junction position with respect to the heterojunction in AlGaAs/GaAs heterobipolar transistors (HBT) is one of the most critical steps in MBE growth of this structure/1,2,3/. Outdiffusion of Be from the base may move the pn-junction into the AlGaAs emitter layer and therefore reduce the injection efficiency. A lower growth temperature reduces the Be diffusion but it also may deteriorate the layer qualities.

In this work we have examined the influence of growth temperature on doping profiles (SIMS, CV), low temperature photoluminescence and device performance of HBT's with a highly Be-doped ($4*10^{19}cm^{-3}$) base. A simple and quick double mesa technology is used to fabricate test HBT's from wafers grown at different temperatures (emitter area 100µm x 100µm). The layer structure is shown in Table 1. Be and Si were respectively used as p-type and n-type dopants. The growth temperature was hold constant at 630°C for all layers up to the collector layer. For the growth of the base and the following layers the temperature was varied between 420°C and 680°C, whereas the V/III ratio was hold constant. The main results are summarized in the following.

As can be seen in Fig.1, the maximum current gain $ß_{max}$ reaches a value of 140 for a growth temperature around 575°C (I_c = 30mA). For temperatures above T = 600°C we observe a sharp reduction of $ß_{max}$. A more gradual reduction of $ß_{max}$ is obtained at lower growth temperatures indicating an increase of recombination. However, even at growth temperatures of 500°C HBT's with a maximum current gain of $ß_{max}$ = 35 were realized. - The strong reduction of $ß_{max}$ for T > 600°C coincides quite well with the onset of Be diffusion into the AlGaAs layer as detected by SIMS (Fig. 2). In particular, we observe a steep diffusion front of Be in AlGaAs which indicates a concentration-dependent

diffusion mechanism. Diffusion of Be into the n^- doped collector is also detected in the same growth temperature range but turns out to be significantly smaller in magnitude.

The onset of diffusion of Be into the AlGaAs emitter is also detected by photoluminescence (PL) measurements at 20K. From the AlGaAs layer we get luminescence with two peaks located at 1.92 eV and 1.86 eV (Fig.4), which can be most probably attributed to bound excitons and a defect complex transition /4/. For growth temperatures higher than T = 600°C the peaks disappear. This strongly correlates with the onset of diffusion of Be into the emitter layer and the drop of the current gain.

A more complex PL emission is observed in the energy range 1.4eV - 1.65eV. These emission lines can be attributed to different HBT layers. The observed peak positions and PL intensities will be discussed in comparison with SIMS, CV and device data of HBT's grown at different temperatures.

Table 1.

Layer	Material	AlAs mole fraction	Thickness (nm)	Carrier conc. (cm^{-3})
cap	n-GaAs	0	100	$3x10^{18}$
graded layer	n-AlGaAs	graded	30	graded
emitter	n-AlGaAs	0.3	100	$2x10^{17}$
spacer	GaAs	0	10	undoped
base	p-GaAs	0	90	$4x10^{19}$
collector	n-GaAs	0	750	$2x10^{16}$
collector contact	n-GaAs	0	1000	$3x10^{18}$
superlattice	(AlAs/GaAs)(1/0)		10x(2+2)	undoped
buffer	GaAs	0	100	undoped

/1/ R.J Malik et al. Appl.Phys.Lett. 46 (6), 1985, p. 600

/2/ H.Ito and t.Ishibashi, Jap.J.Appl.Phys. 26 (3),1987, p.439

/3/ F.Alexandre et al. proceedings of EURO MBE 89

/4/ M.Minara et al. J.Appl.Phys. 55 (10), 1984, p.3760

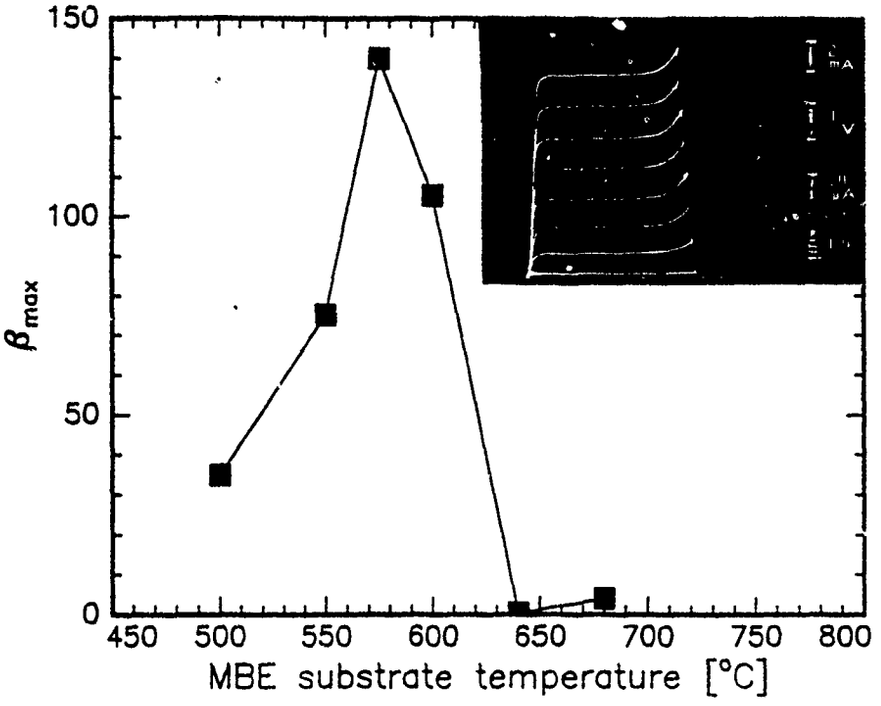

Fig. 1. Influence of growth temperature on max. current gain

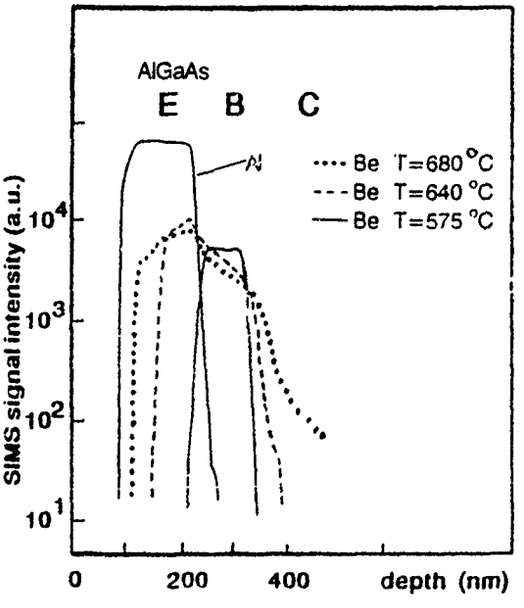

Fig. 2. SIMS profiles of Be and Al

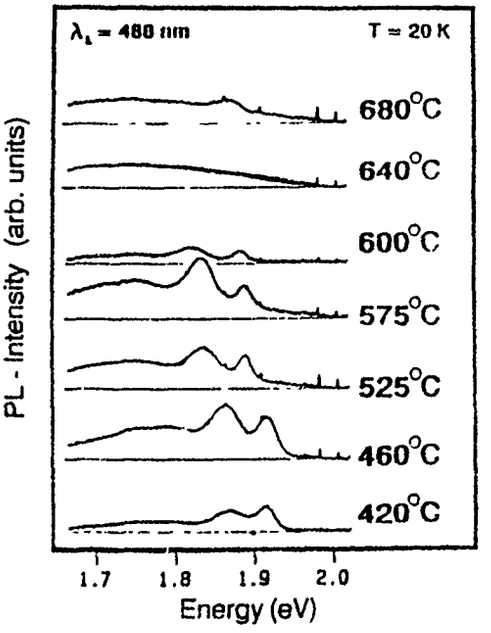

Fig. 3. PL emission from AlGaAs emitter

InP SOLAR CELLS GROWN BY GAS-SOURCE MOLECULAR BEAM EPITAXY

J.P. Zibin, K. Rakennus, K. Tappura, G. Zhang,
J. Lammasniemi, and H. Asonen

Department of Physics, Tampere University of Technology
P.O. Box 527, SF-33101 Tampere, Finland

In recent years InP has received considerable interest as a material for solar cells in space applications. This is because although it can achieve efficiencies roughly comparable to those of GaAs and Si cells, its radiation resistance is substantially better than that of GaAs or Si. Hence by the end of a long mission, InP cells may exhibit much higher efficiencies than cells of the more common materials.

We have grown InP solar cells on InP substrates by the gas-source molecular beam epitaxy (GSMBE) technique. The cells were of the $n^+/p/p^+$ shallow-homojunction type and included an InGaAs contact layer (see figure 1). It was our intent to assess the capability of GSMBE in InP solar cell growth, and in particular to investigate the design of the emitter layer and the nature of the surface grown by GSMBE.

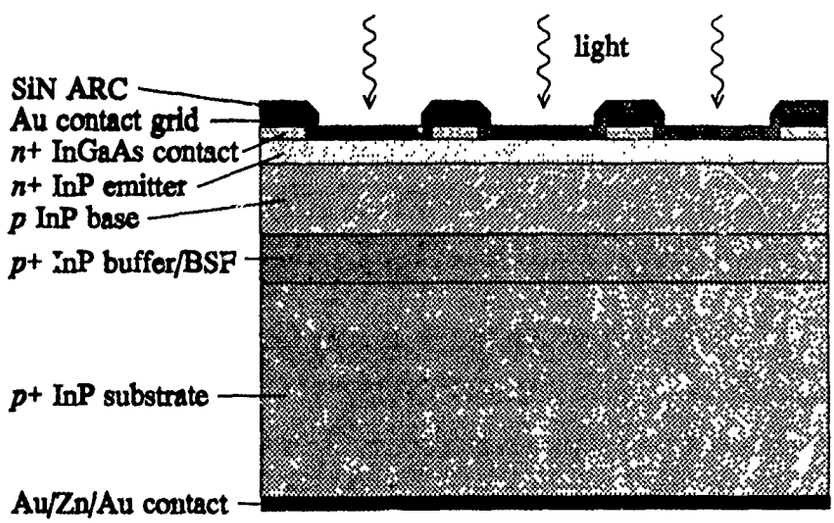

Figure 1. Cross-sectional structure of our InP solar cells. Thicknesses and doping levels vary. ARC = antireflection coating, BSF = back surface field.

Our GSMBE system is equipped with solid indium, gallium, silicon, and beryllium cells while phosphorus and arsenic were generated from thermally cracked PH_3 and AsH_3, respectively. The quality of our undoped InP layers is good according to Hall mobility and photoluminescence (PL) measurements. Undoped InP was *n*-type (~10^{14} cm^{-3}) and the 77 K mobility was above 100 000 cm^2/Vs. PL spectra of these films were dominated by the free exciton transition and showed only minor intensity from the acceptor-bound exciton transition, indicating a very low compensation effect in our samples.

All processing and characterisation of the cells is done in our facilities. Processing steps include lithography, electron-beam metallisation, electroplating, rapid thermal annealing, chemical etching, antireflection coating (ARC) deposition, and bonding. We can measure dark and illuminated current-voltage (*I-V*) curves as well as absolute spectral responses. In addition, a simple technique has been developed to measure approximate efficiencies under any standard illumination conditions.

The properties of the emitter layer are known to be important in the performance of $n^+/p/p^+$ shallow-homojunction InP solar cells. We have grown cells with emitter thicknesses ranging from 3000 to 200 Å. The spectral response and the illuminated *I-V* curve of a 200 Å emitter cell are presented in figures 2 and 3, respectively. The effect of a plasma-deposited SiN_x ARC has also been examined. We have observed anomalously high improvements in spectral response after the deposition of such a coating. This was especially apparent in the cells with the 200 Å emitters, for which the AM0 (space illumination) active-area short-circuit current density increased from 10 mA/cm^2 before ARC to 32 mA/cm^2 after ARC deposition.

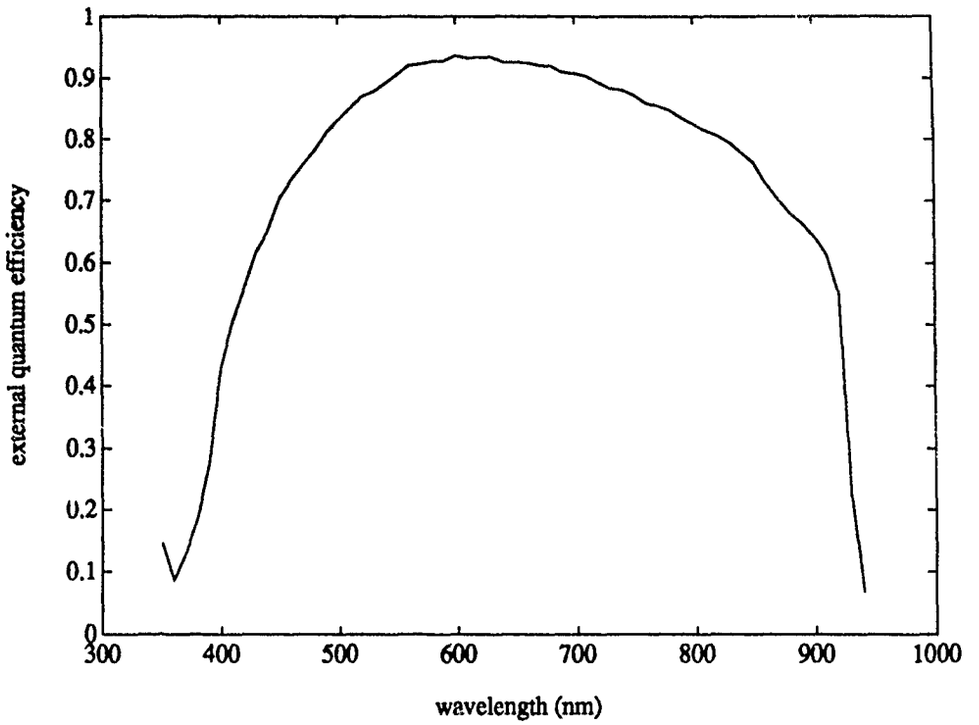

Figure 2. Absolute external active-area quantum efficiency of a SiN_x coated 200 Å emitter InP solar cell.

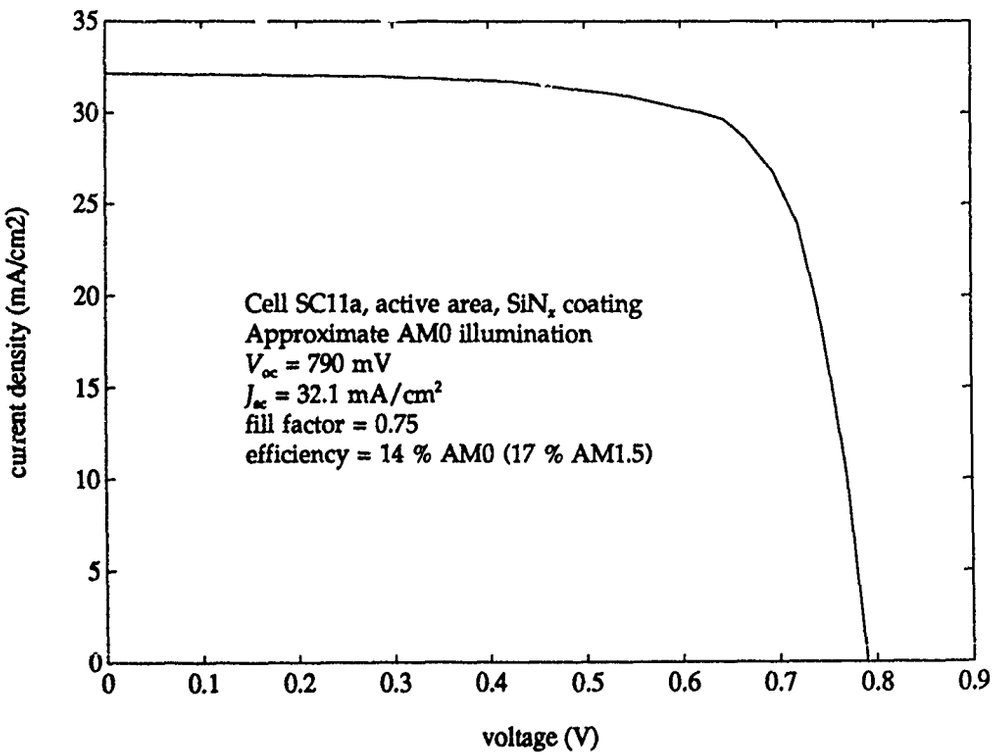

Figure 3. Illuminated current-voltage curve and cell parameters for the same cell as in figure 2 under AM0 (space) illumination. The AM1.5 (terrestrial illumination) efficiency is also given.

AlInAs/GaInAs Metal-Semiconductor-Metal photodiode with graded AlGaInAs transition regions.

A. Temmar, J.P. Praseuth* and A. Scavennec

Centre National d'Etudes des Télécommunications
Laboratoire de Bagneux 196, Av Henri Ravera
92220 Bagneux France
Phone: 33 1 45295159, Fax 33 1 45295405

Owing to its small capacitance and suitability for integration with microelectronic devices, the GaInAs Metal-Semiconductor-Metal photodiode has recently received a large interest. In order to obtain a low enough leakage current, either a semi-insulating material is used (1) or an AlInAs Schottky enhancement barrier is added on top of the absorption region (2). In this latter case, carriers may be trapped at the heterojunction,thus reducing the photodiode bandwidth under low optical excitation, as found in most optical fibre transmission links. To prevent such carrier accumulation, a graded AlGaInAs region has to be inserted between the GaInAs absorption layer and the AlInAs barrier enhancement layer (3,4).

Epitaxial growth:

- The MSM photodiode structure consists of a 0.3 µm $(Al_{0.48}In_{0.52}As)_z(Ga_{0.47}In_{0.53}As)_{1-z}$ buffer layer linearly graded between z=0.9 and z=0.1, followed by a 2 µm $Ga_{0.47}In_{0.53}As$ absorbing layer, a 0.2 µm $(Al_{0.48}In_{0.52}As)_z(Ga_{0.47}In_{0.53}As)_{1-z}$ transition layer linearly graded between z=0.1 and z=0.9, and a 0.05µm $Al_{0.48}In_{0.52}As$ Schottky enhancement layer.
The main difficulty of solid source MBE growth of such structure is to achieve simultaneously the lattice-matching and the linear composition variation of the graded quaternary layers. One way to obtain this is to use superlattice (3); however, this induces interface related defects due to the flux transient associated with shutter operation. Another way is to vary the InAs,GaAs, AlAs growth rates as determined by RHEED oscillation intensities (4); this requires a rather difficult control. Here, we used an adaptation of the two indium cells method developed in our laboratory (5). The excellent characteristics of the MSM-PD we obtained as described in the next section illustrate the quality of the gradual layers. Relevant characterisations of such growth techniques will be presented.

Device processing and characteristics:

- MSM photodetectors have been fabricated, starting with mesa etching down to the SI substrate. This is followed by the TiAu interdigitated Schottky contacts with e-beam deposition, mesa edge isolation and contact pads formation. After the anti-reflection coating deposition, devices are diced and mounted on alumina substrates for characterization. Contacts width is 1 μm with a spacing of 1.5 or 2 μm. The photosensitive area varies from 10x10 μm^2 up to 70x70 μm^2.

Very low leakage current have been observed (0.1 nA at 10 V bias on 40x40 μm^2 devices) with symmetrical characteristics, indicative of a very good material quality. Device capacitance can be very low also (2.5 fF /100μm^2). The responsivity is about 0.7A/W at 1.5 μm. This translates to a quantum efficiency close to 100 % when considering the electrode/sensitive area ratio. No photoconductive gain is observed, and under 10 V bias, no tail is observed in the response to a 35 ps optical pulse at 1.3 μm. (The observed response with a FWHM of 64 ps is limited by the ceramic submount). These two features are illustrative of the efficiency of the graded region in preventing carrier accumulation at the surface and in easing the carrier transport from the absorption region to the collecting Schottky electrodes.

Acknowledgement:

The authors wish to thank M. Allovon for contribution in MBE growth control, Y. Gao for SIMS analysis, J. Primot for x-rays data, L. Nguyen and J.P. Chandouineaux for the set of masks, Y. Le Bellego, L. Giraudet, G. Post and A. Clei for guidance in technology, M. Billard for characterization and J.F. Palmier for fruitful discussions and modeling.

References:

(1) C.J. Wei, D. Kuhl, E.H. Bottcher, D. Bimberg and E. Kuphal
IEEE Electron Dev. Lett. EDL11, 334 (1990)

(2) J.B.D. Soole, H. Schumacher, H.P. LeBlanc, R. Bhat and M.A. Koza
IEDM Washington DC, 3-6 December, Technical Digest, 713 (1989)

(3) O. Wada, H. Nobuhara, H. Hamaguchi, T. Mikawa, A. Tackeuchi and T. Fujii
Appl. Phys. Lett. 51, 16 (1989)

(4) H.T. Griem, S. Ray, J.L. Freeman and D.L. West
Appl. Phys. Lett. 56, 1067 (1990)

(5) J.P. Praseuth, M.C. Joncour, J.M. Gerard, P. Hénoc and M. Quillec
J. Appl. Phys. 63, 400 (1988)

PROPERTIES OF PSEUDOMORPHIC $In_xGa_{1-x}As/Al_{0.3}Ga_{0.7}As/GaAs$ HIGH ELECTRON MOBILITY TRANSISTORS ($0 < x < 0.5$)

T. Schweizer, K. Köhler, P. Ganser, A. Hülsmann, and P. Tasker*

Fraunhofer Institut für Angewandte Festkörperphysik 78 Freiburg, Tullastr. 72, FRG

ABSTRACT

Modulation doped $Al_{0.3}Ga_{0.7}As/In_xGa_{1-x}As/GaAs$ high electron mobility transistor structures for device application have been grown using molecular beam epitaxy. Initially the critical layer thickness for InAs mole fractions up to 0.5 was investigated. For InAs mole fractions up to 0.35 good agreement with theoretical considerations was observed. For higher InAs mole fractions disagreement due to a strong decrease of the critical layer thickness was observed. Using the molecular beam epitaxy technology $Al_{0.3}Ga_{0.7}As/In_xGa_{1-x}As/GaAs$ high electron mobility transistor structures with InAs mole fractions between 0 and 0.35 were grown for device applications. For the presented field effect transistors best device performance is obtained for InAs mole fraction in the range of 0.25-0.3.

INTRODUCTION

Pseudomorphic $Al_yGa_{1-y}As/In_xGa_{1-x}As/GaAs$ high electron mobility transistor (HEMT) structures grown on GaAs are of great interest for high speed device applications. A superior electron confinement and a higher conduction band offset resulting in higher sheet densities can be achieved in comparison to the conventional $Al_yGa_{1-y}As/$ GaAs HEMT structure[1]. However, the lattice mismatch between the GaAs substrate and the $In_xGa_{1-x}As$ layer could only be accomodated within the layers by elastic strain if the $In_xGa_{1-x}As$ layer thickness is below the critical layer thickness[2] (CLT). If the layer thickness is above the CLT the strain energy can force the formation of misfit dislocations. A high dislocation density leads to a strong degradation of the electrical[3] and optical[4] properties. For best performance of $Al_yGa_{1-y}As/In_xGa_{1-x}As/GaAs$ HEMT structures for device application, it is necessary to know the dependence of the CLT of the $In_xGa_{1-x}As$ layers on the InAs mole fraction. Previous work has been concerned with the determination of the CLT with different measurement methods such as photoluminescence[4], x-ray[5], and Hall effect measurements[6]. These methods yield different values for the CLT, which is due to the sensitivity of the different methods[7].

In this paper we report on the growth of $Al_{0.3}Ga_{0.7}As/In_xGa_{1-x}As/GaAs$ HEMT structures for electrical devices. The CLT is determined by Hall effect measurements.

MATERIAL PROPERTIES

The $Al_{0.3}Ga_{0.7}As/In_xGa_{1-x}As/GaAs$ HEMT structures were grown in a Varian Gen II MBE system on semi-insulating LEC grown (100) GaAs 2" substrates. The As-to-Ga beam-equivalent pressure ratio was 15. For the $In_xGa_{1-x}As$ layer growth the As-to-Ga beam equivalent pressure ratio was increased to 30. The InAs mole fraction and the growth rates for GaAs, $Al_{0.3}Ga_{0.7}As$ and $In_xGa_{1-x}As$ were determined using reflection high energy electron diffraction intensity oscillations. The layer sequence of the HEMT structures consists of a 150 nm undoped GaAs buffer layer followed by a 3.5 nm/8.5 nm $GaAs/Al_{0.3}Ga_{0.7}As$ superlattice and a 600 nm undoped GaAs buffer. The structure continues with the $In_xGa_{1-x}As$ quantum well (QW) which is varied in thickness and InAs mole

fraction (x). The layer sequence for the electron supply consists of a 5 nm $Al_{0.3}Ga_{0.7}As$ spacer and a 1.7 nm wide GaAs QW with a δ-doping of $3.5*10^{12}cm^{-2}$ followed by 60 nm undoped $Al_{0.3}Ga_{0.7}As$. The structure is capped by 20 nm GaAs.

At low temperature the Hall mobility is sensitive to structural degradation of the $In_xGa_{1-x}As$. Fritz and coworkers[3] observed a reduction in low temperature mobility by a factor 4-5 on their samples. They attributed this reduction in the Hall mobility to the strain being beyond the critical value required for the generation of misfit dislocations. To study the onset of structural degradation of the $In_xGa_{1-x}As$ layer resulting in a reduction of the Hall mobility series of $Al_{0.3}Ga_{0.7}As/In_xGa_{1-x}As/GaAs$ HEMT structures were grown with varying $In_xGa_{1-x}As$ layer thickness but constant InAs mole fraction (x). With increasing $In_xGa_{1-x}As$ QW width an increase in the Hall mobility is observed. This behaviour can be understood by the fact that the contribution of scattering due to interface roughness decreases with increasing QW width. However exceeding a certain value for the $In_xGa_{1-x}As$ QW width a drop in the Hall mobility is observed. This behaviour can be explained by structual degradation of the $In_xGa_{1-x}As$ layer due to misfit dislocations. In Fig. 1 the determined layer thickness is plotted as a function of InAs mole fraction where no structual degradation is detected. However exceeding this thickness results in a drop in the Hall mobility. The solid curve represents the theoretical expression proposed from Matthews and Blakeslee[2] for the CLT using the mechanical equilibrium theory. For an InAs mole fraction below 0.35 good agreement between the calculated curve and our experimental results is observed. However above 0.35 InAs mole fraction a strong drop of the CLT is observed. For an InAs mole fraction of 0.38 a CLT of only 3 nm is obtained, while for InAs mole fraction of 0.5, only the fact that the CLT must be below 1.5 nm can be determined. The exact CLT could not be determined because for a 1.5 nm wide $In_xGa_{1-x}As$ QW the electrical properties, such as carrier concentration and electron mobility of this structure behave as $Al_yGa_{1-y}As/GaAs$ HEMT structures. The lower carrier concentration is due to an increase in the energy level of the $In_xGa_{1-x}As$ QW with decreasing QW width resulting in a lower band offset. The higher mobility can be understood by the fact that the wave function receives a considerable contribution from the GaAs barrier layer just below the InGaAs QW.

DEVICE PROPERTIES

Using the above discussed molecular beam epitaxy technology for $In_xGa_{1-x}As$ layers we have grown pseudomorphic $Al_{0.3}Ga_{0.7}As/In_xGa_{1-x}As/GaAs$ HEMT structures with different InAs mole fractions. The InAs mole fraction was varied from 0 to 0.35. The $In_xGa_{1-x}As$ QW widths used, were 15 nm, 13 nm, 10 nm, 8 nm and 5nm corresponding to InAs mole fractions of 0.1, 0.2, 0.25, 0.3 and 0.35 respectively. The structure for the formation of the two dimensional electron gas is identical to that already described. For device fabrication there is in addition a 3 nm GaAs layer followed by a 3 nm $Al_{0.3}Ga_{0.7}As$ layer to stop the dry etched gate recess. In Fig. 2 we show the transit frequency of FET structures with a gate length of 0.25 μm as a function of the InAs mole fraction. With increasing InAs mole fraction an increase of the transit frequency is observed. Beyond an InAs mole fraction of 0.3 a decrease of the transit frequency follows. This behaviour can be explained by a decrease of the Hall mobility with increasing InAs mole fraction due to the decreasing CLT. The FETs with a InAs mole fraction of 0.25 show a f_T of 115 GHz for a gate length of 0.15 μm.

REFERENCES

1. A.A. Ketterson, W.T. Masselink, J.S. Gedymin, J. Klem, C.K. Peng, W.F. Kopp, H. Moorkoc and K.R. Gleason, IEEE Transactions on Electron devices, ED-33, 564, (1986)

2. J.W. Matthews and A.E. Blakeslee, J.Cryst.Growth 27, 118 (1974)

3. I.J. Fritz, T. Picraux, L.R. Dawson, W.D. Laidig, and N.G. Anderson, Appl.Phys.Lett. 46, 967 (1985)

4. T.G. Andersson, Z.G. Chen, V.D. Kulakovskii, A. Uddin, and J.T. Vallin, Appl. Phys. Lett. 51, 752 (1987)

5. P.J. Orders and B.F. Usher, Appl.Phys.Lett. 50 980 (1987)

6. I.J. Fritz, P.L. Gourley, and L.R. Dawson, Appl.Phys.Lett. 51, 1004 (1987)

7. I.J. Fritz, Appl.Phys.Lett. 51, 1080 (1987)

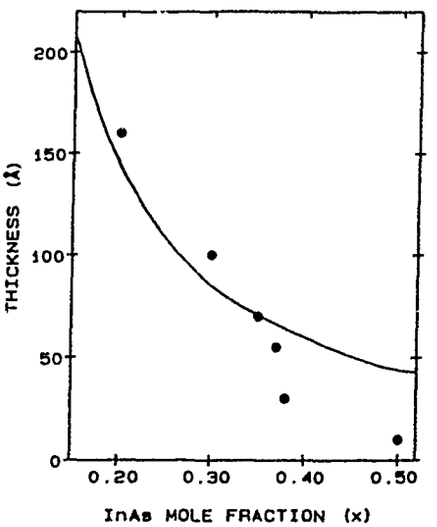

Fig. 1 Determined layer thickness where no structural degradation is detected as a function of InAs mole fraction, using Hall effect measurements (circles). The solid line represents the calculated curve for the critical layer thickness from Matthews and Blakeslee.

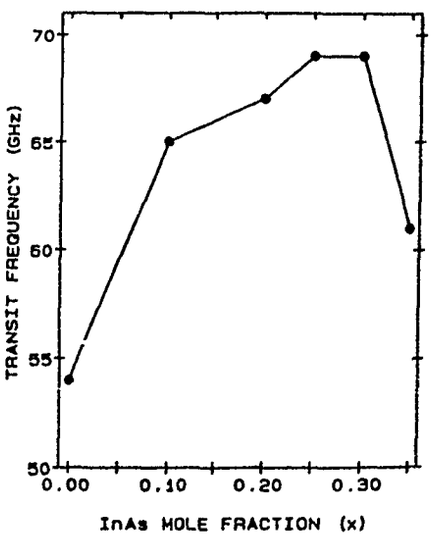

Fig. 2 Transit frequency of FET structures with a gate length of 0.25 μm as a function of the InAs mole fraction.

STM IMAGING OF MBE-GROWN (Al)GaAs (110) CROSS SECTIONS

O. Albrektsen#, H.W. Salemink* and H.P. Meier
IBM Research Division, Zurich Research Laboratory,
CH-8803 Rüschlikon, Switzerland
Tel. (+41) 1 724 8416, FAX (+41) 1 724 3170
#Present address: Telecommunications Research Laboratory,
DK-2970 Hørsholm, Denmark

The abruptness of lattice matched semiconductor interfaces is a topic of current interest in GaAs and Si epitaxy; one area of importance is the description of the alloy composition and the electronic band structure on an atomic or (sub)nanometer spatial scale. Regarding the microscopic description of the growth process, such issues as composition fluctuations, terracing and step density are outstanding.

The atomic sequencing in epitaxially grown semiconductor structures is usually inferred from analysis techniques such as RHEED and TEM, which sample a large number of crystalline unit cells. Scanning tunneling microscopy (STM) is a tool which accesses the electronic structure of surfaces in real space with atomic resolution. This has recently been applied to the study of exitaxial growth of Si on its preferential (001) growth face [1]. An alternative method to study epitaxial material is to employ STM on cross sections of MBE-grown structures (GaAs/AlGaAs multilayers): with this technique the atomic registry in epitaxial GaAs, AlGaAs and across their interface has been observed (Fig. 1) [2]. In this paper, we study the UHV cleaved (110) surface, which is cross-sectional to the preferential <001> growth direction; an SEM is used to move the STM probe towards the layer structure of interest.

From the acquired images, the interface can be defined to an accuracy of $\pm$ one unit cell. The effect of composition fluctuations is also observed via the change in the atomic charge density. It should be noted that the atomic charge densities essentially determine the interface in terms of 'atomic potentials' [3]; the energetic position of the valence band on the other hand will respond to the local composition on a slightly larger length scale. This length scale is of basic importance in nanometer structures.

Since the (110) cross-sectional plane is imaged, the occurrence of steps separating the growth terraces can be observed at the hetero-interfaces; an example of a step separating two terraces is shown in Fig. 2 for the interface of AlGaAs on GaAs (normal interface); it is seen that the step height amounts to multiple atomic layers. This is often observed and can indicate the occurrence of step bunching. For the particular image in Fig. 2, there were no other steps along that interface within 15 nm and the other heterostructure interfaces were more than 10 nm away. In this image,

Fig. 1. Atomically resolved As lattice on (110) cross section of GaAs (lower left) - AlGaAs (upper right) interface, grown with MBE. The <00i> growth direction is indicated. Note the abruptness of the interface and the effect of the composition fluctuations in the ternary compound (from Ref. 2).

the actual step ledge is obscured by a topographic feature, probably an adsorbed C or O atom (cluster) from the residual gas in the UHV environment, as observed frequently on the Al-compounds. The possibility cannot be excluded however, that a preferred nucleation site was present at the step ledge; this may be either the step itself or an incorporated defect. The images prove that it is possible to analyze the terrace growth in layered structures with unit cell resolution and in direct space.

An example of an ultra-thin layer structure is displayed in Fig. 3. The cross-sectional STM image shows the 2.0 nm (4 layers) of AlGaAs, embedded in adjacent GaAs layers. The transition from the binary to the ternary is clearly visible on each side of the 2.0 nm AlGaAs barrier layer. In connection with this image, we note that the ternary AlGaAs appears i nomogeneous on the scale of a few unit cells: we attribute this topographic non-uniformity in the AlGaAs layer to composition fluctuations [2]. Such investigations open the possibility of analyzing the compound interface on the scale of a single unit cell.

Since the STM tool is sensitive to the electronic structure, local current-voltage spectroscopy can also be used to derive a valence band edge and semiconductor band gap [4]. Examples of spectroscopy in (Al)GaAs will be discussed.

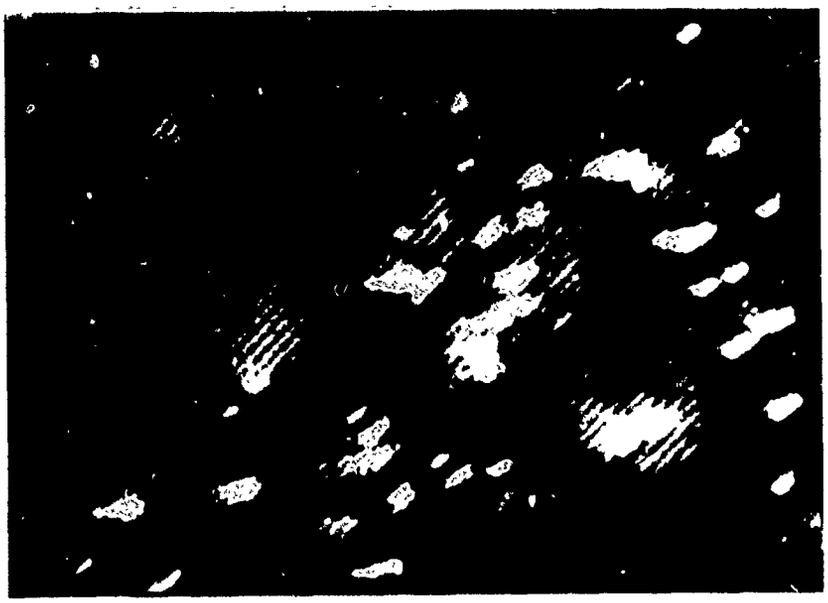

Fig. 2. Cross-sectional view of the (110) cleavage face of GaAs-AlGaAs interface, displaying two terraces and a six-atom-high step separating the terraces (center). The actual step ledge is obscured by a defect.

Fig. 3. Example of the observation of very thin MBE-grown GaAs/AlGaAs multilayers on (110) plane. The 2.0 nm AlGaAs layer is embedded between a 5.0 nm and a 2.0 nm GaAs layer.

References

[1] Proc. 4th Int'l Conf. on STM, J. Vac. Sci. Technol. A8, 195-209 (1990)

[2] O. Albrektsen, D.J. Arent, H.P. Meier and H. Salemink, Appl. Phys. Lett. 57, 31 (1990)

[3] S.B. Ogale *et al.*, Phys. Rev. B36, 1662 (1987)

[4] R.M. Feenstra and J.A. Stroscio, J. Vac. Sci. Technol. B5, 923 (1987)

IN-SITU MONITORING OF III-V MBE GROWTH PROCESSES USING LASER LIGHT SCATTERING

G.W.Smith*, C.R.Whitehouse, J.L.Glasper and D.J.Robbins

Royal Signals and Radar Establishment, St Andrews road, Malvern, Worcestershire, WR14 3PS, United Kingdom.

Tel 684 895324

Fax 685 894540

ABSTRACT

Over the past years, RSRE has pioneered the use of the laser light scattering (LLS) technique for in-situ real-time optical monitoring of vacuum-based epitaxial growth, with particular emphasis on silicon MBE and LPCVD [1,2].

The present paper will describe our more recent work in which we have applied the LLS technique to the study of GaAs/GaAlAs MBE growth processes. As an introduction, the experimental configuration required to perform LLS experiments will be described, along with details of additional steps which need to be taken to record valid real-time LLS data from a rotating substrate. LLS data recorded during all the major phases of GaAs/GaAlAs MBE growth on (001) GaAs substrates, including in-vacuo oxide desorption, GaAs buffer layer growth, GaAs/GaAlAs multilayer fabrication, and growth interrupts will then be described.

FIG 1

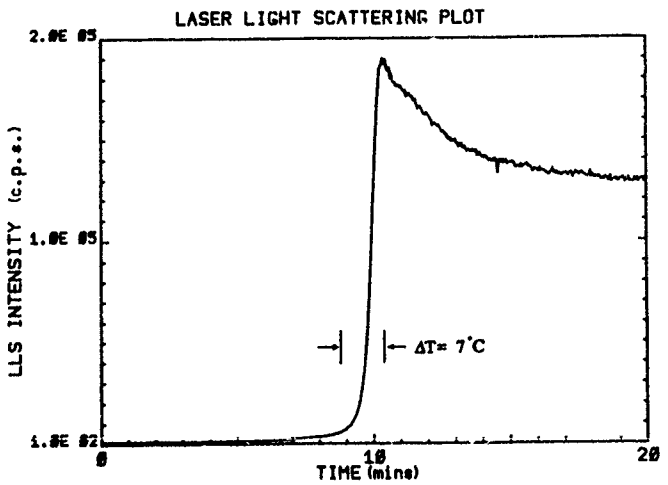

As is the case of our earlier silicon studies [1,2], LLS is found to be very sensitive to the in-vacuo oxide desorption process used to prepare the GaAs substrate prior to MBE growth. A very significant increase in scattered light intensity ($>10^2$) is

observed at the point where the in-situ RHEED system indicates that oxide desorption has occurred (FIG 1).

The subsequent MBE growth of GaAs layers and GaAs/AlAs multilayer structures is then found to generate very complex changes in scattered light intensity, depending upon both the precise growth conditions used , and also the azimuth of the incident laser beam. A full description of these variations will be presented, along with details of our current understanding of the physical processes involved.

As is the case of RSRE's earlier LLS studies of silicon epitaxial growth, our paper will conclude that LLS has much to offer as a real-time, ex-vacuo monitoring technique for III-V MBE growth processes. The technique could not only play a very important role in the control of production-scale multi-wafer III-V MBE growth procedures, but should also be capable of being translated immediately to higher pressure III-V growth processes, including chemical beam epitaxy (CBE) and MOCVD.

REFERENCES

(1) D.J.Robbins, A.J.Pidduck, A.G.Cullis, N.G.Chew, R.W.Hardeman, D.B.Gasson, C.Pickering, A.C.Daw, M.Johnson and R.Jones. J.Crystal Growth 81, 421, (1987).

(2) A.J.Pidduck, D.J.Robbins, A.G.Cullis, D.B.Gasson and J.L.Glasper Proceedings 2nd International Si MBE Conference, Honolulu, (1987).

IN SITU CONTROL OF EPITAXIAL GROWTH USING REFLECTANCE-DIFFERENCE

LARS SAMUELSON*, JAN JÖNSSON AND GERT PAULSSON
Department of Solid State Physics, University of Lund, Box 118, S-221 00 LUND, Sweden, Phone: +46 46 107679, Fax: +46 46 104709

INTRODUCTION

With the increasing demands for control on the atomic level of materials structures, different advanced methods for epitaxial growth and sophisticated techniques for *in situ* studies of growth have emerged. The strong dependence of the energy structure of such ultra-thin layers makes it necessary to know, preferably during growth, the thicknesses of individual layers with an accuracy to the discrete atomic layer thickness level. Two methods for this type of growth control are of special interest, namely the reflection high-energy electron diffraction (RHEED) [1] and the reflectance-difference (RD) [2] techniques. The two-dimensional periodicity of the surface reconstructions can be determined by RHEED and, under certain conditions, growth can be followed in real-time as RHEED oscillations.

The RD technique is a complementary technique which is sensitive to the absorption of photons by bonds which have a symmetry lower than tetrahedral [2]. This sensitivity is achieved by a subtraction of the reflection in the two orthogonal orientations, $(r_{110} - r_{1\bar{1}0})$. This difference vanishes for reflection components originating from tetrahedrally oriented bonds in the bulk of the crystal as well as from randomly oriented molecules above the surface. The RD method is especially sensitive to absorption by dimers which are a part of the different reconstructions of the surface.

THE REACTION OF TEG ON GaAs (001)

The use of RD [3] for real-time observation of growth oscillations [4] is exemplified in figure 1. Curve c) shows the conventional initiation of growth, starting from an AsH_3-saturated surface. When TEG is added to the molecular flux, the RD signal rapidly increases from the level corresponding to the As-terminated surface, and goes into a continuous but damped oscillatory behaviour. Typically, these oscillations can be followed for 30 periods, where each such period corresponds to the growth of exactly one bi-layer, 2.8 Å thick. Curve b) shows that if first the AsH_3 flux is terminated and only TEG is injected, to an amount which deposits one monolayer of Ga, then the initiation of growth by adding AsH_3 gives approach to the RD-level corresponding to growth. Also in this case growth oscillations are observed, indicating that this monolayer of Ga was formed in a well-controlled, two-dimensional fashion. However, if TEG corresponding to the deposition of more than one monolayer of Ga is injected, then reinitiation of growth occurs much less perfectly. This is shown in curve a) where the transient resulting from the reinitiation of growth shows an approach to the

RD-level of growth but without any traces of growth oscillations. Over-saturation of the surface with TEG clearly results in three-dimensional island formation [5,6].

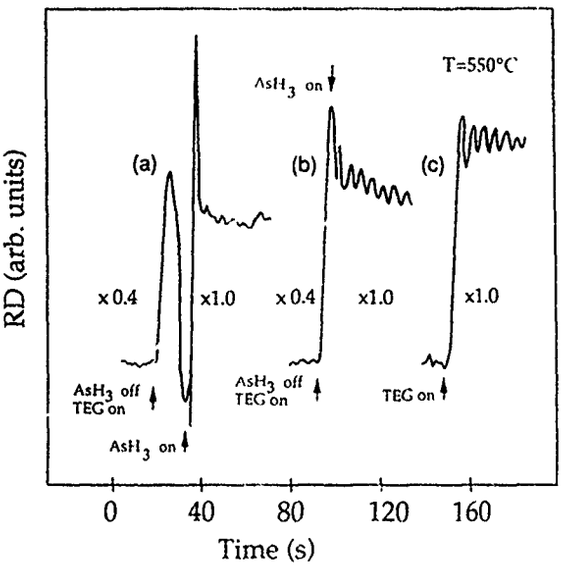

Figure 1. RD-detection of the coherence of the surface during continuous growth of GaAs after pretreating the surface with different amounts of TEG. The amount of TEG injected during discontinuation of the arsine flow corresponds to the formation of (a) three monolayers (b) one monolayer and (c) no TEG. The presence of growth oscillations in curve (b) shows that surface coherence remained during this TEG exposure.

REMOVAL OF EXCESS TEG-DERIVATIVES ON A Ga-RICH GaAs (001) SURFACE

To study the mechanisms by which TEG forms a chemisorbed monolayer of Ga on GaAs (001) we study the removal of excess TEG from a TEG-saturated surface as a function of temperature. Examples of such transformations are shown in figure 2 for four different temperatures. The experiments are performed in such a way that after the AsH_3 flux is closed a dose of TEG is injected nominally corresponding to between 2 and 3 monolayers of Ga. At high temperatures is the initial peak, corresponding to the incorporation of one monolayer of Ga, followed by a dip which is believed to be due to absorption by TEG derivatives which are oriented by the structured, reconstructed Ga-terminated surface. It is clear that the mechanisms by which excess TEG derivatives are removed from the surface are considerably slower at lower temperatures.

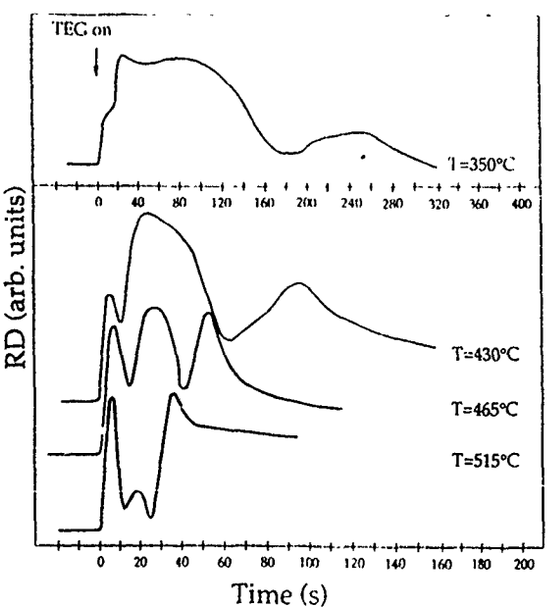

Figure 2. After stabilization with arsine, the surface is exposed to a dose of TEG corresponding to the formation of more than one monolayer of Ga. After a certain time the excess TEG, or its derivatives, becomes undetectable for the RD-probe either by forming Ga droplets or by desorbtion.

REAL-TIME RD-CONTROL OF PULSING SEQUENCES FOR REALIZATION OF ALE

Atomic layer epitaxy is not only of fundamental interest for studies of surface physics, but has also a great potential for obtaining homogeneity over large areas in the growth of quantum well structures. In most cases, conditions for ALE are only obtained by measuring the thickness of the grown layer, with the requirement that it be equal to the number of cycles used times the thickness of one bi-layer. In figure 3 we demonstrate the potential of RD monitoring, in real-time, of complex pulsing sequences during which the self-limitation of TEG-adsorption on the surface has to be controlled. The pulsing sequence used in the experiment shown in figure 3 consists of four periods in each cycle; during period A the surface is saturated by AsH_3; during period B an integrated flux of TEG is injected which nominally gives 2 - 3 monolayers of Ga (or derivatives thereof) to the surface; during period C the Ga-saturated surface is allowed to rid itself of excess Ga molecules whereby it approaches the equilibrium value of Ga coverage; and, finally, during period D (which is the same as period A) the Ga- terminated surface is transformed back to the As-terminated state. The sensitivity of the RD technique and the reproducibility of the rather complex chemical pulsing sequences and of the surface processes is illustrated in figure 3 by three RD-sequences taken from a pulse train of ALE like pulsing sequences. However, in order to prove that the processes chosen to be monitored and controlled in the experiments in figure 3 really result in ALE growth, the thicknesses of the thin layers should be measured.

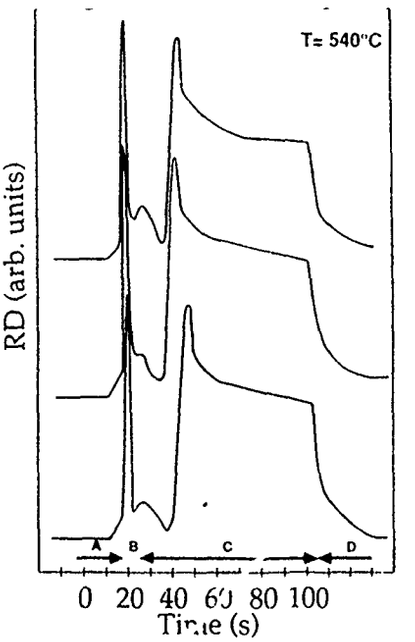

Figure 3. An example of how the RD signal can be used to follow the the different surface processes during an ALE-like valve switching sequence. Three of the ten consecutive sequences are shown. The first sequence is shown at the top and the last sequence at the bottom.

Acknowledgements
S. Jeppesen is acknowledged for technical support. This work was performed within the *nm- structure* consortium in Lund, and was supported by the Swedish National Board for Technical Development and the Swedish Natural Science Research Council.

References

1. J. H. Neave, B. A. Joyce, P. J. Dobson and N. Norton, Appl. Phys. **A31** (1983) 1
2. D. E. Aspnes, R. Bhat, E. Colas, L. T. Florez, J. P. Harbison, M. K. Kelly, V. G. Keramidas, M. A. Koza and A. A. Studna, Proc of SPIE 1037 (1989)2
3. G. Paulsson, K. Deppert, S. Jeppesen, J. Jönsson, L. Samuelson and P. Schmidt, J. Crystal Growth **105** (1990) 312
4. J. Jönsson, K. Deppert, S. Jeppesen, G. Paulsson, L. Samuelson and P. Schmidt, Appl. Phys. Lett., **56** (1990) 2414
5. T. H. Chiu, W. T. Tsang, J. E. Cunningham and A. Robertson, Jr. J. Appl. Phys. **62** (1987) 2302
6. L. Samuelson, K. Deppert, S. Jeppesen, J. Jönsson, G. Paulsson and P. Schmidt, J. Crystal Growth **107** (1991) 68

SELECTIVE AREA N-TYPE DOPING IN MBE GROWTH OF GaAs USING TIN IONS

J.H. Thompson*, E.H. Linfield, D.A. Ritchie, G.A.C. Jones, J.E.F. Frost, A.C. Churchill
Cavendish Laboratory, Madingley Road, Cambridge CB3 0HE, UK.
(Telephone 0223 377482 Fax. 0223 337271)
G.W. Smith, D. Lee, M. Houlton, C.R. Whitehouse
RSRE, St Andrews Road, Malvern, Worcestershire WR14 3PS, UK.
(Telephone 0684 895324 Fax. 0684 894540)

Introduction

This abstract describes how a specially designed tin focussed ion beam (FIB) column has been used for the first time in an MBE growth chamber to produce high quality GaAs doped n-type in selected areas. In order to produce satisfactory resolution at the low ion energies required, the experiments used a system combining a conventional high energy FIB design with the facility to lower the incidence energy of the ions by applying a retarding potential to the sample. The n-type doping of MBE GaAs using ionised beams has previously been attempted by several groups[1,2] using either non focussed or high energy beams .

Experimental Apparatus

A tin FIB column has been developed for very low energy ion deposition in an MBE growth chamber. The ion gun consisted of a tin (n-type dopant in GaAs) liquid metal ion source (LMIS) followed by an electrostatic asymmetric three element lens. The beam position was controlled by electrostatic deflection plates. The ion gun was mounted in the growth chamber of a VG Semicon V80H MBE machine, normal to the substrate position during growth. An electrically isolated sample holder was used which was connected by a wire to a feedthrough on the manipulator flange. The beam was transported at high energy and the incident ion energy was reduced by applying a retarding potential to the sample. Thus a spot size of 90μm at 1nA was achieved with incident ion energies as low as 50eV. Note that the LMIS is known to emit approximately 40% Sn^+ ions and 60% Sn^{++} ions[3]. The energies given in this abstract are for Sn^+ ions although a large proportion of the ions will have twice this energy.

Sample growth and assessment

All substrates were two inch diameter nominally undoped semi-insulating GaAs prepared using a standard wet-etch process. The epilayers were grown at 1μm/hr at substrate temperatures between 590°C and 615°C with a typical As to Ga beam equivalent pressure ratio of 6.5:1. In order to allow the patterning of the epilayer during growth, the substrate was not rotated. The FIB was used to produce a number of discrete areas with different doping levels within the same sample. Incident ion energy was varied between 50eV to 500eV.

The samples were assessed by four different methods. Electron mobility and carrier concentration values were obtained by taking Hall and resistivity measurements at 77K and depth profiles of the

carrier concentration were taken at 300K using a Hall strip and etch system. A Polaron C-V electrochemical etch profiler was used to measure the carrier concentraion depth profile. SIMS was used to measure the concentration of tin as a function of depth. Photoluminescence spectroscopy also provided some information on acceptor levels.

Results and Discussion

Figure 1 shows measurements made on a sample (C378) of bulk GaAs doped with a constant tin ion current density. The ion incidence energy was increased as a function of depth in six 0.7 μm steps from 50eV to 500eV. The beam was briefly switched off at 1μm below the final surface. Figure 1 compares the tin concentration obtained by SIMS with the carrier concentration obtained by 300K Hall profiler as a function of depth. The tin and carrier concentrations both dip at 1μm as expected. The SIMS profile remains constant with increasing depth after this point, demonstrating that the intended structure was grown. The carrier concentration however decreases in a series of steps each approximately 0.7μm in length. Each step corresponds to a particular ion energy as marked. This effect is also present in the 300K Hall mobility. The insert contains a C-V etch profile of the carrier concentration (the depth calibration of which is inaccurate) displaying similar steps.

These results suggest that as the incident ion energy is increased, fewer conducting electrons are produced as a fraction of the total number of tin atoms in the material. This may be due to either compensating acceptors caused by implantation damage or a lower activation level for the tin donor.

Figure 2 plots the 77K Hall mobility versus carrier concentration in the dark for four different ion energies for samples grown with constant dose and energy throughout along with results obtained during the same period with silicon doping from a thermal source. The best sample achieved with tin doping had a mobility of 73000 $cm^2V^{-1}s^{-1}$ at a carrier concentration of 1.1×10^{14} cm^{-3}. This compares with a silicon doped sample with a mobility of 97000 $cm^2V^{-1}s^{-1}$ at 5×10^{14} cm^{-3}.

Finally, figure 3 provides a photoluminescence spectrum for a sample doped with 50eV tin ions at 3×10^{14} cm^{-3}. The narrow linewidths infer that the material is of good quality. No photoluminescence attributable to damage was detected up to 10000Å. The tin acceptor level is also quite clear. This can be compared to the spectrum obtained by Bamba[1] et al from GaAs implanted using a 1kV tin ion beam.

Conclusions

For the first time, high quality GaAs has been grown using MBE with a tin FIB as the dopant source. The FIB has been used to pattern the doping concentration in the lateral plane of MBE material during growth. The evidence for this is presented in the form of 77K and 300K Hall and resistivity data, and photoluminescence measurements.

Acknowledgments

Technical assistance was provided by D Heftel, A Stone, D Charge, D Hall and T Stubbings. The LMIS was provided by Dr P Prewett. EHL is funded by a studentship from Trinity College, Cambridge. JHT is funded by a CASE award with RSRE Malvern.

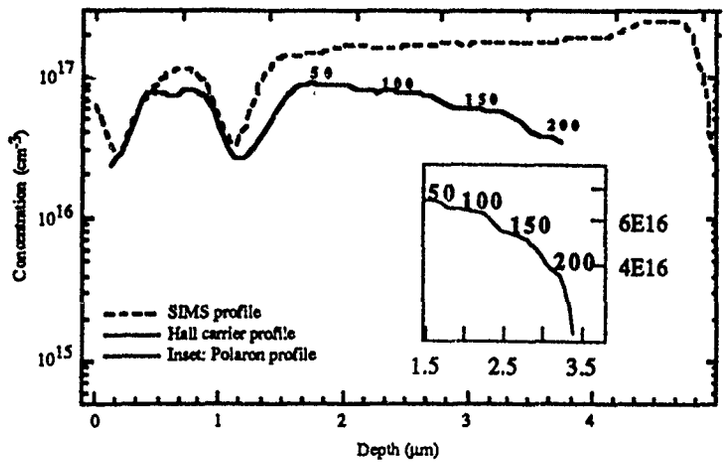

Figure 1: The carrier concentration and tin concentration are compared for a sample doped with tin ions. The ion energy was decreased in steps during growth, causing similar steps in the carrier concentration (indicated by the ion energy in eV). This contrasts with the approximately constant level of tin given by SIMS. The insert plots the C-V etch profile with axes the same as those in the main graph.

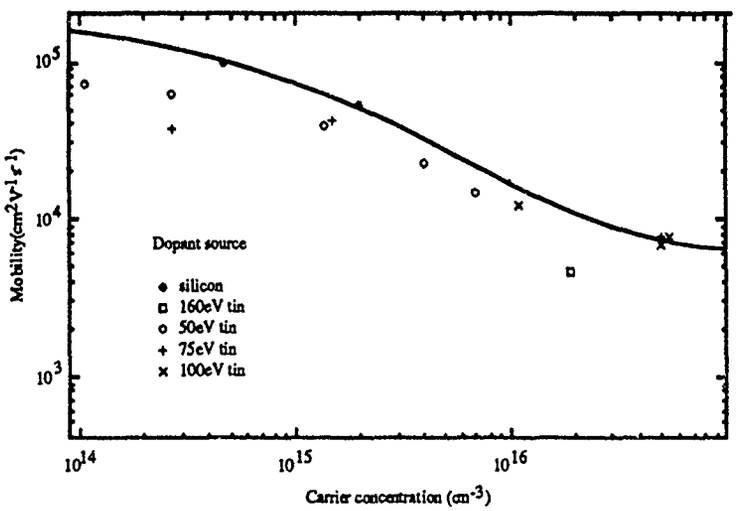

Figure 2: The electron mobility as a function of carrier concentration is displayed for samples doped at constant ion energy. The tin ion energies range from 50eV to 160eV. For comparison, the compensation ratio equal to two is plotted as a line along with results from silicon doped samples from the same growth run.

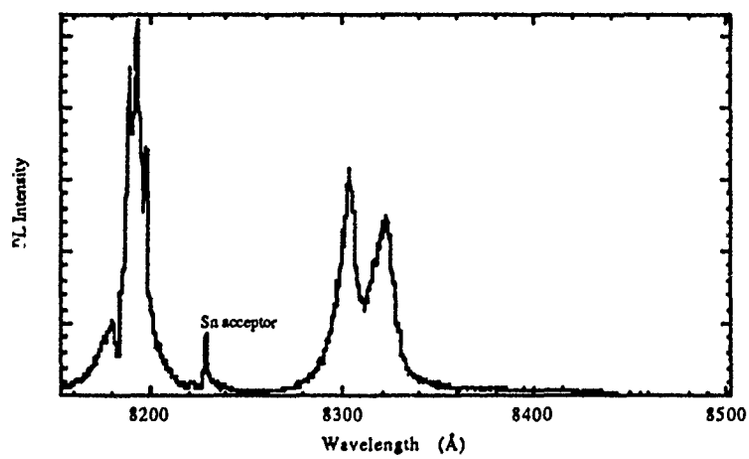

Figure 3:
A photoluminescence spectrum for bulk GaAs doped at 2.7×10^{14} cm^{-3} using 50eV tin ions.

References

1 Y.Bamba, E.Miyauchi, K.Kuramoto, A.Takamori, and T.Furuya, Jpn. J. Appl. Phys. 22, L331 (1983).

2 S.Cavalieri, Ph. Gaucherel, G.Monnom, C.Paparoditis, and J.C.Roustan, J. Vac. Sci. Technol. A5(4), 1421 (1987)

3 P. Sudraud Private communication

283000 cm^2/Vs MOBILITY IN GaAs GROWN BY MBE USING As_4

*Ronald Sivertsen and André Paulsen
Norwegian Telecom, Research, P. O. Box 83, N-2007 KJELLER
Phone: (06)809100, Fax: (06)810076

The highest mobility in GaAs grown by MBE has been achieved using As_2.[1] Growth with As_4 can also give mobilities as high as $3x10^5$ cm^2/Vs under optimal growth conditions and the use of very pure materials.[2] We here report results which are very close to the best mobilities achieved with As_4.[2] Our results were obtained with very simple growth procedures.

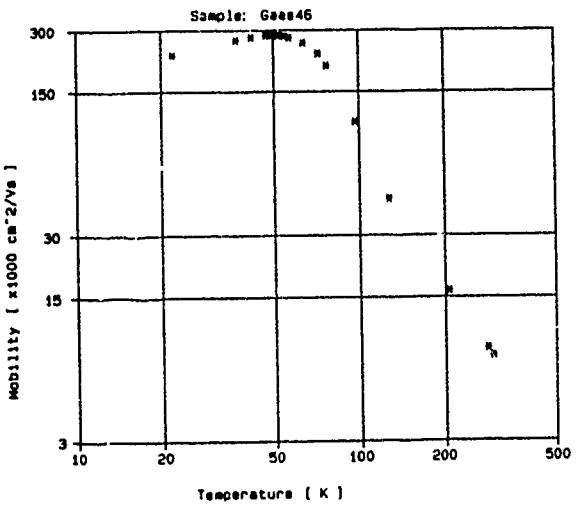

Figure 1
Mobility versus temperature for our highest mobility sample

A temperature scan of the mobility of our best sample is shown in figure 1. The mobility was measured in the dark by the Van der Pauw method, and the peak value was 283000 cm^2/Vs at a temperature of 50 Kelvin. The carrier concentration of the 12µm sample was $5x10^{13}$ cm^{-3}. Several samples with mobility of more than 200000 cm^2/Vs have been grown.

The layers were grown on a new RIBER 32P MBE-machine which was installed in our lab last summer (1990). The machine is a conventional solid sources system using As_4. The cells were loaded with 7N arsenic from Johnson Matthey and 8N gallium from Rhône-Poulenc. Undoped superclean substrates polished 2^0 off {100} from Sumitomo was mounted on indium-free holders. The substrates were loaded from a class 100 cleanroom directly into the introduction chamber without any preparation. After loading, the substrate was degassed 5 minutes at 250 ^{0}C. The growth started less than 30 minutes after the substrate was introduced into the growth chamber. During the growth the substrate was rotated at maximum speed (65 RPM) and the main ion-gauge was left on. The RHEED-gun was used in the beginning of the growth. The background pressure in the chamber before growth was in the range $4\text{-}10\text{x}10^{-11}$. For our best sample this pressure was $7\text{x}10^{-11}$.

The arsenic flux and the Si concentration were the dominating parameters that influenced the mobility. Maximum mobility was obtained for an As_4/Ga ratio of 5.6 and an Si dopant source temperature of 500 ^{0}C. Undoped layers turned out to be p-type with a carrier concentration of $<5\text{x}10^{13}$ cm^{-3} at room temperature. The layers have been analysed by photoluminescence measurements which indicate that the acceptor concentration is very low.

[1]C. R. Stanley, M. C. Holland, A. H. Kean, Sixth International Conference on MBE August 1990, Abstracts VIA-1

[2]N. Chand, R. C. Miller, A. M. Sergent, S. K. Sputz, and D. W. Lang, Appl. Phys. Lett. 52, 1721 (1988)

LOW-OXYGEN ARSENIC FOR AlGaAs MBE

R. G. L. Barnes *
Johnson Matthey PLC,
Orchard Road, Royston, Hertfordshire, SG8 5HE, UK.
Tel: (0) 763 244161
Fax: (0) 763 241862
and
A. Chew
Institute of Surface Science and Technology
Loughborough University of Technology
Leicestershire, LE11 3TU, UK.
Tel: (0) 509 222947
Fax: (0) 509 231983

Very high purity elemental arsenic is well established as a source for the molecular beam epitaxy of compound semiconductors such as gallium arsenide. Technologically useful devices commonly require the fabrication of layers of more complex composition, such as aluminium gallium arsenide, (Al,Ga)As. Unfortunately, the introduction of aluminium places new demands on the purity of the constituent elements, including arsenic. This is because of the very high chemical affinity of aluminium for oxygen, which increases the incorporation of any background or impurity oxygen present into the epilayer.

A process for the manufacture of 99.99999% (7N) shaped arsenic charges has already been reported [1], utilising specialised vapour phase deposition technology. To obtain sufficiently low oxygen levels in the condensed solid product, it is necessary to ensure that unacceptable oxygen concentrations are not introduced from any of the source materials, ambient gases within the reactor, or container materials, or by ingress of

atmospheric oxygen. Thermodynamic studies of the As-O system have identified regimes needed to ensure that residual oxygen impurity in the bulk remains at required levels.

Arsenic charge surfaces provide sites for higher local concentrations of oxygen via oxide formation. Particular attention has been given to surface reactions between arsenic and trace oxygen in controlled atmospheres. Optically thin oxide layers have been studied using secondary ion mass spectrometry. The ability has been established to discriminate between layers of different thicknesses and oxide contents produced under different conditions. This is illustrated in Figure 1. The contribution of local surface concentrations to net oxygen impurity content has been calculated.

By applying these various data to control of the charge fabrication process, effectively oxygen-free surfaces are routinely produced. The SIMS technique has been standardised to permit routine examination of surface trace oxygen profiles. A representative result is shown in Figure 2. Background bulk oxygen impurity levels have been measured by calibration against implanted ^{16}O. Values of 5×10^{14} atoms cm^{-3} have been obtained as typical of this quality of material.

Such material is capable of yielding epilayers whose electrical performance is not limited by oxygen arising from the arsenic source. For example, sheet carrier densities at $77^{0}K$ of 3.5×10^{11} cm^{-2} have been reported for the GaAs/AlGaAs heterojunction [1].

REFERENCES

1. R. G. L. Barnes, M. T. Emeny, C. R. Whitehouse and D. Lee
J. Cryst. Growth 106 (1990) 143

ACKNOWLEDGEMENTS

Thanks are due to A. C. Forbes and T. G. Purcell for the painstaking provision of test samples; and to Cascade Scientific Ltd. for ion implantation and bulk SIMS measurement services.

FIG. 1. Surface oxygen depth profiles for a range of oxide layers on arsenic.

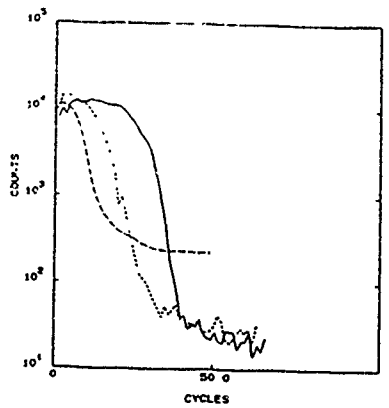

FIG. 2. Surface oxygen depth profile of a typical clean arsenic surface.

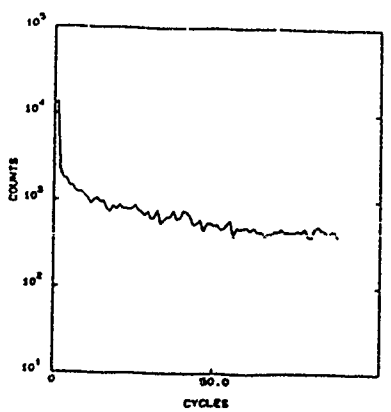

SURFACE STOICHIOMETRY VARIATION IN "ATOMIC LAYER" MOLECULAR BEAM EPITAXY OF GaAs

C. Deparis and J. Massies*
Laboratoire Physique du Solide et Energie Solaire,
Centre National de la Recherche Scientifique,
Sophia Antipolis, 06560 Valbonne FRANCE
tel: (33) 93 95 42 14 fax: (33) 93 95 83 61

As we have previously shown [1], a surface stoichiometry change induces a variation of the RHEED specular beam intensity (Fig. 1). In the present work, we have used RHEED intensity as a probe of the surface stoichiometry changes occuring in the so-called atomic-layer MBE (ALMBE), or migration-enhanced epitaxy (MEE), growth procedure [2-4].

The comparison of the As-surface coverage before ALMBE growth and the one reached at the end of each ALMBE cycle, indicates that As-desorption becomes significant above ≈ 550°C (Fig. 2). An extended As deposition time is then needed to recover, at the end of each ALMBE cycle, the As coverage obtained in standard MBE growth using the same growth conditions (temperature, Ga and As_4 flux intensities). However, even if the surface stoichiometry can be effectively recovered by such a procedure, a degradation of the material properties is still observed through photoluminescence experiments on GaAs QWs grown at 600°C. This indicates that an increase of the As-exposure time is not sufficient to balance the As-outdiffusion from the near-surface region, which occurs during Ga deposition. Therefore the use of the ALMBE procedure is, for thermodynamic reasons, limited to the low growth temperature range.

On the other hand, the analysis of both the specular beam intensity and the surface stoichiometry reached after each cycle, gives information about the ALMBE growth mechanisms. From such analysis, it is concluded that these mechanisms involve the formation of liquid Ga droplets on the surface for an amount of deposited Ga lower than one

atomic layer. Finally, the results of the comparison of the GaAs growth by standard MBE and ALMBE are in agreement with an improvement of the surface diffusion for the ALMBE growth procedure.

[1] C. Deparis and J. Massies, J. Cryst. Growth 108, in press (1991)

[2] M. Pessa, P. Huttunen and M.A. Herman, J. Appl. Phys. 54, 6047 (1983)

[3] Y. Horikoshi, M. Kawashima and H. Yamaguchi Jpn. J. Appl. Phys. 25, L868 (1986)

[4] L. Gonzalez, A. Ruiz, A. Mazuelas, G. Armelles, M. Recio and F. Briones, Superlattices and Microstructures 5, 5 (1989)

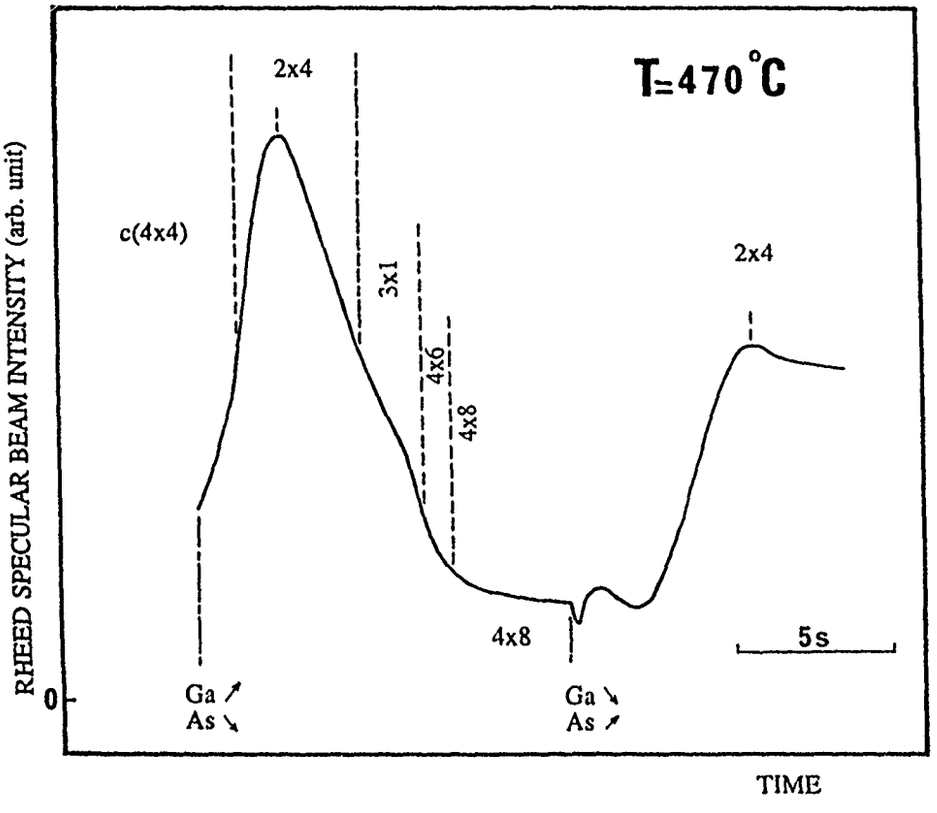

Figure 1: Typical RHEED specular beam intensity variation associated with structural transitions induced by Ga deposition and subsequent As exposure. (Ga deposition rate = 0.12 ML/s and maximum As incorporation rate = 0.20 ML/s).

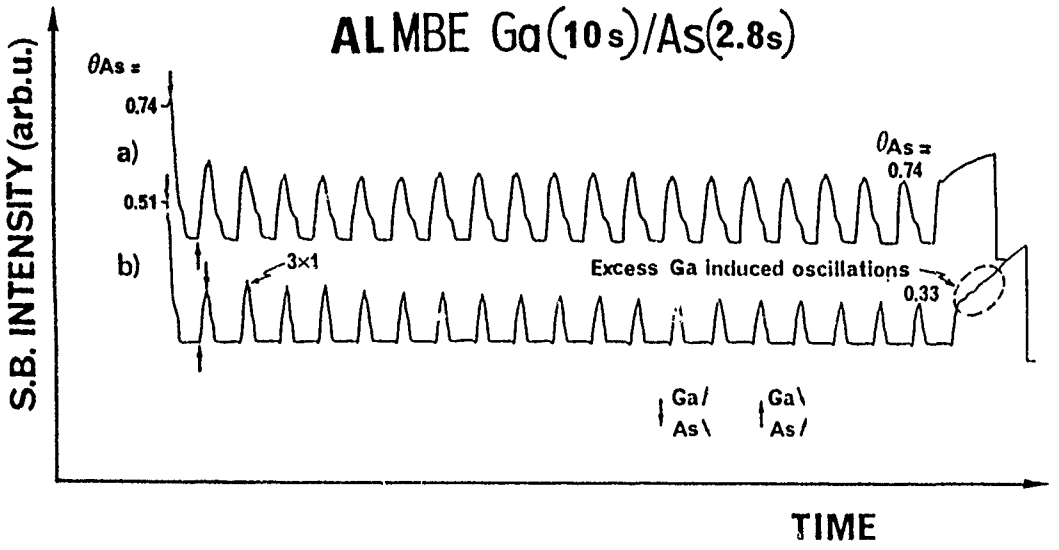

Figure 2: RHEED specular beam intensity recorded during GaAs growth by ALMBE at (a) 550°C et (b) 580°C. The estimated As surface coverage (θ_{As}) is indicated before ALMBE growth and at the end of the 19th ALMBE cycle (Ga deposition rate = 0.10 ML/s and maximum As incorporation rate = 0.36 ML/s).

MBE-overgrowth of patterned substrates by an $Al_{0.4}Ga_{0.6}As$-GaAs superlattice: contours and defects analyzed by TEM.

K. Johannessen*, ELAB-RUNIT, N-7034 Trondheim, Norway
Y.X. Guo and B. Skurdal, Department of Physics, University of Trondheim NTH, N-7034 Trondheim, Norway
R. Høier, SINTEF Applied Physics, N-7034 Trondheim, Norway

The overgrowth of patterned surfaces in the GaAs-AlGaAs system is of potential interest in many electronic and optical integrated circuits and devices. If we allow the wafer to be taken out of the MBE-machine, processed and grown for a second time in the MBE-system, special contacting and confinement structures can be made, which opens the way to new devices. In miniaturizing optical devices there is a need for doing regrowth into narrow trenches, almost as deep as they are wide. Such trenches will normally have sharp edges in the miniaturized structures.

An experiment to test the overgrowth of such trenches including sharp edges, was designed. By standard photolithographic methods we patterned plain GaAs (100) substrates with alternating 5 μm openings and 5 μm stripes in sets of ten. With this geometry 0.75 μm deep trenches were etched using a 1:8:160 H_2SO_4:H_2O_2:H_2O solution. We utilized ridges having both the (011) and the (0$\bar{1}$1) cross-sections on the same wafers. This system includes a variety of planes and sharp edges on which to study the overgrowth . The samples were given two rinses for 5 minutes each in concentrated sulphuric acid and rinsed again for 20 minutes in flowing DI H_2O and spun dry and mounted indium free for the MBE-machine. Whole wafers (2") were used. The overgrowths were performed in a Varian Gen II Modular MBE-machine using As_4,Ga and Al from conventional effusion cells. The growths presented here were performed at two different growth conditions.

The first wafer was grown under conditions typically utilized for HEMTs and MQW components. The substrate temperature (estimated real temperature) was kept at approximately 620 °C and approximately 20 % excess arsenic flux (for AlGaAs layers) was used. The second wafer was grown at conditions typically applied for growing lasers and waveguide components. The substrate temperature used was approximately 720 °C. The gallium flux was increased (approximately 30 %) to compensate for gallium loss. The arsenic flux was approximately doubled compared to the first wafer. The samples were overgrown with 15 periods of superlattices consisting of 50 nm $Al_{0.4}Ga_{0.6}As$ and 50 nm GaAs. The whole structure was doped 10^{17} cm^{-3} with Si. For both wafers the GaAs was growing at 1 μm/h. The structure of the overgrown samples were studied with TEM, both in normal and high resolution. Both the contours of the overgrowth and the defects arising from the overgrowth were studied.

For the low temperature grown sample a rather large amount of defects occurred particularly following {1$\bar{1}$1} planes leading out from the ridge sidewalls. Ridges with a (011) cross-section showed the poorest material quality (see Fig. 1). The high temperature grown samples showed a rather improved material quality. Few defects were found except in the close vicinity of the ridge sidewalls. Also for this temperature the best crystalline growth occurs for ridges with (0$\bar{1}$1) cross-sections (see Fig. 2). As the growth proceeds an in-filling of the trenches occur. The mesa areas shrink as the growth proceeds. This evening of the surface occur predominantly at high temperature growth. (Other samples have shown that the mesas may rather expand under different growth conditions with low As-flux, low substrate temperature and high Al content). The amount of surface evening coincide with improved crystalline quality. Analyzing the contour of the overgrowth and the individual layers give reason for expecting that a considerable transport of group III atoms (predominantly Ga) along the wafer surface occur. The characteristic length of this transport is in excess of 1 μm for the (0$\bar{1}$1) cross-section ridges at high substrate temperature, decreasing to less than 100 nm for the (011) cross-section ridges at low substrate temperature.

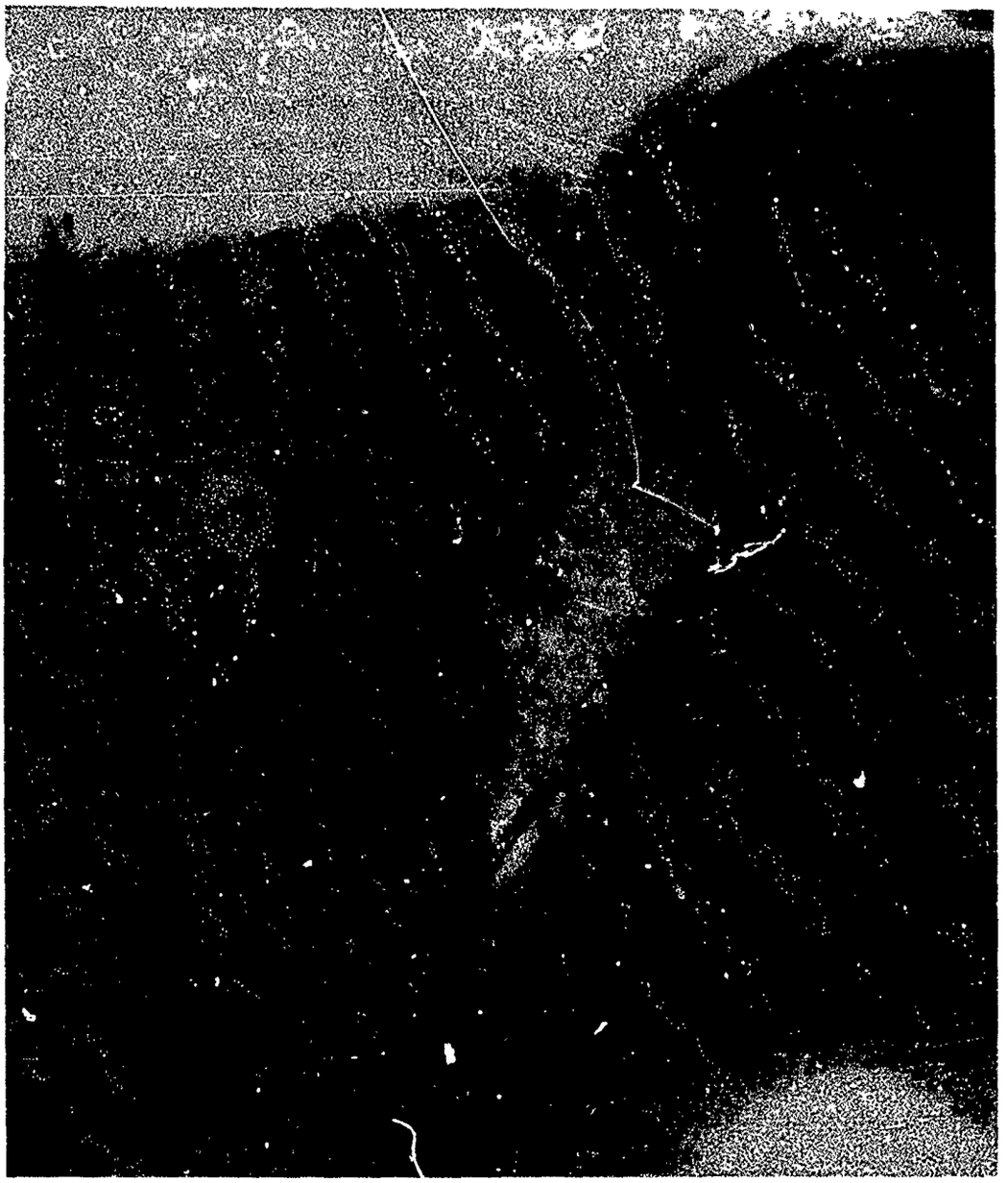

Fig. 1 *TEM dark field picture of low temperature (620 °C) $Al_{0.4}Ga_{0.6}As$-GaAs superlattice overgrowth of an edge on the (011) cross-section of a patterned (100) GaAs substrate. The edge of the substrate may be seen in the lower central part of the picture.*

Fig. 2 *(Next page) TEM bright field picture of high temperature (720 °C) $Al_{0.4}Ga_{0.6}As$-GaAs superlattice overgrowth of an edge on the $(0\bar{1}1)$ cross-section of a patterned (100) GaAs substrate. The edge of the substrate may be seen in the central part of the picture.*

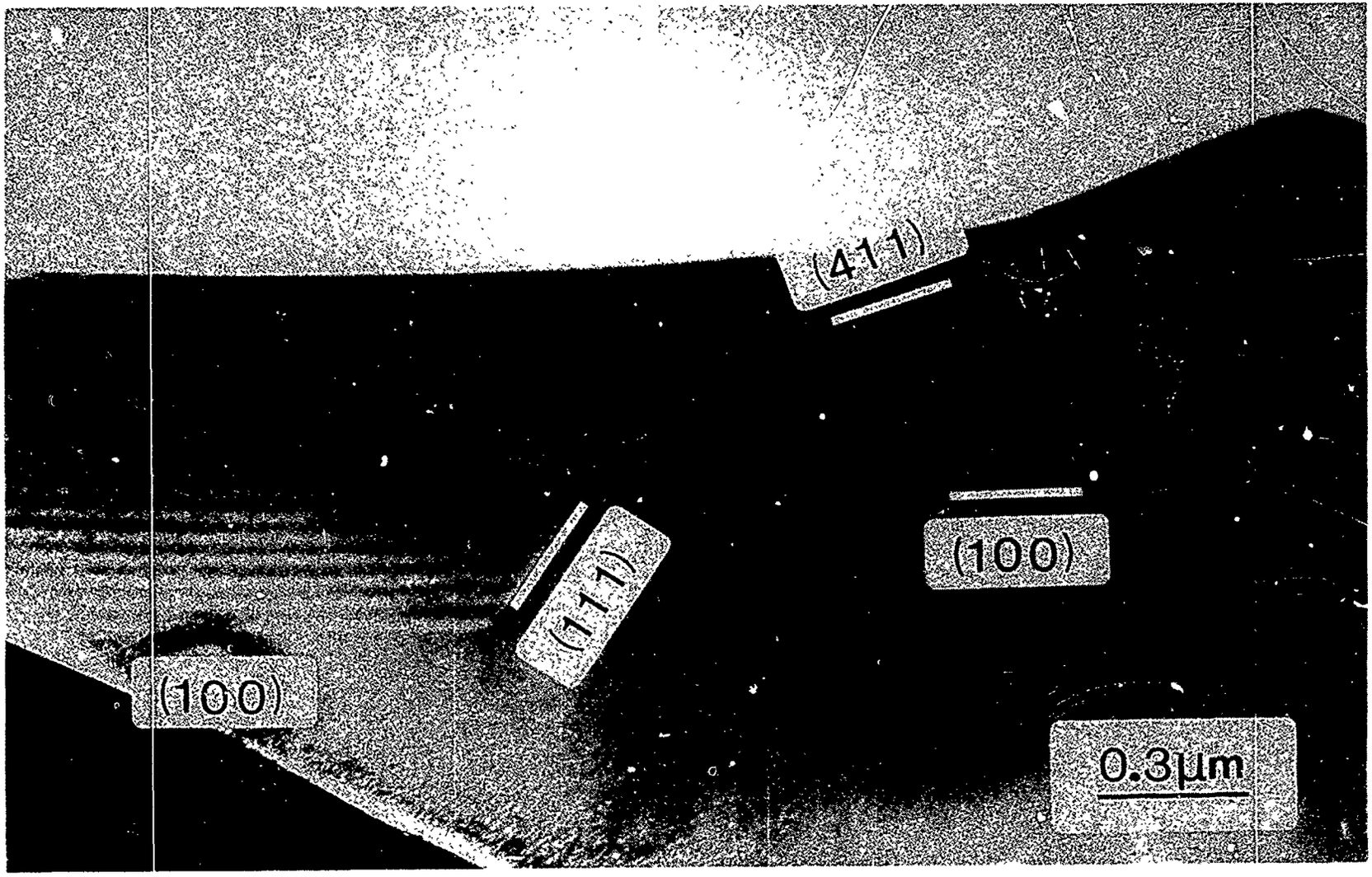
(411)
(111)
(100)
(100)
0.3μm

INFLUENCE OF GROWTH TEMPERATURE ON MBE GROWN $Al_{0.48}In_{0.52}As$

H. Künzel*, J. Böttcher, A. Hase, and C. Schramm
Heinrich-Hertz-Institut für Nachrichtentechnik Berlin GmbH
Einsteinufer 37, D-1000 Berlin 10, Germany
Telefon: (030)31002-0, Telefax: (030)31002-213

$Al_{0.48}In_{0.52}As$ (referred to as AlInAs) is one of the basic materials for InP-based optoelectronics. It is used as the barrier material in layer sequences for heterostructure devices based on elemental source MBE grown layers. The crystalline quality of the material and the impurity incorporation are an important subject for the use of AlInAs in electronic devices. Especially, for HEMT structures a careful analysis of the growth temperature dependence of crystalline and electrical properties is a stringent requirement for the appropriate design of the growth temperature variation during the epitaxial process. An optimum growth temperature sequence has to result in high resistivity AlInAs for the buffer layer, large doping efficiency in the AlInAs:Si layer and high breakdown voltage/low leakage current of the Schottky assist layer.

In this work we have systematically varied the growth temperature between 200 and 580 °C. The growth temperature is calibrated by means of the RHEED pattern of the InP substrate. The change from the (2X4) As stabilized pattern to the (4X2) pattern in the presence of an As beam is found to coincide with a substrate temperature of 530 °C. The growth rate is kept close to 1.0 μm/h and a III/V beam equivalent pressure ratio of 15 is applied, a value as low as possible to maintain As-stabilized growth. Solely for growth temperatures in excess of 500 °C the As flux is increased.

At the growth temperatures commonly used, which are near the the point of oxide desorption from InP substrate, the surface mor-

phology is found to be slightly deteriorated. Examination by an interference microscope or a scanning electron microscope reveals as wavy surface. A lowering of the growth temperature results in a reduction of the roughness, which completely vanishes below 350 °C. Simultaneously, the (400) X-ray diffraction pattern of the AlInAs layers reveals a non ideal bulk crystallinity of the grown layer. At 500 ° C the half-width of the diffraction peak of a 2 μm thick layers is in excess of 50 arcsec. A reduced growth temperature of 300 °C results in an AlInAs half-width of 20 arcsec compared to a value of 15 arcsec for the InP substrate used. This excellent crystalline quality is maintained down to the lowest growth temperature used in this study.

The incorporation of impurities is strongly affected by the growth temperature. Fig. 1 shows the influence of the temperature on the Hall free electron concentration in $1.3\times10^{17}cm^{-3}$ and $2.0\times10^{17}cm^{-3}$ silicon doped material. For all growth temperatures used, the free electron concentration is substantially lower than the amount of dopants incorporated. In addition, the electron concentration decreases with reduced substrate temperature and is below the detection limit beyond 400 °C. CV mesurements on the same set of samples give identical results. The reduction of the free electron concentration is found to coincide with the presence of a high level of deep traps incorporated, which, however, can only partially explain the free carrier deficiency observed. At a growth temperature of 500 °C a total concentration of deep levels, as measured by DLTS, amounts to 1.0×10^{16} cm^{-3} in a 1.0×10^{17} cm^{-3} Si doped sample. Two levels at 250 meV and 760 meV below the conduction band dominate the spectrum.

For growth temperatures beteen 200 and 500 °C, undoped AlInAs is found to be semi-insulating with a restistivity typically in excess of 10^7 Ω·cm and maximum values of 5×10^7 Ω·cm, measured for single layers. DLTS measurements show the same amount of deep electron traps as in Si doped material with compara-

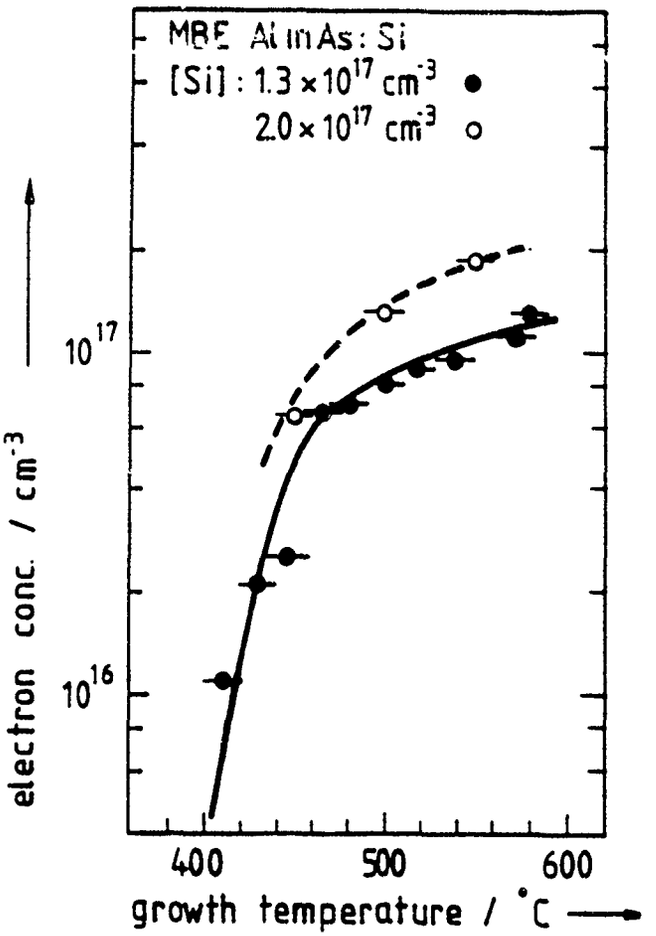

Fig.1: 300 K electron concentration of n-AlInAs:Si versus growth temperature

ble activation energies. Thus, the residual net electron concentration, estimated to be in the order of 10^{15} cm^{-3} in undoped material, is overcompensated. Resistivity measurements of $n^+/i/n^+$-AlInAs structures indicate a dramatically reduced semi-insulating behaviour. High doping levels were found to reduce the i-AlInAs resistivity. Probably, silicon diffusion during growth is responsible for the observed reduction of the resistivity.

Based on the subsequent results, growth of AlInAs/GaInAs HEMT structures can be optimized. An adequate growth temperature profile will be outlined.

DEPENDENCE OF $Al_xGa_{1-x}As$ CRYSTALLINE QUALITY ON SURFACE RECONSTRUCTION DURING GROWTH IN MOLECULAR BEAM EPITAXY

M. I. Etinberg, N. N. Faleev, G. A. Fokin, G. de la Kruz, V. E. Myachin,
Yu. V. Pogorelski*, I. Yu. Rusanovich, I. A. Sokolov

A. F. IOFFE PHYSICO-TECHNICAL INSTITUTE

Polytekhnicheskaya 26 , 194021 Leningrad , USSR

Phone: (812)-247-93-89 Telex: 121453 FTIAN SU

Surfase reconstruction phase diagrams of GaAs and ternary compounds $Al_xGa_{1-x}As$ observed during the epitaxial growth are the subjects of investigation in a number of papers. These studies should be expanded by systematic information about material properties depending on growth temperature (T) and component fluxes. In this abstract we present results of $Al_xGa_{1-x}As$ ($x = 0.23$ and $x = 0.39$) crystalline quality investigations along horizontal crossection of the phase diagram: with increasing T and keeping constant flux ratio $As_4/(Ga+Al) \simeq 2$ and growth velosity ~ 1 μm/hour.

Model structures - 1 μm-width GaAs layer followed by 1.6 μm- width AlGaAs layer grown on a semi-insulating substrate were studied with the double-crystal X-ray spectrometer. Fig.1 shows rocking curves for the sample with $x = 0.23$, prepared under ternary compound growth temperature $T = 610^{\circ}C$ (growth temperature of GaAs layers in all cases was maintained $580^{\circ}C$). Peak 2 is connected with (400)-Bragg reflection from the lattice of GaAs , peak 1 presents reflection from the ternary compound lattice. The width of the second peak is about 8.0" it exceeds to some extent the minimum value of 8.0÷8.2" obtained for GaAs . Minimum value of the first peak width is connected, because of interference, with the ternary compound layer depth. However the width of AlGaAs peak is informative when comparing crystalline quality of layers of the same depth but with different amount of point defects Electron mobility of AlGaAs (Si: $n \simeq 8 \cdot 10^{14}$ cm^{-3}) was mesured 2500 $cm^2/V \cdot s$ under 300 K for this sample.

Fig.2 shows the behaviour of AlGaAs-peak width versus growth temperature and surface reconstruction (we would like to note that the value of T corresponding to the boundary between (2×4) and (1×1) surfase structures sharply increases if we change GaAs to ternary

compound with x = 0.23, however, we didn't observe the difference between boundary positions for x = 0.23 and x = 0.39). Sharp increase of the peak width inside the (1×1)-area suggests that a lot of point defects was created during epitaxial growth. There is no notable dependence of the peak width versus T inside the (1×1)-area. The electron mobility also degradeds when growing in the (1×1)-area. Crystalline quality of material as well as mobility are restored to the level obtained in (2×4)-area at the beginning of the (3×1)-area (near the boundary between (1×1) and (3×1) surfase structures). The amount of point defects notably increases again with further temperature rise resulting in degradation of cristalline quality and carrier mobility.

The peak width of reflection from GaAs layer for the structure prepared in the (1×1)-area was about 25" . It is connected with the structure bent to the radius of 7÷8 m (bending radius of samples prepared in the (2×4)-area was not less than 40 m). The etching of ternary compound layer removes elastic stress , but the width of GaAs peak does not restore up to 9.0" and remains about 12.0" and more . It is connected with the diffusion of point defects into GaAs from the ternary compound layer during growth.

In conclusion, it was observed non-monotonic behaviour of AlGaAs defectness when increasing the growth temperature; higher defectness in the interval of 650-700^{o}C is obviously connected not with the temperature rise but with the absence of surfase reconstruction during growth.

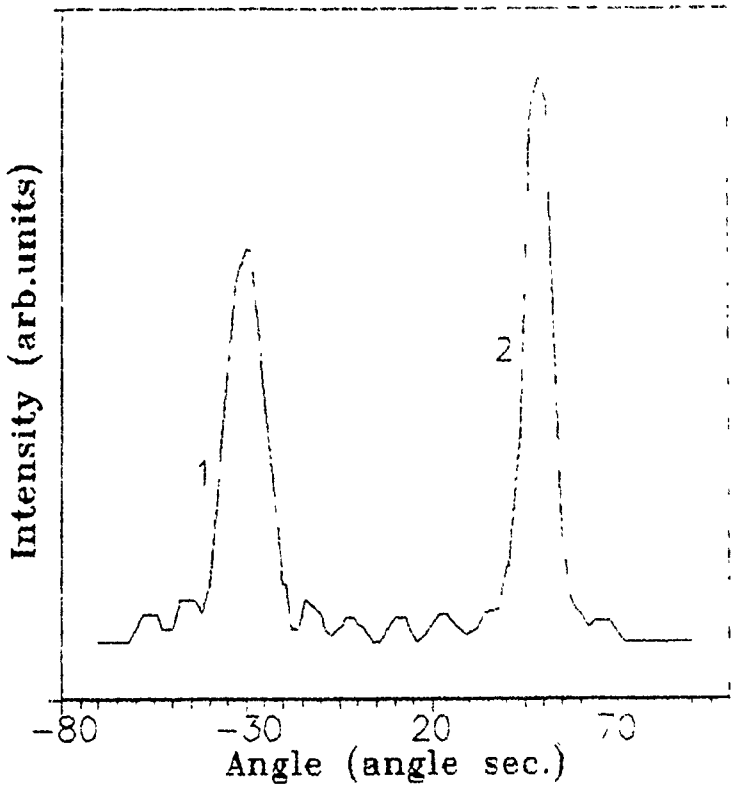
Intensity (arb.units)
1
2
-80
-30
20
70
Angle (angle sec.)

Fig.1

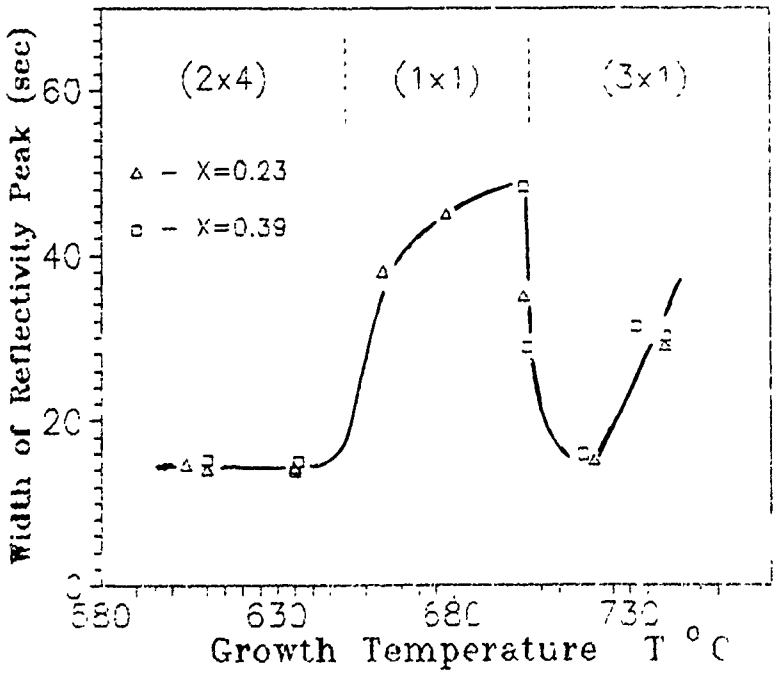
Width of Reflectivity Peak (sec)
60
40
20
(2x4)
(1x1)
(3x1)
Δ - X=0.23
□ - X=0.39
580
630
680
730
Growth Temperature T °C

Fig.2

Nonlinear optic "in-situ" diagnostics of a crystalline film in molecular beam epitaxy facilities

V.F. Krasnov, N.A. Kultchitsky, S.L. Musher, L.A. L.A. Osadchev, V.I. Prots, A.M. Rubenchik, V. E. Ryabchenko, and M.F. Stupak

Institute of Automation and Electrometry, Siberain Branch of USSR Academy of Sciences, 630090 Novosibirsk, USSR

A new method of film structure "*in situ*" monitoring is proposed for MBE and MOCVD technologies. It is based on the analysis of second harmonic (SH) radiation induced in a growing film irradiated by a laser beam. If a film contains amorphous part and regions with different symmetry, then the value and direction of the nonlinear polarization may significantly differ from the value calculated for an ideal crystal. Hence, the measurement of the SH intensity in different points presents local information on film crystalline quality and its distribution over a surface.

SH intensity can change as a result of film thickness variations. We demonstrate that this effect can be eliminated by data processing. Also, we demonstrate that SH measurement during the growth provides the film thickness monitoring and the information on the film refractive index. Also, the information on a transient layer near a wafer can be obtained.

The SH intensity measurement *versus* laser polarization rotation provides the information on crystal structure orientation. We can define crystallographic axes orientation with an accuracy of about 0.1°. The presence of a polycrystal component and its features can be obtained.

The presented method can be complementary to the well-known technique of fast electron diffraction (RHEED) and is supposed to be especially suitable for research groups since it allows a correlation between technological and crystallographic parameters to be quickly determined.

POST-DEADLINE PAPERS

P1, P2, P3, P4, P5, and P6

Resonant tunneling structures based on the GaAs/AlAs System

A. Förster, H. Lüth,

Institut für Schicht und Ionentechnik, Forschungszentrum Jülich, Postfach 1913, D-5170 Jülich

H. Brugger and U. Meiners

Daimler Benz Forschungsinstitut, Wilhelm Runge Straße 11, D-7900 Ulm

Double barrier AlAs/GaAs resonant tunneling diodes were grown by molecular beam epitaxy for high frequency applications. The influences of the AlAs barrier thickness (d_B) and spacer length (L_S) were studied in the range from d_B=3 monolayers (ML) up to 10 monolayers. The peak current density (jp) shows an exponential dependence on the barrier thickness and reaches a maximum value of $4*10^5$A/cm^2 for the 3ML barrier and a current density of jp=$2.6*10^3$A/cm^2 for the 10ML- barrier at room temperature. A maximum peak to valley current ratio (PVR) is observed for the 6ML- barrier sample (PVR=5.0 at 300K, PVR=12 at 77K).

Negative differential resistence in GaAs/AlGaAs structures is well known /1-3/. There are many possible applications like mixers, oscillators, frequency doublers and so on. To achieve high yield from such devices one needs high current densities and high peak to valley ratios. Therefore we investigated the current/-voltage I(V) dependence on AlAs-barrier thickness (d_B) and spacer width (L_S) systematically to achieve a maximum peak current density and PVR.

All resonant tunneling diodes (RTD's) structures were grown on silicon-n-doped GaAs substrates (n=$1*10^{18}$cm^{-3}-$4*10^{18}$cm^{-3}, [100]-orientated) by molecular beam epitaxy using a Varian MBE Mod-GenII System. The MBE-System was equipped with 60cc cells for group III material and 120cc cells for arsenic. Growth rates were controlled by evaluation of intensity oscillations from RHEED spots. The growth rate for GaAs- layers was set to 0.9 μm/h and 0.24 μm/h for AlAs, respectively. A sixty second growth interruption was made only at the 'normal' interface GaAs/AlAs. Both GaAs- and AlAs layers were grown at a substrate temperature of 640C and at a V/III-beam flux ratio of 20. I/V measurements were made on mesa structures with different geometries down to 2 x 2 μm in size. The RTD diodes have the following structure: n+ GaAs substrate, 1μm GaAs buffer n=$1*10^{18}$ cm^{-3}(n+), 100A GaAs n=$1*10^{17}$cm^{-3} (n), 100A GaAs n=$1*10^{16}$cm^{-3} (n-), 50A GaAs spacer, d_B monolayers AlAs, 18 ML GaAs, d_B ML AlAs, 50 A GaAs spacer, 100A GaAs n-, 100A GaAs n, 0.5μm GaAs n+.

RTD's based on AlAs symmetric double barriers in the GaAs-System show negative differential resistence (Fig.1) with a PVR which is dependent on d_B and

was varied from 3 monolayers (ML) up to 10 ML. The GaAs well and the undoped spacer was kept fixed at 18 ML. For this structure the peak- current density (j_P) shows an exponential dependence on the AlAs barrier thickness (Fig.2) and an optimum PVR for d_B=6ML.

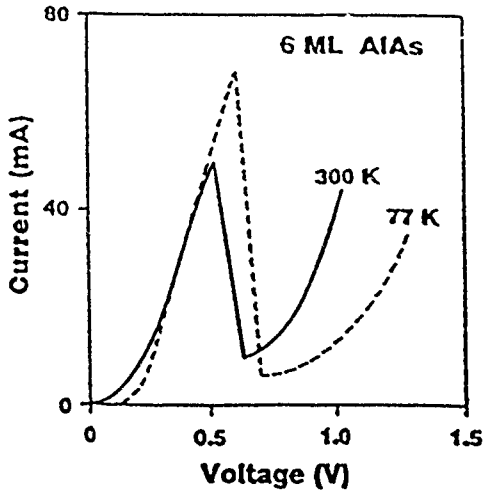

Fig. 1: I/V-curve of AlAs/GaAs-RTD

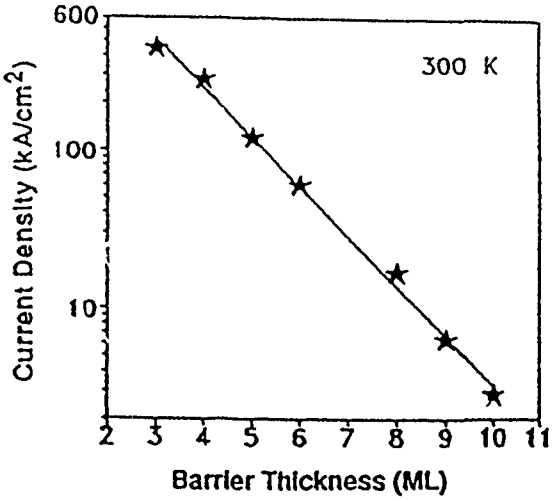

Fig. 2: Peak current density dependence

The PVR-value of 5.0 at a current density of $5.5*10^4$ A/cm^2 is to our knowledge the best reported value at room temperature for the symmetric AlAs/GaAs system. Better PVR's are known for structures with prebarriers /4/ or with different material systems only /5/. Measurements at 77K show higher PVR of typically 12 for the 6 ML barrier sample. A reduction of the emitter side spacer layer thickness from L_S=10 nm to L_S=0.5 nm improves the current density by about 60%.

Literature

1.) R. Tsu and L. Esaki, Appl. Phys. Lett. 22, 562 (1973).

2.) L. L. Chang, L. Esaki, and R. Tsun, Appl. Phys. Lett. 24, 593 (1974)

3.) TV. J. Goldman, D. C. Tsui, J. E. Cunningham, and W. T. Tsang, j. Appl. Phys. 61, 2693 (1987)

4.) Peng Cheng and James S. Harris, Jr, Appl. Phys. Lett.56(17), 1676 (1990); H. Riechert, D. Bernklau, J.P. Reithmaier, Electronic Lett., 26, 340 (1990); V. K. Reddy, A. J. Tsao, and D. P. Neikirk to be published

5.) Tom P. E. Broekert, Wai Lee, and Clifton G. Fonstad, Appl. Phys. Lett. 53(16) 1545 (1988); I. Mehdi and G. Haddad, J. Appl. Phys. 67(5), 2643 (1990)

P2

Doping of CdTe(100) on BaF_2/CaF_2 covered Si(100) for solar cell fabrication

A.N. Tiwari, H. Zogg*, S.Blunier

AFIF (Arbeitsgemeinschaft für industrielle Forschung) at Swiss Federal Institute of Technology, ETH-Hönggerberg, CH-8093 Zürich, Switzerland
phone ++41 1 377 2209 fax ++41 1 371 2419

CdTe was grown by MBE on Si(100) using a BaF_2/CaF_2(100) intermediate buffer layer. The orientation of the CdTe layer is always (100) on fluoride covered Si(100). (We already described CdTe(111) layers on BaF_2-CaF_2/Si(111), [1]). Despite the large (19%) lattice mismatch, good structural quality as judged from low temperature PL and x-ray line widths is achieved. The quality improves somewhat if the surface is illuminated with an Ar-laser (PAMBE) during growth. According to the streaky RHEED-patterns, growth is 2-D. However, microscopy of the surface reveals small hillocks. The surfaces are macroscopically smooth, but not perfectly shiny.

Doping of these lattice mismatched CdTe layers proved to be much more difficult than in CdTe layers grown on CdTe substrates. We were not able to obtain comparable dopant activation using the PAMBE principle, as has been done successfully by Schetzina's group for homoepitaxial layers [2]. For these experiments, we used a single CdTe source together with a furnace containing the dopant element (In or Sb). The structural quality improved with the laser illumination. We obtained resistivities down to 10^3 Ohm cm with Sb-doping [3,4], while we did not observe any decrease in resistance using In as a dopant.

For As doping we have used a self fabricated As cracker cell and an additional Cd source. The excess of Cd helps to lower down the substrate temperature for epitaxial growth and als enhances doping activation. With only a CdTe source, the growth is 3-D below 250°C and polycrystalline below 200°C. With the additional Cd source 2-D growth is obtained down to 210°C and polycrystalline growth below 180°C. With PAMBE and by properly optimizing the Cd and CdTe flux ratio, we obtained layers showing streaky RHEED patterns down to 70°C.

For As doping, a CdTe and Cd flux of $8x10^{-7}$ and $5x10^{-8}$ Torr were used. The substrate temperature was varied in the range of 250-180°C and the As cell temperature between 150-280°C. We obtained lowest resistivities (≈20 ohm cm) for layers deposited at a substrate temperature of 200°C and As cell temperature of 260°C. The illumination intensity and Cd/CdTe flux ratio are important parameters controlling stoichiomety and desorbed sites. Further optimization is being persued to still lower down the resistivity.

The effect of the laser beam again helps to increase the structural quality. The illumination changes the surface reconstruction (as observed by RHEED) in the same way as with homoepitaxial growth. It indicates Te-desorption, which seems to help the p-dopant to be incorporated at the correct lattice sites.

Solar cells were fabricated using such layers. They consist of epitaxial p-CdTe/i-CdTe overgrown with (polycrystalline) CdS as a window layer. The stacks are removed from the substrates by dissolving the fluoride buffer layer and glued on a metal/glass plate (epitaxial lift off). With this technique, thin film, but single crystal solar cells are formed. Since only 1-2 μm thick CdTe layers are needed, high efficiency solar cells with enhanced material economy are expected.

References:

[1] H.Zogg, S.Blunier, Appl. Phys. Lett. 49, 1531, 1986.

[2] R.N. Bicknell, N.C. Giles, and J.F. Schetzina, J. Vac. Sci. Technol. B5, 701 (1987).

[3] A.N. Tiwari, W. Floeder, S. Blunier, H. Zogg, H. Weibel, Appl. Phys. Lett. 57, Sept. 1990, 1108.

[4] A.N. Tiwari, W. Floeder, S. Blunier, H. Zogg, H. Weibel, J. Cryst. growth, 1991, to be published

P3

Low temperature growth and IR-device fabrication with $Pb_{1-x}Sn_xSe/BaF_2$-CaF_2 on Si(111) substrates

H. Zogg, S.Blunier, T. Hoshino, C. Maissen, J. Masek

AFIF (Arbeitsgemeinschaft für industrielle Forschung) at Swiss Federal Institute of Technology, ETH-Hönggerberg, CH-8093 Zürich, Switzerland

phone ++41 1 377 2209 fax ++41 1 371 2419

Photovoltaic IV-VI-(lead-chalcogenide)-on-Si infrared sensors have the potential for a low cost technique of large heteroepitaxial IR focal plane arrays for thermal imaging applications, both for the 3-5 µm and 8-12 µm wavelength range. Sensitivities are as large as in other narrow gap systems like InSb or $Hg_{1-x}Cd_xTe$. However, the signal processing can be performed in the Si-substrate with standard Si-technology. As is well known, sensors in narrow gap material need much less cooling than silicide focal plane arrays or III-V multi quantum well detectors to achieve comparable sensitivities.

We describe our new development of low temperature MBE growth and IR-sensor fabrication in $Pb_{1-x}Sn_xSe$. Depending on the chemical composition x, any cut-off wavelength can be chosen between 7 and >12 µm. (The 3-5 µm range is covered with PbTe or $PbS_{1-x}Se_x$.)

The large lattice- and thermal expansion mismatch between the Si-substrate and the infrared sensitive IV-VI layer is overcome with an about 200nm thick epitaxial stacked CaF_2-BaF_2 buffer layer grown by MBE.

The optimal substrate temperature for the beginning of CaF_2 growth is known to lie around 700°C. This is the highest temperature in the whole growth process. (The IV-VI layers do not need higher growth temperatures than 400°C, while the IR-sensor fabrication steps are performed at temperatures much below). However, this temperature is too high if one wishes to grow the layers on <u>active</u> Si-substrates which already contain completely processed circuits for the read-out electronics. The limiting temperature to use such substrates is due to the Al-metallization, which can withstand temperatures up to 450°C-500°C only for a short time. However, from a practical point of view, it would be advantageous to deposit the layers directly on such completely processed and already electrically tested substrates.

We therefore developed a technique to grow the CaF_2-BaF_2 layers at substrate temperatures never exceeding 450°C. The (processed and aluminized) Si-substrates are cleaned with a low temperature technique in dry N_2 and immediately transferred in dry N_2 to the MBE growth chamber. Epitaxy of the CaF_2 is achieved even at 450°C if the growth rates are low enough. However, the RHEED-patterns at the initial stages of growth are rather blurred, but sharpen considerably during the following BaF_2 growth. We obtained Rutherford backscattering channelling yields of 10%. This is somewhat higher than for the layers deposited with initial substrate temperatures of 700°C, but still satisfactory for the subsequent IV-VI growth.

The 2-4 μm thick IV-VI layers deposited on these buffers in a second growth chamber are untwinned single crystal and exhibit perfectly smooth surfaces with surface defect concentrations down to 10^3 cm^{-2}. Apart from somewhat larger X-ray line widths, the quality of these layers grown on low-temperature buffers is near indistinguishable from IV-VI layers on high temperature grown fluoride buffers. Despite the large thermal expansion mismatch, the layers withstand multiple cooling cycles down to 15K without problems due to some plasticity at

higher temperatures.

A linear photovoltaic IR-sensor array was fabricated in such a low temperature material. The array consists of 66 sensors, each with 50 x 100 μm^2 areas and is illuminated from the backside. The active sensor areas are defined by vacuum deposited Pb which forms a blocking contact on p-type material, thereby creating an induced p-n junction.

The uniformity of the array is excellent. The spread in 50% cut-off wavelength (nominal cut-off wavelength 10.5 μm) is below our measurement accuracy, i.e. below 0.1 μm. The external quantum efficiencies are about 60% (without AR-coating) and with a standard deviation over the whole array of 3%. This was achieved even without substrate rotation and despite our simple IR-device fabrication technique is far from optimized.

Compared to $Hg_{1-x}Cd_xTe$ technology, the sensitivities (resistance area products) of our $Pb_{1-x}Sn_xSe$ arrays are somewhat lower due to the unoptimized device processing, while the uniformities of the spectral response is much better with $Pb_{1-x}Sn_xSe$.

References:

T. Hoshino, C. Maissen, H. Zogg, J. Masek, S. Blunier, A.N. Tiwari, S. Teodoropol, W.J. Borer, Infrared Phys. 32, 1991, pp. 169-175.

H. Zogg, C. Maissen, J. Masek, T. Hoshino, S. Blunier, Mat. Res. Soc. Symp. Proc. Vol. 216, 1991, to be published.

Observation of Reflected–High–Energy–Electron Diffraction Oscillations during Atomic–Layer Epitaxy Growth of CdTe

W.Faschinger, P.Juza, and H.Sitter

Institut für Experimentalphysik, University of Linz, Austria

Recently we presented experimental results of Atomic–layer epitaxy (ALE)–growth of CdTe on GaAs [1–3]. The main result was that the substrate temperature range, in which the average growth rate is one monolayer, is quite narrow. We presented a model which allows to calculate the proper growth parameters for monolayer growth. However, all the data were obtained from post growth characterizations, which means the results represent mean values over several thousand growth cycles. In order to study the growth process in situ in a monolayer scale we built a new growth chamber which allows the use of Reflected High Energy Electron Diffraction (RHEED) to observe the surface during growth.

The experiments were performed in a custom designed vertical MBE–system equipped with 7 Knudsen cell ports together with fast magnetically coupled shutters for operation in the ALE mode. For ALE growth of CdTe elemental Cd– and Te–Knudsen–cells with two separately adjustable heating zones were used. The RHEED–observations were carried out with a 30 keV electron gun (Staib Instruments) which was operated at 12.5 keV. As substrate material we used (100)–oriented semi–insulating GaAs, which was chemically cleaned in a standard H_2SO_4/H_2O_2 etch and preheated to 600 ^{0}C before growth in order to desorb the oxide layer. A nude ionisation gauge placed near the substrate was calibrated for Cd– and Te–beam intensities by depositing polycrystalline Cd– and Te–films on etched and preheated GaAs substrates at a substrate temperature of –10 ^{0}C to avoid any reevaporation. The thickness of the deposits was measured by viewing the cleaving edge of the calibration samples in a SEM. The substrate temperature was calibrated by a second thermocouple which was in direct contact to the surface of a GaAs sample.

The ALE experiments were performed after the growth of a 3 μm thick MBE buffer to avoid the influence of a possible dislocation network at the interface. RHEED–patterns in the (100)–, (110)– and (–110)–azimuth were qualitatively observed during ALE growth in a substrate temperature range between 260 and 340 ^{0}C in order to find substrate temperature dependent features in the RHEED-patterns.

During the ALE growth cycle the surface changes from a Cd–stabilized to a Te–stabilized state. The RHEED patterns of the Cd–stabilized surface show a mixture of a (2 x 1)– and a c(2 x 2)–reconstruction, those of the Te–stabilized surface a (2 x 1)–reconstruction. Althogh the ALE growth rate decreases in the substrate temperature range between 260 and 340 ^{0}C from one to half a monolayer per reaction cycle, a fact that implies that there must be a significant change in the adsorption and arrangement of the surface atoms, the surface periodicity of both the Cd– and Te–stabilized surface does not change with substrate temperature. However, the observed surface periodicity reflects mainly the dimerization of surface atoms which also occurs at submonolayer coverages. The periodicity itself is therefore not an appropriate measure of the surface coverage.

As a consequence it was necessary to study not only the periodicity of the RHEED patterns but also intensity changes. In contrast to previous works on ZnSe [4] we did not monitor the intensity of the specular beam, but of integral and half order streaks in the (110)–azimuth under surface resonance conditions. This new method allows to significantly enhance the absolute signal intensities of single RHEED–spots and the contrast between the signal of the Cd– and Te–covered surface. Surface resonance is a secondary scattering event where the primary electrons are scattered into the surface plane and act there as source beam for the

finally observed diffraction. It occurs always when a reciprocal lattice rod is tangential to the Ewald sphere and significantly enhances the intensity of a spot on the corresponding reciprocal lattice rod [5]. Since a surface resonance wave propagates directly in the uppermost surface layer, it should be extremly sensitive to coverage changes in this layer. The condition of a reciprocal lattice rod being tangential to the Ewald spere can easily be adjusted by turning the azimuthal angle a few degrees off the exact (110)–direction. In our case it was even possible to reach approximate surface resonance for one integral order and one half order streak simultaneously. In this way we could adjust conditions where a bright surface resonance spot (spot 1) appeared on the integral order streak for the Cd–stabilized surface, and another bright spot (spot 2) on the adjacent half order streak for the Te–stabilized surface. During MBE growth both spots appear simultaneously and their intensity ratio is extemely sensible to surface stoichiometry changes during growth.

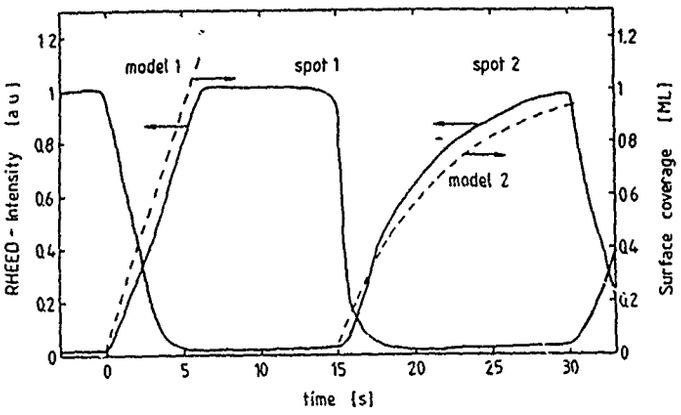

Fig.1: Intensity of two RHEED-spots under surface resonance conditions as a function time during a slow ALE cycle. The Cd pulse starts at t = 0, the Te pulse at T = 15 s. The beam fluxes are $9 \cdot 10^{13}$ and $8 \cdot 10^{13}$ atoms/cm^{2}s for Cd and Te respectively. The dotted lines represent model calculations described in the text.

Fig.1 shows the intensity variation of both spots during a very slow ALE process (pulse times 14.8 s, dead times 0.2 s) with a Cd beam intensity of $9 \cdot 10^{13}$ atoms/cm^2 s and a Te beam intensity of $8 \cdot 10^{13}$ atoms/cm^2 s. During Cd–deposition the intensity of spot 1 increases linearly with time up to a saturation value. The dotted line marked "model 1" is the Cd surface coverage calculated from the known Cd beam intensity under the simple assumption that every offered Cd atom sticks. This assumption seems reasonable if one considers that the Cd atoms are relatively small and as single atoms quite mobile at the surface, so that an adsorbed Cd can change its site if it is hit by a following Cd atom. The two curves correspond within the experimental error of the beam flux calibration ($\cong \pm 5\%$). So we conclude that the intensity of spot 1 is a direct measure of the Cd surface coverage. As soon as a surface coverage of one monolayer is reached, the intensity saturates.

During Te–deposition spot 2 increases, but not proportional to the offered Te flux. The time until the saturation value of spot 2 is reached, is much longer than for spot 1, although the Cd– and Te–flux are approximately equal. We assume that the different behaviour reflects a different adsorption behaviour of Te compared to Cd. This seems reasonable if one considers that Te adsorbs as a large and comparably immobile Te_2–molecule, that cannot easily change its site if it is hit by a second Te_2–particle. Under the simple assumption that a Te_2–molecule sticks only if it hits an empty surface site and re–evaporates if it hits an occupied site one would expect a surface coverage C as a function of time which is given by $C = 1 - \exp(-j \cdot t)$ where j is the Te beam flux in monolayers/s. With the actual value of 0.16 monolayers/s for the Te flux the result of such a calculation is the dotted line marked "model 2". Again the correspondence between the intensity of the spot and the simple model is very good. This confirms that, in analogy to spot 1, the intensity of spot 2 is a direct measure of the Te coverage.

It is very important to note that the intensity of spot 1 can no longer be taken as a measure of the Cd coverage as soon as one starts to deposit Te. Then the

intensity drops to nearly zero within 2 s, although the Te coverage at that time, as measured by spot 2, is only about 0.2 monolayers. A possible explanation is that even a low Te coverage shadows the Cd surface for the incident electrons and so effectively prevents the Cd–related surface resonance. For Cd deposited on Te the effect on spot 2 is not as strong but of the same tendency. So one can only monitor the coverage of the uppermost monolayer with a spot that is *rising* in intensity with rising coverage. The behaviour of spot 1 is very similar to the results obtained by Zhu et al. [4] for the specular spot in the case of ZnSe: The intensity rises approximately linearly when the Zn shutter is opened. But when Se is offered, the intensity drops much faster than the Se coverage can be formed, if one considers the given fluxes. Nevertheless Zhu et al. use the intensity *drop* of the specular spot as a measure of the Se–coverage, which might be very unprecise according to our observations.

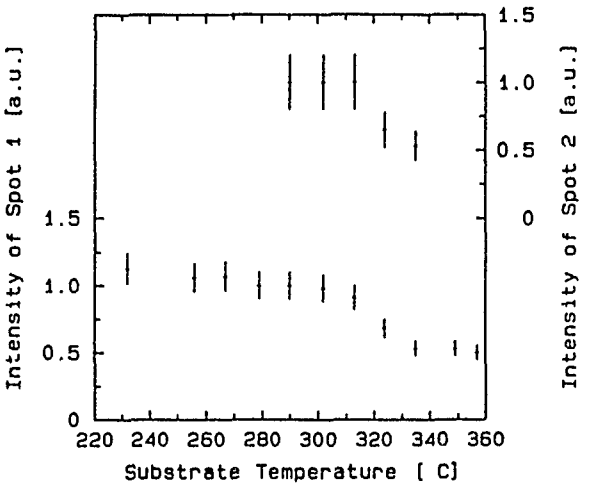

Fig.2: Intensity of the Cd–related surface resonance spot (spot 1) under Cd–stabilized, and of the Te–related spot (spot 2) under Te–stabilized conditions as a function of substrate temperature.

We also measured the intensity of spot 1 under Cd–stabilized and spot 2 under Te–stabilized conditions as a function of substrate temperature. The results are depicted in fig.3. It is clearly visible that the intensity of spot 1 drops to approximately 50% at substrate temperatures higher than 315 ^{0}C. The behaviour of spot 2 is tendentially similar. This result shows that the surface accepts only half a monolayer of Cd and Te at higher substrate temperatures, with the consequence that the average growth rate drops to 0.5 monolayers per cycle, as shown by our previous results. Such a measurement is consequently a fast and easy way to determine appropriate parameters for monolayer ALE growth.

In conclusion we showed that the observation of RHEED spots under surface resonance conditions is a powerful tool for the in–situ investigation of surface adsorption processes. The intensity of these spots is extremely sensitive, and, under proper conditions, proportional to the coverage of the topmost layer. One can observe different spots for the observation of different adsorbates. This is an important advantage compared to the observation of the specular spot, whose intensity seems to be a reliable measure only for one component. We think that these advantages are not limited to CdTe and this new method will be of use for other II–VI– and even III–V–materials.

1) W.Faschinger, and H.Sitter, J.Crystal Growth 99 (1990) 566
2) W.Faschinger, P.Juza, and H.Sitter, Acta Polytechnica Scandinavica 195 (1990) 171
3) H.Sitter, and W.Faschinger, Festkörperprobleme (Advances in Solid State Physics) 30 (1990) 219
4) Z.Zhu, M.Hagino, K.Uesugi, S.Kamiyama, M.Fujimoto, and T.Yao, Japanese J.Appl.Phys. 28 (1989) 1659
5) P.K.Larsen, P.J.Dobson, J.H.Neave, B.A.Joyce, B.Bölger, and J.Zhang, Surf.Sci. 169 (1986) 176

Deep level analysis of undoped $Ga_xIn_{1-x}P$/GaAs heterostructures grown by MOMBE and MOVPE

E. C. Paloura[a)], A. Ginoudi, G. Konstandinidis and G. Kiriakidis
FORTH-IESL, P.O. Box 1527, GR-71110 Heraklion, Crete, Greece
[a)] Permanent address : Aristotle Univ. of Thessaloniki, Physics Dept.313-1, GR-54006 Thessaloniki, Greece

The lattice matched $Ga_{0.51}In_{0.49}P$/GaAs heterojunction is an important alternative to the AlGaAs/GaAs system for applications in modulation doped field-effect transistors and heterojunction bipolar transistors[1]. Device quality and reliability are directly dependent on the electrical properties and the deep levels in the alloy semiconductor[2]. In this paper we report on the deep level characteristics of undoped $Ga_xIn_{1-x}P$/GaAs heterostructures grown with two novel growth techniques, Metallorganic Molecular Beam Epitaxy (MOMBE) and Metallorganic vapour Phase Epitaxy (MOVPE).

The residual doping of the $Ga_xIn_{1-x}P$ epilayer, for both the MOMBE and MOVPE samples, is n-type. The free carrier concentration (N_D-N_A), as calculated from the room temperature capacitance-voltage (C-V) characteristics, for all the MOVPE and a number of the MOMBE samples is in the range of 10^{15} cm^{-3}. Au Schottky barrier diodes with a diameter of 500μm were used for the C-V and the Deep Level Transient Spectroscopy (DLTS) measurements. The barrier heights of the MOVPE samples, as calculated from current-voltage (I-V) characteristics, varied in the range 0.9-0.96 eV while the ideality factor n was 1.1 and the forward characteristics were thermionic. On the other hand the barrier heights for the MOMBE samples were about 0.7 eV and ideality factors $n \approx 2$. Furthermore, a "ledge" (pseudosaturation of the current over a range of the applied gate bias) indicating defect assisted conduction, was observed in the forward I-V characteristics for small values of the forward bias[3]. The low ϕ_B values for the MOMBE samples could be attributed to the phase decomposition phenomena which were observed in TEM analysis[4] in these samples and which have been attributed to the rather low growth temperature ($T_G < 520^oC$).

A typical DLTS spectrum, recorded with emission rate windows 400 and 1000 s^{-1}, from an undoped lattice-matched MOMBE $Ga_{0.51}In_{0.49}P$/GaAs heterostructure, where the active epilayer is 0.5μm thick, is shown in Fig.1. Two traps, thereafter labeled A and B are detected. Trap A, with E_A=817eV, σ_A=2.3x10^{-13} cm^2 and N_{TA}=8.5x10^{14} cm^{-3}, where E_A is the activation energy, σ_A is the capture cross-section and N_{TA} is the trap concentration, is a $Ga_xIn_{1-x}P$ trap since it appears only for a filling pulse height high enough to completely flatten

the bands (i.e.filling pulse height ≥ ϕ_B+gate bias). Trap B has a very strong bias dependence and the peak position shifts from 199 K to 340 K when the applied gate bias varies from +0.2 to -2 V. Therefore, trap B is an interface trap which essentially dominates the device behavior.

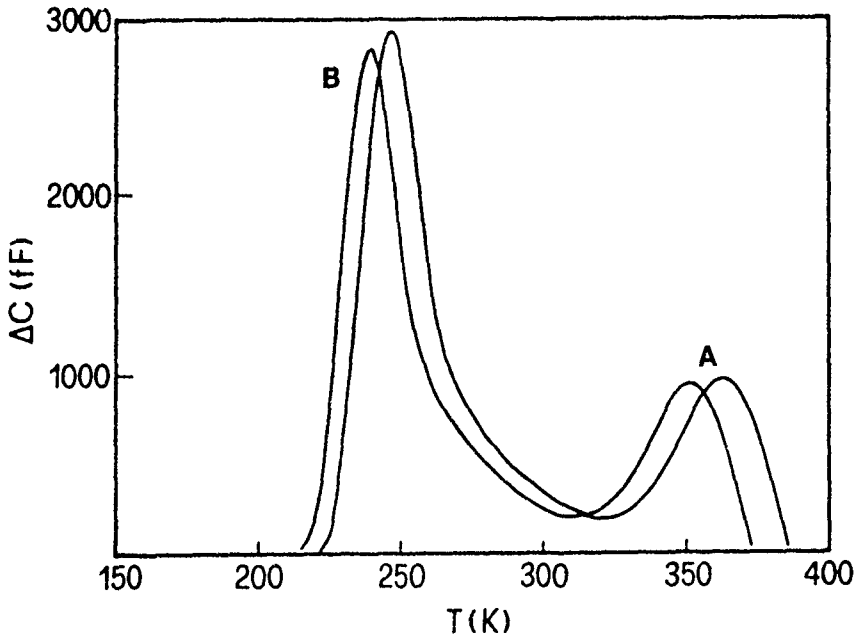

Fig.1 : DLTS spectrum from a lattice matched GaInP/GaAs heterostructure, recorded with a bias of -0.2 V and filling pulse height of +0.9 V

Trap A is characteristic of the MOMBE samples (epilayer thickness : 0.5-1.7μm) and is also present in Ga-rich samples. The DLTS spectrum from a MOMBE Ga-rich sample (x=0.68) with $\Delta\alpha/\alpha$=1.2% (where α is the GaAs lattice constant) reveals the presence of two electron traps with the following characteristics : E_A=875 meV, σ_A=1.3x10^{-15} cm^2, N_{TA}=4x10^{15} cm^{-3} and E_C=537 meV, σ_C=2x10^{-16} cm^2, N_{TC}=1.3x10^{15} cm^{-3}. We propose that the trap labeled A for the lattice matched and Ga-rich samples has the same origin and is characteristic of the growth method. The difference in the measured activation energy (about 60 meV) could be attributed to the conduction band offset. Trap C in the Ga-rich sample is most probably related to defects induced by the large lattice mismatch.

The MOVPE samples are lattice matched ($\Delta\alpha/\alpha<10^{-3}$) and the thickness of the epilayer in the examined samples varies from 1.6 to 2.2μm. DLTS analysis reveals the presence of a single electron trap with E_a=0.7 eV, σ=1x10^{-15} cm^2 and N_T=2x10^{14}-1x10^{15} cm^{-3}. A common feature of the DLTS spectra in all the examined samples is alloy broadening due to microscale variations of the Ga_xIn_{1-}

$_x$P alloy composition[4]. It could be suggested that a local variation of the band gap result in fluctuations of activation energies or capture cross-sections.

The electron trapping centers in all the examined samples exhibit persistent photoconductivity (PPC) at T<100 K and upon exposure to white light the device capacitance increases due to carrier photoexcitation. After exposure to white light the diode capacitance increases and recovers to the initial dark value at about 250 K for the lattice matched samples while in the lattice mismatched samples the PPC effect is still observable even after heating up to 300 K.

In summary we present evidence that the interface trap concentration at the $Ga_xIn_{1-x}P$/GaAs interface dominates the device behavior when the epilayer is thinner than 1μm. The undoped MOMBE samples, lattice matched and mismatched, contain a characteristic deep trap (trap A) with an activation energy that takes values in the range 817-870 meV while the lattice mismatch introduces an additional deep trap with an activation energy of 537 meV. Trap A also dominates the forward I-V characteristics and it could be suggested that a small increase of the growth temperature might improve the ϕ_B and ideality factor of the Schottky diodes on MOMBE material. On the contrary, the Schottky barriers on the MOVPE samples grown on at T_G>520°C have a higher ϕ_B and an ideality factor closer to the ideal value of 1. Finally, all the examined samples suffer from microscale variations of the alloy composition which becomes evident on the DLTS spectra as a broadening of the trap peaks.

---

[1] J. M. Olson, R. K. Ahrenkiel, D. V. Dunlavy, B. Keyes and A. E. Kibbler, Appl. Phys. Lett. **55** (12), 1208 (1989)

[2] R. Fischer, T. J. Drummand, J. Klem, W. Kopp, T. S. Henderson, D. Perrachione and H. Morkoc, IEEE trans. Electron. Dev. **ED-31** (8), 1028 (1984)

[3] J. F. Chen, J. C. Chen, Y. S. Lee, Y. W. Choi, K. Xie, P. L. Liu, W. A. Anderson and C. R. Wie, J. Appl. Phys. **67**(8), 3711 (1990)

[4] J. Stoemenos, private communication (1990)

Extended Abstract for 91 Euro MBE W... ...pere, FINLAND, 21-24 April 1991

RHEED STUDIES AND THE GROWTH OF HIGH MOBILITY INDIUM PHOSPHIDE BY SOLID SOURCE MBE

by

C.R. Stanley*, V.M. Airaksinen+ , R.H. Hutchins and M. McElhinney,

MBE Research Group, Department of Electronics and Electrical Engineering,

University of Glasgow, Glasgow, G12 8QQ, Scotland, U.K.

* I.D.D.; 44-(0)41-330-4798: FAX; 44-(0)41-330-4907

Abstract

A detailed investigation by RHEED of the MBE growth of InP from solid sources has been undertaken. It has been established that the incorporation rate of phosphorus from P_4 tetramers is at least 20 times lower than from P_2 dimers. An anomolous behaviour has been observed between ≈480-520°C whereby the phosphorus incorporation rate remains approximately constant rather than continuing to decrease exponentially with increasing temperature. By growing thick unintentionally doped layers at temperatures towards the upper limit of this range with the minimum of excess P_2, mobilities up to ≈170,000$cm^2V^1s^1$ at 77K with electron densities ≈2x$10^{14}cm^3$ have been achieved despite a steady deterioration in the surface morphology. These are believed to be the highest mobilities recorded for InP whether grown by solid or gaseous source MBE.

1. Introduction

Little fundamental information exists on the MBE growth of indium phosphide although it is generally agreed that the use of P_2 dimers is preferable to P_4 tetramers for reasons largely connected with the higher background pressures which occur both during and after growth with P_4. The highest reported 77K electron mobility for InP grown by solid source MBE from In and P_2 fluxes is ≈55,000$cm^2V^1s^1$ [1], but mobilities up to ≈150,000$cm^2V^1s^1$ have been measured for epitaxial layers grown from gas sources.[2,3] The purpose of the investigations summarized here has been twofold; (i) to determine the phosphorus-limited incorporation rates as a function of the phosphorus species and substrate temperature through the use of RHEED intensity oscillations, and (ii) to use this information to optimize the conditions for the growth from solid sources of high mobility, unintentionally doped InP.

2. Experimental Procedures

The experiments were carried out in an essentially standard Varian Modular Gen II MBE system equipped for the growth of both (Al,Ga)As and InP, but fitted with a turbomolecular pump and liquid nitrogen trap configured specifically to handle phosphorus under UHV conditions. The phosphorus flux was generated from 6N's purity form 1 red phosphorus contained in the graphite sublimator section of a group V cracker source. The cracker was identical to the unit recently used in the same MBE system to grow GaAs of

+ Permanent address; Electron Physics Laboratory, Helsinki University of Technology, Otakaari 1, SF-02150 Espoo, FINLAND.

exceptional purity [4,5], and operated at a temperature of T_{cr}≈700°C for conversion of ≥90% P_4 tetramers into P_2 dimers. The oscillations at the commencement of growth on to (100)-InP substrates in the intensity of the specularly reflected beam from a 15kV electron gun were detected with an optical fibre and photomultiplier tube to determine growth rates. Substrate temperatures were estimated with an Ircon optical pyrometer.

3. RHEED Results

(a) (100)-InP Surface Reconstructions

The (100) surface symmetries have been examined over a wide range of substrate temperatures (T_S) and P_2:In flux ratios (F_r) along both the [110] and [1$\bar{1}$0] directions. As T_S is progressively raised, the surface transforms from a (2x2) to a (2x1) reconstruction at T_S≈400°C and to what is apparently a (2x4) phosphorus-stable reconstruction at T_S≈440°C, with the exact temperatures being dependent on the P_2 flux. This (2x4) reconstruction is then retained even when the growth is severely limited by the P-incorporation rate. No combination of T_S and F_r has been found which leads to a (4x2) In-stable surface. These observations are broadly in agreement with those reported by Morishita et al. [6] for GSMBE InP.

(b) Phosphorus-limited growth conditions

The absence of the (4x2)-(100)-InP In-stable surface has required that a more involved procedure to be adopted for quantifying the incorporating P-flux as a function of phosphorus species and T_S. The growth rate G_r has been measured by RHEED intensity oscillations at T_S≈450°C where the proportion of the incident P_2 flux which is not able to incorporate is small. The In cell temperature, and hence G_r, is then increased (In-incorporation rate limited) until growth becomes limited by the P-incorporation rate; G_r then remains constant despite further increases to T_{In} and the retention of the "P-stable" reconstruction.

P-incorporation rate limited growth has been studied as a function of the incident P-species simply by varying T_{cr} from a low value of ≈400°C where essentially no cracking of P_4 to P_2 occurs, up to and beyond ≈700°C where the conversion efficiency is >90%. The results of these experiments reveal that the incorporation rate of phosphorus is at least 20 times less efficient from P_4 tetramers than from P_2 dimers.

The dependence of P-incorporation rate limited growth vs T_S will be discussed. This shows anomolous behaviour between ≈480-520°C where the phosphorus incorporation rate remains approximately constant rather than continuing to decrease exponentially with increasing temperature.

4. MBE Growth of High Mobility InP

The information from the RHEED studies has been used to optimize the conditions for the growth of thick undoped layers of InP, particularly with regard to minimizing the P_2:In flux ratio that is needed at a given substrate temperature. A summary of the growth parameters and

Hall data for a series of thick un-InP layers is given in table 1. The F_t's quoted in the table are BEP ratios although these have also been determined as incorporation rate ratios.

Sample #	P_2:In Flux ratio	T_s °C	d μm	n_{300} cm^{-3}	μ_{300} $cm^2V^{-1}s^{-1}$	n_{77} cm^{-3}	μ_{77} $cm^2V^{-1}s^{-1}$
B72	3.3:1	450	10	$3.6x10^{15}$	≈3000	$1.2x10^{15}$	67750-78800
B76	1.8:1	440	7	$4.5x10^{15}$	2800	$\approx 1.2x10^{15}$	67400-75800
B79	1.9:1	420	6	$\approx 5x10^{15}$	≈2500	$\approx 1.2x10^{15}$	62300-70962
B85	6.8:1	520	5	$7x10^{14}$	≈4000	$\approx 5x10^{14}$	80000-122000
B86	7.0:1	515	8	$1x10^{15}$	≈4000	$6.3x10^{14}$	117850
B87	7.0:1	520	8	$4.1x10^{14}$	5433	$4.8x10^{14}$	152880
B89	6.8:1	480	8	$\approx 2x10^{15}$	3534	$7.9x10^{14}$	102077
B90	6.4:1	460	8	$2.46x10^{15}$	3186	$7x10^{14}$	86906
B91	18.7:1	≈530	8	$1.4x10^{15}$	$7x10^{14}$	$7x10^{14}$	110000
B92	8.0:1	≈525	8	$6x10^{14}$	≈4800	$5.5x10^{14}$	≈130000
B93	7.0:1	≈525	8	$7x10^{14}$	≈5000	$5.8x10^{14}$	≈120000
B96	5.6:1	≈520	8	$\approx 4x10^{14}$	≈4400	$2\text{-}3x10^{14}$	149500-170868

Table 1: Summary of growth conditions and Hall data for a series of un-InP layers grown by solid source MBE.

The mobilities up to $\approx 170{,}000 cm^2V^1s^1$ at 77K with electron densities $\approx 2x10^{14}cm^3$ are believed to be the highest recorded for InP whether grown by solid or gaseous source MBE. 5K photoluminescence spectra are dominated by excitonic transitions, confirming that the concentrations of compensating acceptor species are very low. The presentation will discuss the relationships between the growth conditions and the measured Hall and photoluminescence data. The surface morphology will also be reviewed since this is believed to provide a clue to the growth mechanisms which appear to be different from GaAs.

5. Acknowledgements

The authors acknowledge discussions with M. Holland and A. Kean, and the technical support of J. Cochrane and W. Reid in the MBE laboratory. The research is partially supported by the U.K. S.E.R.C. through grants GR/F/80890 and GR/F/65248

6. References

[1] J.S. Roberts et al., Electron. Lett, **22**, 506 (1986).
[2] H. Heinecke et al., Electron. Lett., **26**, 213 (1990).
[3] A. Rudra et al., Proc. 6th Int. Conf. on MBE, to be published J. Crystal Growth.
[4] C.R. Stanley et al., Appl. Phys. Lett., **57**, 1992 (1990).
[5] C.R. Stanley et al., Appl. Phys. Lett., **58**, 478 (1991).
[6] Y. Morishita et al., Appl. Phys. Lett., **53**, 42 (1988).